Systems approaches to the biology of the spindle pole body

Howell, Rowan

Awarding institution:
King's College London

Systems Approaches to the Biology of the Spindle Pole Body

Rowan Howell

Supervised by:

Dr Peter Thorpe

Dr Attila Csikász-Nagy

Randall Division of Cell and Molecular Biophysics

King's College London

and

The Francis Crick Institute UK

July 15, 2020

A thesis presented for the degree of

Doctor of Philosophy

Abstract

The yeast centrosome or Spindle Pole Body (SPB) is an organelle situated in the nuclear membrane, where it nucleates spindle microtubules and acts as a signalling hub. The SPB is reproduced conservatively, meaning an existing SPB is required to form a new SPB. Additionally, the Mitotic Exit Network (MEN), a group of proteins controlling exit from mitosis localize to the SPB, in an essential step in MEN activation. These properties are conserved in the MicroTubule Organising Centre's (MTOC) of higher eukaryotes, which also duplicate conservatively and act as signalling hubs. Various studies have explored the effects of forcing individual proteins to interact with the yeast SPB, however no systematic study has been performed. Furthermore, while the MEN has been studied intensively, a unified understanding of how localization and protein activity function together as a system is lacking. I have used Synthetic Physical Interaction (SPI) screening to detect proteins that inhibit growth when forced to associate with the SPB. I found that the SPB is especially sensitive to relocalization, necessitating a novel data analysis approach for the SPI data. In addition, I found a set of forced associations that perturb SPB duplication, resulting in elevated SPB number and, in some cases, multi-polar spindles. In order to study spatial aspects of MEN regulation in parallel to control of enzymatic activity by post-translational modifications I developed a compartmental, logical model of the MEN that is capable of representing both aspects of regulation. I found that my model is capable of correctly predicting the phenotype of 80% of mutants we tested, including mutants representing mislocalizing proteins. I use this model to uncover new aspects of MEN regulation, study the role of the FEAR (Cdc Fourteen Early Anaphase Release) network in determining anaphase length and investigate stochasticity in the Spindle Position Checkpoint (SPoC). Altogether this project presents a systematic view of which proteins are regulated through interaction with the SPB and how this functions as a mechanism of protein regulation.

Acknowledgements

I would like to extend my deepest gratitude to my supervisors Peter Thorpe and Attila Csikász-Nagy for their dedicated support and guidance.

Many thanks go to the members of my thesis committee Fabrice Caudron, Ulrike Eggert, Willy Taylor, Paul Bates and Silvia Santos for their advice throughout the project. Outside of the Crick and KCL, I would like to thank Laurence Calzone and Julio Saez-Rodriguez for their support and direction with logical modelling tools.

It has been a pleasure to work alongside colleagues in both the Thorpe and Csikász-Nagy labs : Gudjon Olafsson, Lisa Berry, Wenjun Guo, Cinzia Klemm, Henry Wood, Grace Heredge Thomas, Zoltan Dul, Rosa Hernansaiz Ballesteros, Kirsten Jenkins, Greg Szep and many others at the Crick Institute, KCL and QMUL. I would like to thank my friends Vidya Chivukula and Saz Basu for providing regular distraction and occasional advice.

I'm deeply indebted to my fiance, Esi, for her unwavering support and for getting through many months of lockdown with me and my thesis. I would like to express my great appreciation for my parents, without whom, of course, none of this would have been possible. I would also like to thank my baby niece Mireia for a memorable interlude in the writing process.

Contents

List of Figures

List of Tables

List of abbreviations

- 5FOA – 5-FluoroOrotic Acid
- APC – Anaphase Promoting Complex
- ASC – Anaphase Specific Component
- CDK – Cyclin-Dependent Kinase
- CFP – Cyan Fluorescent Protein
- CV – Coefficient of Variation
- DDC – DNA Damage Checkpoint
- EM – Electron Microscopy
- ER – Endoplasmic Reticulum
- FBA – Flux Balance Analysis
- FEAR – Cdc Fourteen Early Anaphase Release
- FPR – False Positive Rate
- FRET – Förster Resonance Energy Transfer
- GAP – GTPase Activating Protein
- GBP – GFP-Binding Protein
- GFP – Green Fluorescent Protein
- GI – Genetic Interaction
- GIS – Genetic Interaction Similarity
- GO – Gene Ontology

- INM – Inner Nuclear Membrane
- LGR – Log Growth Ratio
- MEN – Mitotic Exit Network
- NE – Nuclear Envelope
- NLS – Nuclear Localization Sequence
- NPC – Nuclear Pore Complex
- ODE – Ordinary Differential Equation
- ONM – Outer Nuclear Membrane
- ORF – Open Reading Frame
- PCR – Polymerase Chain Reaction
- PDE – Partial Differential Equation
- PDF – Probability Distribution Function
- PKN – Prior- Knowledge Network
- PP1 – Protein Phosphatase 1
- PP2A – Protein Phosphatase 2A
- RENT – REgulator of Nucleolar silencing and Telophase exit
- RFP – Red Fluorescent Protein
- SAFE – Spatial Analysis of Functional Enrichment
- SAC – Spindle Assembly Checkpoint
- SDE – Stochastic Differential Equation

- SGA – Synthetic Genetic Array
- SPA – Selective Ploidy Ablation
- SPB – Spindle Pole Body
- SPI – Synthetic Physical Interaction
- SPIN – Spindle Pole Insertion Network
- SPoC – Spindle Position Checkpoint
- STG – State-Transition Graph
- UDS – Universal Donor Strain
- Y2H – Yeast 2-Hybrid
- YFP – Yellow Fluorescent Protein
- γ-TuSC – γ-Tubulin Small Complex
- γ-TuRC – γ-Tubulin Ring Complex

Chapter 1

Introduction

1.1 Introduction

The aim of this project is to understand how localization at the Spindle Pole Body (SPB) is used as an aspect of protein regulation in the cell cycle of the budding yeast, *S. cerevisiae*. The SPB is the MicroTubule Organising Centre (MTOC) of the cell and is crucial for accurate segregation of genetic material between the mother and daughter cells. Beyond nucleation of microtubules, the SPB acts as a signalling hub, controlling both its own duplication and exit from mitosis. Understanding how localization is utilised in these pathways not only improves our understanding of the pathways themselves but also provides a blueprint for understanding localization as a regulatory mechanism more broadly. I have drawn on approaches from systems biology to develop a systems-level view of the SPB as a signalling scaffold. Firstly, I have used a screening tool known as Synthetic Physical Interactions (SPI) to test which proteins are sensitive to forced localization at the SPB. I then developed a novel modelling framework to incorporate spatial effects into a logical network in order to model localization of Mitotic Exit Network (MEN) proteins at the SPB. In this chapter I will introduce some of the key aspects of cell cycle and SPB regulation in budding yeast. I will then move on

to discuss systems biology approaches to the cell cycle and review the existing literature on the subject.

1.2 The Biology of the Spindle Pole Body

1.2.1 Yeast as a model organism

In this project I have used the budding yeast *Saccharomyces cerevisiae* as a model organism. Budding yeast is one of the most commonly used model organisms in the cell cycle community and has a number of properties making it attractive for these kinds of studies. Firstly, it is straightforward to genetically engineer and has well-established transformation and crossing protocols. Secondly, it can easily be grown in both haploid and diploid forms and has a compact genome. Finally, it is well established as a model organism meaning that much is already known about its cell cycle. There is a long history of genes and mechanisms being discovered in yeast before being translated into discoveries in higher eukaryotes.

While the cell cycle of budding yeast is similar to that of higher eukaryotes, there are of course differences. Throughout the thesis I will refer to the *S. cerevisiae* cycle when referring to cell cycle regulation. However, I will, at times, reference the conservation of proteins and mechanisms in other organisms.

1.2.2 Fundamentals of cell cycle regulation

Eukaryotic cells reproduce by alternating between stages of DNA replication and cell division. The *S. cerevisiae* cell cycle begins in G1-phase, where the cell grows to an appropriate size. Once this size has been reached, the cell commits to the cell cycle, passing the START checkpoint and forming a protrusion called a bud. The cell then passes into S-phase, where each of the chromosomes is replicated

resulting in paired sister chromatids. Once replication is completed, the cell enters mitosis. In this stage, the cell divides the genetic material between the mother and bud in 3 well-defined stages: metaphase, anaphase and telophase (Figure 1.1, Weiss (2012)). In metaphase the cell starts to exert force on the sister chromatids via the mitotic spindle. This spindle consists of microtubules emanating from the SPB and at the opposing end is connected to the kinetochores which bind to the centromeric DNA of the chromosomes. The Spindle Assembly Checkpoint (SAC) will arrest the cell cycle until this process is completed (Ibrahim (2015)). When the kinetochores are correctly attached to the sister chromatids, the cell will enter anaphase. At this point, the sister chromatids lose cohesion, leading to extension of the mitotic spindle. In budding yeast, one pole of the spindle must enter the bud in order that a full complement of chromosomes is delivered to the daughter cell. A second mitotic checkpoint, called the Spindle Position Checkpoint (SPoC) monitors this process (Ibrahim (2015)). When the spindle is extended and aligned, the cell enters telophase and the process of nuclear fission and cytokinesis occur. The DNA Damage Checkpoint (DDC) can also arrest cells in mitosis in yeast (reviewed in Matellán and Monje-Casas (2020)). After the cells have divided both mother and daughter re-enter into G1-phase of the cell cycle.

Cyclin-Dependent Kinase (CDK) activity is the main driver of cell cycle progression in yeast. The CDK complex is formed of the catalytic subunit, Cdc28, and one of the cyclins: Clns 1-3 or Clbs 1-6 (Andrews and Measday (1998)). Expression of indivdual cyclins is temporally controlled (Figure 1.1), *CLNs 1-3* are expressed during G1, *CLBs 5-6* are expressed during S-phase and *CLBs 1-4* are expressed in mitosis. CDK activity increases from G1 until it reaches a peak in metaphase. At the metaphase-anaphase transition, the Anaphase-Promoting Complex (APC) subunit Cdc20 becomes active (Sullivan and Morgan (2007)). APC-Cdc20 ubiquitinates securin, Pds1, leading to its destruction and consequently loss of sister chromatid cohesion. Simultaneously, APC-Cdc20 also tar-

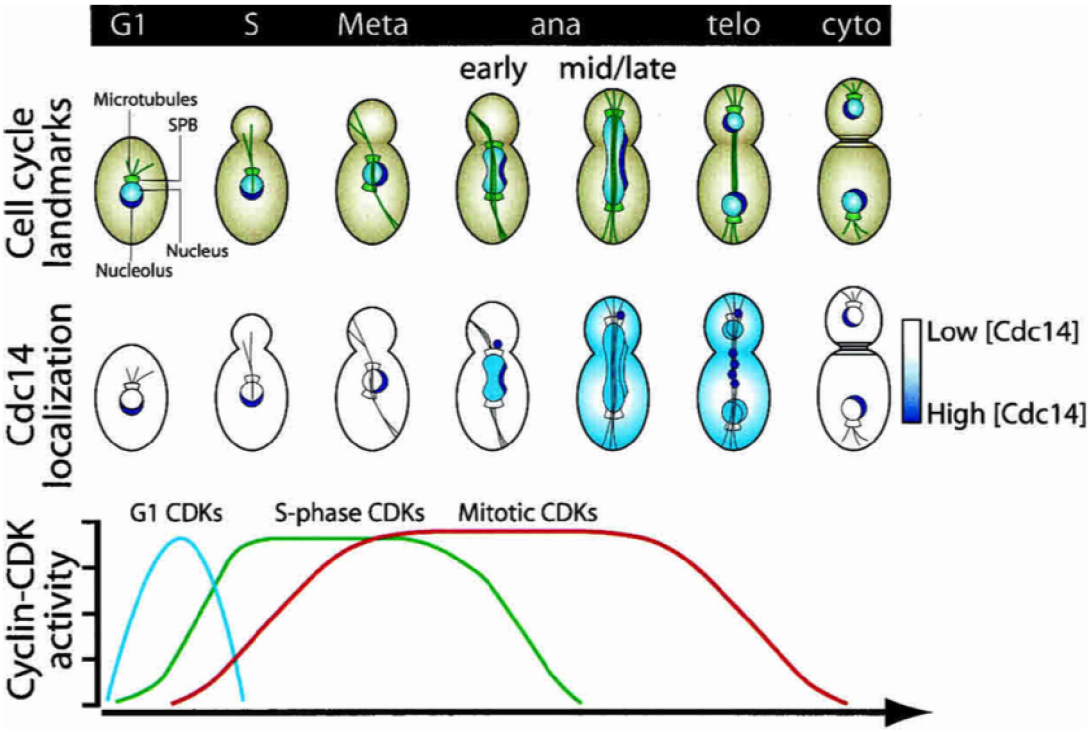

Figure 1.1: Cell cycle events and their coupling to Cdc14 localization and CDK activity. Adapted from D'Amours and Amon (2004).

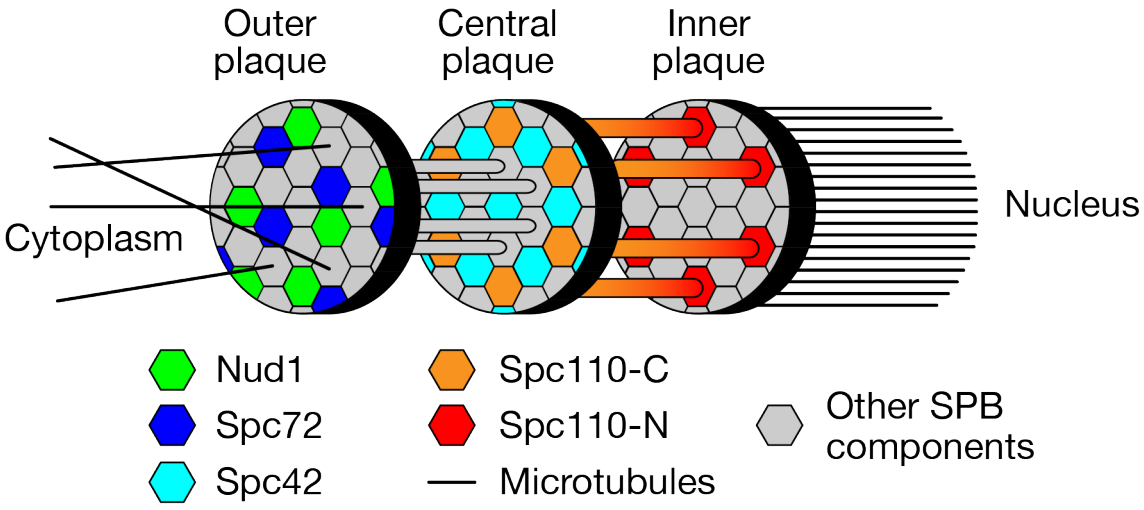

Figure 1.2: The structure of the SPB, showing the location of GBP-tags used in the SPI screens.

gets cyclins for destruction, leading to a lower level of CDK activity in anaphase than in metaphase. When the spindle is aligned, the MEN will become active, leading to release of Cdc14 phosphatase from the nucleolus, where it has been sequestered since G1-phase (Figure 1.1, Stegmeier and Amon (2004)). Liberation of Cdc14 leads to entry into telophase, cytokinesis and eventually the resetting of the cell into G1-phase. It achieves this by reversing CDK phosphorylation, activating the alternative APC subunit, Cdh1, as well as the CDK inhibitor Sic1.

The SPB plays two vital roles in the cell cycle. Firstly, it nucleates the microtubules that form the mitotic spindle, without which cells will arrest at the SAC (Rüthnick and Schiebel (2018)). Secondly, it is an essential scaffold for the MEN (Scarfone and Piatti (2015)). Disruption of either of these processes can lead to a mitotic arrest.

1.2.3 The structure of the spindle pole body

The SPB is a multi-protein assembly that sits embedded in the Nuclear Envelope (NE), with one side facing into the nucleus and the other facing out into the cytoplasm (reviewed in Jaspersen and Winey (2004); Fu et al. (2015)). Byers and

Goetsch (1974) used Electron Microscopy (EM) to image the SPB and showed that it is formed of three distinct plaques. The inner plaque faces into the nucleus and is responsible for nucleation of microtubules that form the mitotic spindle. The outer plaque faces into the cytoplasm and the astral microtubules controlling nuclear positioning are nucleated here. The central plaque joins the inner and outer plaques and is also attached to a structure called the half-bridge. The length of the SPB from outer to inner plaque is roughly 150nm, while the diameter varies from 80nm in G1-phase to 110nm in M-phase (Jaspersen and Winey (2004)). The diameter of the SPB increases with ploidy, averaging 160nm in diploid cells.

SPB components were originally identified by a variety of techniques, including mass spectrometry of SPB-enriched extracts, screens for physical interaction with known SPB components and genetic screens to identify mutants with phenotypes indicative of SPB defects (Kilmartin (2014)). Once identified, immuno-EM has been used to identify the region of the SPB these proteins localize to specific regions of the SPB. As a large, multi-protein assembly, the structure of the SPB has proven challenging to determine. An approach using FRET (Förster Resonance Energy Transfer) data found a unique geometrical configuration of proteins for the SPB (Muller et al. (2005)). A more sophisticated approach produced a structure using Bayesian integrative modelling to combine data from FRET, Y2H (Yeast 2-Hybrid), EM, x-ray crystallography and small-angle x-ray scattering experiments (Viswanath et al. (2017)).

Spc110 is a long, coiled-coil protein which functions as the receptor for the γ-TuSC (γ-Tubulin Small Complex) at the inner plaque (Fu et al. (2015)). The γ-TuSC consists of a single copy of both Spc97 and Spc98 as well as 2 copies of γ-tubulin (Tub4); this complex recruits other tubulin subunits, leading to the formation of microtubules. The N-terminus of Spc110 lies on the inner plaque but the C-terminus resides on the central plaque where it is linked to Spc42 via Spc29 and Cmd1 (Figure 1.2, Jaspersen and Winey (2004)). Spc42 forms a hexagonal

crystalline structure at the central plaque (Figure 1.2, Bullitt et al. (1997)). Cnm67 is another coiled-coil protein that is thought to act as a spacer between the central and outer plaques, its C-terminus interacts with Spc42, while its N-terminus is connected to Nud1 at the outer plaque (Jaspersen and Winey (2004)). Nud1 binds Spc72, which acts as the γ-TuSC receptor at the outer plaque of the SPB (Figure 1.2, Fu et al. (2015)). The half-bridge is attached to the central plaque and has components on both sides of the nuclear envelope (Rüthnick and Schiebel (2016)). Sfi1 is a long, α-helical protein that spans the cytoplasmic side of the half bridge, it contains 21 Cdc31 binding sites (Li et al. (2006)). Cdc31 in turn binds Kar1, while Mps3 is a membrane protein which localises to the nuclear side of the half-bridge.

Protein	**Localization**	**Role**
Spc110	Outer plaque	γ-TuSC receptor
Spc29	Central plaque	Spacer
Cmd1	Central plaque	Ca^{2+} binder
Spc42	Central plaque	Membrane interaction?
Cnm67	Outer plaque	Spacer
Nud1	Outer plaque	MEN scaffold
Spc72	Outer plaque	γ-TuSC receptor
Sfi1	Half-bridge	Structural half-bridge component
Cdc31	Half-bridge	SPB duplication
Kar1	Half-bridge	SPB duplication
Mps3	Half-bridge	SPB duplication
Spc97	γ-TuSC	Microtubule nucleation
Spc98	γ-TuSC	Microtubule nucleation
Tub4	γ-TuSC	Microtubule nucleation

Table 1.1: SPB proteins and their roles.

1.2.4 The life cycle of the spindle pole body

A new SPB starts its life in G1-phase as a satellite formed of Spc42, Spc29, Nud1 and Cnm67 connected via two extended half-bridges (the full-bridge) to an existing SPB (Figure 1.3, Adams and Kilmartin (1999)). This satellite sits on the cytoplasmic face of the nuclear membrane until the cell passes the START

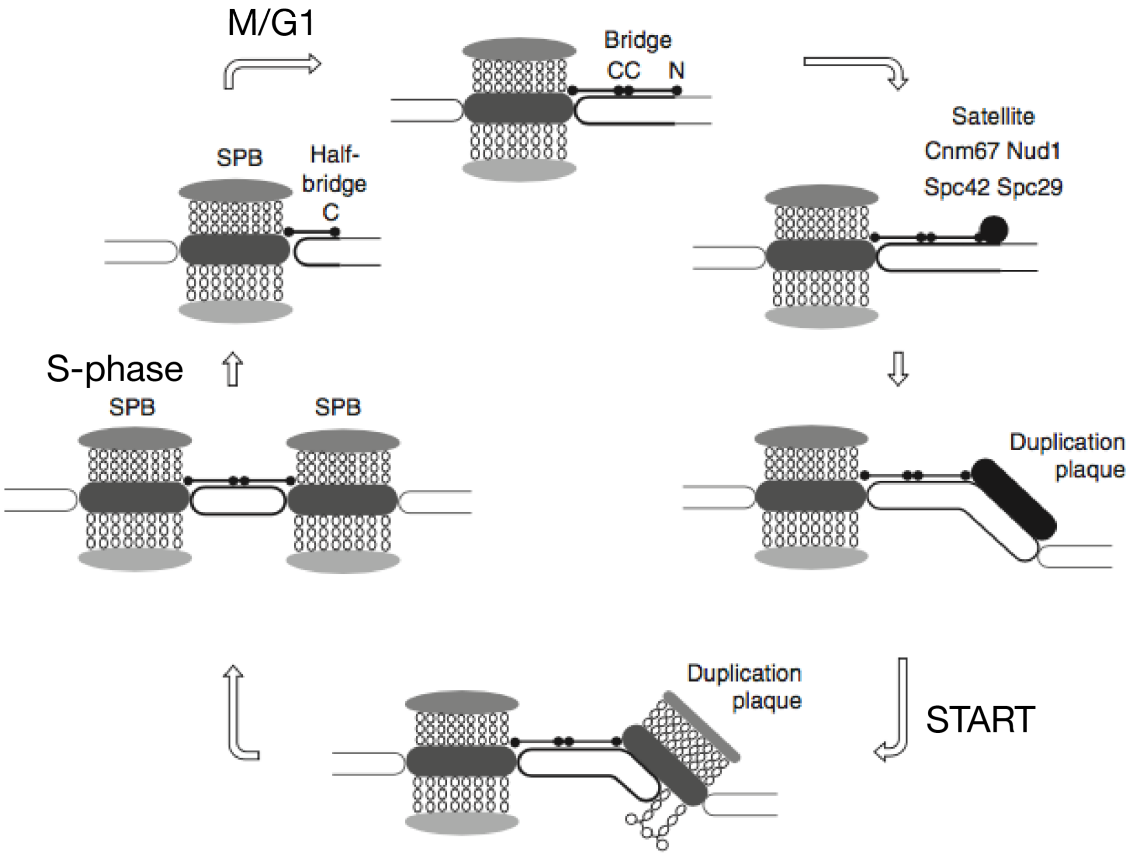

Figure 1.3: Life cycle of the SPB. The first step in SPB duplication is half-bridge extension occurring at the M/G1 transition. Then an SPB satellite formed of Cnm67, Nud1, Spc42 and Spc29 is formed on the cytoplasmic face of the NE. This grows into a duplication plaque which is then inserted into the NE after the START checkpoint. The duplication plaque grows into a full SPB and then the half-bridge is cleaved during S-phase, leading to separation of the SPBs. Figure adapted from Fu et al. (2015).

checkpoint, at which point it is inserted into the membrane (Rüthnick and Schiebel (2018)). Once embedded, the satellite develops into a full SPB. By S-phase, the cell has two fully formed SPBs embedded in the nuclear membrane but tethered together by the full bridge. As CDK activity rises in S-phase, Sfi1 is phosphorylated by CDK leading to separation of the SPBs (Avena et al. (2014); Elserafy et al. (2014)).

In mitosis, the SPBs nucleate microtubules into the nucleus which form the mitotic spindle and interactions between these microtubules force the SPBs to opposing ends of the nucleus. The SPBs also nucleate astral microtubules which

interact with the cell cortex controlling nuclear positioning. There are two pathways that contribute to this process, one dependent on Dyn1 (dynein) and the other on Kar9 (Juanes and Piatti (2016)). These motor proteins help to align the mitotic spindle with the mother bud axis. When one of the SPBs enters the bud, the SPoC is satisfied and the MEN becomes active, leading to mitotic exit and cytokinesis. Dephosphorylation of Sfi1 by Cdc14 at mitotic exit allows the half-bridges of both SPBs to extend into full-bridges and formation of new SPB satellites (Li et al. (2006); Avena et al. (2014); Elserafy et al. (2014)). After cytokinesis, the cycle begins anew.

The current paradigm of SPB development is that SPBs are formed through the above cycle of satellite formation, insertion, half-bridge abscission, SPB separation and half-bridge extension (Rüthnick and Schiebel (2016)). This cycle is tied to the chromosomal cell cycle by regulation of the half-bridge through oscillations in CDK and Cdc14 activity. This results in perfect once-per-cycle duplication of the SPBs.

There are many mutants that prevent SPB duplication, for example the temperature sensitive allele of *CDC31* leads to cells with a single SPB (Baum et al. (1986)). However, it is not just structural SPB components that lead to this phenotype. A screen for mutants with a mono-polar spindle phenotype identified *MPS1* and *MPS2* (Winey et al. (1991)). While *MPS1* mutants fail to initiate satellite formation, *MPS2* mutants form a satellite but fail to insert it into the nuclear envelope. Together with Bbp1, Nbp1 and Ndc1, Mps2 is part of the Spindle Pole Insertion Network (SPIN), a group of proteins essential for insertion but not duplication of the SPB (Rüthnick and Schiebel (2018)). While mutants that prevent SPB duplication are reasonably common, mutations that cause SPB over-duplication are more rare. This phenotype is seen in cells with relatively large perturbations to cell cycle dynamics, for example cells overexpressing Cdc5 (Song et al. (2000)) or lacking the cyclins Clb1-4 (Haase et al. (2001)). The *sfi1-C4A* allele causes

aberrant SPB duplication but is also unable to separate these SPBs (Avena et al. (2014)).

Insertion of the SPB-satellite

The Nuclear Envelope (NE) is a double lipid-bilayer consisting of the Inner- and Outer-Nuclear Membranes (INM and ONM), with a small volume enclosed between the two known as the perinuclear space (Rüthnick and Schiebel (2018)). NPCs (Nuclear Pore Complexes) and SPBs traverse both membranes and as a result, the INM and ONM are fused in the region around an NPC or SPB. The discovery, by Adams and Kilmartin (1999), of a pore-like structure near the un-inserted SPB satellite raised the possibility that these two structures share a common mechanism of insertion through the nuclear envelope. Furthermore, the SPIN protein Ndc1 is found at both the SPB and the NPC (Chial et al. (1998)). There are also genetic interactions between SPB and NPC genes, for example the monopolar spindle phenotype of *mps3-1* can be rescued by deletion of *NUP157* (Witkin et al. (2010)). This has lead to a model in which the machinery used to insert NPCs is also used to insert SPBs (Jaspersen and Ghosh (2012)). Recent evidence has shown that the pore-like structure observed by Adams and Kilmartin (1999) is indeed an NPC and that NPC activity is required for SPB insertion (Rüthnick et al. (2017)). Rüthnick et al. (2017) also showed that the SPIN network proteins, which are all - except Bbp1 - transmembrane proteins, form a ring around the satellite as it is inserted.

Age-dependent segregation of the SPBs

During mitosis, one of the SPBs enters the bud compartment and will go on to become the SPB of the daughter cell. This SPB is termed the dSPB (daughter SPB), in opposition to the mSPB (mother SPB), which remains in the mother cell. The SPBs are also distinguished by their age. As the cell enters M-phase one

SPB will have existed for less than a single cell cycle (the “new” SPB), while the other will have existed for at least one (the “old” SPB). The fate- and age-based identities of the SPBs are linked, with the old SPB becoming the dSPB in nearly every case (Pereira et al. (2001)). Deletion of *KAR9*, disrupts this association, randomising the fate of the SPBs.

There are two theories to explain the mechanism of age-dependent segregation patterns of SPBs. Lengefeld et al. (2018) propose that this pattern relies primarily on Kar9, a microtubule motor that they argue is directed to the older SPB by components of the MEN pathway, specifically by phosphorylation of Kar9 by Dbf2 (Hotz et al. (2012a,b)), which then acts to pull this SPB into the bud (Hotz and Barral (2014)). According to this theory the age-based identity of the SPB is established by phosphorylation of Nud1 by Swe1 in G1-phase and maintained by the kinase Kin3 and acetyltransferase NuA4 (Lengefeld et al. (2017)) However, this theory controversially relies on the activity of Dbf2 kinase in metaphase and the evidence showing that the MEN can influence Kar9 localization has proven not to be reproducible (Campbell et al. (2019)). Alternatively, Geymonat et al. (2020) propose that asymmetry of astral microtubules at the SPBs is sufficient to explain their segregation pattern. They propose that age-dependent CDK-phosphorylation of Nud1 underlies Spc72 asymmetry, which in turn leads to asymmetric nucleation of microtubules.

Why this process is regulated at all is something of a mystery, as mutants that randomize SPB fate are generally healthy, for example *kar9*Δ (Miller and Rose (1998b)). One theory is that this regulation prevents premature aging of the daughter cell (Lengefeld and Barral (2018)). By tethering Kar9 to the mother cortex, Manzano-López et al. (2019) were able to reverse the pattern of SPB inheritance, leading to old SPBs remaining in the mother cell. These cells showed a reduced replicative lifespan, in support of the theory of Lengefeld and Barral (2018).

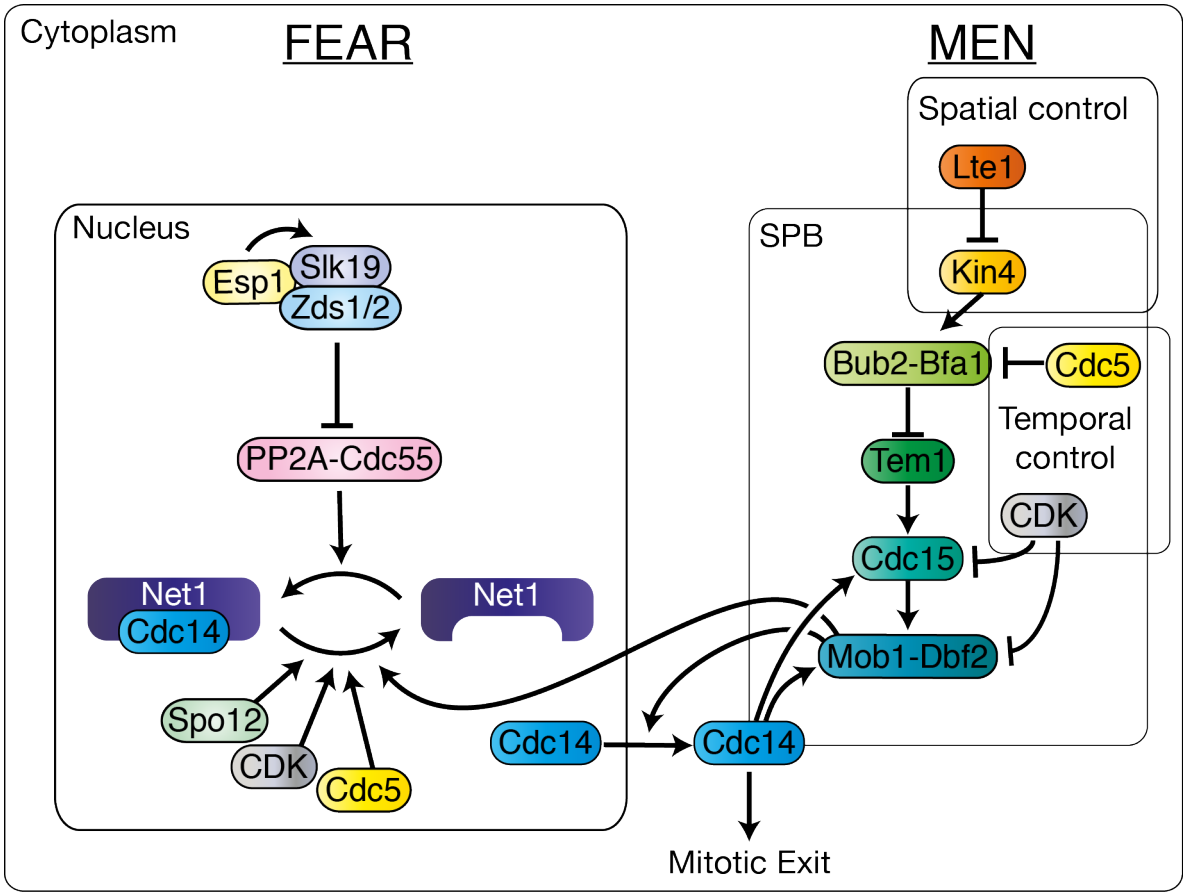

Figure 1.4: A simplified graphical description of the MEN and FEAR pathways.

1.2.5 Regulation of mitotic exit and the SPB

In budding yeast, there are 3 clearly defined stages in mitosis: metaphase, anaphase and telophase. The transition between metaphase and anaphase is controlled by the SAC, which will delay the transition until the kinetochores are correctly attached to the centromeres (Ibrahim (2015)). The transition from anaphase to telophase is controlled by the SPoC, which will delay the transition until an SPB enters the bud, signalling alignment of the spindle (Ibrahim (2015)). These stages are characterised not just by mitotic events but also by the balance of CDK and Cdc14 activity. In metaphase, CDK activity is high while Cdc14 is tightly sequestered in the nucleolus. At the metaphase-anaphase transition, APC-Cdc20 becomes active (Sullivan and Morgan (2007)). APC-Cdc20 targets cyclins for destruction, leading to a lower level of CDK activity in anaphase. Simul-

taneously, it ubiquitinates Pds1, leading to liberation of seperase, Esp1. Esp1 not only cleaves securin, leading to sister-chromatid seperation, it also initiates activation of the FEAR (Cdc Fourteen Early Anaphase Release) network (Reviewed in Rock and Amon (2009)). Prior to anaphase, Cdc14 is sequestered in the nucleolus as a result of interaction with a stoichiometric inhibitor, Net1, forming the RENT (REgulator of Nucleolar silencing and Telophase exit) complex. The FEAR network causes phosphorylation of Net1 leading to disassociation of RENT. This allows Cdc14 to diffuse around the nucleus. When the cell passes the SPoC, the MEN becomes active, leading to release of Cdc14 throughout the cell. Cdc14 reverses CDK phosphorylation, in particular phosphorylation of Swi5, Sic1 and Cdh1 (Sullivan and Morgan (2007)). Cdh1 is an APC subunit that is required for full destruction of Clb2, and CDK phosphorylation prevents Cdh1 activity. Sic1 is a stoichiometric inhibitor of the CDK complex and it is rapidly degraded when phosphorylated, Cdc14 phosphatase activity allows it accumulation. Swi5 is a transcription factor that drives *SIC1* expression and CDK phosphorylation inhibits this activity. Therefore, through multiple mechanisms, Cdc14 release leads to reversal of CDK phosphorylation, setting the stage for entry into a new cell cycle.

The FEAR network

The FEAR network releases Cdc14 from the RENT complex through phosphorylation of Net1 (Figure 1.4, Rock and Amon (2009)). Throughout mitosis, Net1 is phosphorylated transiently by CDK and Cdc5, with this phosphorylation largely reversed by Protein Phosphatase 2A (PP2A), in its Cdc55-bound isoform, in metaphase (Shou et al. (2002); Azzam et al. (2004); Ptacek et al. (2005); Queralt et al. (2006)). Upon entry into anaphase, Esp1 is released from Pds1, allowing it to form a complex with Slk19 and, together with Zds1/2, downregulate PP2A-Cdc55 (Sullivan and Uhlmann (2003); Queralt and Uhlmann (2008a)). There is some debate over the nature of this downregulation, with Rossio and Yoshida

(2011) arguing that it is a result of exclusion of Cdc55 from the nucleus while Játiva et al. (2019) posit that phosphorylation of Cdc55 by CDK leads to a reduction of phosphatase activity in anaphase. Either way, the result is that Net1 phosphorylation accumulates, allowing Cdc14 to be released throughout the nucleus. The nucleolar proteins Spo12 and Fob1 also contribute to this process through a poorly understood mechanism (Stegmeier et al. (2004); Tomson et al. (2009)). It is interesting that CDK activity drops from metaphase to anaphase but it is in anaphase that CDK activity is required for FEAR. However, there is clear evidence of this with *clb2*Δ and *clb5*Δ mutants as well as a *net1-6CDK* allele, in which CDK sites have been mutated, all showing FEAR phenotypes (Azzam et al. (2004); Manzoni et al. (2010)). FEAR release is transient, if the MEN is not activated then Cdc14 will return to the nucleolus and the cell will not exit mitosis (Stegmeier et al. (2002)). The FEAR network is not essential, as demonstrated by the viability of FEAR mutants such as *slk19*Δ, however these mutants show a delay in exit from mitosis (Stegmeier et al. (2002)). FEAR and rDNA condensation appear to be interlinked, as FEAR release aids in segregation of rDNA (Clemente-Blanco et al. (2009)) but condensation of the rDNA is required for FEAR (de los Santos-Velázquez et al. (2017)). FEAR release may also be important for other mitotic events including spindle midzone assembly (Khmelinskii et al. (2007)) and spindle microtubule stabilization (Higuchi and Uhlmann (2005)), as well acting as a feedback mechanism to make the metaphase-anaphase transition irreversible (Holt et al. (2008)).

The MEN

The MEN is responsible for interpreting the signal that the SPoC has been satisfied and, as a result, releasing Cdc14 fully into the cytoplasm (Figure 1.4, Weiss (2012); Scarfone and Piatti (2015); Ibrahim (2015)). At the root of the SPoC is a distinction between the mother and bud compartments (Figure 1.5). A protein

kinase, Kin4, localises to the mother compartment (Pereira and Schiebel (2005)), while another protein, Lte1, localises specifically to the bud (Bardin et al. (2000)). This leads to the establishment of MEN activating and inhibiting zones (Bardin et al. (2000); Chan and Amon (2010)). The key switch in the MEN is the small GTPase, Tem1, whose activity and localization is controlled by the Bub2-Bfa1 GAP (GTPase Activating Protein) complex (Pereira et al. (2000); Caydasi et al. (2012)). Bfa1 in the mother compartment is phosphorylated by Kin4, forcing it to turn over rapidly at the SPBs (Caydasi and Pereira (2009)). When an SPB enters the bud compartment, Bub2-Bfa1 is removed from Kin4 control and localizes stably at the SPB. Bfa1 is then phosphorylated by Cdc5 which resides at the SPB, inhibiting its GAP activity (Geymonat et al. (2003)). The result of these modifications of Bfa1, is that Tem1 is recruited to the SPB, and accumulates its active GTP-bound form there (Figure 1.5). Lte1 was originally thought to act as a GEF for Tem1, due to its homology to other GEFs (Shirayama et al. (1994a)) however it was shown not to act as a GEF *in vitro* (Geymonat et al. (2009)). Instead Lte1 is thought to act primarily to control Kin4 localization and activity (Bertazzi et al. (2011); Falk et al. (2011)). Tem1 goes on to recruit the protein kinase Cdc15 to the SPB (Asakawa et al. (2001)). Cdc15 phosphorylates Nud1, creating a docking point for the Mob1-Dbf2 (Rock et al. (2013)). Cdc15 then phosphorylates Dbf2 specifically at the SPB, leading to activation of the Mob1-Dbf2 complex (Mah et al. (2001)), which in turn leads to Cdc14 release. Dbf2 has a paralog, Dbf20, which can partially play the role of Dbf2 in *dbf2*Δ cells (Toyn et al. (1991)). The exact mechanism by which Cdc14 is released by Mob1-Dbf2 is not yet understood, however it is known that Mob1-Dbf2 enters the nucleus (Stoepel et al. (2005)), phosphorylates Net1 (Ptacek et al. (2005)) and phosphorylates Cdc14 near to its NLS (Nuclear Localization Sequence), allowing Cdc14 to leave the nucleus (Mohl et al. (2009)). A recent pre-print (Zhou et al. (2020)) offers clues to the exact mechanism by which Mob1-Dbf2 promotes Cdc14 release from the nucleolus,

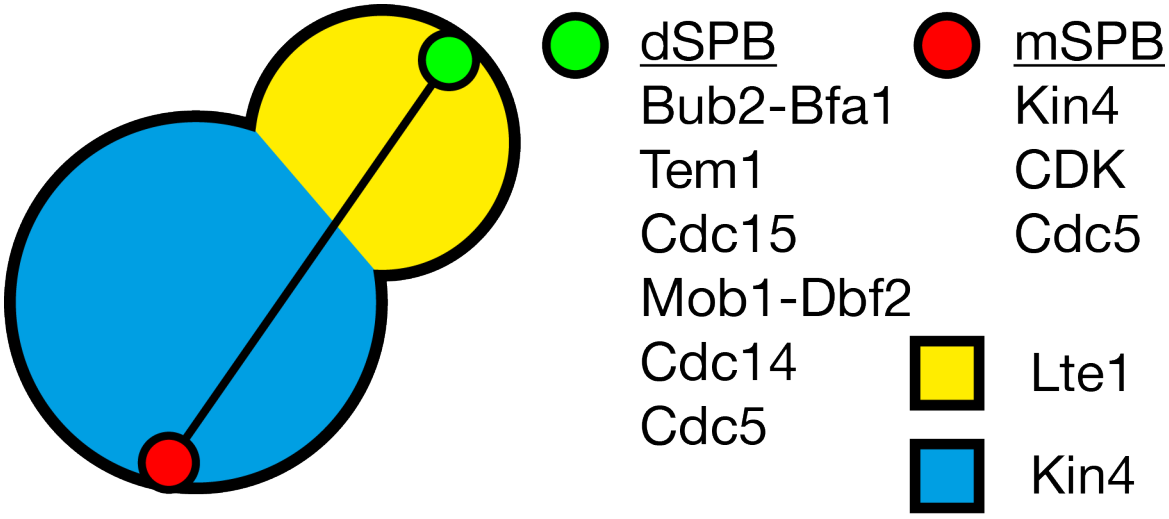

Figure 1.5: Spatial organization of MEN proteins in a late anaphase cell. Lte1 localizes to the bud compartment, establishing the MEN activatory region, while Kin4 localizes to the mother compartment, characterizing the MEN inhibitory region. The dSPB carries MEN-promoting proteins, while the mSPB carries MEN inhibitors.

suggesting Cdc5 phosphorylation of Net1 targets Mob1-Dbf2 to the nucleolus, allowing the complex to phosphorylate Net1.

The MEN at the SPB acts as a sensor for spindle alignment. When an SPB enters the bud, the MEN senses the change in environment from inhibitory to activatory and converts this signal, through the cascade, into a decision to exit mitosis.

Localization of the MEN

Nud1 is the main scaffold for MEN proteins at the SPB, the mislocalizing *nud1-2* allele leads to a mitotic arrest with an inactive MEN at restrictive temperature (Gruneberg et al. (2000)). Gryaznova et al. (2016) used FRET to show that Bfa1 binds to both Nud1 and Spc72, while Kin4 interacts only with Spc72. They also showed that *spc72*Δ cells (viable in the W303 background) can exit from mitosis but lack a functional SPoC. Rock et al. (2013) showed, using a Nud1 phosphomutant and crystalization of human Mob1 with a Nud1 peptide, that Mob1 binds to Nud1 only when Nud1 has been phosphorylated by Cdc15. Bub2-Bfa1 is im-

portant for localization of other MEN proteins at the SPB, especially Tem1 and Cdc14 (Pereira et al. (2002)), although a small amount of Tem1 localizes at the SPB in *bub2*Δ*bfa1*Δ cells (Caydasi et al. (2012)).

Mitotic kinases and phosphatases

CDK and polo kinase Cdc5, as well as the phosphatases Cdc14 and PP2A play a role in regulation of mitotic exit. CDK phosphorylation inhibits Cdc15 (Jaspersen and Morgan (2000)) and Mob1 (König et al. (2010)), this is thought to limit the activity of the MEN in metaphase, when CDK activity is high. These modifications are reversed by Cdc14, seemingly leading to a paradox: how can Cdc14 be released if it is required for its own release?

Firstly, in an unperturbed cell cycle it may be FEAR rather than full scale Cdc14 release that is reponsible for this dephosphorylation. Yellman and Roeder (2015) argue that FEAR is limited to the nucleus preventing cross-talk between the FEAR and the MEN, which acts in the cytoplasm. However, the detectable delay in mitotic exit signalling seen in FEAR mutants is usually interpreted as an indication that FEAR plays a role in MEN activation (Stegmeier et al. (2002)). While fluorescently-labeled Cdc14 is generally restricted to the nucleus during anaphase, it may be that a small proportion escapes and is sufficient to make these modifications. Secondly, it can be argued that Cdc14's role in MEN activation is a form of positive feedback that helps to make the M/G1 transition irreversible.

CDK does not just regulate Cdc15 activity, it also is thought to engage in a negative feedback loop with Cdc15, preventing their co-localization at SPBs (Figure 1.5), König et al. (2010)). CDK and Cdc14 also regulate Bfa1; a *bfa1-6A* mutant, in which 6 CDK phospho-sites are mutated is SPoC deficient, and the SPoC deficiency of *kin4*Δ can be rescued by the FEAR mutant *spo12*Δ (Caydasi et al. (2017)).

The role of the polo-kinase, Cdc5, in the regulation of mitotic exit has been difficult to study due to its many roles in mitosis (Botchkarev and Haber (2017)). A bioinformatic approach discovered 192 proteins containing Cdc5 consensus sites and polo-box domain binding sites, including Bfa1, Cdc15, Cdc20, Cdc55, Cdh1, Dbf20, Esp1, Lte1, Net1, Sic1 and Spc72 (Snead et al. (2007)). In the absence of Cdc5 activity, cells arrest in anaphase with Cdc14 remaining in the nucleolus, suggesting that Cdc5 is required for both FEAR and MEN pathways (Stegmeier et al. (2002); Rodriguez-Rodriguez et al. (2016)). On the other hand, overexpression of Cdc5 can cause premature Cdc14 release and mitotic exit in cells arrested in metaphase and in the absence of FEAR proteins (Shou et al. (2002); Sullivan and Uhlmann (2003)). The primary role of Cdc5 in the FEAR is thought to be phosphorylation of Net1, alongside CDK (Rock and Amon (2009)). In the MEN, it has a role in inhibiting Bfa1 (Geymonat et al. (2003)) and also appears to positively regulate Cdc15 binding at the SPB (Rock and Amon (2011)). CDK is required for Cdc5 to function in regulation of mitotic exit (Mortensen et al. (2005); Rodriguez-Rodriguez et al. (2016)). Cdc5 kinase activity remains constant throughout mitosis (Cheng et al. (1998)), which suggested that rather than acting as a switch, Cdc5 may act as a mitosis specific signal. However, recent work from the Haber lab suggests that Cdc5 localization is regulated, with Cdc5 restricted to the nucleus in metaphase, before being released into the cytoplasm in anaphase (Botchkarev et al. (2014)). Although Cdc5 shows an SPB localization throughout mitosis, Botchkarev et al. (2017) show that it moves from the inner to outer plaque at the metaphase-anaphase transition. This shows that Cdc5 may act as an anaphase specific signal for MEN regulation.

Similarly to Cdc5, the role of PP2A in control of mitotic exit has been difficult to establish. PP2A-Cdc55 has a clear role in the FEAR network, where it prevents FEAR release by reversing phosphorylation of Net1 until it is removed from the nucleus (Queralt et al. (2006); Queralt and Uhlmann (2008a)). The alternative

isoform PP2A-Rts1 also has an established role regulating Kin4 localization at the SPB (Bertazzi et al. (2011)). Baro et al. (2013) also found evidence that Bfa1 and Mob1 are substrates of PP2A-Cdc55, arguing that *cdc55*Δ cells have an active MEN in metaphase but do not exit mitosis due to CDK inhibition of Mob1. SILAC screens have identified various residues in Mob1 and Bfa1 with phospho-regulation that depends on Cdc55 and Rts1 (Baro et al. (2018); Touati et al. (2019)). However, there is a lack of definitive genetic evidence that PP2A-Cdc55 regulates the MEN, aside from the established roles. Rossio and Yoshida (2011) demonstrate with a *CDC55-NLS* mutant that Cdc55's role in the FEAR network depends on its localization. However, Queralt et al. (2006) also show that PP2A-Cdc55 phosphatase activity in synchronized cell extracts was lower in anaphase than metaphase. Játiva et al. (2019) propose that Cdc55 activity is regulated by CDK phosphorylation and show that mutating CDK sites in Cdc55 can change its activity towards Net1. These findings present PP2A as a factor that generally opposes mitotic exit, helping to restrict it to anaphase.

The extended MEN

Aside from the core MEN proteins, and mitotic kinases and phosphatases, a number of proteins have been found to play some role in control of mitotic exit. The *AMN1* gene was identified in a screen for synthetic dosage lethality in a *cdc5-1* background (Wang et al. (2003)). While *AMN1* is primarily expressed in G1-phase in daughter cells where MEN activity is suppressed, *amn1*Δ cells were also found to be SPoC deficient (Wang et al. (2003)). The 14-3-3 protein Bmh1 is also though to regulate the MEN, playing a role alongside Kin4 regulating Bfa1 localization at the SPB (Caydasi et al. (2014); Gryaznova et al. (2016)). However, it is worth noting that subsequent studies disagreed with Caydasi et al. (2014), finding no SPoC defect in *bmh1*Δ cells (Falk et al. (2016a)).

Lte1 is known to play a number of roles activating the MEN however it is

not essential, although *lte1*Δ cells are cold sensitive. A screen for high-copy suppressors of *lte1*Δ cold sensitivity identified the PAK kinase Ste20 (Höfken and Schiebel (2002)), which has also been shown to drive mitotic exit in *lte1*Δ*kin4*Δ*spo12*Δ cells (Caydasi et al. (2017)). Therefore, Ste20 is thought to act in parallel to Lte1, by targeting Tem1 through a poorly understood mechanism (Chiroli et al. (2003)). The cortical proteins Kel1 and Kel2 were found to precipitate with Tem1 and Lte1 in pull-down experiments (Höfken and Schiebel (2002)). However, *kel1*Δ and *kel2*Δ mutants suppress the cold sensitivity of *lte1*Δ strains, suggesting they are negative regulators of the MEN. The GTPase Cdc42 and its GEF Cdc24, which are key determinants of cell polarity, function upstream of Lte1 and Ste20 (Höfken and Schiebel (2002)). In particular, Lte1 is controlled by Cdc42 through the kinase Cla4, which phosphorylates Lte1, regulating Lte1 localization and activity (Höfken and Schiebel (2002); Chiroli et al. (2003); Bertazzi et al. (2011)). Cdc42 and the formin Bni1 have also been shown to regulate asymmetry of Bub2-Bfa1 localization at the SPBs (Monje-Casas and Amon (2009)).

Although Lte1 and Kin4 are thought of as the key determinants of the MEN-activating and -inhibiting zones, their localization is controlled indepedently. Kin4 will still localize at the mother cortex in *lte1*Δ cells, although Lte1 does seems to be important to prevent Kin4 loading at the dSPB (Falk et al. (2011)). Kin4 activity and localization is regulated by Elm1 kinase (Caydasi et al. (2010); Moore et al. (2010)). Elm1 localizes to the budneck and this localization is regulated by septin dynamics, in particular as regulated by ubiquitin ligases Dma1&2 (Merlini et al. (2012)). Septins have themselves been implicated in the SPoC, with *sep7*Δ and *cdc10*Δ cells lacking a functional checkpoint (Castillon et al. (2003)). However, this may be because these septins form a diffusion barrier required to establish Lte1 and Kin4 localization.

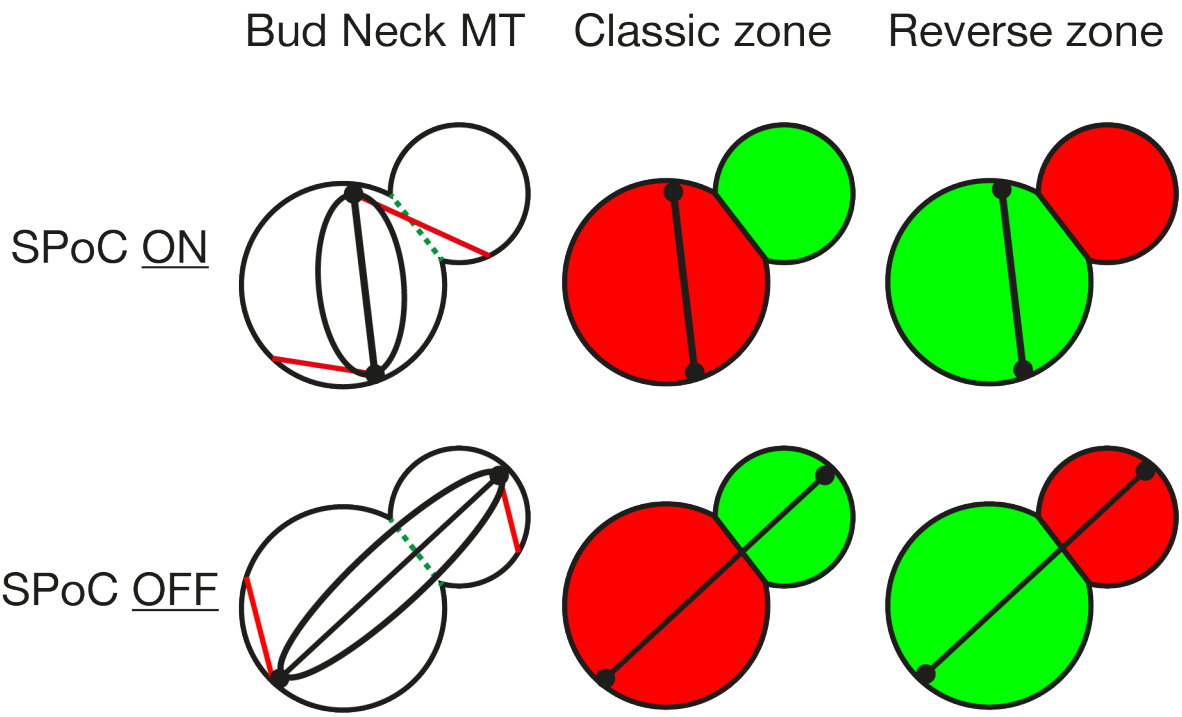

Figure 1.6: The three main theories of SPoC regulation. According to the bud neck microtubule model, astral microtubules interact with the budneck, inhibiting mitotic exit. The classic zone model posits that the bud is a MEN-activating zone and that entry of an SPB into this zone activates the MEN. The alternative zone model reverses the zones, arguing that entry of an SPB into the bud allows accumulation of active MEN proteins at the mSPB.

Alternative models of MEN activation

Various models of the SPoC have been suggested and are illustrated in Figure 1.6. An early theory, the bud neck microtubule model, proposed that astral microtubules connecting the SPB to the cytoskeleton interact with the bud neck, leading to MEN inhibition while the spindle is misaligned (Adames et al. (2001)). However, recent experiments using multinucleate cells, which can have both microtubules in the bud neck and an SPB in the bud, suggest that the entry of an SPB into the bud is the trigger for mitotic exit (Gryaznova et al. (2016); Falk et al. (2016b)). These experiments lend support to a 'zone' model, which posits that the cell is divided into a MEN-activating zone and a MEN-inhibiting zone. The original zone model (referred to as the classic zone model in Figure 1.6) identifies the bud as the MEN-activating zone and posits that the entry of an SPB loaded with MEN proteins into the bud leads to MEN activation which then spreads through the cell (Chan and Amon (2010)). A variant on this model (denoted the reverse zone model in Figure 1.6) flips the zones suggesting the bud is the MEN-inhibitory zone (Hotz and Barral (2014)). The idea behind the reverse zone model is that symmetry of MEN components at the SPB inhibits MEN activation by preventing accumulation at a single SPB. Entry of an SPB into the bud causes Bub2-Bfa1 to accumulate at the dSPB, removing it from the mSPB, allowing activation of Tem1 there. However, the reverse zone model has significant issues. The model suggests that asymmetry of Bub2-Bfa1 is necessary for MEN activation. Geymonat et al. (2009) found that the mutant Lte1-8N protein mislocalizes to the mother compartment. They found that these cells will exit mitosis with a misaligned spindle – when Bub2-Bfa1 is symmetric – in contradiction of the prediction of the reverse zone model. Campbell et al. (2020) have recently shown that a single SPB is sufficient to initiate mitotic exit, disproving the reverse zone model hypothesis. They used the *cdc31-2* mutation to generate cells with a single SPB and showed that in these cells, mitotic exit occurs after entry of the SPB into the bud.

However, they found mitotic exit is much slower in these cells, demonstrating the importance of signal amplification at the mSPB.

The MEN outside anaphase

The conventional understanding of the MEN is that its activity is limited to late anaphase, however evidence that Dbf2 kinase may be active earlier in the cycle has challenged this view (Reviewed in Hotz and Barral (2014)). Dbf2 and Dbf20 were found to regulate *SWI5* and *CLB2* mRNA stability, with the activity of Dbf2 independent of its kinase activity (Trcek et al. (2011)). Dbf2 was also implicated in regulation of the G1/M transition through phosphorylation of the arginine methyl-transferase Hmt1 (Messier et al. (2013)). Furthermore, Dbf2 and Dbf20 phosphorylate Kar9 in metaphase, and this modification is required for age-depedendent segregation of the SPBs (Hotz et al. (2012a,b)). Dbf2 kinase activity towards calf thymus H1 histone is known to be regulated through phosphorylation of Ser-374 and Thr-544 by Cdc15 as well as by interaction with Mob1 (Mah et al. (2001)). Mob1 is phosphorylated by CDK at a number of sites, and incubation of Dbf2-Mob1 with Clb2-CDK reduces Dbf2 kinase activity towards the C-terminus of Cdc14 (König et al. (2010)). Therefore, how Dbf2 could act in metaphase is something of a mystery. One possible resolution is that Dbf2 substrate specificity could depend on its phosphorylation, meaning that Dbf2 activity towards Hmt1 may be independent of phosphorylation by Cdc15 but not its activity towards MEN targets. Another interesting finding is that overexpression of *MOB1* can rescue a *dbf2*$\triangle$ *dbf20*$\triangle$ double mutant (Komarnitsky et al. (1998)), perhaps suggesting that Dbf2's MEN promoting activity may be independent of its kinase activity.

Beyond mitotic exit, the MEN has been shown to play a role in the execution of cytokinesis (Reviewed in Juanes and Piatti (2016); Tamborrini and Piatti (2019)). Release of Cdc14 initiates cytokinesis (Sanchez-Diaz et al. (2012)), and

so clearly a major contribution of the MEN to cytokinesis is through the liberation of Cdc14. However, there is evidence that MEN proteins play a role independently of Cdc14. An early indicator of this role was the discovery of a *CDC15* allele that is competent in MEN activation but fails to accomplish cytokinesis, leading to the formation of cell chains (Jiménez et al. (1998)). A similar phenotype is seen in *net1-1 GAL1-UPL-TEM1* cells which can release Cdc14 in the absence of MEN activity (Lippincott et al. (2001)). Dbf2 displays a clear bud neck localization in telophase, and this localization depends on other MEN proteins (Frenz et al. (2000)). This localization is functionally relevant, as Dbf2 phosphorylates proteins involved in cytokinesis such as the chitin synthase Chs2 (Oh et al. (2012)). Tamborrini et al. (2018) went further to show that localization of MEN proteins at the SPB is important for cytokinesis. Overexpression of the ubiquitin ligase *DMA2* prevents proper cytokinesis without impairing mitotic exit, again forming cell chains (Merlini et al. (2012)). Tamborrini et al. (2018) showed that Dma2 ubiquitinates Nud1 and suggest this impairs localization of MEN components at the SPB. They further show that the growth defect caused by overexpression of *DMA2* can be rescued by forced interaction of Cdc14 with Nud1. While the roles of Cdc14 at the budneck are well documented (Kuilman et al. (2015)), it is currently unclear exactly how MEN activity and Cdc14 at the SPB contribute to cytokinesis. However, it is established that localization of Dbf2 at the SPB is necessary for its activation before it performs its necessary function in the nucleus. It seems likely that the role of MEN proteins during cytokinesis requires prior activation at the SPB too.

Mitotic oscillators

Cdc14 has been observed engaging in cycles of release and re-sequestration (Lu and Cross (2010); Manzoni et al. (2010)). These oscillations are observed in cells expressing *CLB2dB*Δ, a non-degradable mitotic cyclin. These oscilla-

tions are thought to result from a Cdc5-Cdc14-Cdh1 feedback loop. Cdc14 is released through the usual MEN pathway which requires Cdc5 activity. Cdc14 activates Cdh1 by dephosphorylation of CDK sites. Cdh1 goes on to target Cdc5 for destruction, leading to MEN inactivation and Cdc14 re-sequestration. This hypothesis is backed up by mathematical modelling (Vinod et al. (2011)).

1.2.6 Conservation of SPB proteins and function

The SPB of *S. pombe*

The *Schizosaccharomyces pombe* SPB shares some characteristics with that of *S. cerevisiae*, performing much the same role as a MTOC (Reviewed in Cavanaugh and Jaspersen (2017)). There is a good degree of conservation, with the *S. pombe* SPB harbouring orthologs of Cmd1, Cnm67, Nud1, Spc110, Spc72 and Spc42. The *S. pombe* SPB also duplicates conservatively via a similar mechanism involving a half bridge with orthologs of Cdc31 and Sfi1 (Rüthnick and Schiebel (2016)). However, there are differences in the SPBs of the two yeasts. The *S. pombe* SPB does not have the clear tripartite structure that the *S. cerevisiae* SPB has, appearing in EM images as an amorphous ellipsoid (Cavanaugh and Jaspersen (2017)). Furthermore, the *S. pombe* SPB sits entirely on the cytoplasmic face of the NE until the onset of mitosis (Rüthnick and Schiebel (2016)).

The Septation Initiation Network

The Septation Initiation Network (SIN) is a pathway in *S. pombe* homologous to the MEN in *S. cerevisiae* (Reviewed in Bardin and Amon (2001); Simanis (2015)). As fission yeast have no SPoC, the SIN controls cytokinesis rather than mitotic exit. Failure of the SIN does not prevent re-entry into the next cycle so cells with an inactive SIN go through multiple cycles of chromosome duplication and nuclear division without cytokinesis, leading to elongated, multinucleate cells. Conversely,

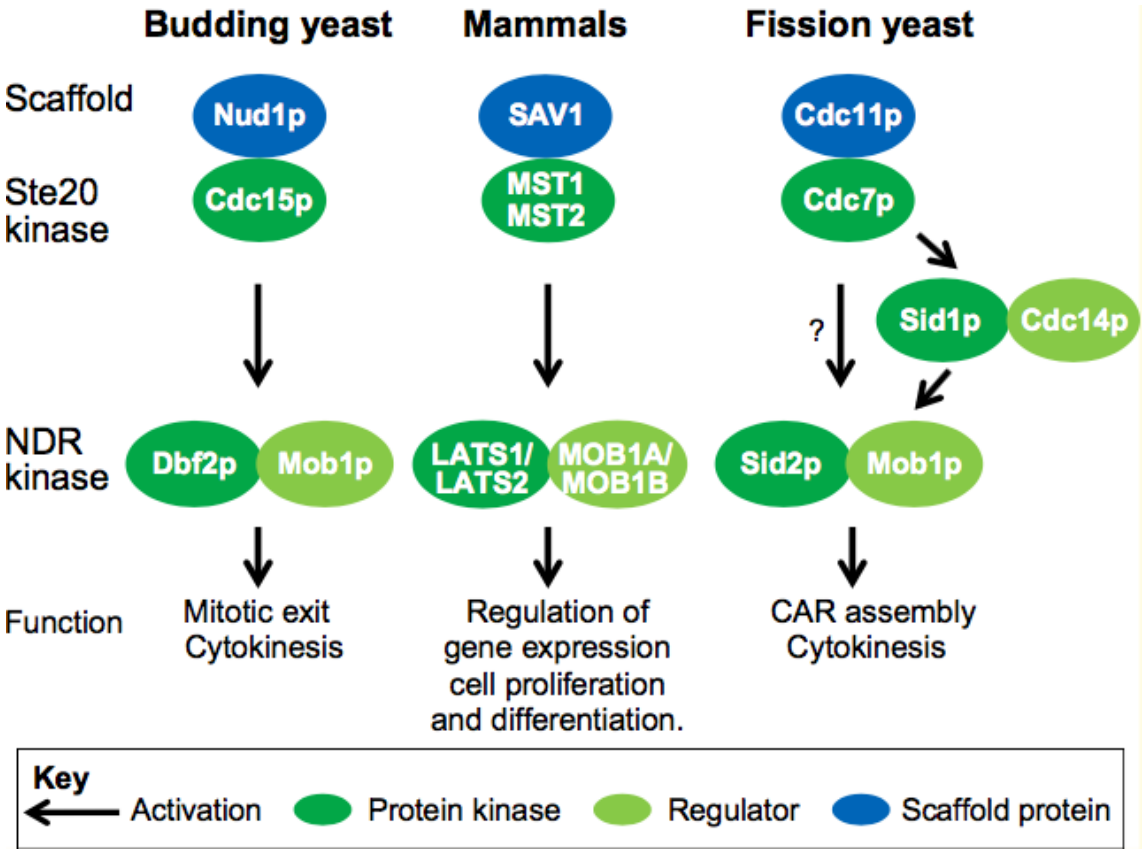

Figure 1.7: Summary of the organization and function of the MEN (budding yeast), Hippo (mammals) and SIN (Fission yeast) pathways. Reproduced from Simanis (2015)) with permission of The Journal of Cell Science.

an overactive SIN leads to the formation of multiple septa. The SIN pathway is highly similar to MEN, and comparative approaches have been fruitful. For example, it was through comparison with the *S. pombe* gene *byr4* that the *S. cerevisiae* gene *BFA1* (Byr-Four Alike) was discovered (Song et al. (1996); Li (1999)).

The close similarity between the pathways makes them an interesting study in how signalling networks are adapted through evolution to different purposes. The phosphatase clp1 (also known as flp1) is an ortholog of *S. cerevisiase* Cdc14, and similarly is retained in the nucleolus during interphase. Much like Cdc14, clp1 seems to engage in a positive feedback loop with the SIN, however its role appears to be limited to cytokinesis and it is not essential for viability (Cueille et al. (2001)). The SIN also localises to SPBs and, intriguingly, it does so in an asymmetric manner. However while in *S. cerevisiae* the asymmetric localization of proteins at the SPBs mirrors the asymmetric morphology of the cell, *S. pombe* cells are symmetric.

Mitotic entry and the SPB

While mitotic exit is not controlled from the SPB in *S. pombe*, mitotic entry is controlled there (Reviewed in Arquint et al. (2014)). Localization of *S. pombe* polo kinase, plo1, or CDK at the SPB is sufficient to drive mitotic entry (Grallert et al. (2012)) and mislocalizing cyclin mutants can prevent mitotic entry (Basu et al. (2020)).

Eukaryotic centrosomes

The MTOC of higher eukaryotes is the centrosome. Although morphologically distinct from the SPB, centrosomes share some features with SPBs. A number of SPB components are conserved in human centrosomes, including Cdc31, Cmd1, Sfi1, Spc72, Spc110 and Nud1 (Jaspersen and Winey (2004)). The γ-TuSC struc-

ture responsible for microtubule nucleation is also conserved in humans, although other eukaryotes also have a larger complex, the γ-TuRC (γ-Tubulin Ring Complex) (Fu et al. (2015)). Centrosomes also duplicate conservatively, although via a different mechanism to SPBs (Fu et al. (2015)). Age-dependent segregation of centrosomes has been observed in the developing mouse brain, where asymmetric divisions are coupled with centrosome fate (Wang et al. (2009)). Defects in centrosomal behaviour have also been linked to human disease, the human protein ASPM localizes to centrosomes, and mutations in this gene are strongly associated with microcephaly (Fu et al. (2015)). Cancer cells frequently display increased numbers of centrosomes, but whether this is a cause or consequence of cancer is unclear (Nigg (2006)). Recent research has shown that centrosome overduplication can drive tumorigenesis (Levine et al. (2017), reviewed in Bose and Dalal (2019)).

The Hippo pathway

The MEN is an example of a type of signalling pathway with deep evolutionary roots (Weiss (2012)). These pathways, known as Mst/*hippo* or Ndr/LATS systems are conserved throughout Eukaryota. The mammalian Hippo pathway is another example of this signalling structure and contains orthologs of many MEN proteins, including Cdc15, Mob1 and Dbf2. The Hippo pathway controls cell proliferation and is important to restrict growth in adult organisms; Hippo mutants often display uncontrolled organ growth (Meng et al. (2016)). Perhaps unsurprisingly, the Hippo pathway is often disregulated in cancer (Harvey et al. (2013)). Orthologs of Cdc14 exist in humans, and overexpression of these proteins leads to defects in mitosis, however they are not thought to be controlled by the Hippo pathway (Queralt and Uhlmann (2008b)). LATS1/2 and NDR1/2, mammalian homologs of Dbf2 and Cdc15, are found on centrosomes, with NDR1/2 thought to play a role in centrosome duplication (Hergovich et al. (2008)).

1.3 Systems approaches to cell biology and genetics

Systems biology encompasses any approach to understanding living organisms as complex, interconnected systems (or parts of such systems). As such, systems biology is primarily a response to a reductionist view of biology, positing that, for example, understanding genes or proteins in isolation is not sufficient to understand a cell. In a famous essay, Lazebnik argued that cell biology can be compared to fixing a radio (Lazebnik (2002)). The radio can be taken apart and each wire, transistor and button analyzed independently for its function, as biologists do. However, an engineer would reconstruct the wiring diagram of the radio, focussing on the connections, rather than the components.

Systems biology uses mathematical and computational concepts to build theoretical frameworks in which to study biology. These approaches can be broadly divided into the categories of top-down or bottom-up (Gunawardena (2014)). Top-down approaches embed large experimental datasets into a theoretical framework. An example of this is the budding yeast genome-wide genetic interaction network (Costanzo et al. (2016)). Alternatively, bottom-up approaches test our scientific understanding by formalizing a view of a particular process and testing whether the formal model fits our expectations. An example of this is a mathematical model of the cell cycle such as the Chen model (Chen et al. (2004)). Not all approaches can easily fit into these categories however, with some relying on inference from a dataset to build a model before testing its behaviour on unseen data. In fact, model development is often thought of as an iterative cycle with alternating stages of model fitting, testing and updating. In this section, I will give an overview of systems biology approaches to studying the yeast cell cycle.

1.3.1 High-throughput yeast screening

High-throughput screening is a discovery driven approach to genetics. In such a screen, a scientist attempts to identify genes involved in a process in an unbiased way, by systematically testing most of, or the entire, genome. There are 3 vital ingredients to a high-throughput screen:

1. A systematic collection of mutants, for example the yeast deletion collection (Winzeler et al. (1999)).

2. A perturbation to be applied to the collection. This may be an additional genetic perturbation, such as in a synthetic lethality screen (for example Goodson et al. (1996)) or could be an external condition such as high salt (Giaever et al. (2002)).

3. A phenotypic measurement, commonly a measurement of growth rate or fitness.

High-throughput screening is an important tool in systems biology as it can be used to identify, in an unbiased way, the constituent parts of a system. High-throughput screening methods were pioneered in yeast, mainly because of yeast's genetic tractability. Since the development of CRISPR-Cas9, which has simplified the genetic modification of mammalian cells, many of these ideas have been applied to study higher eukaryotes (Reviewed in Shalem et al. (2015)). Unbiased approaches like screening are particularly important in complex systems. For example, when the yeast sequencing project was completed, researchers were surprised to learn that the majority of predicted ORFs (Open Reading Frames) had not been identified by previous methods (Dujon (1996); Giaever and Nislow (2014)).

Genetic and Synthetic Physical Interactions

The study of single gene deletions has been remarkably fruitful. Since the yeast deletion collection was release in 1999 (Winzeler et al. (1999)), it has been used in over 1,000 genome wide screens (Giaever and Nislow (2014)) and has even been sent into space (Nislow et al. (2015)). However, more insight can be gained by testing pairwise combinations of loss-of-function mutants (often using temperature sensitive alleles of essential genes) (reviewed in (Baryshnikova et al. (2013)). These Genetic Interaction (GI) screens aim to identify combinations of genes which are more (or less) sick when lost together than either is individually. The most comprehensive of such studies is that of Costanzo et al. (2016), which tested the fitness of $\sim 23,000,000$ double mutants, identifying nearly a million genetic interactions. To achieve this required the development of robot-assisted protocols to perform the experiments and sophisticated statistical analysis to test for significance (Baryshnikova et al. (2010)). However, in its essence, this experiment resembles many other yeast high-throughput screens, using Synthetic Genetic Arrays (SGA) to cross libraries of loss-of-function mutants together and imaging colony size to estimate growth rate.

Since the first genetic interaction screens in yeast, the results have been organised as genetic interaction networks. However, genetic interactions can occasionally be misleading as an indication of shared function. A better measure of this relation is actually the correlation between the interaction profiles of two genes which can be used to construct a Genetic Interaction Similarity (GIS) network (Tong et al. (2004)). If we consider an array M, where $M_{i,j}$ gives the strength of the genetic interaction between gene i and gene j, then each row $M_{i,}$ is a vector showing the different genetic interactions of gene i. The correlation between these rows can then be used to define an appropriate level of similarity. For example, Costanzo et al. (2010) included edges between genes in their GIS network when the Pearson correlation coefficient between genes exceeded a threshold of

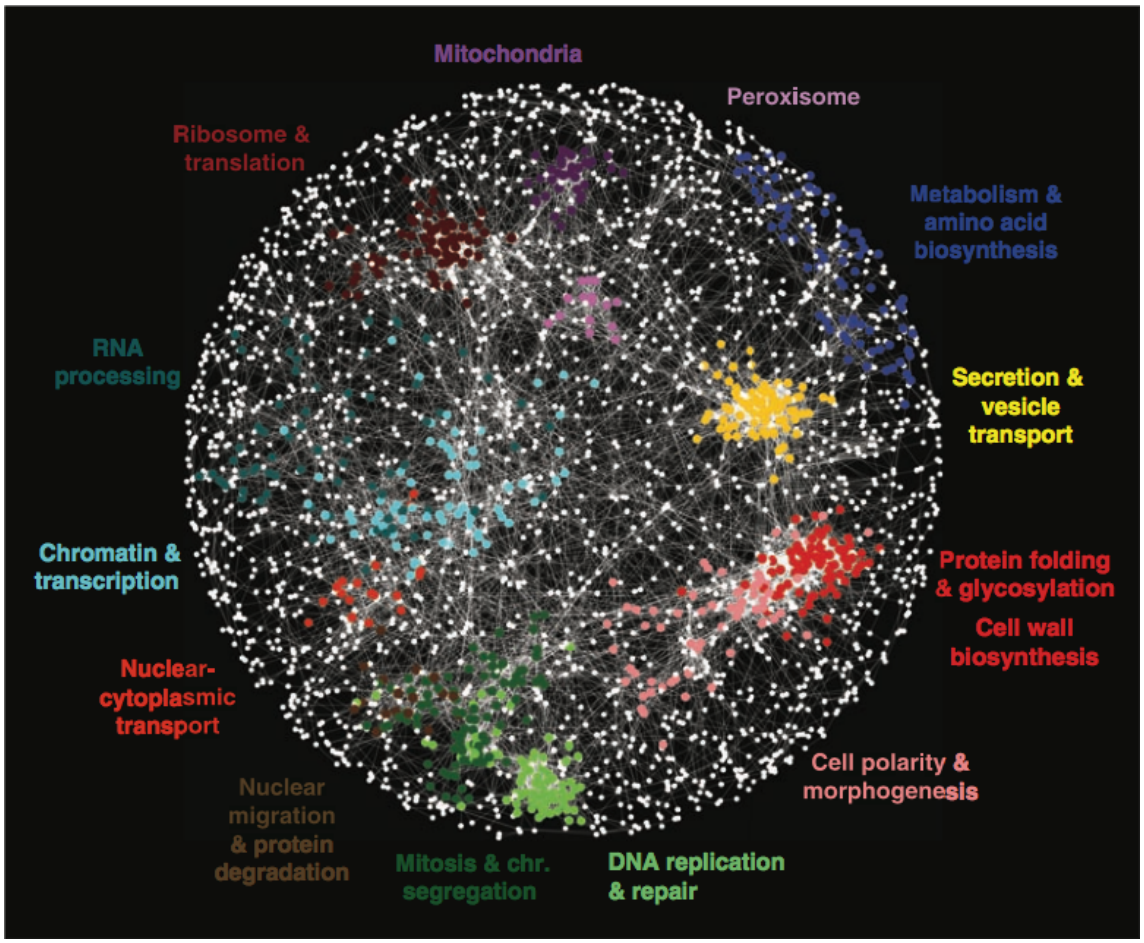

Figure 1.8: GIS network showing regions of the network associated with specific cellular functions. Reproduced from Costanzo et al. (2010). Reprinted with permission from AAAS.

0.2. In this representation, regions of the network can be associated with specific cellular functions (Costanzo et al. (2010)). These GIS networks have lead to a network-based approach to enrichment analysis, known as SAFE (Spatial Analysis of Functional Enrichment) (Baryshnikova (2016); Usaj et al. (2017)). Note that GIS networks do not necessarily overlap with physical interaction networks, although the hubs of these networks tend to overlap (Costanzo et al. (2010); Baryshnikova et al. (2013)).

Synthetic Physical Interaction (SPI) screens test the effect on fitness of pairwise protein fusions (Ólafsson and Thorpe (2015)). This is achieved by introducing a gene tagged with GFP-Binding Protein (GBP) (Rothbauer et al. (2007)) into a library of strains expressing genes tagged with GFP (Huh et al. (2003)). Tkach et al. (2012) identified a subset of the Huh et al. (2003) library consisting of GFP strains that had a discernible GFP signal, and it is the library of Tkach et al. (2012) that is often used for SPI screens. By introducing the GBP-tagged gene on a plasmid, a rapid high-throughput plasmid transfer protocol called Selective Ploidy Ablation (SPA) (Reid et al. (2011)) can be used, avoiding the need for the use of slower SGAs. The SPI methodology was originally developed to study regulation of the kinetochore (Ólafsson and Thorpe (2015, 2016)). Berry et al. (2016) have also used the method to study the effects of protein re-localization to different regions of the cell, although the SPB was not included in this study.

1.3.2 Mathematical modelling of cell biology and genetics

Mathematical models are a key component of systems biology, but why is this? Firstly, while our intuition is an important tool to understand biological systems, such systems can display counter-intuitive behaviour (Tyson (2007)). An example of this is seen in the behaviour of scaffolded signalling pathways. A scaffold can increase the rate of reaction between two interacting proteins, for example a kinase and substrate, and so our intuition states that more scaffold will increase

the rate of phosphorylation. This is true for concentrations of a scaffold up until a threshold, at which point increasing scaffold concentration will actually slow down the reaction. This is predicted by models of scaffolded reactions (Levchenko et al. (2000)) and has been verified experimentally (Whitaker et al. (2012)). Secondly, as Lazebnik argues, it may be that quantitative rather than qualitative details may be fundamentally the origin of disfunction (Lazebnik (2002)). If we wish to develop medical interventions to cancer, for example, we may need to understand how mutations affecting the quantitative behaviour of proteins feed into behaviour of the system. Finally, biological systems are complex, meaning that it is difficult for humans – but not computers – to keep track of all the moving parts (Brenner (1999)). The yeast genome contains 6,000 genes while humans are estimated to have at least 20,000 protein-coding genes (Salzberg (2018)). Understanding how each of these genes work together is certainly beyond any human mind and may well be beyond computer technology. However, computers can keep track of many more variables than a human can and are therefore an important tool in combating this complexity. A key aim of modern biology is to bridge the genotype-phenotype gap and computational models will be required to meet this aim.

A number of different modelling formalisms have been developed. I will describe and contrast two of the most commonly used formalisms before giving a brief overview of the wider field of methods.

Ordinary Differential Equations

Systems of Ordinary Differential Equations (ODEs) are the most widely used formalism. An ODE model is created from a set of chemical reactions, for example phosphorylation of a substrate, S, by a kinase, X:

$$\mathrm{X + S} \xrightarrow{\mathrm{k_1}} \mathrm{XS} \xrightarrow{\mathrm{k_2}} \mathrm{X + S_p}. \tag{1.1}$$

This can then be transformed into a set of ODEs using the law of mass action:

$$\begin{aligned} \frac{d[X]}{dt} &= -k_1[X][S] + k_2[XS] \\ \frac{d[S]}{dt} &= -k_1[X][S] \\ \frac{d[XS]}{dt} &= k_1[X][S] - k_2[XS] \\ \frac{d[S_p]}{dt} &= k_2[XS]. \end{aligned} \tag{1.2}$$

In these ODEs, we track the evolution of the concentration of each species over time. While mass action is a simple, linear assumption it requires the inclusion of intermediate states (here XS). In some cases the ODE system is simplified by using non-linear terms to approximate the effects of intermediates, for example:

$$\frac{d[S_p]}{dt} = k[S]\frac{[K]^h}{a^h + [K]^h}. \tag{1.3}$$

The advantage of this formulation is that systems of ODEs are well studied mathematically in the field of dynamical systems theory (see the textbook of Strogatz (2001)). Smaller systems of ODEs can be analyzed analytically, and desirable behaviours such as self-sustained oscillations or bistability identified. A toolbox of 'motifs', small ODE systems with well characterised properties, has been developed over time and often even large systems can be understood by breaking them down into their constituent motifs (Reviewed in Tyson et al. (2003); Tyson and Novák (2010)). Conversely, new systems can be designed by combining these motifs (for example Perez-Carrasco et al. (2018)). Furthermore, even large systems can be easily simulated computationally, and many tools exist to do this.

While ODEs are widely used in systems biology, they have limitations. Firstly, they are deterministic, while biological systems often display stochastic behaviour. This is a fundamental limitation of ODE models, however such systems can easily be translated into stochastic frameworks. A mass action ODE sys-

tem may be simulated with the Gillespie algorithm, which treats the system as a Markov jump process (reviewed in Warne et al. (2019)). Alternatively, for larger systems the chemical langevin equation may be used to generate Stochastic Differential Equations (SDEs) (Wilkinson (2009)). ODEs can be thought of as representing the evolution of the mean of a stochastic system. As many biological assays measure the bulk behaviour of cells, rather than single cells, a deterministic model can often accurately describe biological data. However, there are occasions when only a stochastic model will suffice. Furthermore, as ODEs measure concentrations, they assume a well-mixed chemical solution. This is often appropriate but in some cases, especially when copy numbers are low, this assumption can break down (Warne et al. (2019)). This is often a problem when modelling protein translation, as mRNA numbers are often much lower than protein numbers (Elowitz et al. (2002)). An additional limitation of ODE models comes from the explicit representation of all species. If we were to model formation of a complex of n components, there are 2^n possible intermediate sub-complexes which would all have to explicitly represented. This is a particular issue for models of large complexes or prions. Finally, ODE models require a large number of parameters and their behaviour can depend critically on these parameters. An ODE model requires a rate parameter for each chemical equation and an initial condition for each species. As these parameters often cannot be measured *in vivo*, they must be inferred, which can be impractical for large models. Tyson and Novák (2020) describe this as the 'curse of parameter space'. They point out that for a model with 100 parameters, testing 10 values for each parameter would require more simulations than there are atoms in the universe.

Logical Models

Logical models were first formulated in the 1960s and 1970s to describe gene regulatory mechanisms (Kauffman (1969); Thomas (1973)). At first the interest

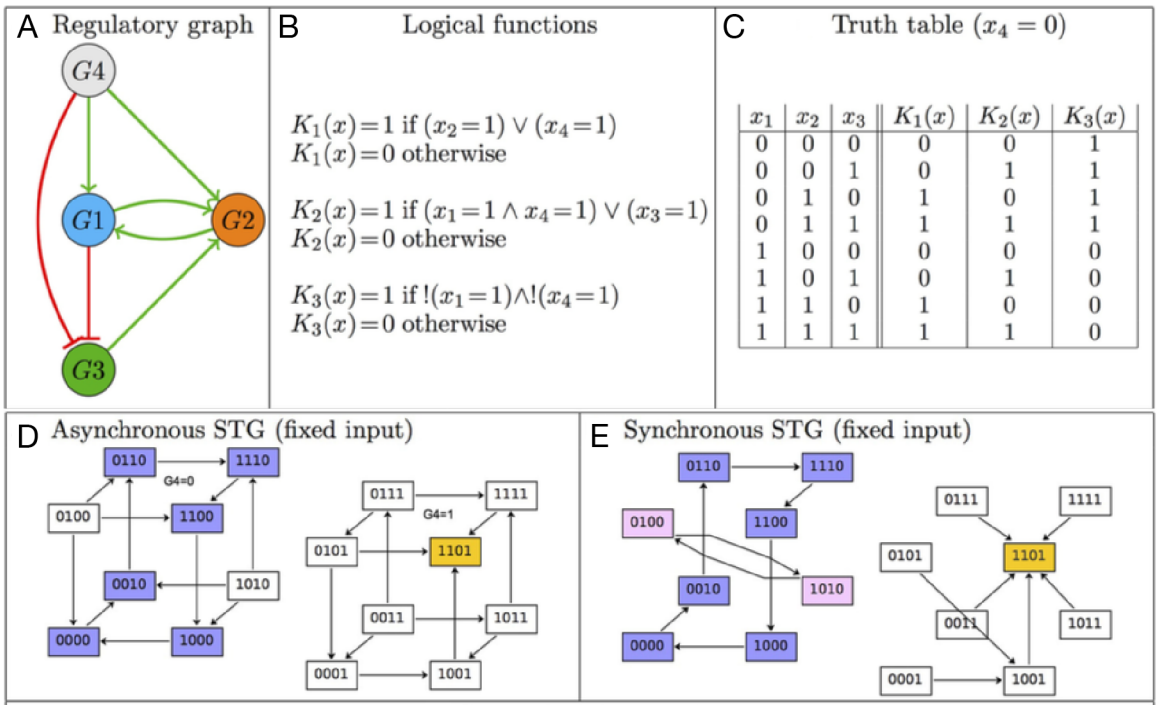

x_1	x_2	x_3	$K_1(x)$	$K_2(x)$	$K_3(x)$
0	0	0	0	0	1
0	0	1	0	1	1
0	1	0	1	0	1
0	1	1	1	1	1
1	0	0	0	0	0
1	0	1	0	1	0
1	1	0	1	0	0
1	1	1	1	1	0

Figure 1.9: Summary of a simple logical model. A: A 4-node logical model, with a single input (G4). B: The logical rules describing the regulation of each node. Note there is no rule for node 4 as it is an input to the model. C: The truth table of the model, when the input is switched off. D: The STG of the model under an asynchronous update scheme. Each node here represents a state of the model. The two isolated subgraphs correspond to the two possible values of the input node. Note how more than one edge leads out of some nodes, depending on which node is updated first. The steady state of the model is highlighted in yellow. E: The STG of the same model under a synchronous update scheme. Note how a single edge leads out of each node. Adapted from Abou-Jaoudé et al. (2016)).

was mainly in the properties of random networks, and their use in modelling specific systems is more recent (Bornholdt (2008)). A logical model can be thought of as a process on a network (Reviewed in Albert and Thakar (2014); Abou-Jaoudé et al. (2016); Barberis et al. (2017)). In this network, nodes are genes and regulatory mechanisms (either activation or repression) are represented by signed (positive or negative), directed edges between nodes (Figure 1.9A). Genes are considered to be in one of two states: either ON (1) or OFF (0). Then from a given state of the network, time is advanced in discrete steps, with the following state of the model depending on the currently active nodes. Nodes whose activators are active or inhibitors are inactive will become or remain active and vice versa. When a node has multiple in-edges, the model must specify a rule describing how the different kinds of regulation interact (Figure 1.9B). These rules are generally described in terms of formal logic (for example $A =!B\&C$), which is the root of the name. These rules can also be understood through a truth table, which enumerates the outcome of each rule under each of the possible states of each node (Figure 1.9C). Generalized logical models allow nodes to take any discrete number of states, while models as described above, in which nodes take only 2 states, are called Boolean models. Logical models can also be used to model signalling networks which function through post-translational modification, rather than transcriptional regulation. In these models, the nodes are proteins and their activity represents the state of the majority of molecules in the cell.

As there are only a finite number of states of a logical model, and the sequence of states is specified deterministically then, by the pigeon-hole principle, the sequence must eventually either fall into a steady state or a cycle. These are called the attractors of the model. There must be at least one attractor of the model but there may be many more, with the choice of initial state determining which attractor is reached. The behaviour of the model can be summarised in a State-Transition Graph (STG, Figure 1.9D&E). The STG is a network where the

states of the model are the nodes with arrows showing the transitions. Attractors are represented in the STG as the regions of the graph which, once entered, can never be left. Mathematically speaking, these are known as the strongly-connected components of the graph – regions in which for every node, there is a permissible path to every other node. Identification of attractors is a difficult problem and two different approaches currently exist. Exhaustive approaches based around construction or sampling of the STG are common (Garg et al. (2008)), and refinements such as the introduction of Hierarchical Transition Graphs have been suggested (Bérenguier et al. (2013)). An alternative approach to attractor identification relies on the computational theory of model checking (Abou-Jaoudé et al. (2016)).

Update Schemes In the process described above, all the nodes are updated at every time point simultaneously. This is known as the synchronous update scheme. While such an update scheme is very simple to describe and simulate it is also unrealistic. This is because in any set of biochemical reactions, some threshold will be overcome first. Asynchronous update schemes, in which nodes are updated individually, are therefore more realistic. Deterministic asynchronous update schemes, in which nodes are updated in a pre-specified order exist, however stochastic asynchronous update schemes are more common. These schemes may be uniformly random, with the next node to update being chosen uniformly at random or sometimes include priority classes of nodes which are more likely to be picked. While steady states identified under the synchronous update scheme are still steady under the synchronous scheme, cycles may behave differently when using an asynchronous scheme. In fact, cycles which rely on more than one node changing at each step are frequently lost when moving from a synchronous to asynchronous update scheme. An STG can also be constructed for a model using an asynchronous update scheme, however multiple

edges may emanate from each node, as the sequence of states is no longer deterministic (Figure 1.9D). Due to the complexities of analysing the STG, a Monte-Carlo or simulation based approach is common to analyse the behaviour of asynchronous networks.

In addition to the synchronous and asynchronous update schemes, a continuous time variant was developed by Stoll et al. (2012). In this framework, each node is updated at random intervals, whose frequency is determined by a rate parameter. Therefore, the order in which the nodes are updated is random, as with an asynchronous model. But in contrast with a traditional asynchronous update scheme, the timing of these transitions can be determined, meaning that conclusions relating to timing can be drawn from the logical model.

The continuous time update scheme is the closest representation of the biochemical processes, as it can produce time-resolved trajectories. However, it requires the specification of numerical rates, leading to the issues of parameter-fitting that occur with ODE models. This is a serious drawback although it is worth noting that some features of the logical model, such as the steady states will not depend on these parameters, unlike an ODE model. The asynchronous update scheme is the next most-realistic scheme and can represent the trajectories leading to a steady state. The synchronous scheme is not very realistic however it is useful to find steady states, which are independent of update scheme.

Representing complexes The formation of protein complexes is an important aspect of post-translational modification and so it is important to consider how they are represented in logical models. There are two approaches, which are illustrated in Figure 1.10 for a bipartite complex formed between proteins A and B which regulate a third protein C. The “explicit" representation includes a node representing the complex itself (“A-B"). The “implicit” representation does not have this node but instead uses the rule for the C node to express the requirement

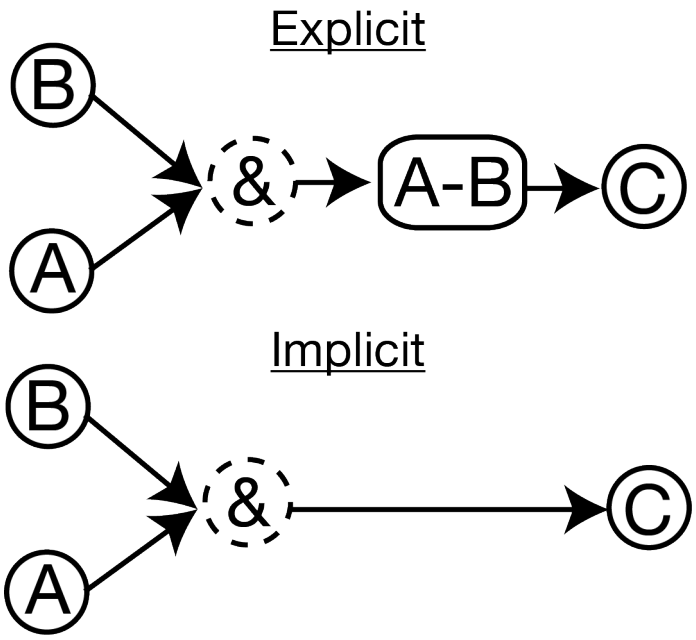

Figure 1.10: Explicit and implicit representations of complexes in logical models. The explicit representation uses a separate node “A-B” to represent the presence of the complex made up of protein A and B. In the implicit representation, this behaviour is subsumed into the rule for the downstream target, C.

for the complex. Both of these approaches are established in the literature, for example Münzner et al. (2019) use the explicit representation while Chasapi et al. (2015) use the implicit representation. While the explicit representation is a more complete representation of biological knowledge, it creates additional nodes and has the potential to contribute to the problem of combinatorial explosion. For this reason, I use the implicit representation in my model.

Stochastic logical models There are a number of modifications to logical models that can be made to introduce stochasticity. The first and most basic is just the randomisation of initial conditions. Asynchronous random update schemes are a more profound way to introduce stochasticity into the network. While this can change the dynamics of the network relative to a synchronous scheme, the behaviour of the network still depends deterministically on the update rules. More drastic changes to the logical modelling framework have been suggested. In one

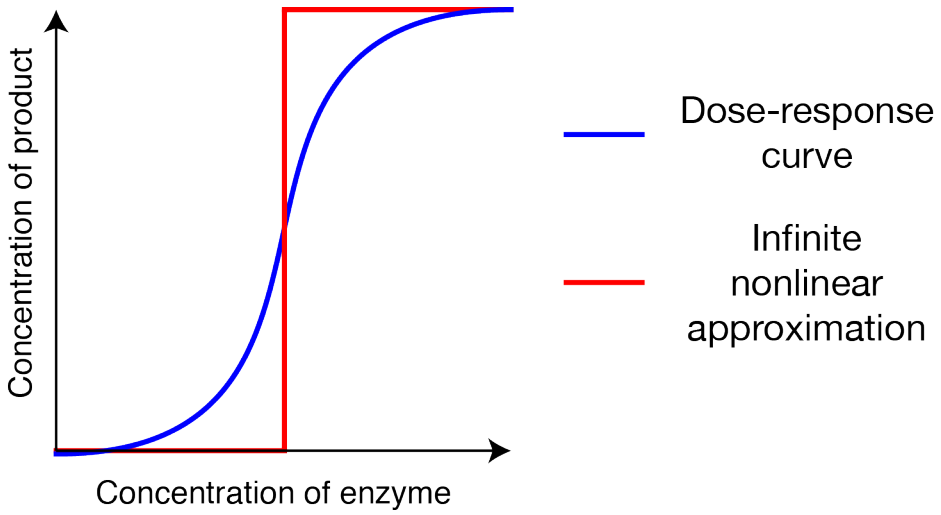

Figure 1.11: The 'infinite nonlinear approximation' of a dose response curve.

approach, at each update stage there is a small chance for each node to be flipped at random (Qu et al. (2002)). In another approach, a continuous variable is assigned to each node that varies according to an ODE, while the behaviour of the node with respect to the rest of the network is still limited to discrete values (Bornholdt (2008)). Noise can be introduced to the system by addition of a noise term to each of the ODEs. Probabilistic Boolean networks include multiple update rules for each node, with a specific rule chosen randomly at each update step according to pre-defined probabilities (Shmulevich et al. (2002)).

Logical vs ODE models The logical modelling formalism offers some advantages relative to ODEs. They are very quick and computationally efficient to simulate, even when simulated stochastically, which is notoriously slow for large ODE systems. Logical models generally have no parameters, instead the dynamics are determined by the structure of the network and the update rules. This means they can be used to investigate the structure of a signalling network directly, without parameter fitting. Barberis et al. (2017) argue that the lack of fitted parameters makes logical models falsifiable as they succeed or fail on the back of the network structure rather than any specific parameterization. While the assumption

that each biochemical species' activity is limited to one of a small number of discrete states may seem unreasonable, it is actually remarkably similar to the way that biochemists tend to think about such systems. A typical dose-response curve is sigmoidal, and can described well by a Hill function, as seen in Equation 1.3. The logical formalism makes an 'infinite nonlinear approximation', that the Hill coefficient here is infinite, flattening the curve into a rigid 'elbow' shape (Figure 1.11,Glass and Kauffman (1973); Bornholdt (2008)).

Fisher and Henzinger (2007) distinguish between mathematical and computational models, identifying ODEs systems as mathematical and logical models as computational. They make this distinction on the basis of executability: computational models are essentially instructions on how to simulate a system while mathematical models are descriptions of the rules governing such systems. Rather than viewing ODE systems and logical models as competing viewpoints, they can be seen instead as complementary approaches. Logical models are fundamentally qualitative rather than quantitative, and therefore generally they can make only qualitative predictions. However, they are an honest representation of a system for which we know few numerical parameters and can easily scale to represent very large systems. Systems of ODEs are accurate models of molecular kinetics and are vital to dissect the dynamic properties of small systems.

Logical modelling tools As the logical modelling community has grown, a number of tools for the creation, analysis and simulation of logical models have been created. Many of these are curated by the Consortium for Logical Models and Tools (colomoto.org). Packages for logical model analysis can be found for R (BoolNet, Müssel et al. (2010)) and Python (PyBoolNet, Klarner et al. (2017)), and a dedicated GUI for such tasks is provided by GINsim (Naldi et al. (2009)). CellNOptR is a package that can be used to train logical models against experimental data (Terfve et al. (2012)). MaBoSS is a set of software that can be used

for continuous time simulation of logical models, and also has a python package (Stoll et al. (2012, 2017)). The Odefy toolbox provides tools for automatic generation of ODE models from logical models (Krumsiek et al. (2010)). Transfer of logical models between different environments is facilitated by a standardised file format, the SBML-qual format (Chaouiya et al. (2013)).

Spatial models

Both logical and ODE models are based around an assumption that all proteins in the cell are well-mixed, so that their concentration is uniform throughout the cell. However, eukaryotic cells have a number of chambers separated by lipid membranes (for example, the nucleus) and many proteins are distributed non-uniformly throughout the cell. When modelling a system where the spatial distribution of components throughout different compartments is important, the standard modelling tool is compartmental ODEs. In this framework, a separate variable is used to represent the concentration of each species in each compartment. A logical equivalent of such a modified system has not yet been developed.

The compartmental framework still assumes spatial homogeneity within the compartment, in cases where this assumption does not hold other spatially-resolved frameworks must be used. Partial Differential Equations (PDEs) are a standard tool in applied mathematics to study systems with spatial heterogeneity. PDEs have been used to study protein-activity gradients (Kholodenko (2006)), and are commonly used to study pattern formation at the multicellular level. A logical modelling approach has been used to study similar systems, using the Epilog tool (Varela et al. (2018)). In this framework, a set of hexagons represents a sheet of epithelial cells with the state of each cell controlled by a logical model. Neighbouring cells can communicate their state, which acts as an input to the logical model. This approach is related to earlier discrete models of biological patterning, including cellular autonoma such as Conway's game of life (Gardner (1970)). If

protein copy numbers are low, then agent-based models where the state and location of each individual molecule is tracked may be appropriate. However, such models will become computationally intractable when tracking large numbers of molecules.

Further modelling formalisms

Apart from the formalisms discussed above, a number of other modelling frameworks have been developed. When studying metabolism, the standard modelling framework is the constraint-based Flux Balance Analysis (FBA). Some attempts to bridge the gap between metabolic and regulatory models have made, for example Barberis et al. (2017) propose a hybrid logical-FBA model to investigate interactions between the cell cycle and metabolism. A number of other hybrid modelling frameworks have been developed, including ODE systems with some deterministic and some stochastic variables (for example Ahmadian et al. (2020)), and ODE systems where some variables are limited to discrete states as in a logical model (for example Singhania et al. (2011)). Petri nets are an alternative network based, discrete modelling framework (for example Mura and Csikasz-Nagy (2008)). The above formalisms all suffer from the problem of combinatorial explosion, resulting from explicit representation of all intermediates. These issues can be resolved with agent- or rule-based approaches (for example Ibrahim et al. (2013)).

1.3.3 Models of the cell cycle

Having discussed the major modelling approaches used in cell biology and genetics, I will now provide an overview of their application to the yeast cell cycle. I will deal separately with two different types of model: whole cell cycle models and models of mitotic exit.

Comprehensive cell cycle models

The first comprehensive model of the yeast cell cycle was an ODE model, known as the Chen model (Chen et al. (2000, 2004)). This model was groundbreaking as not only one of the largest ODE models at the time but also the first to describe a quantitative model of eukaryotic cell cycle control. This model established a paradigm for cell cycle modelling and many subsequent whole cell cycle models can be seen as "descended" from this model. The original model has been updated and expanded a number of times, notably in Kraikivski et al. (2015). Stochastic implementations of the model have been used to establish the robustness of the cell cycle (Barik et al. (2010)) and to predict the penetrance of given phenotypes (Barik et al. (2016)). The model has also been expanded to study the control of cell size both deterministically (Heldt et al. (2018)) and stochastically (Ahmadian et al. (2020)). Additionally, the model has been used as the basis to explore new modelling strategies, such as standard component modelling (Laomettachit et al. (2016)) and hybrid SDE-ODE systems (Ahmadian et al. (2020)), as well as to test out new parameter fitting strategies (Chen et al. (2017)). The model has also been converted into a generic model of eukaroytic cell cycle control (Csikasz-Nagy et al. (2006)). These models have been highly successful at explaining the yeast cell cycle and can reproduce many genetic phenotypes, as well as playing a key role in developing the cell cycle as a testing ground for methods in systems biology. However, their treatment of mitotic exit has generally been coarse-grained. Models such as that of Kraikivski et al. (2015) contain a MEN module, representing Tem1, Cdc15, Cdc5, Lte1 and Bub2-Bfa1, alongside Cdc14, Net1 and other cell cycle regulators. However, they do not include extended MEN proteins and, crucially, do not represent protein localization.

Comprehensive logical models of the yeast cell cycle have also been developed. The first of these was the model of Li et al. (2004). This model consisted of just the main regulatory connection between 11 key cell cycle regulators

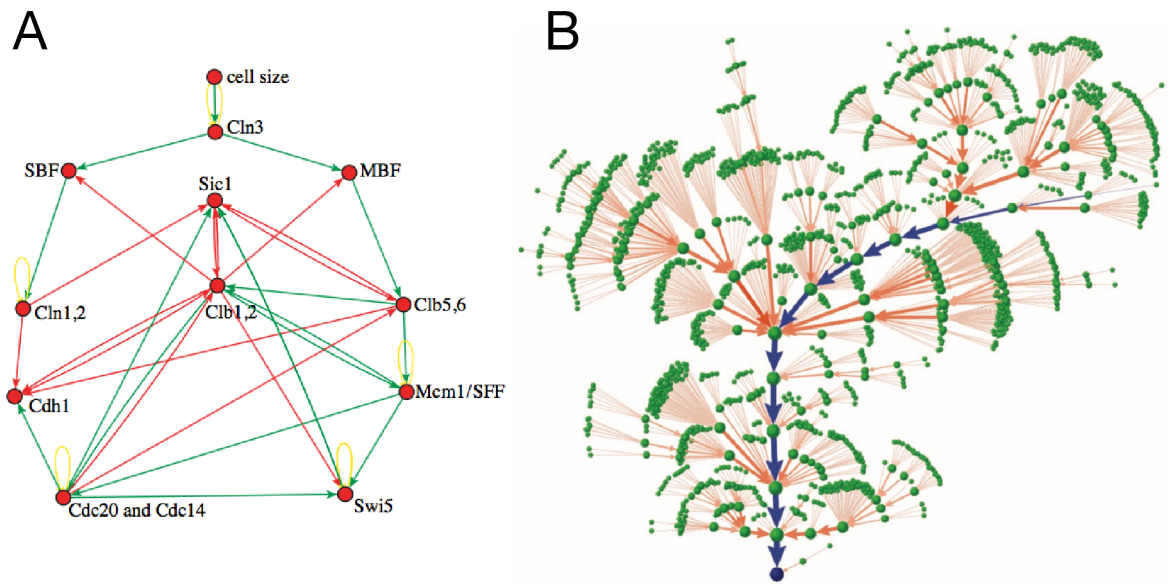

Figure 1.12: The Li et al. (2004) logical model of the cell cycle. A: Structure of the network, adapted from Bornholdt (2008). B: The STG of the model, showing how many different states converge onto the G1 state of the model, adapted from Li et al. (2004).

and a node representing cell size. However it recapitulated the key features of the cycle and the authors were able to show that the attractor representing normal cycle function was remarkably robust to randomization of initial condition, although other attractors also exist. The model has since been developed, including stochastic implementations (for example Zhang et al. (2006)). More detailed models were created by Irons (2009) and Fauré et al. (2009), both of which include a rudimentary treatment of mitotic exit control. A probabilistic Boolean network approach was taken by Todd and Helikar (2012), who used the cell cycle as a system to establish the power of this approach. Despite modelling the entire cycle, all of these networks are reasonably small, with fewer than 30 nodes (Barberis et al. (2017)). The model of Rubinstein et al. (2013) is significantly larger, with 67 nodes representing proteins, RNA species and cellular events, with some taking values in the range $\{0, 1, \ldots 9\}$. There is a divergence of approach within logical modelling, with some researchers seeking minimal models which refine the essence of the system (for example Li et al. (2004)) and others

favouring extensive models that aim to represent all the players in the system (for example Rubinstein et al. (2013)). Linke et al. (2017) took the former approach, building a minimal oscillator from 4 cyclins and testing which network architectures could fit experimental observations. In contrast, Münzner et al. (2019) take the opposing approach, building a comprehensive model of cell cycle regulation consisting of 357 components, including proteins, genes, RNAs and explicit representation of complexes. The model of Münzner et al. (2019) is an incredible feat of knowledge aggregation and significant attention is devoted to control of SPB duplication and separation, and the role of the MEN in Cdc14 control and cytokinesis. In this model, complex formation is represented explicitly, for example a "Dbf2Mob1Nud1" node represents binding of Mob1-Dbf2 at the SPB. However, not all localizations are represented, for example Bub2-Bfa1 localization at the SPB.

These comprehensive cell cycle models are the first steps towards executable genome-scale models of the cell. While their scale is impressive it undoubtedly leads to simplification of individual pathways. As a result, even the most detailed of these models does not represent the mitotic exit pathways to a high degree of precision. Next, I will discuss models created to investigate mitotic exit specifically.

Mitotic exit models

The first model built to investigate mitotic exit specifically is that of Queralt et al. (2006). In this paper, the authors show that downregulation of PP2A-Cdc55 is the key switch responsible for FEAR and build a simple ODE model to back this proposal up. The theoretical properties of the model were investigated further in a follow up paper, which revealed that the mitotic exit transition was underpinned by two positive feedback loops (Tóth et al. (2007)). The first is a positive feedback loop between Cdc14 and Cdc15 and the second a double negative feedback loop

between CDK and APC-Cdh1. This model, known as the Queralt model, has been subsequently expanded on. Firstly, Vinod et al. (2011) expanded the model to include more detail on cyclin regulation and Net1 phosphorylation. Importantly, they were able to recapitulate the cycles of Cdc14 release and sequestration observed by Lu and Cross (2010) and Manzoni et al. (2010). Then Hancioglu and Tyson (2012) developed the Queralt model along similar lines, focussing on examining the role of Cdc5 in mitotic exit. They concluded that Cdc5 has multiple roles but can phosphorylate Net1 alone, leading to Cdc14 disassociation. All of these models are focussed on the execution of mitotic exit and resetting of the cell to its G1 state, as opposed to the signalling of the decision to exit from mitosis. As a result, they generally do not represent the MEN pathway in much more detail than the comprehensive cell cycle models. None of these models represent the spatial organization of the MEN at the SPBs. In contrast, a compartmental ODE model of the SPoC was created by Caydasi et al. (2012). This model represents the regulation of Bub2-Bfa1 and Tem1 and their interdependent localization in high detail, and match the model to *in vivo* measurements of localization. However, its focus is limited to a small number of proteins and does not represent the entire network.

SIN models While there are differences between the mechanisms of mitotic exit control in *S. cerevisiae* and *S. pombe*, there are significant similarities between the SIN and MEN. In particular both are regulated through localization at the SPB. Therefore, I will discuss the existing models of SIN regulation.

Csikasz-Nagy et al. (2007) created a minimal model of the SIN, splitting the system between variables representing the “top” and “bottom” of the network, and embedding this model within a larger model of the *S. pombe* cell cycle. This was sufficient to represent to represent wild type and mutant behaviours, such as deposition of multiple septa in *cdc16*^{ts} cells. However, this model did not

take account of spatial organization of the SIN. Bajpai et al. (2013) expand on the Csikász-Nagy model and represent the localization of SIN components at the SPB. The SIN localizes asymmetrically at the SPBs, despite minimal morphological differences between them. Bajpai et al. (2013) establish the minimal requirements for such a system to function, and apply these to the SIN model. Intriguingly, they found that a full representation of the phosphostate of cdc11 (Nud1 ortholog) is required. This model is capable of representing the behaviour of many mutants, including double and triple mutant combinations, as well as other experimental perturbations such as laser ablation of SPBs. Both of these models use a crude representation of the SIN, differentiating simply between the top and bottom of the network. In contrast, Chasapi et al. (2015) built a comprehensive logical model of the SIN, explicitly representing all of the key regulators of septation. While they do not represent localization explicitly, they do so implicitly with scaffold proteins required for activation of some proteins, for example cdc11 (Nud1 ortholog) activates spg1 (Tem1 ortholog). They use multiple nodes to represent different levels of CDK activity (interphase, early and late mitosis). Their model has 2 steady states in late mitosis, lining up closely with the asymmetric pattern of protein localization at the SPB. This model is capable of making testable predictions, for example the model suggests that septation can be initiated from the cytoplasm when cdc7 (Cdc15 ortholog) is overexpressed.

1.4 Project Aims

The aims of the project are to address the following questions:

1. Which proteins are regulated through interactions with the SPB?

2. How is localization at the SPB used as an aspect of protein regulation?

3. Why does the cell use localization at the SPB to regulate proteins?

I have addressed Question 1 by performing SPI screens with the SPB, this is presented in Chapter 3. I have addressed Question 2 primarily by studying the role of SPB localization in control of mitotic exit. I present a compartmental, logical model of mitotic exit in Chapter 4. Question 3 is addressed through various findings from both the SPI screens and the modelling work in both Chapter 3 and 4. Altogether, this project gives a systems-level view of the SPB and how localization there is used to regulate cell cycle events.

Chapter 2

Methods

2.1 Introduction

This chapter is included to specify the details of methods used in this project. It is written as a guide for an expert in the respective fields to use to reproduce the work in the project and takes the form of protocols and technical descriptions.

2.2 Yeast & Bacterial Methods

All plasmids are shown in Table 2.1. All GFP strains originate from the GFP library (Huh et al. (2003), Tkach et al. (2012)). GFP strains with a *kar9*Δ genotype were constructed by transformation of strains from this library. All other yeast strains are shown in Table 2.2.

2.2.1 Yeast strains

Table 2.1: Plamids used in this study.

Plasmid	Genotype	Type	Selection	Source
pHT4	*CUP1p-GBP-RFP*	CEN	*LEU/AMP*	G. Olafsson (Ólafsson and Thorpe (2015))
pHT11	*CUP1p-SPC42-GBP-RFP*	CEN	*LEU/AMP*	This study
pHT99	*(empty plasmid)*	CEN	*NAT/AMP*	P. Thorpe
pHT222	*CUP1p-SPC42-RFP*	CEN	*LEU/AMP*	Gift from E. Herrero
pHT297	*CUP1p-SPC42*	CEN	*LEU/AMP*	This study
pHT575	*CUP1p-SPC110-GBP-RFP*	CEN	*LEU/AMP*	This study
pHT576	*CUP1p-GBP-RFP-SPC110*	CEN	*LEU/AMP*	This study
pHT577	*CUP1p-SPC110*	CEN	*LEU/AMP*	This study
pHT584	*CUP1p-NUD1-GBP-RFP*	CEN	*LEU/AMP*	This study
pHT585	*CUP1p-NUD1*	CEN	*LEU/AMP*	This study
pHT615	*CUP1p-SPC72*	CEN	*LEU/AMP*	This study
pHT616	*CUP1p-SPC72-GBP-RFP*	CEN	*LEU/AMP*	This study
pHT651	*GALSp-NUD1-GBP-RFP*	CEN	*LEU/AMP*	This study

Continued on next page

Table 2.1 – continued from previous page

Plasmid	Genotype	Type	Selection	Source
pHT667	*CUP1p-nud1-2-GBP-RFP*	CEN	*LEU/AMP*	This study
pHT706	*CUP1-HTB2-AZURITE*	CEN	*NAT/AMP*	This study
pHT708	*CUP1-AZURITE*	CEN	*NAT/AMP*	This study
pHT790	*MET3p-GBP-RGP*	CEN	*LEU/MET /AMP*	C. Klemm
pHT795	*MET3p-CLB2-CDC28-GBP-RFP*	CEN	*LEU/MET /AMP*	C. Klemm
pX29	*(empty plasmid)*	CEN	*LEU/AMP*	Gift from R. Rothstein (Reid et al. (2011))
pX75	*HIS3p:mRuby2-Tub1+3'UTR::URA3*	Integrating	*AMP*	Gift from W. Lee (Markus et al. (2015))
pX76	*HIS3p:mTurquoise2-Tub1+3'UTR::URA3*	Integrating	*AMP*	Gift from W. Lee (Markus et al. (2015))

Continued on next page

Table 2.1 – continued from previous page

Plasmid	Genotype	Type	Selection	Source
pX78	*CDC5*	2μm	*LEU/AMP*	Gift from G. Pereira (Caydasi et al. (2017))
pX79	*MOB1*	2μm	*LEU/AMP*	Gift from G. Pereira (Caydasi et al. (2017))
pX80	*MOB1*	CEN	*URA/AMP*	Gift from G. Pereira (Caydasi et al. (2017))

Table 2.2: Strains used in this study.

Strain	Genotype	Background	Source
E224	*MATα trp1-1 his3-11,15 leu2-3,112 ura3-1 RAD5 MET17 ADE2 LYS CEN1-16::Gal-Kl-URA3*	W303	Gift from R. Rothstein Reid et al. (2011)
Continued on next page			

Table 2.2 – continued from previous page

Strain	Genotype	Background	Source
E438	*MAT***a** *his3Δ1 leu2Δ0 met15Δ0 ura3Δ0*	S288c	Brachmann et al. (1998)
T622	*MAT***a** *his3Δ1 leu2Δ0 met15Δ0 ura3Δ0 TEM1-GFP::HIS3*	S288c	This study
T687	*MAT***a** *his3Δ1 leu2Δ0 met15Δ0 BBP1-YFP::KAN ura3Δ0::mTurq2-TUB1 URA3*	S288c	This study
T688	*MAT***a** *his3Δ1 leu2Δ0 met15Δ0 NUP133-YFP::KAN ura3Δ0::mTurq2-TUB1 URA3*	S288c	This study
T689	*MAT***a** *his3Δ1 leu2Δ0 met15Δ0 NUP170-YFP::KAN ura3Δ0::mTurq2-TUB1 URA3*	S288c	This study
T690	*MAT***a** *his3Δ1 leu2Δ0 met15Δ0YJL021C-YFP::KAN ura3Δ0::mTurq2-TUB1 URA3*	S288c	This study
T724	*MAT***a** *his3Δ1 leu2Δ0 met15Δ0 ura3Δ0 CDC15-YFP:: KAN*	S288c	This study
T725	*MAT***a** *his3Δ1 leu2Δ0 met15Δ0 ura3Δ0 TEM1-YFP::KAN*	S288c	This study
T731	*MAT***a** *his3Δ1 leu2Δ0 met15Δ0 ura3Δ0 CDC28-GFP::HIS swe1Δ::KAN*	S288c	This study

Continued on next page

Table 2.2 – continued from previous page

Strain	Genotype	Background	Source
T744	*MAT***a** *his3Δ1 leu2Δ0 met15Δ0 CDC14-CFP::shHPH HIS3p-mRuby2-TUB1+3'UTR::URA3*	S288c	This study
T747	*MAT***a** *his3Δ1 leu2Δ0 met15Δ0 CDC14-CFP::shHPH HIS3p-mRuby2-TUB1+3'UTR::URA3 spo12Δ::KAN*	S288c	This study
T753	*MAT***a** *his3Δ1 leu2Δ0 met15Δ0 ura3Δ0 NUD1-GFP::HIS3 bfa1Δ::KAN*	S288c	This study
CKY329-3	*MAT***a** *ura3-52 leu2Δ1 his3Δ200 trp1Δ63 mob1Δ::klTRP1*	S288c	Gift from G. Pereira Caydasi et al. (2017)
W8224-16C	*MAT*α *ADE2 leu2-3,112 ura3-1 trp1-1 LYS2 SPC110-CFP::KAN RAD5*	S288c	Gift from R. Rothstein
PT327	*MAT***a***/MAT*α *his3Δ1/his3Δ1 leu2Δ0/leu2Δ0 met15Δ0/MET15 ura3Δ0/ura3Δ0 LYS2/lys2Δ0*	S288c	This study

Continued on next page

Table 2.2 – continued from previous page

Strain	Genotype	Background	Source
PT328	*MAT***a***/MAT*α *his3*Δ*1/his3*Δ*1 leu2*Δ*0/leu2*Δ*0 met15*Δ*0/MET15 ura3*Δ*0/ura3*Δ*0 LYS2/lys2*Δ*0 CDC28-GFP::HIS3/CDC28*	S288c	This study

2.2.2 Yeast growth

Yeast were cultured in either liquid media or on solid agarose plates. Liquid media was shaken at 300rpm. Cultures were incubated at either 23℃, 30℃ or 37℃.

Yeast Media

Solid media differs from liquid media by addition of 2% w/v agarose. All media contains 2% w/v sugar – either glucose, galactose or raffinose. In addition to sugar, media is an aqeuous solution containing the following ingredients.

- **YP** 1% w/v yeast extract, 2% w/v peptone.
- **Synthetic Complete** 109μM adenine sulfate, 95μM L-arginine sulfate, 95μM L-histidine HCl, 229μM L-isoleucine, 457μM L-leucine, 164μM L-lysine HCl, 134μM L-methionine, 303μM L-phenylalanine, 98μM L-typtophan, 166μM L-tyrosine, 178μM uracil, 1290μM L-valine, 0.67$\%$ w/v yeast nitrogen base without amino acids (BD, USA).
- **Synthetic Complete without ammonium sulfate** 109μM adenine sulfate, 95μM L-arginine sulfate, 95μM L-histidine HCl, 229μM L-isoleucine,

457μM L-leucine, 164μML-lysine HCl, 134μML-methionine, 303μM L-phenylalanine, 98μM L-typtophan, 166μM L-tyrosine, 178μM uracil, 1290μM L-valine, 0.17$\%$ yeast nitrogen base w/v (without amino acids and ammonium sulfate) (BD, USA), 0.1$\%$ w/v monosodium glutamate.

- **Drop-out synthetic media** As synthetic complete, but without a specific amino acid (or combination). For example, -leu media lacks leucine.

Drugs

The following drugs are added to media to select or counter-select specific genotypes:

- **Hygromycin B** Used at 200μg/ml concentration, stock 50mg/ml in PBS (Roche, Switzerland). Selects for the *shHPH* gene. Cannot be used in media containing ammonium sulfate.

- **G418** Used at 300μg/ml concentration. Stock 60mg/ml in H_20, made from powder (ChemCruz, USA). Selects for the *KAN* gene. Cannot be used in media containing ammonium sulfate.

- **Nourseothricin** Used at 100μg/ml concentration, stock 200mg/ml in H_20, made from powder (Werner BioAgents, Germany). Selects for the *NAT* gene. Cannot be used in media containing ammonium sulfate.

- **5FOA (5-FluoroOrotic Acid)** Used at 750μg/ml concentration, stored as solid powder (Fluorochem, UK). Selects against the *URA3* or *klURA3* genes. In order to fully suppress the uracil synthesis pathway, 5FOA is used in synthetic media supplemented with additional uracil, to a final concentration of 445μM.

The following drugs are added to media to activate a specific checkpoint:

- α-**factor** Used at 3μg/ml concentration, stock 1mg/ml in H_20, made from powder (Peptide Chemisty STP, The Francis Crick Institute, UK). Cells arrest at the Start checkpoint in G1-phase. Arrest can be verified by checking cell morphology, arrested cells will develop a "schmoo" morphology with no bud. Cells can be released by washing twice in sterile H_20.

- **Nocodazole** Used at 15μg/ml concentration, stock 5mg/ml in DMSO, made from powder (Sigma-Aldrich, Germany). Cells arrest at the SAC checkpoint in M-phase. Arrest can be verified by checking cell morphology, arrested cells will appear as "dumb-bell" shaped cells, with a large bud. Arrest is most effective in YPD media.

2.2.3 Yeast transformations

Yeast were transformed with either plasmid DNA or linear DNA fragments for homologous recombination using a lithium acetate-based protocol.

Solutions

- **TE/LiOAc** 10mM Tris-HCl pH7.5, 1mM EDTA, 100mM LiOAc in H_20.

- **TE/LiOAc-40$\%$PEG** 10mM Tris-HCl pH7.5, 1mM EDTA, 100mM LiOAc 40$\%$ w/v PEG_{3350} (Sigma-Aldrich, Germany) in H_20.

Protocol

1. Grow 5ml culture, shaking, overnight, typically at 30℃ in YPD.

2. Dilute 500μl of overnight culture in 50ml fresh media and grow for a further 5 hours, until OD_{600} is roughly 0.6.

3. Spin down culture at 4000rpm for 5 minutes, resuspend in 10ml of TE/LiOAc solution.

4. Spin down cell-suspension at 4000rpm for 5 minutes, resuspend in 600μl of TE/LiOAc solution.

5. In a 1.5ml Eppendorf tube, mix 15μl salmon sperm DNA solution (Sigma-Aldrich, Germany), 200-500ng DNA, 200μl cells and 700μl TE/LiOAc-40$\%$PEG solution.

6. Incubate for 30 minutes, typically at 30℃.

7. Heatshock at 42℃ for 15 minutes.

8. *If using drug selection* - Spin down at 2,500 rpm for 1 minute, resuspend in 1ml fresh media and grow shaking for at least 1 hour.

9. Plate cells, dry fully under a flame and incubate. Colonies should be usually visible after 2 days.

2.2.4 Yeast genomic DNA extraction

Different protocols were used to extract yeast DNA depending on what the DNA was used for. DNA used for bacterial transformation was extracted using a CHELEX-based protocol. DNA used for PCR was extracted using an ethanol-based protocol.

Solutions

- **CHELEX suspension** 5$\%$ w/v CHELEX (Sigma-Aldrich, Germany) in H_20. This is a suspension and the CHELEX will visibly settle out over time, shake before use.
- **LiOAc/SDS** 200mM LiOAc, 1$\%$ w/v SDS in H_20.
- **TE** 10mM Tris-HCl pH7.5, 1mM EDTA in H_20.

Protocol for DNA extraction with CHELEX

1. Grow 5ml culture, shaking, overnight.
2. Spin down 2ml culture at 13,000rpm for 1 minute and resuspend in 250μl CHELEX suspension (shake before use).
3. Move suspension to 1.5ml Eppendorf tube and add 250μl 0.5mm-diameter glass beads.
4. Vortex suspension for 4 minutes on highest setting.
5. Incubate tube at 100℃ in heat block for 2 minutes.
6. Spin down suspension at 13,000 rpm for 1 minutes.
7. Collect top 100μl of supernatant, avoiding cell debris and CHELEX.
8. Repeat spin down and collect top 50μl of supernatant.

Protocol for DNA extraction with ethanol

1. Grow 5ml culture, shaking, overnight.
2. Spin down 200μl of culture at 13,000rpm for 1 minute, resuspend in 100μl of LiOAc/SDS solution.
3. Incubate at 70℃ in heat block for 5 minutes.
4. Add 300μl of 96$\%$ ethanol and vortex for 4 minutes.
5. Spin down suspension at 13,000rpm for 3 minutes.
6. Remove supernatant without disturbing the pellet.
7. Add 500μl of 70$\%$ ethanol, washing the pellet.
8. Spin down suspension at 13,000rpm for 1 minute.

9. Remove supernatant with a pipette without disturbing the pellet.

10. Dissolve pellet in TE.

11. Spin down suspension at 13,000 rpm for 30s before use.

2.2.5 Bacterial transformation and plasmid purification

Plasmids were amplified in *E. coli* before sequencing or transformation into yeast.

Solutions

- **LB Amp** 1% w/v tryptone, 0.5% w/v yeast extract, 1% w/v NaCl, 100μg/ml Ampicillin (Sigma) in H_20. Optional - 1.5% w/v agarose (for solid media).
- **SOC** 2% w/v tryptone, 0.5% w/v yeast extract, 1mM NaCl, 10mM $MgCl_2$, 10mM $MgSO_4$, 25mM KCl, 20mM glucose in H_20.

Transformation protocol

1. Thaw ElectroMAX DH10B cells (ThermoFisher, USA) on ice.
2. Dilute DNA to 30μl total with 10% glycerol and mix with 15μl cells, move to cold, 2mm cuvette.
3. Electroporate at 2.5KVm, 200Ω, 25μFd.
4. Immediately add 1ml SOC to cuvette, mix with pipette.
5. Transfer to 5ml tube and incubate for an hour, shaking at 37℃.
6. Plate cells, dry fully with a flame and incubate. Colonies should be visible the next day.

Bacterial growth

Bacterial cultures expressing plasmids were grown in LB Amp media, shaking, at 37℃.

Plasmid purification

Plasmids were purified according to the GeneJET Plasmid Miniprep Kit protocol (Thermo Scientific, USA).

2.2.6 Spot assay

Protocol

1. Grow 5ml culture of all strains, shaking, overnight.
2. Measure OD_{600} of overnight cultures with spectrophotometer. If necessary, dilute denser cultures with fresh media so all cultures have roughly the same density.
3. Using a multi-well plate make 10-times serial dilutions of the cultures.
4. Use a multi-channel pipette to plate these dilutions, dry fully with a flame and incubate.
5. Grow until control colonies have grown to the same extent. Plates grown at lower temperature, on less efficient sugars (such as galactose) or with drugs may take longer to achieve the same amount of growth. Scan plates when they have grown sufficiently.

2.2.7 Inducible promoters

The *GALS* and *MET3* promoters were used as inducible promoters.

***GALSp* induction Protocol**

1. Grow 5ml culture of all strains, shaking, overnight in media containing raffinose sugar.
2. Spin cells at 4,000rpm for 5 minutes, resuspend in 5ml sterile water.
3. Spin cells at 4,000rpm for 5 minutes, resuspend in 5ml media containing galactose sugar.
4. Grow culture, shaking and monitor for expression of gene. It may take 2 hours to see significant expression and longer to see phenotypic effects.

***MET3p* induction Protocol**

1. Grow 5ml culture of all strains, shaking, overnight in synthetic media supplemented with 2mM methionine to repress the *MET3p*.
2. Spin cells at 4,000rpm for 5 minutes, resuspend in 5ml sterile water.
3. Spin cells at 4,000rpm for 5 minutes, resuspend in 5ml media containing 10μM methionine (usually -MET media with additional methionine added).
4. Grow culture, shaking and monitor for expression of gene. It may take 2 hours to see significant expression and longer to see phenotypic effects.

2.3 Molecular Biology

2.3.1 PCR and gel electrophoresis

Polymerase Chain Reaction (PCR) was used to amplify small sections of DNA prior to transforming into yeast or *in vitro* plasmid construction. DNA primers

were designed using the SeqBuilder application (DNASTAR, USA), and synthesised by Sigma-Aldrich, Germany. DNA primer stocks were prepared at 20μM concentration in TE solution.

Solutions

- **TAE buffer** 40mM tris, 20mM acetic acid, 1mM EDTA in H_20.

PCR protocol

Different polymerase mastermixes were used for different types of reaction. For diagnostic PCRs (to determine genotype after transformation), DreamTaq PCR mix (ThermoFisher, USA) was used. For preparative PCRs (to transform yeast cells), Q5 High-Fidelity PCR mix (NEB, USA) was used.

1. For 100μl reaction: 1μl of each primer solution, 1μl of genomic DNA, 47μl of H_20, 50μl of polymerase mastermix. In practice, this was scaled to 20μl reactions for diagnostic PCRs or 50μl reactions for preparative PCRs.

2. Standard PCR reaction (timing and temperature often optimised for specific reactions):

   (a) 95℃ - 5 minutes

   (b) 94℃ - 30s

   (c) 55℃ - 30s

   (d) 72℃ - 1 minute

   (e) Return to (b) 29 times

   (f) 72℃ - 5 minutes

   (g) 4℃ - indefinitely

3. Determine concentration of product with NanoDrop spectrophotometer.

PCR product purification

PCR products were purified according to the GeneJET PCR Purification Kit protocol (Thermo Scientific, USA).

Gel electrophoresis

Agarose gel electrophoresis was used to determine the length of linear DNA fragments. Gels were prepared with TAE buffer and 0.5% electrophoresis-grade agarose (Invitrogen, UK). GelRed DNA dye was added at 0.1μl/ml to visualize DNA. Samples were loaded with 10x loading dye into separate wells, alongside 1kb GeneRuler DNA ladder (Thermo Scientific, USA). The gels were run in TAE buffer on a mini submarine Hoefer HE33 unit (Amersham Biosciences, UK) at 90V for roughly 60 minutes. Bands were visualized by UV illumination using a ChemiDoc imaging system (Bio-Rad, USA), and images were analyzed with the ImageLab application (Bio-Rad, USA).

2.3.2 Plasmid construction

Plasmids were constructed through gap repair of linearized plasmids by homologous recombination either in yeast or *in vitro*. In either case, the plasmid was then transferred to *E. coli* for amplification and sequencing.

Plasmid linearization

To linearize plasmids, 1μg of plasmid DNA was incubated with restriction enzyme in 50μl of the appropriate buffer at the appropriate temperature (see Table 2.3), for 1 hour. The linearized DNA was purified according to the PCR purification protocol and the linearization was verified by gel electrophoresis.

Table 2.3: Restriction enzymes used in this study.

Enzyme	Manufacturer	Buffer	Temperature
HpaI	NEB, USA	CutSmart	37° C
NdeI	Roche, Switzerland	SuRE/Cut H (Red)	37° C
NruI-HF	NEB, USA	CutSmart	37° C
ZraI	NEB, USA	CutSmart	37° C

Gap repair protocol in yeast

Gap repair in yeast was performed as the transformation protocol, using 50ng of linearized plasmid DNA and 50ng of insert DNA.

Gap repair protocol *in vitro*

Gap repair *in vitro* was performed according to the NEBuilder HiFi DNA Assembly Cloning Kit protocol (NEB, USA).

Site-directed mutagenesis

Site-directed mutagenesis was performed according to the Quikchange Mutagenesis Kit protocol (Agilent Technologies, USA).

2.3.3 Sequencing

Plasmids and some genomic transformations were verified by Sanger sequencing. DNA primers were prepared as described for PCR. Sequencing was performed either by the Genomics Equipment Park STP (The Francis Crick Institute, UK) or by Genewiz (UK) or by Source BioScience (UK). The results were analyzed with the SeqMan Pro application (DNASTAR, USA).

2.4 Microscopy

2.4.1 Live-cell Microscopy

Cells were imaged with a Zeiss Axioimager Z2 microscope (Carl Zeiss AG, Germany), with a 63x 1.4NA oil immersion lens and using a Zeiss Colibri LED illumination system (RFP=590 nm, YFP = 505 nm, GFP=470 nm, mTurq = 445 nm, azurite=385nm). Bright field images were obtained and visualised using differential interference contrast (DIC) prisms. Images were captured using a Hamamatsu Flash 4 Lte. CMOS camera containing a FL-400 sensor with 6.5 μm pixels, binned 2x2.

Slide preparation protocol

1. Grow 5ml culture of all strains, shaking, overnight.
2. Dilute 1ml culture in 25ml of fresh media and return to incubator, shaking, for at least 2 hours. If inducing expression with a conditional promoter, use media that will activate the promoter.
3. If necessary - spin down 5ml of culture, remove supernatant and resuspend in 50μ of fresh media.
4. Put 2.5μl of culture onto glass slide, add 2.5μl media containing 1.4$\%$ LMP agarose and pipette up and down. Remove 2.5μl of mixture and cover the remaining with 22mm cover slip (#1.5 thickness).

2.4.2 Image analysis

Images were analyzed and prepared with the Volocity application (Perkin Elmer Inc., USA). In general, cells with high levels of autofluorescence were excluded as dead cells.

2.4.3 Time-lapse microscopy

Time-lapse microscopy was used to measure the length of anaphase. Cells were imaged using a DeltaVision®Elite (GE Healthcare), with a 60x 1.42NA Oil Plan apochromatic lens and an InsightSSI 7 Colour Combined Unit illumination system (CFP = 438nm, mRuby2 = 575nm). Images were captured with a front illuminated sCMOS camera, 2560 x 2160 pixels, 6.5μm pixels, binned 2x2. Time lapse videos were captured over 2 hours, with images captured at 2 minute intervals.

Imaging chamber preparation protocol

1. Grow 5ml culture of all strains, shaking, overnight in SC media.
2. Dilute 2.5ml culture in 25ml of fresh media and return to incubator, shaking, for 3 hours.
3. Transfer cells to an agarose cube made from -URA media and allow to dry.
4. Place cube(s) into an imaging chamber and seal with parafilm.
5. Pre-incubate chamber for 1 hour at 30℃.

2.4.4 Time-lapse analysis

Images were analysed using FIJI (Schindelin et al. (2012)), with the Bio-formats plugin (Linkert et al. (2010)).

2.5 Synthetic Physical Interaction Screening

2.5.1 SPI method

The SPI screening process was performed as described in Ólafsson and Thorpe (2018). A library of GFP strains is transformed with a plasmid expressing either

a fusion of a protein of interest with GBP or a control, through a mating-based method known as Selective Ploidy Ablation (SPA) (Reid et al. (2011)). This method relies on a Universal Donor Strain (UDS), which has a *klURA3::GAL1* promoter adjacent to each centromere. This strain will mate with cells of the opposite mating type. When this diploid is given media containing galactose sugar, the *GAL1* promoter will become active leading to loss of the UDS chromosomes. Haploid cells are then selected for with 5FOA, which counterselects against cells retaining UDS chromosomes and *klURA3* genes.

1. Transform the UDS (E224) with the plasmids of interest.
2. Make 'lawns' - plates covered with dense layer of UDS cells.
3. Copy the lawns onto the required number of YPD plates.
4. Copy the GFP library on top of the YPD plates bearing the UDS cells.
5. Incubate these plates for 6 hours, to allow cells to mate.
6. Copy plates onto 2% galactose -leu plates, to select for cells bearing the plasmid and to induce loss of UDS chromosomes. Incubate for 24 hours.
7. Copy plates onto 2% galactose -leu + 5FOA plates, to select for haploid cells bearing the plasmid. Incubate for 48 hours.
8. Scan plates with desktop flatbed scanner (Epson V750 Pro, Seiko Epson Corporation, Japan) at a resolution of 300 dpi.

2.5.2 Basic quantitative analysis of SPI data

Scanned images were analysed computationally to extract measurements of the colony sizes. The online tool ScreenMill (Dittmar et al. (2010)) was used to perform normalisation and calculate Log Growth Ratios (LGRs) and Z-scores by

comparison of experimental and control colony sizes. Two controls were used (plasmids expressing GBP or the SPB protein alone) but, as in previous studies, we found strong agreement between the two and we used an average of the two values. In some cases, the library contained multiple copies of the same GFP strain, in these cases data was aggregated by averaging. In the proteome-wide screens plates were normalised to the plate median while in the validation screens GFP-free controls were used for normalisation. LGRs were further normalised using a spatial smoothing algorithm as described in Berry et al. (2016).

2.5.3 Mixture model analysis of SPI data

Bimodal normal mixture models were fitted to the smoothed LGR data using the "Mclust" package (Scrucca et al., 2016). This analysis is anticipated to be made available as part of a new screen analysis tool "ScreenGarden" being developed in the Thorpe lab.

2.5.4 Further bioinformatic tools for analysis of SPI screen results

The GOrilla website (`http://cbl-gorilla.cs.technion.ac.il/`, Eden et al. (2009)) was used to perform all gene ontology enrichment analysis. The "cluster" program (version 3.0, Eisen et al. (1998)) was used to perform hierarchical clustering of the SPI data; Java Treeview (Saldanha (2004)) was used to visualize the results. Clustering was performed using the correlation of the LGRs, minimizing the average linkage of the clusters. Spatial Analysis of Functional Enrichment (SAFE) analysis of SPB SPI hits was performed using the Cell Map website (`www.thecellmap.org`, Usaj et al. (2017)). Venn diagrams were created at `http://bioinformatics.psb.ugent.be/webtools/Venn/`.

2.5.5 Scripts

R scripts for data formatting and analysis are freely available at `https://github.com/RowanHowell/data-analysis`.

2.6 Logical Modelling

2.6.1 Training logical models

The CellNOptR package (Terfve et al. (2012)) was used to train logical models. CellNOptR employs a genetic algorithm to optimise the model against an array of experimental data (Saez-Rodriguez et al. (2009)). Starting from the PKN, all possible combinations of AND gates (up to a maximum number of inputs defined in the package) are generated and then a given model is defined by an edge-inclusion vector $P \in \{0,1\}^r$, where r is the number of possible edges. Therefore only edges which are included in the PKN are considered during training, although they can be combined in different logical rules. For any given model, CellNOptR can then calculate an objective function for a given model which is defined as

$$\theta(P) = \frac{1}{n_g} \sum_{k=1}^{s} \sum_{l=1}^{m} \sum_{t=1}^{n} \left(B^M_{k,l,t} - B^E_{k,l,t}\right)^2 + \alpha \frac{1}{v^s_e} \sum_{e=1}^{r} v_e p_e,$$

where n_g is the number of data points, B^M are the models predictions and B^E are the experimental data across m readouts, n time points and s experimental conditions (or mutants). α is a tunable parameter balancing the fit to data and size penalty terms. v_e is the number of inputs per edge and is used to ensure that AND gates are not penalised more harshly than OR gates, v^s_e is the sum of all v_e. In all instances of model training, I used a set of mutant phenotypes defined by the steady state localization of Cdc14.

CellNOptR uses a genetic algorithm to optimise the objective function $\theta(P)$, taking the following steps:

1. **Initialize** The algorithm needs a model to use as a starting point, usually the "full" model $P = \{1\}^r$.

2. **Fitness** The algorithm ranks all models by the value of the objective function and assigns fitness from the ranking.

3. **Selection** A number of models is selected to continue, based on their fitness.

4. **Recombination** Individual models mate producing new models where the vector P is produced from uniform crossover of the parents. Models with high fitness are selected to mate at higher frequency.

5. **Mutation** Mutation occurs at random across each of the loci (entries of P) of the models.

6. **Replacement** The old generation is replaced by the new, with the fittest member of the old generation maintained.

7. **Stop** The algorithm will stop if either a model achieves an objective function below a given tolerance or the algorithm has been through a given number of iterations without an improvement to the optimal value of the objective function.

8. **Loop** If the stop criteria are not met the algorithm will loop back to 2.

All Prior-Knowledge Networks (PKNs) and phenotype lists were constructed by hand using Excel (Microsoft, USA). Custom R scripts were written to convert the hand-written lists to the format required by CellNOptR. Generally, when training, the scripts were run 100 times in parallel. This was achieved using custom

Bash scripts to submit tasks in parallel on the High-Performance Computing cluster at the Francis Crick Institute. R scripts were used to collate the results of these runs and analyze the resulting ensemble of models.

2.6.2 Construction of compartmental logical models

Compartmental logical models

In a compartmental ODE model, the concentration of each protein in each compartment is described by separate variables. Similarly in a compartmental logical model, a node exists for each protein in each compartment it is permitted to localize to. The state of this node corresponds to whether the protein is present in this compartment (1) or not (0). In addition to these localization nodes, an activity node for each protein and each compartment exists to track whether the protein is active in this compartment (1) or not (0). Activation of the localization node is a pre-requisite for activation of the activity node. The rules of the network are then built from an activity network and a localization network. The former network describes how proteins control each others' enzymatic activity through post-translational modifications while the latter network describes how proteins control each others localization. The resulting network can be expressed as a logical network, albeit one where each protein appears multiple times for each compartment. This means that compartmental logical networks are larger than the underlying networks. If there are n proteins represented in the model and C compartments, the resulting compartmental logical network has $2 \times n \times C$ nodes.

Construction of the mitotic exit model

The FEAR network was trained using the CellNOptR package, run 100 times in parallel. The max inputs per gate was set to 4 as this is maximum permitted by the package. Activity and localization networks as well as a set of location

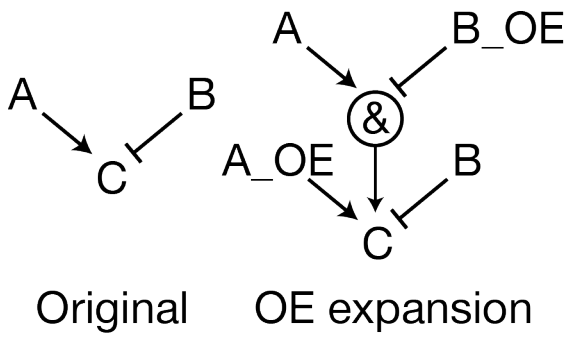

A	B	A_{OE}	B_{OE}	C
0	0	0	0	1
0	1	0	0	0
1	0	0	0	1
1	1	0	0	1
-	-	1	0	1
-	-	0	1	0
-	-	1	1	1

Figure 2.1: Schematic showing how logic gates are expanded to include overexpression (OE) nodes and the corresponding logic gate.

specific rules were created in BoolNet format and custom R scripts were used to generate the compartmental logical model. Briefly, the relevant nodes were created for each of the permitted locations and then the rules were read in and distributed across the nodes by creating an edge list. This edge list included modifications, such as requiring localization to be on for the activity node to be switched on. Generally, protein activity can only be regulated by proteins in the same compartment. The exception is the SPB, where proteins that can localize to the SPB can be regulated by these proteins or, if their regulator cannot localize to the SPB (for example Lte1), by proteins in the surrounding cytoplasm. The "Spindle alignment" node controls whether proteins at the dSPB can exchange with the cytoplasm ("Spindle alignment" = 0) or with the bud compartment ("Spindle alignment" = 1) (see Figure 4.4). All R scripts for logical modelling may be accessed at `https://github.com/RowanHowell/CLM-R`.

2.6.3 Simulation of mutant strains

To analyse the phenotypes of mutant strains, we placed all mutations into one of the following categories:

1. **Hyperactive**, an allele which is resistant to inhibition and will be active wherever it is localized.

2. **OE**, overexpression either by the *GAL1* promoter or provision of the gene on a multicopy plasmid, the protein is present and active everywhere. This high level of expression a protein can break the usual rules of protein regulation (see below).

3. **KD**, (knock-down), a functionally inactive allele, often temperature or analogue sensitive, which is inactive wherever it is localized.

4. **Delete** or **Deplete**, either deletion of the protein or depletion via a conditional promoter, localization prevented everywhere.

5. **Location** or **!Location**, the forced localization of the protein in one compartment or (!) the prevention of that localization.

6. **Phosphomutants**, phosphomutants represent a re-wiring of the network and therefore were considered on a case-by-case basis.

Of the above, most are straightforward, however overexpression can have many effects on protein function, and in some cases the sheer quantity of the overexpressed protein can alter the wiring of the network, for example activating a downstream component despite the presence of an inhibitor (Moriya (2015)). To account for these effects we introduced additional overexpression nodes for each protein. In the case where a protein activates its downstream components in a way that could be blocked by an inhibitor, the overexpression node circumvents this inhibition (Figure 2.1). However, note that localization of a protein in a compartment is always a necessary requirement for that protein's activity in that compartment. Similarly overexpression of an inhibitor may block the activation of a protein even in the presence of an activator. The only exceptions to this are the cases of non-physiological conditions of high Tem1 activity and lack of low level of Bub2 and Bfa1 activity in models 3 and higher. These modifications were applied to the edge list described above, and were used to produce a variant of

the model, usually suffixed “OE”. Similarly, we treated forced localization at the SPB as equivalent to a local overexpression, so a model variant suffixed “SPB” included the forced localization nodes needed to model this pertubation.

2.6.4 Attractor analysis

We represented the logical model as a Boolean network, in which each level of activity is represented as an individual node, in order to make use of computational tools designed for Boolean networks. As synchronous steady states are necessarily steady states in an asynchronous setting, all steady states were identified on the synchronous model. This was performed by solving the satisfiability problem using the BoolNet package for R (Müssel et al. (2010)), which employs the PicoSAT solver (Biere (2008)), based on the algorithm of Dubrova and Telsenko (Dubrova and Teslenko (2011)). In some cases multiple steady states exist for the same cell cycle stage, in order to determine the phenotype in such situations we used Monte Carlo simulations of the asynchronous model with nodes chosen uniformly at random, again using BoolNet functions. Unless otherwise stated all simulations were performed from the same, physiological initial conditions and were ran until either steady state was reached, the “Mitotic Exit" node was activated or the number of timesteps reached $10,000$. All R scripts may be accessed at `https://github.com/RowanHowell/CLM-R`.

2.6.5 Continuous time implementation with MaBoSS

We used the MaBoSS package (Stoll et al. (2012)), using scripts developed for the MaBoSS python package (Stoll et al. (2017)), to perform continuous time simulations of the logical model. The BoolNet model was converted to MaBoSS format using the GINsim tool (Naldi et al. (2009)). Rate parameters were fit to match experimentally determined length of mitosis in *bub2*Δ and *kin4*Δ cells,

Falk et al. (2016a), Table 4.2).

Spindle alignment times were simulated as a Wiener process, using a custom Python script. A Wiener process $W(t)$ is defined by the following properties (Durrett (2019)):

1. **Continuity** $W(t)$ is continuous in t.
2. **Independent increments** $W(t+u) - W(t)$ is independent of $W(s)$ for $s \in [0, t)$.
3. **Gaussian increments** $W(t+u) - W(t) \sim N(0, u)$, where $N(\mu, \sigma^2)$ is a normal variable with mean μ and standard deviation σ.

Generally a Wiener process is assumed to start from $W(0) = 0$, however in this case I assume the spindle alignment (denoted $x(t)$) starts from uniformally distributed initial conditions $x(0) \sim U(-\pi/2, \pi/2)$. Trajectories of $x(t)$ were approximated using property 3 above:

$$x(t + \Delta t) = x(t) + n(0, \sigma^2 \Delta t),$$

where $n(0, \sigma^2 \Delta t)$ is a normally distributed variable with mean 0 and variance $\sigma^2 \Delta t$, and σ is a variable representing the speed of the process.

All Python scripts may be accessed at `https://github.com/RowanHowell/CLM-Python`.

2.6.6 ODE simulations

Simulations of the ODE model of Caydasi et al. (2012) (BioModels database ID: BIOMD0000000702) were performed with Copasi (Hoops et al. (2006)), using the CoRC package for R. Parameters were unchanged from the original model, except initial conditions which were chosen to match the steady states of the

pre-alignment model. Forced localization of Bfa1 at the SPB was modelled by decreasing the off-rate of Bfa1 species by a factor of 1,000.

Chapter 3

Results 1: Synthetic Physical Interactions with the yeast centrosome

3.1 Introduction

The SPB is an important signalling hub; physical interaction of signalling proteins with the SPB is critical for duplication of the SPB and mitotic exit. I wanted to explore the impact of forcing physical interactions with the SPB. I used the SPI methodology to induce physical interactions with 5 proteins from different locations around the SPB. This screening approach allowed me to test the impact on growth of forced localization at the SPB for over $4,000$ proteins. In reference to genetic interactions, a SPI is a forced association that results in a significant growth defect.

I found that the SPB is especially sensitive to forced localization, relative to other regions of the cell. This lead to issues with the statistical methodology used to assess the significance of growth defects and detect SPIs. I developed a novel way to analyze SPI data, using an empirical Bayes approach based on

mixture models. This methodology allowed me to establish robust definitions of SPIs and also derive screen-specific parameters to compare the impact of forced localization to different regions of the cell.

I found that the hits from the Spc42 screen were enriched for nuclear pore components, and hypothesized that this was due to disruption of SPB copy-number homeostasis. I screened 80 interactions for aberrant SPB copy-numbers and identified a number of proteins that reliably induce additional Spc42 foci when forced to localize at the SPB. Imaging of microtubules in these strains indicate that these foci nucleate microtubules and otherwise behave as regular SPBs. These findings have consequences for our understanding of SPB duplication.

I re-screened a number of MEN proteins in a genetic background lacking the *KAR9* gene, in order to detect defects in SPoC maintenance. I found that some SPIs with Spc72, for example Tem1, were dependent on *kar9*Δ, indicating SPoC disruption. I also re-screened for SPIs using the temperature sensitive *nud1-2* allele, rather than wild type Nud1. I found that some interactions, especially Tem1 and Bfa1, were drastically different using this target protein, suggesting scaffold specific effects are important at the SPB. I developed an alternative *GALSp* based conditional SPI system, and showed that this recapitulates the effects seen in the original Nud1 screen. I used this system to show that the SPI between Cdc28 and Nud1 is a result of the sequestration of Cdc28 outside of the nucleus, preventing mitotic entry.

The bulk of the work in this chapter was published in Howell et al. (2019).

3.2 Synthetic Physical Interaction Screens

Synthetic Physical Interaction screens are a method used to assess the impact of forcing proteins to associate with another protein (Ólafsson and Thorpe (2015)). This screening methodology makes use of the strong binding between GBP and

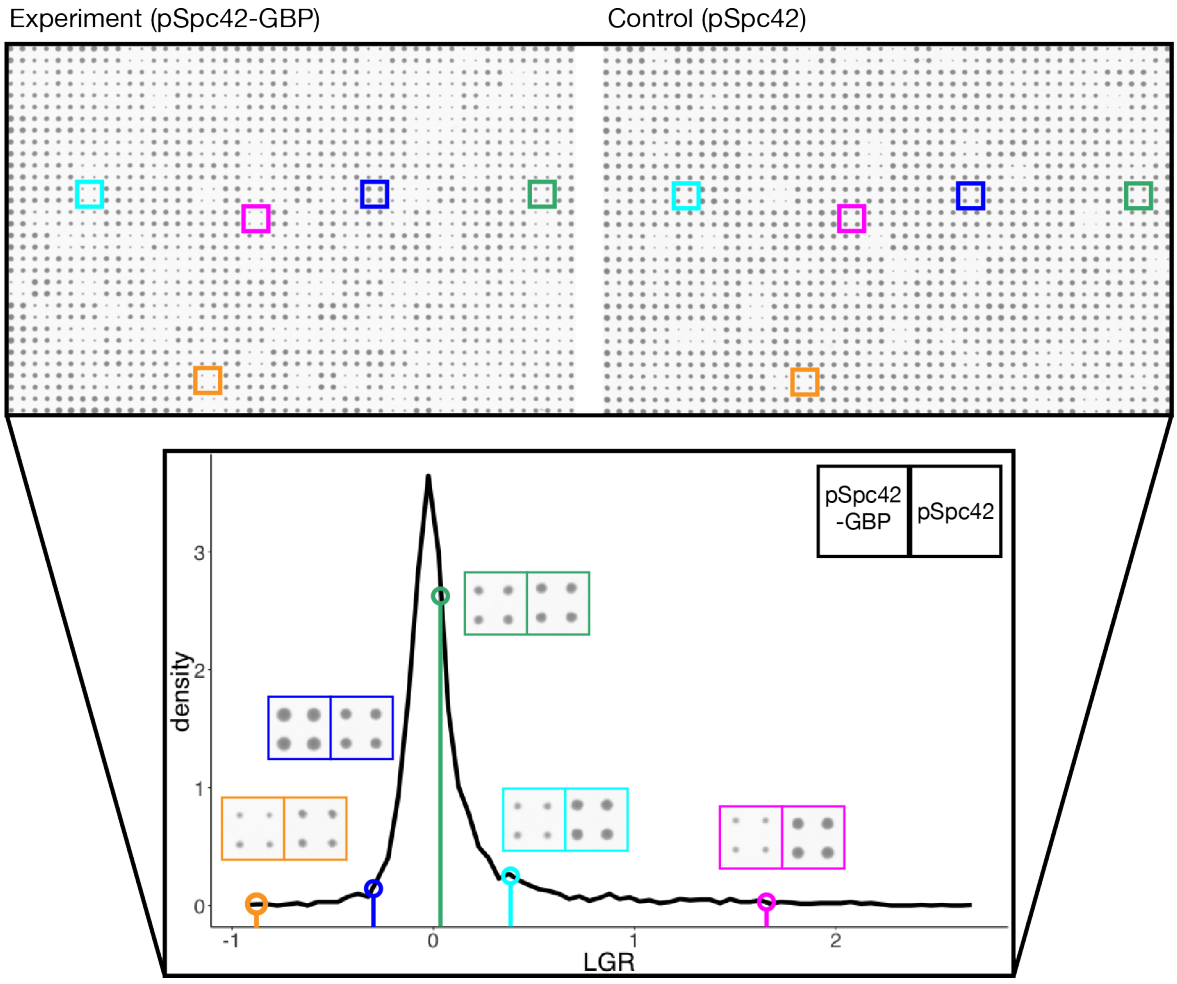

Figure 3.1: Schematic of the SPI screening process. The top panel shows scans of a single library plate with the plasmid expressing either Spc42-GBP-RFP (denoted Spc42-GBP) or Spc42 (the plate with the plasmid expressing GBP alone is not shown). The lower panel shows a histogram of LGRs in the screen. Five strains are highlighted to show the difference in colony size associated with different LGRs. Note that strains with low negative LGRs, such as that shown in orange are often the results of slow-growing GFP strains, which can register as having enhanced growth due to plate normalization and proportionally high levels of measurement error.

GFP to induce binary fusions between a target protein, tagged with GBP, and a GFP-tagged protein. Using a library of yeast strains expressing GFP-tagged proteins (Tkach et al. (2012)), the SPI method can be used to test forced interactions across the proteome. This is achieved using a high-throughput mating-based approach, known as Selective Ploidy Ablation, to transfer a plasmid expressing the target protein-GBP fusion into the library (Reid et al. (2011)). The impact of the forced localization is measured by the Log Growth Ratio (LGR), which is calculated from the areas of colonies grown with the target protein tagged with GBP and two controls. These controls are cells expressing either GBP alone or the target protein in the same GFP strain. A high LGR (generally > 0.4) is indicative of a growth defect while a low LGR (< -0.4) can indicate a growth enhancement (Figure 3.1).

A Z-transformation is applied to the data to examine the significance of any effect on growth. This procedure transforms LGRs to Z-scores, with the set of Z-scores having a mean of 0 and a standard deviation of 1. In Z-space, the region $(-2, 2)$ is the 95% confidence interval, assuming normally distributed data. Therefore a Z-score greater than 2 or less than -2 is considered statistically significant.

3.2.1 Identification of SPI targets

The SPB is spans the nuclear membrane and consists of 3 plaques: the inner plaque, which faces into the nucleus; the outer plaque facing into the cytoplasm; and the central plaque bridging the other two (Figure 1.2, Jaspersen and Winey (2004)). I decided to perform SPI screens with 5 target locations around the SPB: Nud1, Spc42, Spc72 and both the C- and N-termini of Spc110. The N-terminus of Spc110 is located on the inner plaque of the SPB, while the C-terminus resides on the central plaque, along with Spc42. Nud1 and Spc72 lie on the outer plaque. I chose these targets as representative of different regions of the SPB. Although Nud1 and Spc72 are both outer plaque proteins I chose to screen with both as

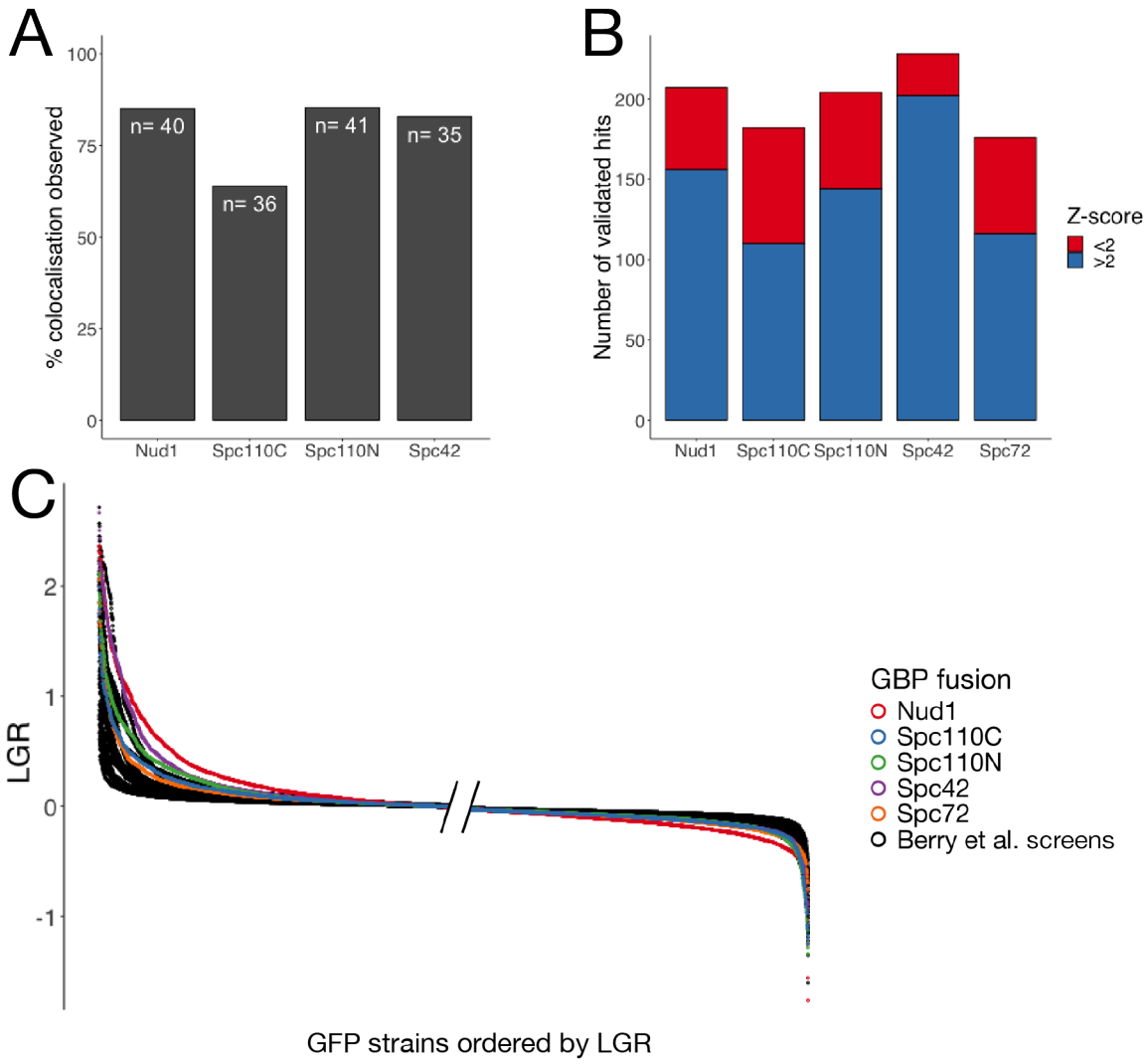

Figure 3.2: Caption located on next page.

there is evidence that MEN proteins localize to specific scaffolds at the outer plaque (Gryaznova et al. (2016)). I performed these 5 SPI screens and analyzed the data using an established automated image analysis pipeline to measure the colony sizes and calculate colony sizes (Dittmar et al. (2010)). Custom R scripts were used to handle and rearrange the data. A custom perl script was used to smooth the data to minimise the effects of plate organisation (Ólafsson and Thorpe (2015)).

Figure 3.2: Analysis of SPI screening data. A: Colocalization of query and target proteins in the Nud1, Spc42, Spc110C and Spc110N screens. A selection of 48 GFP strains were chosen to represent different regions of the cell and a mixture of strong and weak growth phenotypes. Each strain was judged to have either colocalization of GFP and RFP at SPB foci or not. In some cases no live cells were imaged due to slow growth, these strains were removed from analysis. The $60\% - 80\%$ colocalization observed in each screen is consistent with previous studies (Berry et al., 2016). B: Validation of SPB SPI screens. For each GBP construct, 240 GFP strains were chosen and rescreened at higher density. These strains were considered to be validated hits if the growth defect measured was greater than a cutoff determined by GFP-free controls. In each screen, we found that strains with Z-scores less than 2 met the criteria for validation, suggesting the cutoff at a Z-score of 2 was overly restrictive. C: Ordered LGRs for each of the 5 SPB screens and 23 screens from Berry et al. (2016), this graph shows only strains present in the subset of the GFP library used in the SPB screens. The left hand side of the graph has left-justified values while the right hand side shows the right-justified values, this is because the regions closest to the edges are the most informative. The SPB screens, shown in colour, are considerably seperated from the screens performed with other regions of the cell.

3.2.2 Validation of results

I had assumed that the GFP-tagged proteins would be recruited to the SPB, rather than the other way around, as a result of the structural integrity of the SPB. I checked this using fluorescence microscopy. I imaged 48 GFP strains, chosen to represent SPIs and non-SPIs, different regions of the cell and regulators of mitosis. Imaging was performed with cells expressing *NUD1-GBP-RFP*, *SPC42-GBP-RFP*, *SPC110-GBP-RFP*, *GBP-RFP-SPC110* and *GBP-RFP*. I found that $60\% - 80\%$ of cells showed colocalization of GFP and RFP consistent with recruitment of the GFP-tagged protein to the SPB (Figure 3.2A). This result is in keeping with the findings of Berry et al. (2016).

In order to assess the rate of false positives (Type I errors), I validated the strains with the highest, or lowest (most negative), LGRs. These validation screens used 16, rather than 4, replicates of each stain. Instead of using an LGR or Z-score threshold, LGRs were compared with GFP-free controls growing on the same plate. A total of 240 strains were validated for each SPB-GBP

construct. For each screen, I validated all strains with a Z-score greater than 2 (~ 150 per screen), with the remaining strains being chosen from those with a Z-score just below 2 and strains with Z-score less than -2. The growth enhancers ($Z < -2$) were found not to validate at a high rate. These strains are generally found to be slow-growing, which can lead to inaccuracies when calculating the LGR (Figure 3.1A). Almost all of the strains, including those with a Z-score below 2, were found to have a significant growth defect relative to GFP-free controls (Figure 3.2B).

3.2.3 Limitations of Z-score analysis

The finding that interactions that were assigned a Z-score less than 2 were validated according to the growth defect relative to GFP-free controls suggested to me that using a threshold of $Z = 2$ was leading to Type II errors (false negatives) and excluding interesting results. Applying a Z-transformation assumes that the data roughly follows a normal distribution. This is a reasonable assumption if the majority of strains in a screen are unaffected, but as the number of strains showing a growth defect increases, this assumption will break down. I hypothesised that the SPB was particularly sensitive to forced localization of proteins, and as a result the Z-score cutoff was too restrictive. I plotted the distribution of LGRs from the SPB SPI screens against the distributions of 23 previously published SPI screens (Berry et al. (2016), Figure 3.2C). The SPB SPI screens show markedly higher LGRs than the other SPI screens, in agreement with my hypothesis. Therefore, I concluded that Z-scores are not an appropriate tool to assess the significance of SPIs with the SPB.

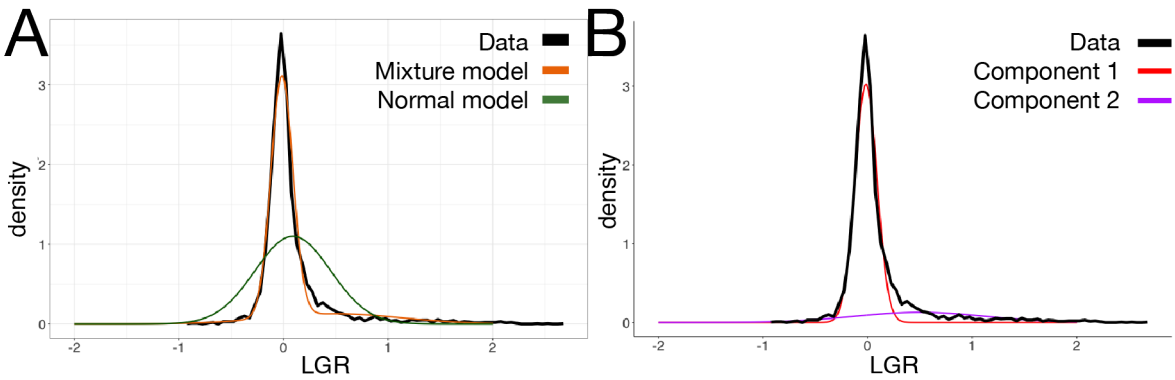

Figure 3.3: Normal and mixture models of the Spc42 SPI screen data. A: A bimodal normal mixture model fits the data more closely than a unimodal normal model. B: The two components of the normal mixture model. Component 1 is the "central" peak, component 2 is the "hit" peak.

3.3 Empirical Bayes approach

In order to overcome the limitations of Z-score thresholding, I developed a novel statistical model for the SPI data. The raw data from a SPI screen is a set of LGRs, based on colony sizes. The sizes of genetically identical yeast colonies are generally assumed to follow a lognormal distribution (see for example Baryshnikova et al. (2010)). So for an experimental colony size E_i and control colony size C_i

$$LGR_i = \log\left(\frac{E_i}{C_i}\right) = \log(E_i) - \log(C_i).$$

If E_i and C_i follow a lognormal distribution, then LGR_i should follow a normal distribution, as it is the difference between two normally distributed variables. However, the variability in this random variable is derived purely from noise in the system (for example the number of cells pinned) and observational errors. In a real screen, there are biological reasons that some strains will grow more slowly than the average. If we calculate a normal model from the mean and standard deviation of the LGRs and plot it against the histogram of the data, it is clear that the data is not normally distributed (Figure 3.3A).

Rather than fitting a uni-modal normal distribution, I reasoned that the data

could be better modelled by fitting a mixture model of two weighted normal distributions (Fraley and Raftery (2002)). This approach is similar to the empirical Bayes approach of Efron (2004), where the prior is inferred from the data, as here I infer the null distribution. These two distributions represent the distribution of proteins unaffected by forced localization at the SPB, and the distribution of the SPIs, whose growth is significantly affected. I used the "Mclust" package (Scrucca et al. (2016)) to fit the mixture models to the SPI data. This package uses an Expectation-Maximization approach to fit normal mixture models. The model fitting process yields 6 parameters: the weights ρ_1 and ρ_2, the means μ_1 and μ_2; and the standard deviations σ_1 and σ_2, which fully define the mixture model. The structure of the mixture model is shown in Figure 3.3B. The mixture models fit the data much better than the uni-modal normal models, see for example the Spc42 data (Figure 3.3A).

In order to evaluate whether my mixture model approach is appropriate as a statistical model of SPI screen data, I fit mixture models to all of the SPB SPI screens and the 23 screens of Berry et al. (2016). Of these 28 datasets, I found that 20 fit the data as we expected, with a clear "central" peak, representing the distribution of unaffected strains, and a "hit" peak shifted to the right. The remaining 8 datasets did not show well defined hit peaks. I defined the fit as a "failure" if

$$\mu_2 < \mu_1 + 1.5\sigma_1.$$

This is likely because these screens had fewer hits, as evidenced by the small number of strains with Z-score greater than 2 (Figure 3.4A). In these cases a Z-transformation approach may be more appropriate.

The screens of Berry et al. (2016) were performed using the full GFP library ($\sim 6,000$ strains, Huh et al. (2003)) while I used a smaller library of strains with confirmed GFP fluorescence ($\sim 4,500$ strains, Tkach et al. (2012)). The parameters of the fitted mixture models were not greatly affected when applied to the

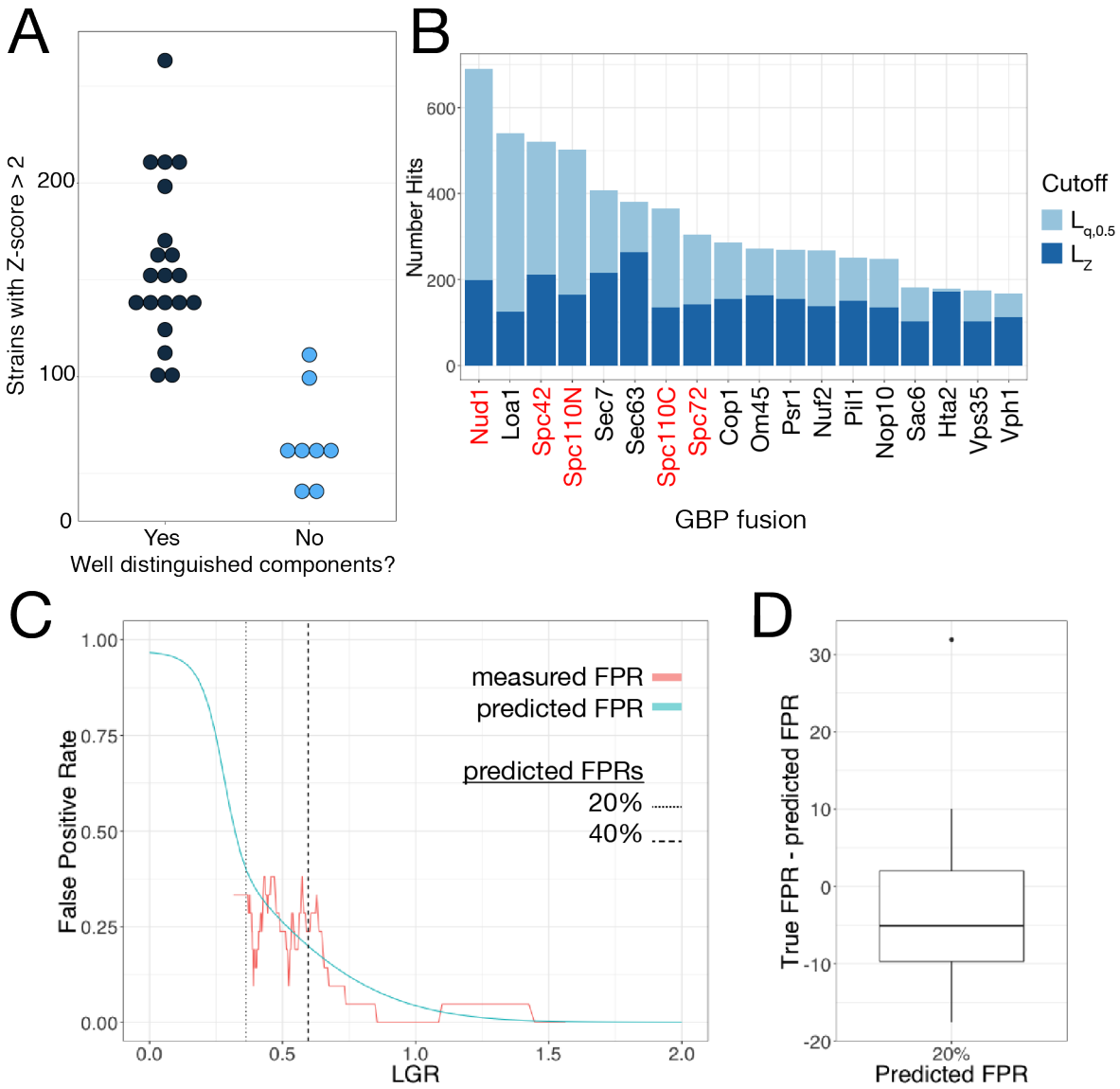

Figure 3.4: Using mixture models to determine thresholds. A: Dot plot showing the number of strains with Z-score greater than 2 for each screen. The screens are split between those where the mixture model identified well distinguished hit and central peaks and screens where it did not. B: The number of hits by both Z-score (L_Z) and q(x) ($L_{q,0.5}$) cutoff for each of the screens where the mixture model was applicable. The q(x) cutoff has a higher dynamic range than the Z-score and is better able to distinguish screens with many hits. C: FPR prediction for the Spc72 screen. The FPR for the screen was predicted from the mixture model and this prediction is overlaid with estimates of the FPR using binned data from the validation screen. In this case, the predicted FPR was reasonably accurate, although the data is quite noisy. The points where the mixture model predicts 20% and 40% FPR are indicated with a dashed line. D: Box-and-whisker plot showing the difference between measured and predicted FPR at the point where the FPR is predicted to be 20% across the screens where the mixture model was applicable. This shows some bias, with the predicted FPR generally higher than the true FPR but generally achieving an accuracy around $\pm 10\%$.

subset of strains used for the SPB SPI screens.

3.3.1 Using mixture models to define cutoffs

Having established that mixture models are an appropriate statistical model for the SPI screen data, I turned my attention to methods to determine cutoffs.

The genome-wide screen can be thought of as a process of generating LGRs for genes in the screen. Let us consider how we could simulate this data. I define the set of hits to be C_2 and the non-hits as C_1. The elements of each of these sets will follow a normal distribution and so these sets are referred to either as the first and second components or the central and hit peaks. First, a gene is designated to be either a hit or not, this is essentially a Bernouilli variable or weighted coin flip, where the probability of being assigned a hit is given by the weighting of the hit peak, ρ_2. In other words, a gene G_i has identity I_i, with:

$$\mathbb{P}(I_i = C_k) = \begin{cases} \rho_1, & k = 1 \\ \rho_2, & k = 2 \end{cases}.$$

Then the LGR of the gene LGR_i is a normal variable distributed with mean and standard deviation μ_1, σ_1 or μ_2, σ_2, depending on its identity.

A standard method when analysing genome-wide screen data is to calculate p-values, the probability of a given value or higher being measured, given a null model. The central peak component of the mixture model is interpreted as describing the variation in unaffected strains, so this is a natural choice for a null model. This allows for the calculation of p-values:

$$p(x) = \mathbb{P}(LGR_i > x | I_i = C_1) = \int_x^\infty f_{LGR_i | I_i = C_1}(z) dz,$$

where $f_X(x)$ represents the Probability Distribution Function (PDF) of the random variable X. In this case $f_{LGR_i | I_i = C_1}(x)$ is the PDF of a normal variable with mean

μ_1 and standard deviation σ_1. These p-values must be adjusted to account for multiple hypothesis testing, to achieve this I calculated FDR q-values (Benjamini and Hochberg (1995)). The cutoff for significance of a p-value is usually 0.05, with a p-value less than this indicating a significant result. Therefore, we may define a cutoff $L_{p,0.05}$ where the adjusted p-value of a measured LGR would pass below 0.05.

The mixture model structure suggests an alternative cutoff definition, based instead around the probability of inclusion in the hit peak component. I define the conditional probability of inclusion in component 2 to be

$$q(x) = \mathbb{P}(I_i = C_2 | LGR_i = x).$$

By Bayes' theorem

$$q(x) = \frac{f_{LGR_i|I_i=C_2}(x)\mathbb{P}(I_i = C_2)}{f_{LGR_i}(x)},$$

where $f_{LGR_i|I_i=C_2}(x)$ and $f_{LGR_i}(x)$ can be calculated from the fitted distributions. The metric $q(x)$ can be thought of as the probability that a strain for which we measure a LGR of x is a hit. A natural cutoff for this metric is then the point at which the strain is more likely to be a hit than a non-hit, in other words where $q(x) = 0.5$. I refer to this cutoff as $L_{q,0.5}$. In comparison, we define the LGR that would correspond to a Z-score of 2 in Z-space to be L_Z.

In practice $L_{q,0.5}$ is always less than L_Z, but the cutoffs were further apart in screens with more hits (Figure 3.4B). Using $L_{q,0.5}$ as a cutoff instead of L_Z increases the dynamic range of hits from 100-250 to 100-700, in the screens where two peaks could be distinguished. This shows that this cutoff is more effective as a tool for distinguishing screens with many and few hits.

3.3.2 Using mixture models to predict validation

I validated the hits from the SPB SPI screens by repeating the screening procedure with more repeats and comparing to GFP-free controls. Validation is important to verify key results but can also be used to establish metrics such as the False Positive Rate (FPR). However, validation uses further resources so it would be preferable to minimise the number of validation experiments performed. I decided to investigate how my empirical Bayes approach to studying the SPI data could be used to optimise validation experiments. A SPI is validated if its LGR in the validation screen is greater than the mean plus two standard deviations of the LGRs of the GFP-free controls on the same plate. This differs from the definition of Berry et al. (2016) who used the maximum of the LGR of the GFP-free controls as a threshold. The probability of validation for a strain with LGR, x in the original screen is defined to be

$$p_V(x) = \mathbb{P}(LGR_i^V > K | LGR_i = x).$$

By conditioning on the identity of G_i and using the law of total probability,

$$\begin{aligned} p_V(x) = &\mathbb{P}(LGR_i^V > K | I_i = C_1)\mathbb{P}(I_i = C_1 | LGR_i = x) \\ &+ \mathbb{P}(LGR_i^V > K | I_i = C_2, LGR_i = x)\mathbb{P}(I_i = C_2 | LGR_i = x). \end{aligned}$$

Each of these quantities can be calculated with no further assumptions using the parameters from the fitted mixture model with the exception of $\mathbb{P}(LGR_i^V > K | I_i = C_2, LGR_i = x)$. To calculate this, I further assume that

$$\mathbb{P}(LGR_i^V > K | I_i = C_2, LGR_i = x) \sim \text{Normal}\left(\mu = x, \sigma^2 = \frac{\alpha(\sigma_2)^2}{4}\right),$$

where α is a parameter than can be tuned. A key assumption here is that strains from the hit peak have a "true" LGR greater than 0, for which x is a reasonable

approximation. This is in contrast to strains from the central peak, which are assumed to have a "true" LGR of 0. This assumption is based on the finding that validation LGRs correlate with the LGR from the original screen. Another assumption is the choice of $\frac{\alpha(\sigma_2)^2}{4}$ as the variance of this distribution. The uncertainty in this measurement derives from both existing noise in the screening system and batch effects. The term $\frac{(\sigma_2)^2}{4}$ is based on the measured uncertainty in the original screen, with the factor of 4 coming from the use of 16 rather than 4 colonies for these measurements. We find that there is a noticeable "batch" effect, meaning that the variance between screens is higher than within them and we can tune the strength of this effect with the parameter α. We found that $\alpha = 4$ yielded good results.

If we plot $pV(x)$ against measured data from the SPI screens, we find that it generally closely matches the measured FPR (Figure 3.4C). Of the 20 SPI datasets for which the mixture model fit the data well, in 18 screens $pV(x)$ accurately predicted the FPR. The other 2 screens had poor validation rates in general. This approach could also be used to calculate SPI thresholds, for example at the point where the FPR is 20% or 40% (Figure 3.4C). Comparing the true and predicted FPRs at the point where the FPR is predicted to be 20%, shows that generally the prediction is accurate (Figure 3.4D). There is a slight bias, with the predicted FPR on average $\sim 5\%$ higher than the true FPR but the overall accuracy is within $\pm 10\%$ in the majority of cases. This approach could be used to define a further cutoff, $L_{V,0.2}$, the point at which a measured LGR has an FPR of 20%.

3.3.3 The SPB is sensitive to forced localization of proteins across the proteome

I have already demonstrated that the empirical Bayes approach to analysis of SPI screens has significant advantages with respect to the definition of thresholds

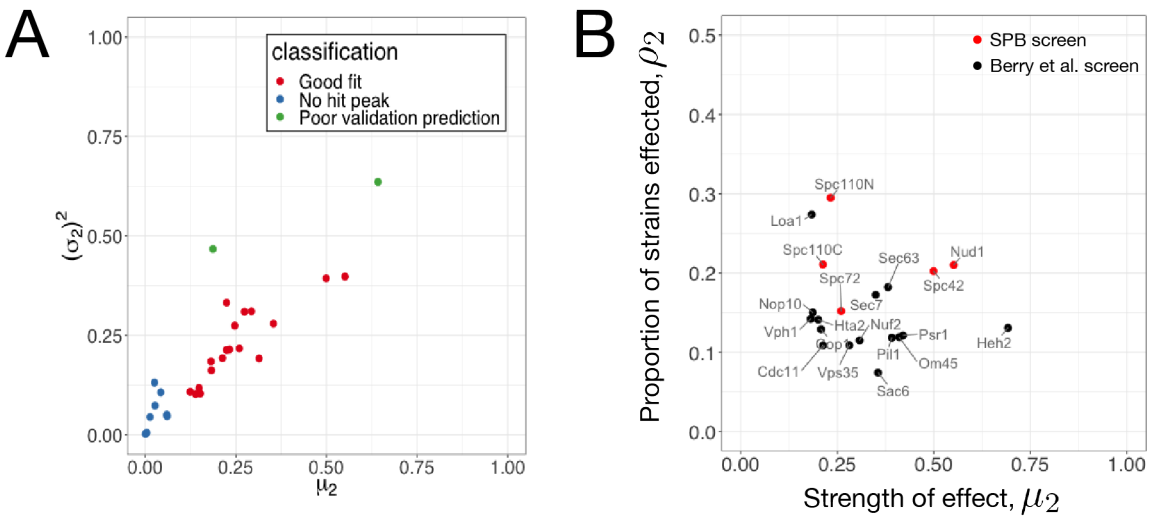

Figure 3.5: Mixture model parameters. A: Classification of mixture model fit for each of the 28 screens analyzed. The mean μ_2 and variance $(\sigma_2)^2$ of component 2 are good indicators of the success of the model with very low means or high variances indicative of the lack of a hit peak or poor validation prediction respectively. B: Classification of screen based on fitted parameters calculated using the subset of GFP strains used in the SPB screen. Each of the screens for which the mixture model fit was appropriate are plotted according to the proportion of strains affected (ρ_2) and the average strength of these effects (μ_2). The SPB screens Spc42 and Nud1 are positioned in the upper right portion of the graph, showing that a large proportion of proteins were sensitive to forced interaction with the SPB and these sensitivities caused significant growth defects.

and prediction of validation experiments. An additional benefit is the calculation of parameters that can be used to compare screens with different target proteins. I found that by plotting the variance of the hit peak, σ_2^2, against its mean, μ_2, I could distinguish different behaviours of the mixture model (Figure 3.5). Very low means and variances were indicative of a failure of the mixture model to identify distinct peaks while high variances were indicative of poor validation.

I previously hypothesized that the SPB is more sensitive to forced recruitment than other regions of the cell. I found that, using the $L_{q,0.5}$ cutoff, the SPB SPI screens were among the screens with the most hits (Figure 3.4B). The parameter μ_2 is the mean of the hit peak, so higher values of μ_2 can be intrepreted as suggesting that forced interaction with the target protein causes more severe growth defects. Similarly, ρ_2 represents the weight of the hit peak, so higher values of ρ_2 suggest that a greater portion of the proteome is sensitive to forced interaction with the target protein. By plotting screens based on these two parameters, we can compare the effects of forcing interactions with different target proteins (Figure 3.5B). The SPB screens sit in the top right part of this graph, demonstrating that generally the SPB is sensitive to forced association with other proteins. Nud1 and Spc42 produce particularly severe SPIs (high μ_2), while Spc110 causes weaker SPIs but with a greater proportion of the proteome (high ρ_2). Spc72 is less distinct from other regions of the cell, possibly reflecting the fact that it is a non-essential gene in the S288C background (Giaever et al. (2002)). Other screens also had high values of μ_2 and ρ_2, notably Loa1, Heh2, Sec7 and Sec63, which are all membrane proteins localising to the ER, golgi or nuclear membrane.

Next I wanted to know whether the SPB screens identified similar hits. I clustered the SPB screens with the 23 screens of Berry et al. (2016), using hierarchical clustering both by GFP strain and by screen (Figure 3.6). All 5 SPB screens were clustered together, apart from the other 23 screens suggesting that the set of hits in these screens are characteristic of the SPB and not other regions of

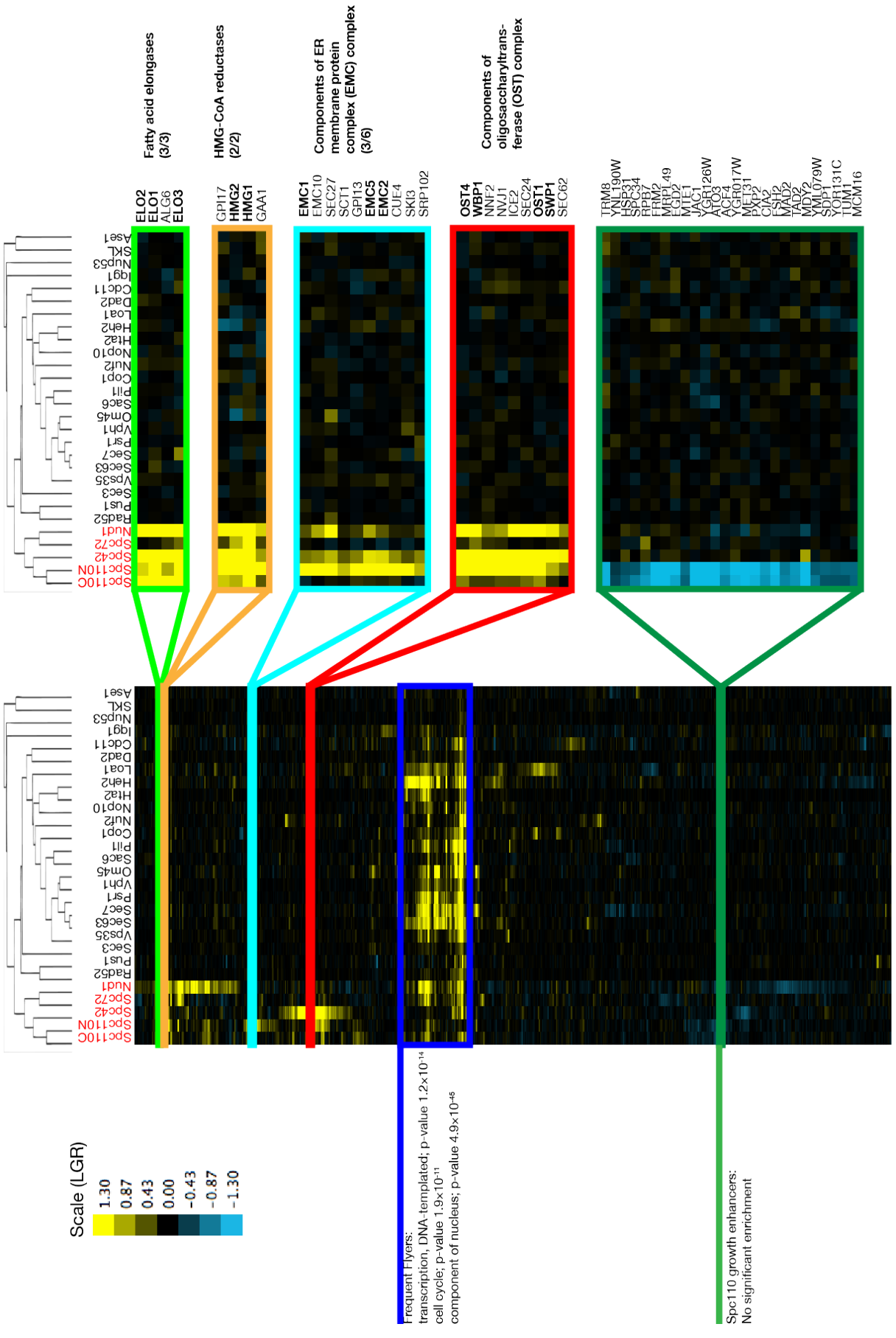

Figure 3.6: Cluster analysis of all 28 SPI screens used in this study. The data is clustered both vertically (by GFP strain) and horizontally (by screen, tree shown). The horizontal clustering tree shows that the SPB screen results are more similar to each other than the other screens. The vertical clustering identifies clusters of biologically related proteins with similar profiles of sensitivity to forcible relocalization.

the cell. The vertical clustering of strains by their SPI profile also reveals biologically relevant clusters of proteins. These clusters include the fatty acid elongases Elo1, Elo2 and Elo3; and the two paralogs of HMG-CoA reductase Hmg1 and Hmg2, which are all SPIs with SPB components (Figure 3.6). This clustering also groups protein complexes together, for example the ER membrane protein complex (EMC) and oligosaccharyltransferase complex (OST) (Figure 3.6). Another cluster identified by this analysis consists of proteins that appear to enhance growth when forced to interact with both ends of Spc110. However, of the 19 growth enhancers from the Spc110N screen that were re-tested in the validation screen, none were found to have a reproducible effect enhancing growth. The likely reason that these strains appear to be growth enhancers in both the Spc110C and Spc110N screens is that they shared both controls (the GBP-free control for both screens was a plasmid expressing Spc110). Furthermore, this cluster is not enriched for any GO terms. Finally this clustering approach allowed me to identify a set of proteins that were SPIs in many screens (Figure 3.6). These so-called “frequent flyers” are sensitive to relocalization to any region of the cell and so are therefore generally not considered of interest when testing for interactions with a specific region of the cell. The frequent flyers are enriched for transcription factors and other nuclear proteins, as previously noted (Berry et al. (2016)).

3.3.4 GO and SAFE analysis

The cluster analysis identified some clusters of related genes that were SPIs with the SPB. I wanted to gain a comprehensive understanding of the kinds of proteins that are sensitive to forced localization at the SPB. To achieve this I used GO (Gene Ontology) enrichment analysis and SAFE (Spatial Analysis of Functional Enrichment).

The SAFE method superimposes a set of proteins - in this case SPIs from my

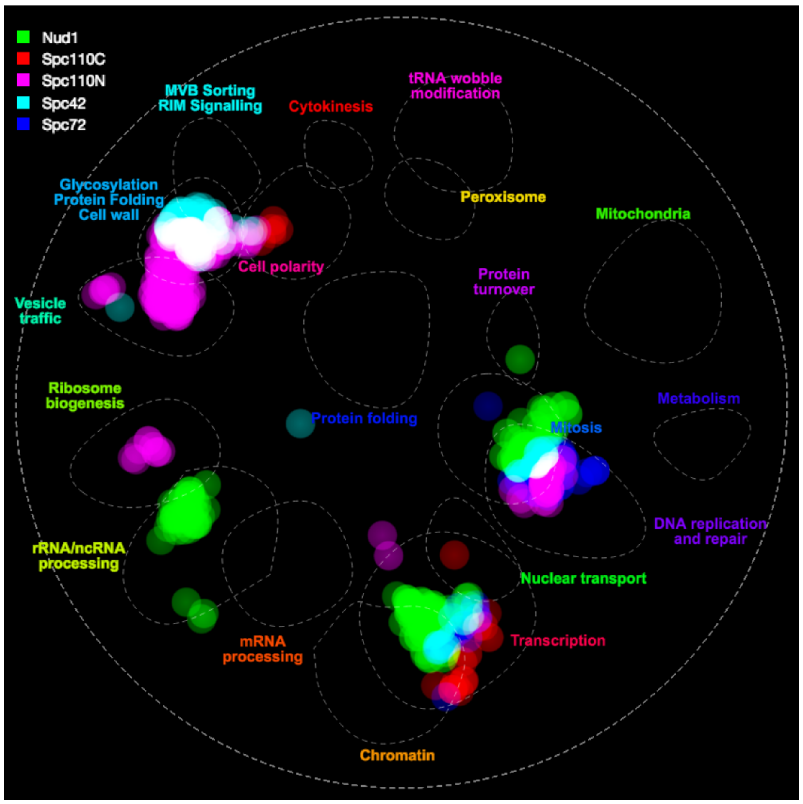

Figure 3.7: SAFE enrichment of hits from SPB SPI screens, visualized using TheCellMap.org. The *S. cerevisiae* genetic interaction network was clustered by density, identifying highly dense regions of space corresponding to shared function. Regions of space containing high densities of hits from each screen are highlighted accordingly showing visually which processes the hits from the screens are related to.

screens as identified using the $L_{q,0.5}$ threshold - onto a genetic interaction similarity profile network (Baryshnikova (2016)). Regions of this network are associated with specific biological functions so by plotting the areas containing high densities of proteins from a screen, a picture of the biological functions perturbed by the screen is formed. I used the online tool `thecellmap.org` (Usaj et al. (2017)) to perform this analysis and visualize the results (Figure 3.7). There are high densities of SPB SPIs in the mitotic regulator and transcription factor regions of the network. Furthermore, for the Spc110 and Spc42 screens there are clusters of hits in the protein folding, glycosylation and cell wall zones. It is interesting to note that, while there is some overlap, each screen shows density in some unique parts of the network. This is especially notable in the cases of Nud1 and Spc72 as well as Spc42 and Spc110C,as these pairs of locations are close within the SPB. This suggests that some of these interactions are scaffold specific.

In addition to SAFE analysis I used GO enrichment analysis to see which categories of proteins are enriched in the SPI datasets. I performed this analysis with the GOrilla tool (Eden et al. (2009)). I used ranked GO analysis, ranking the genes by the LGRs from the screen, as this approach does not require a threshold. I plotted heatmaps showing significant enrichments for each of the SPB SPI screens (Figure 3.8). Note these heatmaps show just the most relevant categories, not the entire set of results. The Spc42 screen and both Spc110 screens were enriched for proteins in the Endoplasmic Reticulum (ER) and involved in lipid metabolic processes, especially sterol and sphingolipid biosynthesis and fatty acid elongation (Figure 3.8C). This is interesting as the SPB is embedded in the nuclear membrane, suggesting these forced interactions may perturb the composition of the nuclear membrane. There may also be a link to SPB duplication as deletion of *SPO7*, a regulator of phospholipid biosynthesis has been found to suppress the mono-polar phenotype of *MPS3* mutants (Witkin et al. (2010)). I found significant enrichment for the microtubule nucleation process term in the

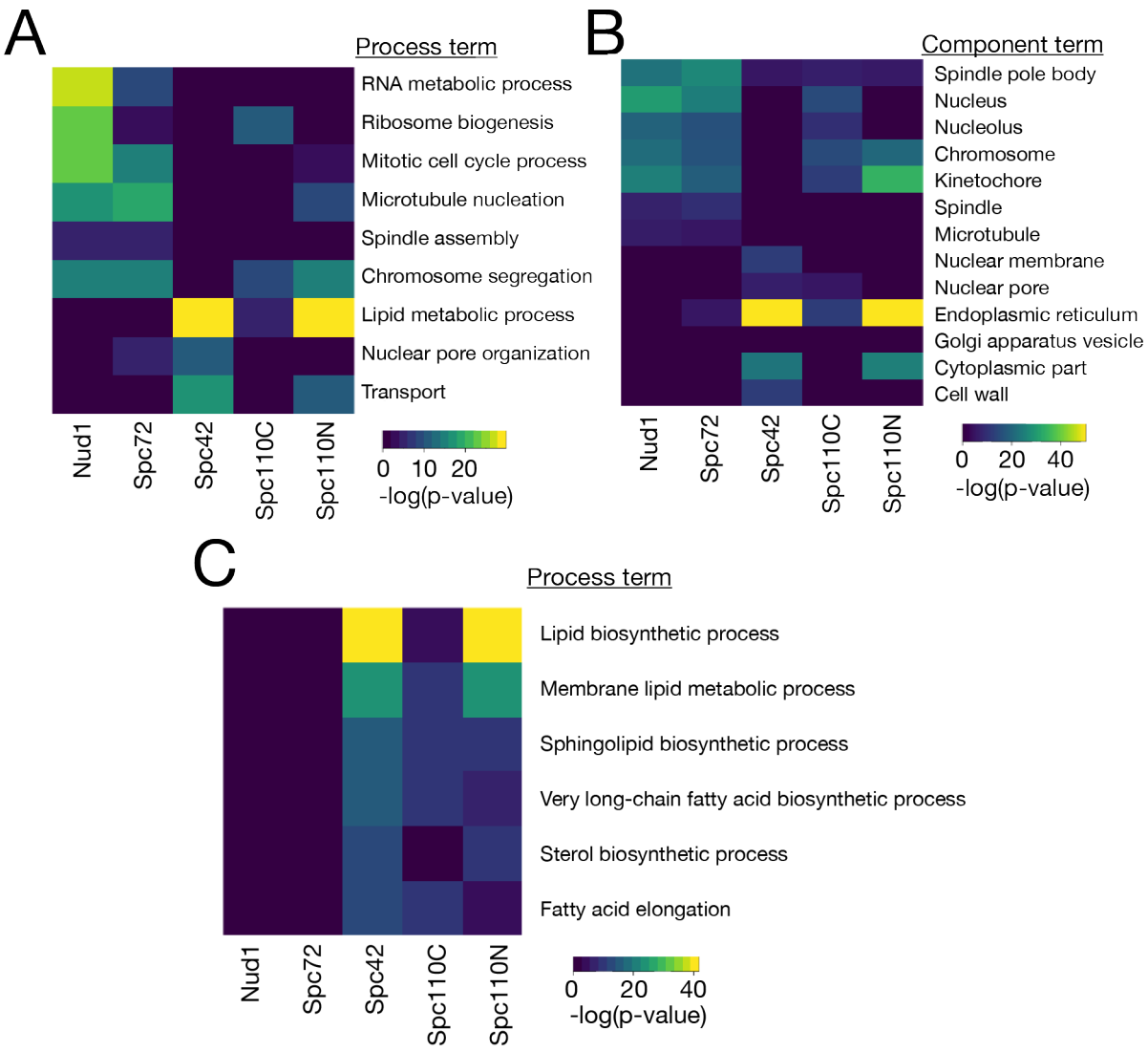

Figure 3.8: GO analysis of SPB SPI screens, performed using the entire, ranked dataset. A: Heatmap of process GO analysis, dark blue tiles represent no significant enrichment while the lighter colours represent significant enrichment, with warmer tones representing higher p-values. B: Heatmap of component GO analysis. C: Heatmap of lipid synthesis process GO terms.

Nud1, Spc72 and Spc110N screens, which are also the proteins closest to the sites of microtubule nucleation. All screens, except for Spc42, are significantly enriched for components of the chromosome and the kinetochore as well as proteins involed in chromosome segregation. Yeast-two-hybrid screens have identified physical interactions between kinetochore components and the SPB (Wong et al. (2007)), suggesting these may be physiologically relevant interactions.

The MEN is known to be regulated from the SPB, with Spc72 and Nud1 being the primary scaffold for MEN proteins (Scarfone and Piatti (2015)). These screens were enriched for proteins involved in the mitotic cell cycle process. The MEN proteins Cdc15, Mob1, Dbf2, Cdc14 and, PP2A scaffold subunit, Tpd3, were validated hits in the Nud1 screen along with Kin4 in the Spc72 screen.

The hits from the Spc42 screen are enriched for components of the nuclear pore and proteins involved in nuclear pore organization (Figure 3.8). These interactions overlap with known genetic interactions, for example Nup157 was a SPI with Spc42 and *nup157*$\triangle$ suppresses the *spc42-11* mutation (Witkin et al. (2010)). It has been proposed that nuclear pore proteins play a role in SPB duplication and insertion so I decided to investigate these results further.

3.4 Synthetic Physical Interactions cause spindle pole body overduplication

3.4.1 Screen for SPB overduplication

I wanted to know if the growth defect caused by forced localization of nuclear pore proteins to the SPB was a consequence of SPB duplication errors leading to aberrant SPB copy-numbers. I decided to use fluorescence microscopy to screen for interactions causing abnormal number of SPBs. I chose 80 proteins to screen with the Spc42-GBP-RFP fusion. These proteins included most nuclear

Protein	Database Location	Screen LGR	Retest LGR
Apq12	ER	1.58	1.46
Crm1	Nucleus	1.23	0.54
Nic96	Nuclear Periphery	1.06	1.20
Nsp1	Nuclear Periphery	0.91	0.36
Nup133	Nuclear Periphery	0.23	0.27
Nup170	Nuclear Periphery	0.19	0.33
Pom34	Nuclear Periphery	0.46	0.77
YDL121C	ER	2.40	1.83
YJL021C*	Punctate	0.74	0.95
YPR071W	ER	0.42	0.82
YPR114W	ER	2.67	2.01

Table 3.1: Proteins identified in the microscopy screen for proteins that induce extra SPBs when forcibly relocalized to the SPB. * YJL021C overlaps the originally identified YJL020C ORF and so has been merged into YJL020C (Brachat et al., 2003), however the GFP strain shows a punctate fluorescent signal. Database locations were accessed from yeastgenome.org/.

pore proteins including SPIs, such as Nsp1, and non-SPIs, such as Nup170. I also included other proteins involved in regulation of SPB duplication, such as SPIN proteins, and uncharacterized proteins that were hits in the screen.

I used the SPA method to generate strains expressing *SPC42-GBP-RFP* as well as one of the query proteins tagged with GFP. I gathered cells to image directly from the agar plates used for the screen and counted the number of RFP foci per cell. In some cases, the RFP signal was not limited to the SPBs, for example in strains expressing GFP-tagged membrane proteins. However, in these cases there were still small regions of high RFP signal which were counted as foci. I identified 11 strains in which cells containing 3 or more foci were observed (Table 3.1). Although cells suggestive of a mono-polar phenotype were observed, we could not rule out the possibility of further SPBs due to the slow-folding nature of RFP (Pereira et al. (2001)).

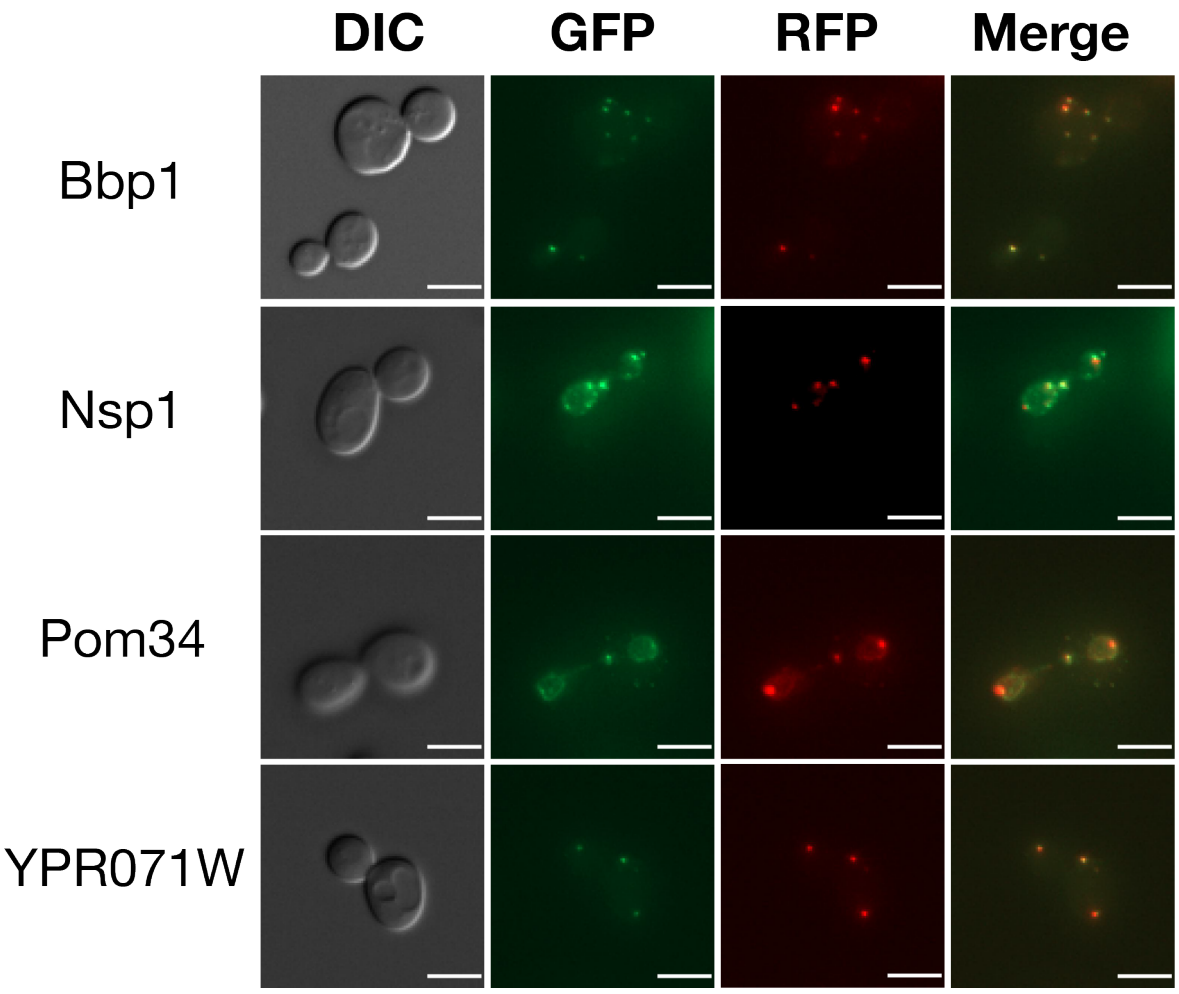

Figure 3.9: Representative images of Bbp1, Nsp1, Pom34 and YPR071W -GFP strains expressing Spc42-GBP-RFP from a plasmid, each showing more than two RFP foci, interpreted as indicative of overduplication of SPBs. All scale bars are 5μm.

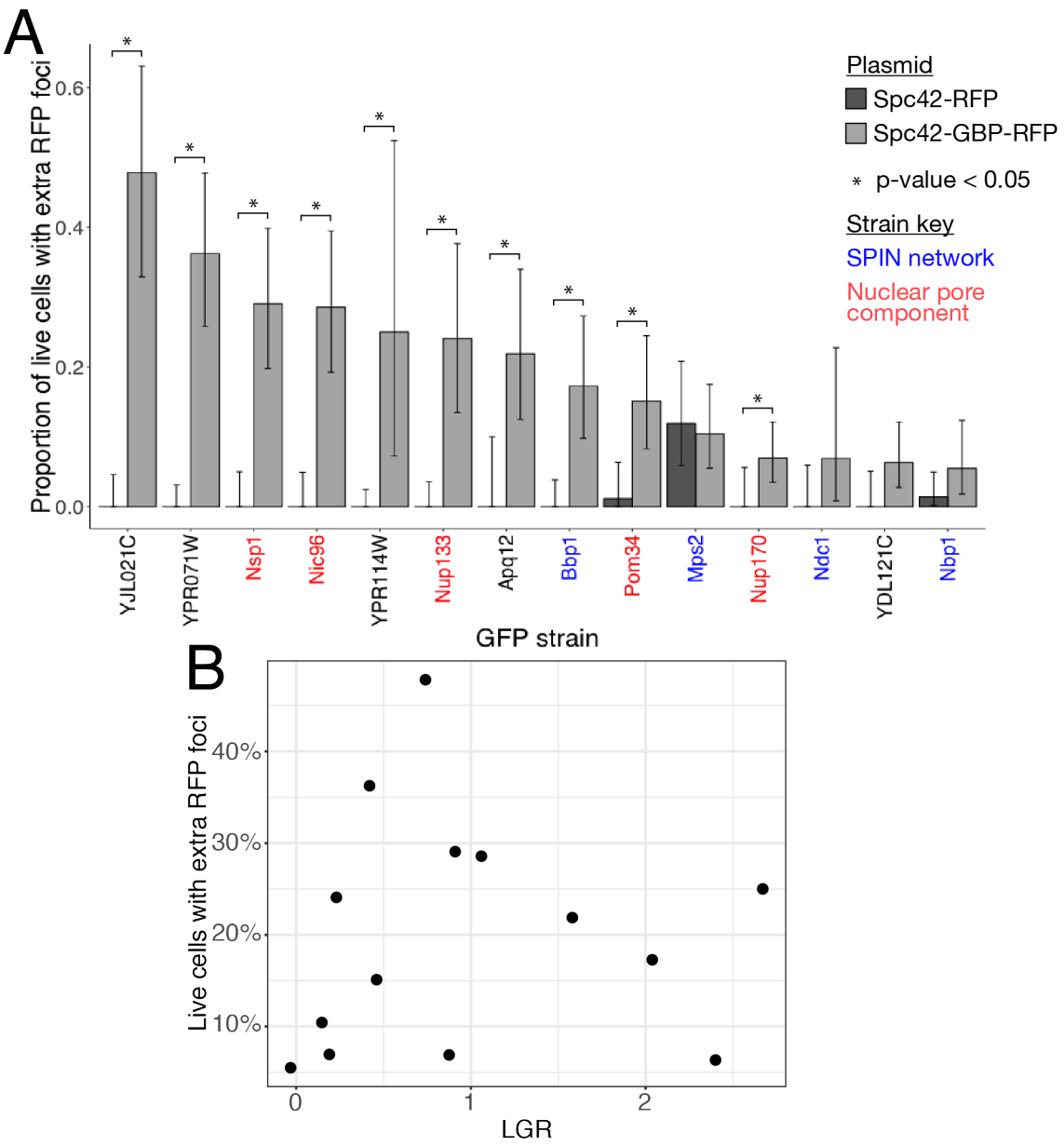

Figure 3.10: Quantification of SPIs causing additional RFP foci. A: The percentage of living cells showing more than two RFP foci, three images were captured for each strain. Error bars show 95% confidence intervals calculated with the Clopper-Pearson exact method; p-values were calculated using Fisher's exact test. B: The percentage of cells with additional foci against the LGR from the original SPI screen with Spc42. The two variables show no statistical correlation (Kendall's $\tau = 0.12$, Kendall rank correlation test $p = 0.59$).

3.4.2 Quantification of SPB overduplication

I found that screening strains directly from the plate meant that only a limited number of cells could be imaged, especially in already slow growing SPI strains. Therefore I transformed the 11 GFP strains identified in the screen, along with the four SPIN proteins, with the plasmid. I could establish colonies of all strains except *CRM1-GFP*. I grew these strains in liquid culture before imaging, allowing larger quantities of cells to be examined. I found cells showing evidence of SPB overduplication in all of the strains tested. I counted these cells and calculated the proportion of living cells with > 2 RFP foci (Figure 3.10A). As a control, I performed the same analysis with a plasmid expressing *SPC42-RFP*. I found a statistically significant proportion of cells with extra RFP foci in all strains tested except Mps2, Nbp1, Ndc1 and YDL121C. In the Mps2-GFP strain I observed cells with additional RFP foci at a similar level with both the experimental and control plasmid, suggesting the *MPS2-GFP* mutation alone causes SPB overduplication. Note that this analysis contains results for the protein denoted by its ORF, *YJL021C*, but this ORF was found to overlap with *YJL020C*, suggesting this growth phenotype could be in part due to disruption of the *YJL020C* ORF (Brachat et al. (2003)).

3.4.3 Forced localization at the SPB can induce SPB overduplication

In the above experiment, I demonstrated that forced interaction between various proteins and Spc42 lead to cells containing more than 2 RFP foci, suggesting cells experience SPB overduplication. However, due to the binding between Spc42-GBP and the GFP-tagged protein, it is unclear whether the RFP foci represent true SPBs or just accumulations of the Spc42-GBP-RFP fusion protein. In order to test whether the foci resulting from some of these interactions are true SPBs, I

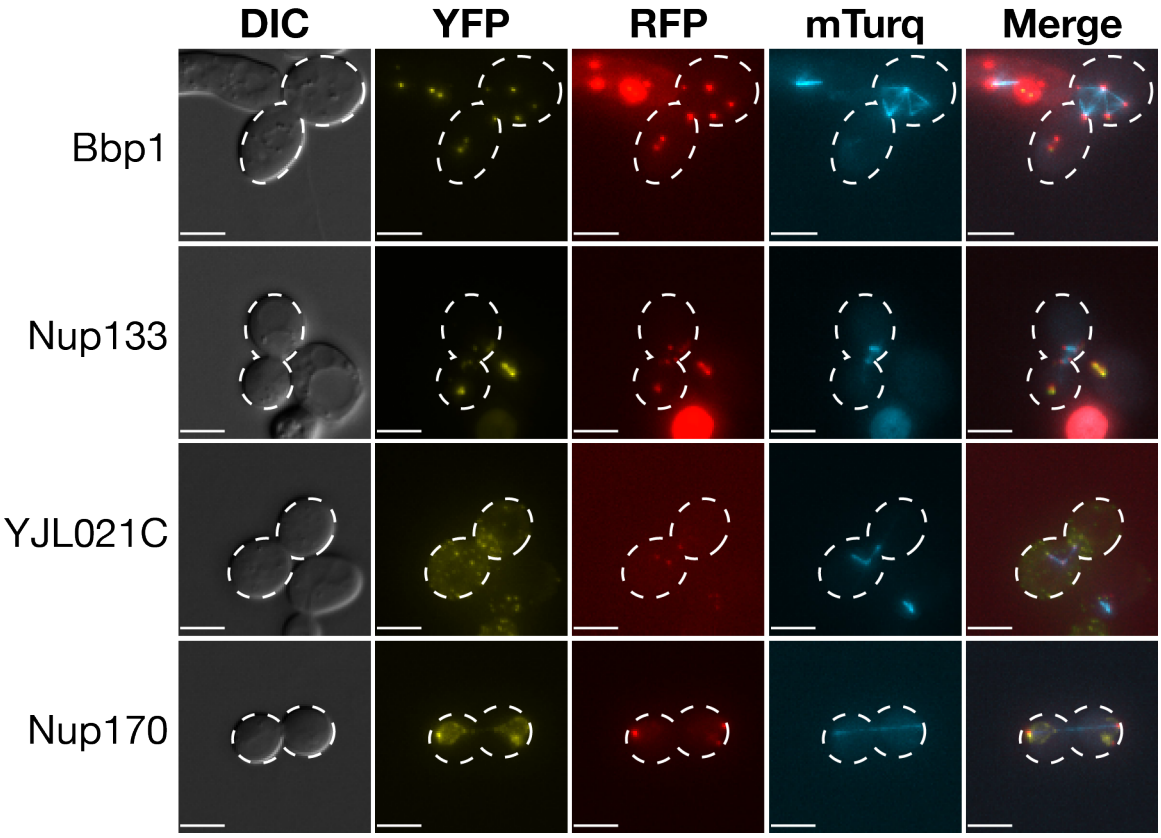

Figure 3.11: SPIs inducing formation of multi-polar spindles. Representative microscope images show spindle morphology in the YFP strains (labeled on left), expressing *SPC42-GBP-RFP*, the spindle is labeled by mTurq-Tub1. Multi-polar spindle are observed in all strains except *NUP170-YFP*. Scale bars are 5μm.

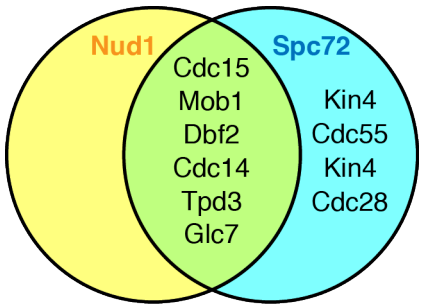

Figure 3.12: Venn diagram showing overlap between MEN hits from the Nud1 and Spc72 screens. Hits are defined using the $L_{q,0.5}$ cutoff. Note that Kin4 was automatically excluded from the Nud1 screen data, and Tem1-GFP was found to be missing from the GFP collection used for screening.

created *BBP1-YFP*, *NUP133-YFP*, *NUP170-YFP* and *YJL021C-YFP* strains and introduced an mTurq-Tub1 marker. GBP binds YFP but not mTurq, meaning that in these strains I could examine the microtubule morphology. I found that each of these strains, except for *NUP170-YFP*, showed evidence of multi-polar spindles (Figure 3.11). This suggests that the RFP foci in these three strains represent SPBs capable of nucleating microtubules which can participate in spindle formation.

3.5 Synthetic physical interaction screens with mitotic exit network proteins

The MEN coordinates late mitotic events from the SPB (Figure 1.4). Previous studies have shown that forced localization of MEN proteins at the SPB can disrupt MEN signalling, either promoting mitotic exit prematurely as with Cdc15 (Rock and Amon (2011)) or inhibiting mitotic exit as with Kin4 (Maekawa et al. (2007)). MEN proteins localize to the cytoplasmic face of the SPB and physically interact with both Nud1 and Spc72. I found a significant enrichment for the GO term “Mitotic Cell Cycle Process” in both the Nud1 screen ($p = 9 \times 10^{-14}$) and the Spc72 screen ($p = 3 \times 10^{-9}$). Upon inspection, I noticed that several MEN proteins

were identified as hits in these screens, based on the $L_{q,0.5}$ cutoff, and that many were identified in both the Nud1 and Spc72 screens (Figure 3.12). Glc7 is the catalytic subunit of the PP1 (Protein Phosphatase 1) holoenzyme. Although PP1 is not currently thought of as a MEN protein, it is known to play a role in control of mitotic events at the kinetochore in budding yeast and to regulate mitotic exit in other organisms, including *S. pombe* (De Wulf et al. (2009)). I decided to include it in this analysis as a potential as yet uncharacterized member of the MEN.

I was interested to note that Kin4 was a hit with Spc72 and not Nud1. However, on further inspection I found that Kin4 had been automatically excluded from the Nud1 screen by the ScreenMill analysis software. Furthermore, I noted that Tem1 was not a hit with either screen. Microscopy of the “Tem1-GFP" strain from our GFP library revealed that it had been contaminated with another GFP strain. The library copy showed a GFP signal localised to the cell membrane, rather than the SPB localization characteristic of Tem1, meaning that Tem1 had effectively not been tested in the original screen. I constructed a *TEM1-GFP::HISMX* strain and used this in the following mini-screens.

Therefore, I decided to perform a mini-screen focussing on MEN proteins, similar to the validation and nuclear pore screens.

3.5.1 Mitotic exit network mini-screen with Nud1 and Spc72

I assembled a single plate of GFP strains for the mini-screen, consisting of MEN proteins, some control non-MEN proteins and GFP-free controls. Additionally, I constructed *kar9*Δ::*KANMX* versions of the GFP strains by transformation of the GFP strains. Kar9 is a protein that, in parallel to Dyn1, promotes alignment of the mitotic spindle with the mother-bud axis. Cells with the *kar9*Δ mutation spend considerably longer with a misaligned spindle (Miller and Rose (1998a)). This means that SPoC mutants, which can exit mitosis with a misaligned spindle, will be more likely to segregate the chromosomes within the mother compartment,

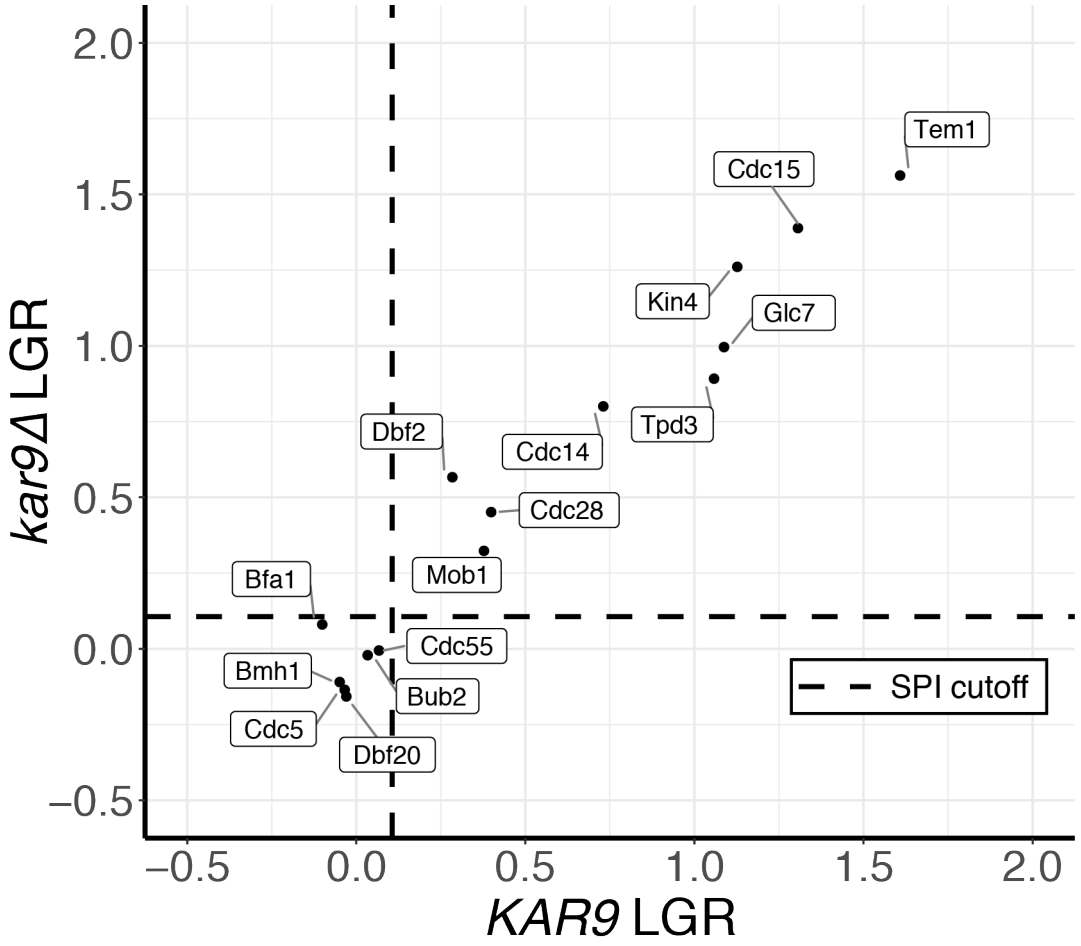

Figure 3.13: LGRs from the *NUD1-GBP* mini-screen for MEN proteins. Each point shows the LGRs for both *KAR9* (x-axis) and *kar9*Δ (y-axis) strains for the given GFP-tagged protein. Cutoffs are determined as the maximum of either *KAR9* or *kar9*Δ GFP-free control strains respectively.

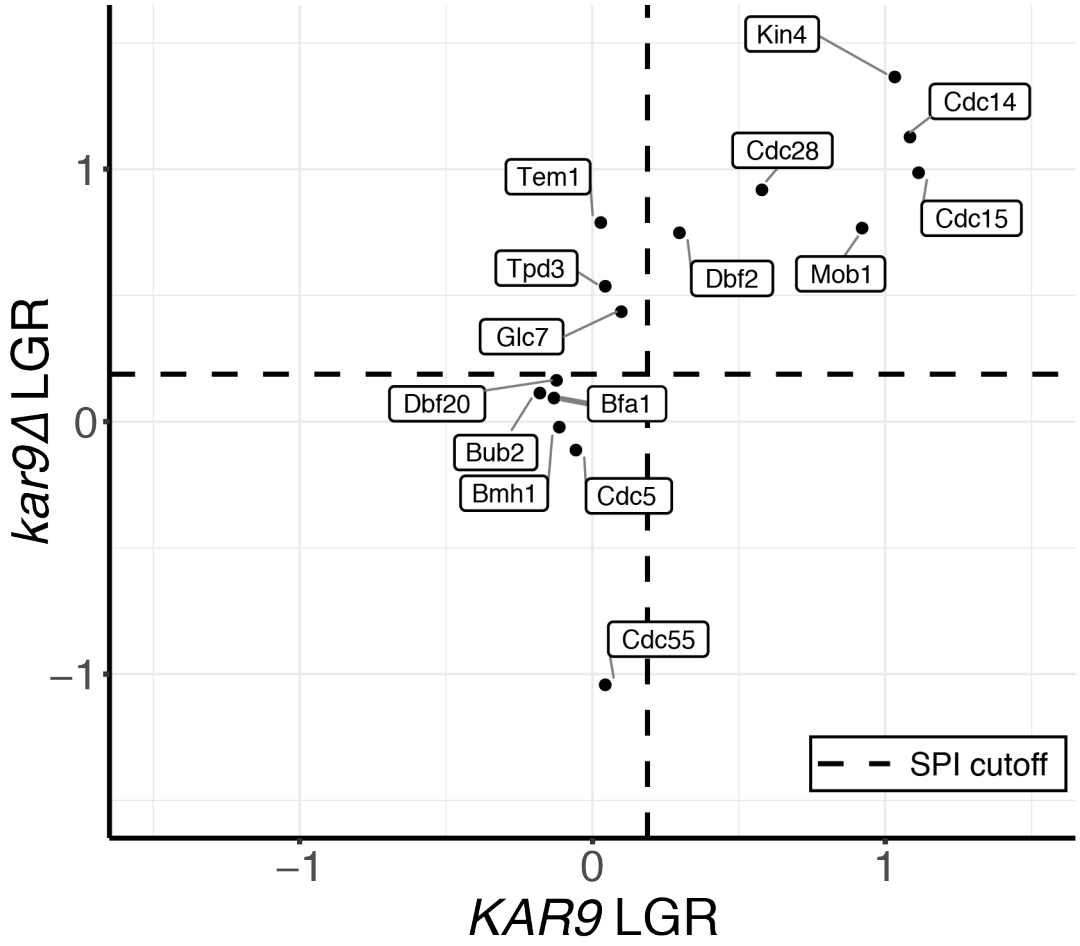

Figure 3.14: LGRs from the *Spc72-GBP* mini-screen for MEN proteins. Each point shows the LGRs for both *KAR9* (x-axis) and *kar9*Δ (y-axis) strains for the given GFP-tagged protein. Cutoffs are determined as the maximum of either *KAR9* or *kar9*Δ GFP-free control strains respectively.

leading to cell death. Therefore, SPoC mutants, such as *bfa1*Δ, which are not lethal alone, are synthetic lethal with *kar9*Δ (Pereira et al. (2000)). I reasoned that if forced localization of some MEN proteins to the SPB interfered with the SPoC then the growth defect caused by this interaction would be enhanced in a *kar9*Δ strain. The plate also includes a *kar9*Δ, GFP-free control.

Unexpectedly, I found that the LGRs of *KAR9* and *kar9*Δ strains were highly correlated in the Nud1 mini-screen (Figure 3.13). In all cases I tested, proteins were SPIs with Nud1 in both the presence and absence of *KAR9* or neither. Additionally, both Tem1 and Kin4, which were not included in my previous analysis, were revealed to have strong SPIs with Nud1 in this analysis. This mini-screen demonstrates the strong impact on growth caused by forced interaction of MEN proteins with Nud1. The fact that no growth defects were enhanced by deletion of *KAR9* indicates that either no forced interactions inhibit SPoC activity or that other growth inhibiting effects are dominant over this effect.

In comparison, I found that forced interaction of Tem1, Tpd3 and Glc7 with Spc72 caused lethality only in the absence of Kar9 (Figure 3.14). However, it worth noting that both Glc7 and Tpd3 were identified as SPIs in the original genome-wide screen, which was performed in a *KAR9* background. Other SPIs with Spc72, such as Cdc15, were showed growth defects with and without the *kar9*Δ mutation. Cdc55 appears to enhance the growth in the *kar9*Δ background, although again it worth noting that it failed to reproduce the SPI phenotype in the *KAR9* background that was identified in the original screen.

These screens contain valuable information about how and when forced localization of MEN proteins at the SPB causes a growth defect. However, they only tell us about growth. I wanted to develop a conditional system to explore precisely the impact of these forced interactions on cell cycle progression.

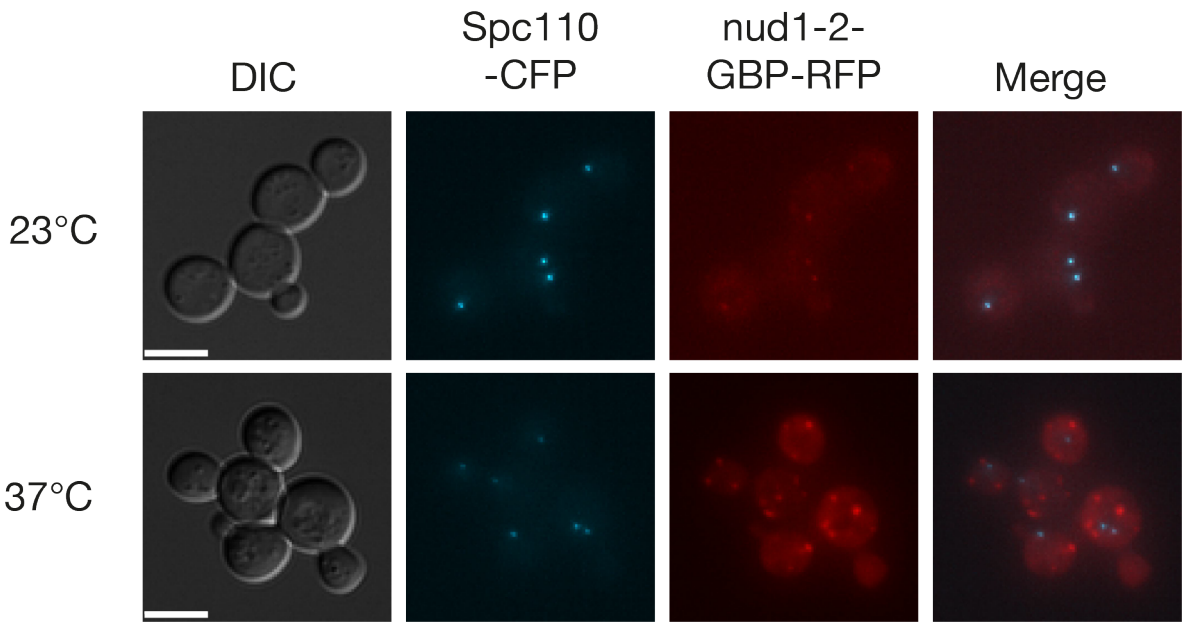

Figure 3.15: Representative images of *SPC110-CFP* cells expressing *nud1-2-GBP-RFP* from a plasmid at $23℃$ and $37℃$. Scale bars are $5\mu m$.

3.5.2 *nud1-2-GBP* screen

The *NUD1* gene has a temperature senstive allele, *nud1-2*, whose protein product localizes to the SPB in a temperature dependent manner (Gruneberg et al. (2000)). At $23℃$, nud1-2 localizes to the SPB as wild type Nud1 does, but at $37℃$ it detaches from the SPB. I constructed a plasmid expressing *nud1-2-GBP-RFP* and tested its localization in a *SPC110-CFP* strain. I found the pattern of localization generally matched that described by Gruneberg et al. (2000) (Figure 3.15), although I also observed distinct RFP puncta, distinct from the SPBs, throughout the cell at the higher temperature. I reasoned that I could use this approach to regulate localization at the SPB through control of temperature. At low temperatures, the nud1-2-GBP protein would localize at the SPB, bringing any GFP-tagged protein with it. At high temperatures, it would disperse into the cytoplasm, allowing the GFP-tagged protein to localize as in wild type cells. Note this would have the opposite behaviour to a standard temperature sensitive mutant, as SPIs would be dead at low temperature but grow normally high temperature.

Therefore I decided to repeat the screening process with the wild type Nud1 and nud1-2 GBP fusions at $23℃$, $30℃$ and $37℃$.

I performed the screens leaving the plates at each stage to grow at the specified temperature. I found that temperature did affect the strength of the Nud1 SPIs to some degree (Figure 3.16). This is probably due to the speed of growth at different temperatures. As I measured the ratio of colony sizes, if temperature affects the rate of growth of two strains in the same way then we would expect a larger divergence in growth at an optimal temperature, leading to a larger LGR. Generally, the LGR is highest at $30℃$, then $23℃$ and then $37℃$. In some cases, such as Cdc14 and Dbf2 the growth defect is completely suppressed at the higher temperature. The reason for this is not clear but may be because the fusion of these proteins to GFP disrupts their function at high temperatures, regardless of their localization, meaning the control colony is also small.

The suppression of SPIs at high temperature is more pronounced in the nud1-2 screen (Figure 3.16). In this case nearly all the SPIs are highly suppressed at $37℃$ but not $23℃$ or $30℃$. In particular cases, such as Dbf2, this approach shows potential, as they are very sick at the lower temperatures but grow reasonably well at high temperature. However, there are clearly significant differences in the behaviour of other strains. Bfa1 is not a SPI at any temperature with Nud1, but is with nud1-2, in a way that is suppressed at $37℃$. In addition, Tem1 is a strong SPI with Nud1 but is not a SPI at any temperature with nud1-2. I plotted the strains according to the LGR in the *KAR9* and *kar9*Δ background from the nud1-2 screen at $23℃$, as I did for the Nud1 and Spc72 screens (Figure 3.17). At $23℃$, the proteins are still forcibly recruited to the SPB. Tem1 is a SPI with nud1-2 only in the *kar9*Δ background, suggesting the interaction disrupts SPoC function. This is reminiscent of the Spc72 screen. However, unlike the Spc72 screen, both Tpd3 and Glc7 are not SPIs in the *kar9*Δ background. The Bfa1 SPI is also independent of the presence of Kar9. Altogether, *nud1-2* at $23℃$ behaves

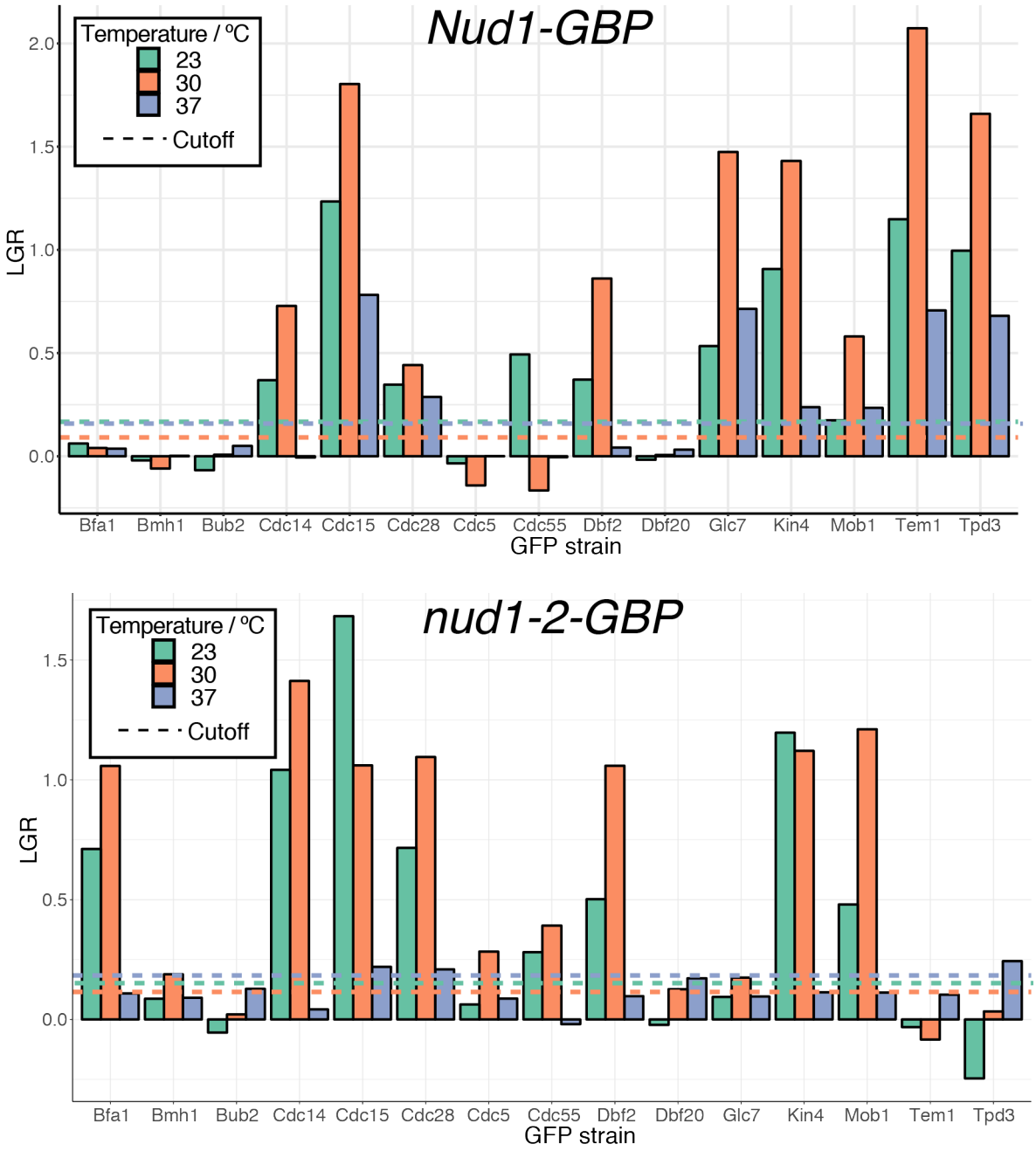

Figure 3.16: LGRs of *KAR9* MEN strains at $23\,℃$, $30\,℃$ and $37\,℃$ with both Nud1-GBP and nud1-2-GBP. Dashed lines show cutoffs for each temperature (indicated by the color of the line) as defined by the maximum of the *KAR9* GFP-free controls.

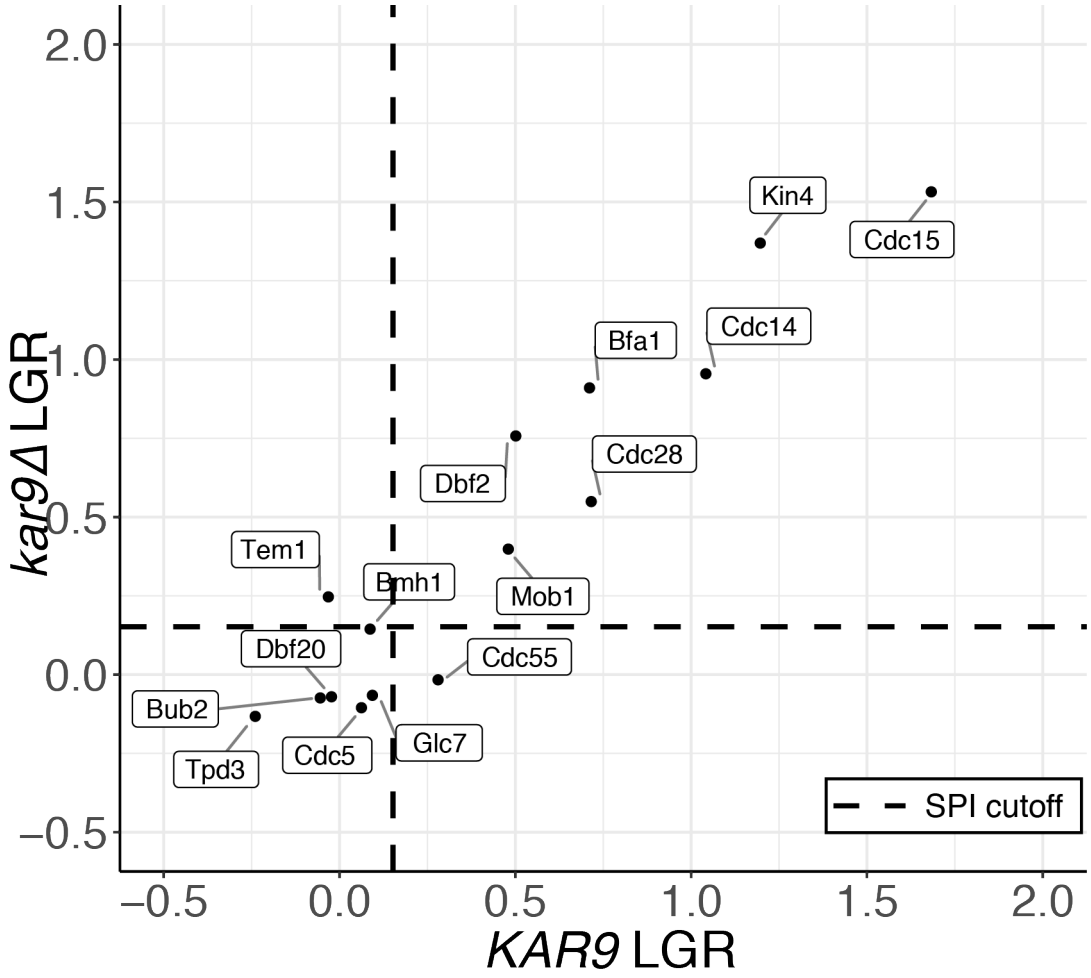

Figure 3.17: LGRs from the *nud1-2-GBP* mini-screen for MEN proteins. Each point shows the LGRs for both *KAR9* (x-axis) and *kar9*Δ (y-axis) strains for the given GFP-tagged protein. Cutoffs are determined as the maximum of either *KAR9* or *kar9*Δ GFP-free control strains respectively.

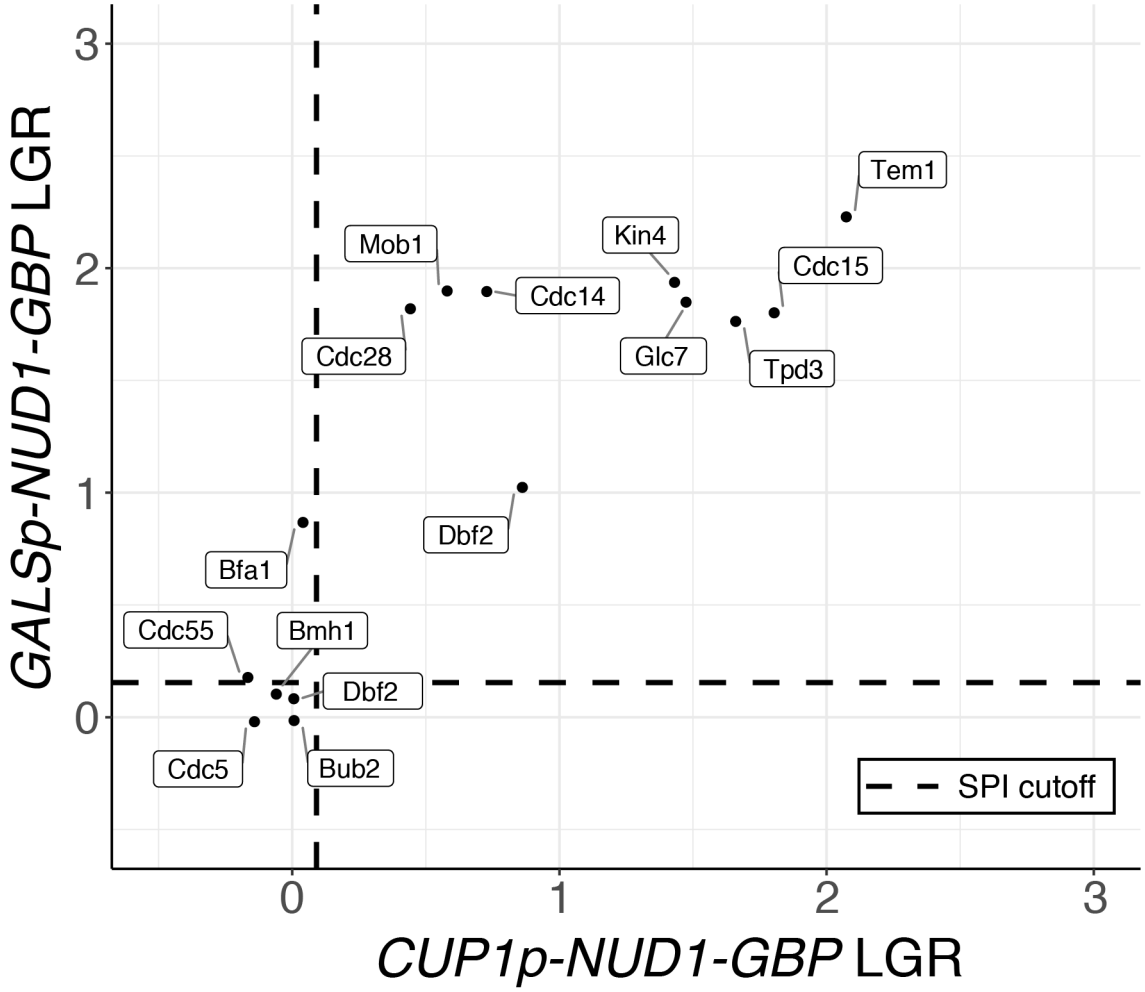

Figure 3.18: LGRs from the *CUP1p-NUD1-GBP* and *GALSp-NUD1-GBP* mini-screen for MEN proteins (all *KAR9*). Cutoffs are determined as the maximum of the *KAR9* GFP-free control strains in each screen respectively.

quite differently to Nud1. This offers an interesting insight into the scaffold specific effects of forced localization. However, it also limits the accuracy of the allele as a tool to conditionally study forced interactions with Nud1.

3.5.3 *GALSp-NUD1-GBP* screen

As an alternative to a temperature based conditional system, I tried expressing *NUD1-GBP* from the conditional *GALS* promoter. *GALSp* is a truncated version of the *GAL1* promoter, it still offers the conditionality of *GAL1p* but has lower overall transcriptional activity (Mumberg et al. (1994)). Nud1 overexpression is

not reported to cause lethality (Gruneberg et al. (2000)). However, *GAL1p* is an incredibly strong promoter so to limit off-target effects I decided to use the weaker promoter.

I repeated the mini-screen with the *GALSp-NUD1-GBP* plasmid and the *CUP1p-NUD1-GBP*. The SPA methodology relies on using galactose media to select against the conditional chromosomes from the donor strain, so the final stages of the screen are always performed on galactose. I compared the results of these screens (Figure 3.18). Generally speaking, the same proteins are hits in both screens. The LGRs of the hits are generally higher in the *GALSp-NUD1-GBP* screen, perhaps because the levels of Nud1-GBP are higher. Bfa1 was not a hit in the *CUP1p-NUD1-GBP* screen but is in the *GALSp-NUD1-GBP* screen. This may be a dose-dependent effect. Overall, the *GALSp* driven system seems to represent the behaviour of the original system more faithfully than the *nud1-2*, temperature-controlled system.

3.5.4 Forced interaction of Cdc28 with Nud1 prevents mitotic entry

Cdc28 is the catalytic subunit of the CDK complex, which is known to play role in the MEN, inhibiting Cdc15 and Mob1. However, CDK has many roles in the cell cycle. I wanted to know whether the SPI between Cdc28 and Nud1 was the result of MEN inhibition or had a different mechanism. I used the *GALS-NUD1-GBP* plasmid to conditionally recruit Cdc28 to the SPB. This worked as expected, the strain *GALS-NUD1-GBP CDC28-GFP* strain grows well on glucose, but grows poorly on galactose (Figure 3.19A). I examined these cells using fluorescence microscopy, and found that on galactose a large proportion of these cells show a “long bud” phenotype (Figure 3.19B). These cells arrest with reasonably short inter-SPB distances ($< 3\mu m$) and abnormally elongated buds. If the MEN were

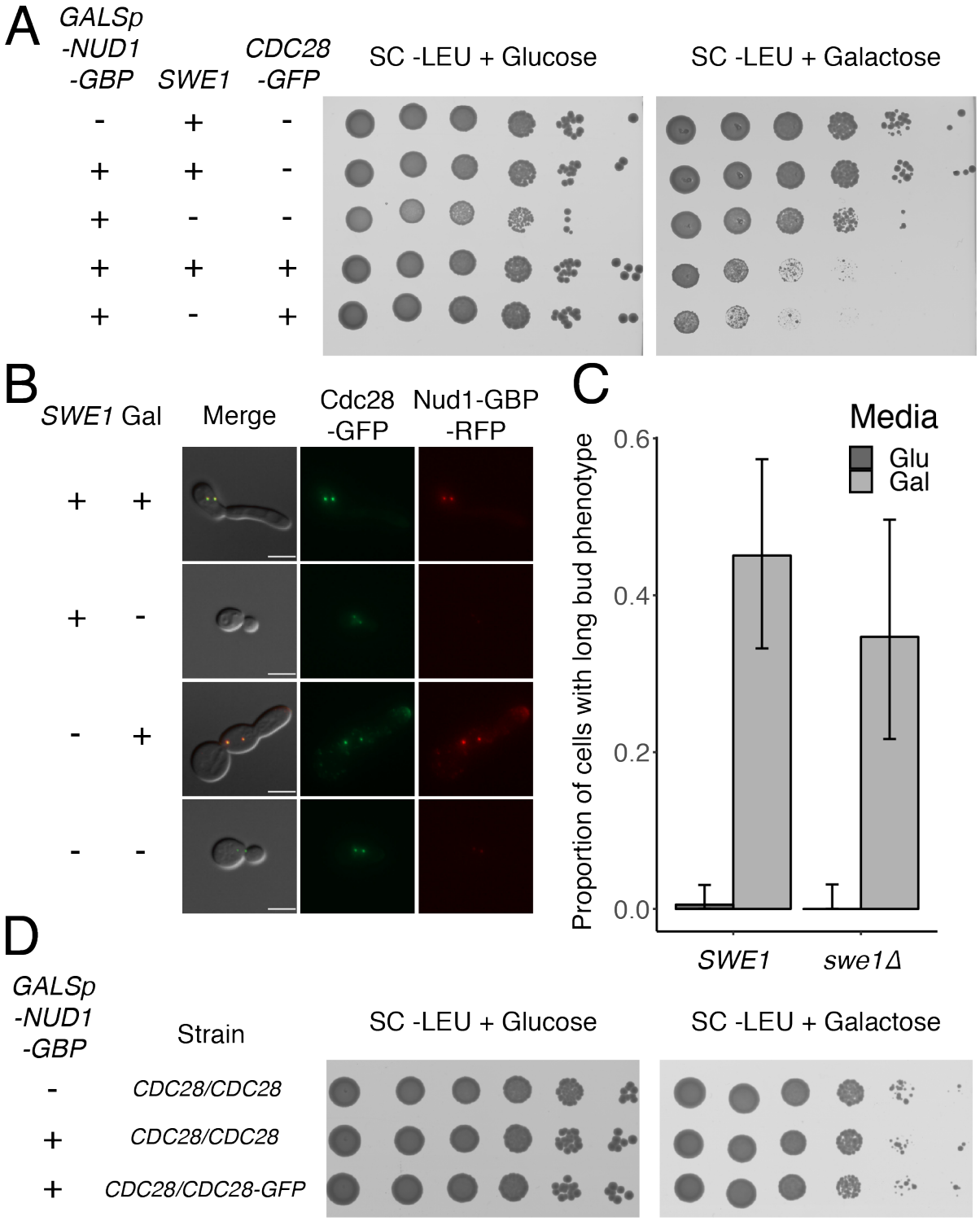

Figure 3.19: Caption located on next page.

Figure 3.19: A: Forced interaction of Cdc28 and Nud1 causes lethality, independently of Swe1. B: Representative images of *GALSp-NUD1-GBP CDC28-GFP* strains. Cells were grown overnight in raffinose media before being diluted into either glucose or galactose media and were grown for 8 hours before imaging. Nud1-GBP-RFP signal is visible in galactose but not glucose media. Scale bars show $5\mu m$. C: Roughly 40% of *GALSp-NUD1-GBP CDC28-GFP* cells in galactose media show a long bud phenotype, while $< 1\%$ show this phenotype in glucose media, independently of *SWE1*. Error bars show 95% confidence intervals calculated using the two-sided Clopper-Pearson exact method. D: The growth defect caused by forced interaction of Cdc28 and Nud1 is suppressed in a heterozygous *CDC28-GFP* strain.

inhibited, we would expect cells to arrest in anaphase with extended spindles ($>$ $3\mu m$ between SPBs). The observed phenotype is reminiscent of the morphology of cells with mitotic entry defects (Lew and Reed (1993)). This phenotype can sometimes be suppressed by deletion of the CDK regulator, *SWE1*, for example in the case of *cdc55*Δ (Rossio and Yoshida (2011)). I tested whether deletion of *SWE1* could suppress the SPI between Nud1 and Cdc28. I found that it could not suppress either the growth defect (Figure 3.19A) or the elongated bud phenotype (Figure 3.19B&C).

Nud1 is on the cytoplasmic face of the SPB so I reasoned that forced binding of Cdc28 to Nud1 may prevent entry of CDK into the nucleus, preventing mitotic entry. Notably, Cdc28 was not a SPI with the N-terminal Spc110 GBP fusion, which is on the nuclear face of the SPB (Supplementary File 5). To test this hypothesis I constructed a heterozygous *CDC28/CDC28-GFP* diploid strain and transformed it with the *GALSp-NUD1-GBP* plasmid. In this strain, the GFP-tagged version of Cdc28 can be forced to localize to the SPB, but the untagged version can still enter the nucleus. This strain showed no growth defect, relative to controls, on galactose (Figure 3.19D). This suggests that the SPI between Nud1 and Cdc28 is caused by a mitotic entry defect cause by prevention of nuclear localization of the CDK complex.

3.6 Discussion

In this chapter I have described the results of 5 SPI screens, systematically forcing proteins to localize to different parts of the SPB. These screens help to answer the first of the key questions set by the project: which proteins are regulated through interactions with the SPB? The screening data has lead to the identification of a number of categories of proteins which cause problems for the cell. These include proteins involved in SPB duplication and members of the MEN.

In this section I will first discuss the novel statistical tools I have used to analyze the SPI data and will then move on to the biological implications of these findings.

3.6.1 Mixture models for SPI data

The first statistical approach I used to analyze the SPI data was to apply a Z-score. While Z-scores are commonly used, they rely on the assumption that the data is normally distributed. I have shown that the SPI LGR data is very poorly fit by a normal distribution, especially when the screen has many hits. To address this shortcoming, I developed an empirical Bayes approach to analyze SPI screens. This approach lead to the construction of a number of tools to determine the significance of results, including the probability of inclusion in the hit peak and the probability of validation. The $L_{q,0.5}$ cutoff offers significant advantages over the L_Z cutoff. Using the $L_{q,0.5}$ cutoff gives a greater variation in the number of hits between screens, meaning that it is not just taking the top ~ 200 LGRs in the screen, as when using L_Z. Some interactions, for example Nup133 with Spc42, were not hits when using L_Z, but were later shown to have a relevant phenotype. This shows that by using the higher cutoff from the Z-score approach, biologically interesting interactions were being missed.

Name	Statistical model	Basis
L_Z	Normal	p-value
$L_{q,0.5}$	Mixture	Probability of inclusion in hit peak
$L_{p,0.05}$	Mixture	p-value, using central peak as null model
$L_{V,0.2}$	Mixture	Probability of validation

Table 3.2: Table of cutoffs.

Comparing cutoffs

I have used the empirical Bayes approach to define 3 new thresholds that could be used to define hits in SPI screens (Table 3.2). I used the $L_{q,0.05}$ cutoff in this study and have demonstrated it performs preferably to the Z-score cutoff L_Z. One drawback to this metric is that it is not adjusted for multiple hypothesis testing. This is because standard methods for multiple hypothesis testing, such as FDR q-values (Benjamini and Hochberg (1995)) and Bonferroni adjustment, are based around adjusting p-values. As the $q(x)$ metric I define is not based on a p-value, these methods do not directly apply. I have also outlined a method to calculate p-values using the mixture model and multiple hypothesis adjustments can be applied to these to get an adjusted cutoff. Future work could be devoted to developing adjustments to the $q(x)$ metric to account for multiple hypothesis testing. These alternative cutoffs look at the data in different ways and so may be appropriate in different situations.

Improvements to SPI screening

Although the empirical Bayes approach I have described is an improvement over Z-scores, it has its limitations. We found that the LGRs from some screens did not have well defined hit peaks. In these cases a normal model is more appropriate. We also found that when variance was too high, the screens were generally not reproducible. Baryshnikova et al. (2010) found evidence of strong batch effects in their genetic interaction screens, likely resulting from subtle difference in media composition or incubator conditions. They use linear discriminant analysis to

calculate “batch signatures” which can be used to adjust colony size measurements. Zackrisson et al. (2016) found that the spatial organisation of colonies on a plate could influence their growth rate. They accounted for this effect by local normalization across the plate. Zackrisson et al. (2016) also improved the precision of their measurements by scanning plates over time, allowing them to plot colony growth curves, and infer growth rates from the curve. Therefore, improvements to the methodology used to conduct SPI screens could also improve their reproducibility and precision.

3.6.2 The SPB is especially sensitive to forced localization

I noticed early on that the SPI screens with the SPB seemed to have many hits. In addition to the thresholds produced by the mixture models, these models have 5 independent and interpretable parameters. I compared these parameters for the SPB screens and the screens of Berry et al. (2016). This backed up my suspicions that the SPB is especially sensitive to forced localization. The root cause of this sensitivity may be simply that the SPB is involved in many processes. Certainly proteins related to many of its known roles, such as regulation of SPB duplication and mitotic exit, were identified in the screen. However, many other proteins such as those involved in lipid synthesis or kinetochore proteins were also identified. Another explanation for the sensitivity may be that its position within the nuclear membrane means that forced localization of proteins to the SPB may affect the nuclear membrane as well. This might mean that recruiting sphingolipid synthases for example, may lead to increased sphingolipid incorporation locally in the region of membrane around the SPB. Another explanation for the sensitivity may be that the SPB is highly effective at sequestering proteins, preventing them from performing their function in other regions of the cell. This seems to be the explanation of the Nud1-Cdc28 interaction, as these cells seem unable to enter mitosis even in the absence of CDK inhibitor Swe1. The pheno-

type is then rescued in a diploid strain containing untagged Cdc28. The ability of the SPB to effectively sequester proteins may explain its use as a signalling scaffold during mitosis. This may be an interesting effect to exploit in synthetic signalling systems.

3.6.3 SPB overduplication

The current paradigm of SPB duplication is that it is tied to the chromosomal cell cycle by phospho-regulation of Sfi1 by CDK and Cdc14. Half-bridge extension is initiated by Cdc14 activity but cleavage of the bridge depends on CDK. This might suggest that tethering Cdc14 to the SPB could lead to perennially extended bridge structures and SPB overduplication. However, I found that Cdc14 had a SPI with Nud1 only, and Nud1 is an outer plaque protein located far from the half-bridge. This contrasts with a previously reported SPI screen with Cdc14-GBP, that identified Spc42-GFP as a hit that depended on the phosphatase activity of Cdc14 (Ólafsson and Thorpe (2015)).

I did find that recruitment of SPIN proteins and NPCs to the SPB caused growth defects, and that some of these interactions lead to additional Spc42-RFP foci, indicating SPB overduplication. In the cases of Bbp1, Nup133 and YJL021C, these foci were confirmed to act as MTOCs. If we accept that this result extends to the other interactions that lead to additional Spc42-RFP foci, then this has important implications for our understanding of SPB duplication. On the face of it, it seems unlikely that these interactions would be sufficient to break the once-per-cycle regulation of SPB duplication. Both SPIN proteins and the NPC are thought to act in the process of insertion of the SPB satellite. Even if recruitment of these proteins is a regulated aspect of insertion, according to the current model, their presence would not be sufficient to initiate half-bridge extension and satellite formation. There are two ways to explain these interactions. Firstly, it could be that the current model needs revision. If there was feedback between the insertion

machinery and the half-bridge then perhaps recruitment of this machinery could induce half-bridge extension in spite of external cues from CDK and Cdc14. Alternatively, it could be that another, as yet uncharacterized, SPB duplication pathway exists. In particular, it could be that recruitment of Spc42 to NPCs could "seed" new SPBs within the nuclear pore. These alternatives could be distinguished by their dependence on half-bridge components like Cdc31, which we would expect to still be essential in the first case but not in the second.

It is interesting to compare my findings to those of Witkin et al. (2010), who found that the requirement for functional Mps3 could be bypassed by deletion of $SPO7$ and either *NIC96* and *POM34* (among other genes). This puzzling result has lead to speculation that another SPB duplication pathway could exist (Witkin et al. (2010)), or that the role of SPIN proteins may be more indirect than previously thought, acting instead to recruit other proteins or regulate the membrane environment (Jaspersen and Ghosh (2012)). Altogether these results suggest connections between membrane environment, NPCs and SPB duplication which are not explained by the current model. My SPI screens were enriched for lipid biosynthesis proteins, so it would be interesting to investigate whether these strains were also deficient in regulation of SPB duplication.

These interactions show potential for use as a model system to explore the impact of aberrant MTOC number. Although I was able to demonstrate that some Spc42-RFP foci resulting from SPIs with the SPB acted as MTOCs, I only tested a subset of the strains showing additional foci. This analysis will need to be extended to the rest of the strains. In order to act as a useful system to explore the impact of increased MTOC number, some optimisation will be required. It would be ideal to both increase the proportion of cells displaying the phenotype and to make the system inducible, in order to minimise the likely chromosomal instability of these strains. Currently the only yeast mutants with aberrant SPB copy-number are either cell cycle mutants with pleiotropic phenotypes (such as

CDC5 overexpression (Song et al. (2000))) or the *sfi1-C4A* mutation, which is also deficient in SPB separation (Avena et al. (2014)). Therefore, if the stated optimisation steps are feasible, this system would have great potential to explore the impact of additional MTOCs. Centrosome overduplication is a characteristic of cancer cells but cancer cells generally manage to assemble a bipolar spindle despite having multiple MTOCs (Nigg (2006)). This is of interest both in terms of understanding the basic biology of cancer but also to investigate potential drug targets. Determining the factors required for cells to survive with extra MTOCs may open up alternative avenues for cancer therapy.

3.6.4 SPIs between MEN proteins and the SPB

I have established SPIs between a number of MEN proteins and Nud1 or Spc72, which are the scaffolds for the MEN. I also tested these interactions in a *kar9*Δ background, as MEN hyperactivation is generally not lethal except in the absence of *KAR9* or *DYN1*. A particularly interesting result is the behaviour of Tem1, which is always a SPI with Nud1, but not with nud1-2 even at low temperature, and with Spc72 only in the absence *KAR9*. This suggests a degree of scaffold-dependent behaviour in Tem1's regulation. Caydasi et al. (2012) argue that there are two pools of Tem1 at the SPB: one which localizes through interaction with Bub2-Bfa1 and another that localizes independently. Physical interactions between Bfa1 and both Nud1 and Spc72 have been detected by FRET (Gryaznova et al. (2016)), but this assay has not been repeated with Tem1 so it is unclear which of these scaffolds is responsible for the Bub2-Bfa1 independent localization of Tem1. Valerio-Santiago and Monje-Casas (2011) used a Cnm67-Tem1 fusion to induce localization of Tem1 at the SPB however my results indicate that the behaviour they observe may depend on the choice of Cnm67 as the scaffold at the SPB. Rock et al. (2013) showed that Nud1 itself is a target of the MEN pathway and phosphorylation of Nud1 by Cdc15 is required for loading of Mob1-

Dbf2. My results provide further evidence that Nud1 may act as more than just a passive scaffold but may contribute to regulation of the MEN actively.

The PP2A scaffold protein Tpd3 was identified as a SPI with Nud1 as well as with Spc72 in the absence *KAR9* (although it is worth noting it was identified as a SPI in the Spc72 screen). PP2A-Cdc55 has a well established role in the FEAR network and PP2A-Rts1 is known to be required for Kin4 localization at the SPB. However there is also evidence that PP2A-Cdc55 regulates Bfa1 and Mob1 (Baro et al. (2013, 2018); Touati et al. (2019)), although genetic evidence for these interactions is limited. The SPI between Tpd3 and Nud1 may be a good system to test the impact of PP2A on MEN regulation. It is also worth noting that the PP1 catalytic subunit, Glc7, has a similar pattern of SPIs to Tpd3. PP1 has established roles in mitotic exit in other organisms and a role for PP1 in mitotic exit in yeast, working through Bud14, has been described in a recent pre-print (Kocakaplan et al. (2020)).

It seems likely that forced localization of Tem1 and Cdc15 at the SPB lead to MEN hyperactivation and this phenotype is explored further in Chapter 4. However, why MEN hyperactivation would cause a growth defect is an interesting question. Other mutations that hyperactivate the MEN, such as deletion of *BFA1*, have no impact on fitness unless combined with mutations that delay spindle alignment, such as *kar9*$\triangle$. While Valerio-Santiago and Monje-Casas (2011) found that a Cnm67-Tem1 fusion was not lethal, Rock and Amon (2011) found that a Cnm67-Cdc15 fusion was highly toxic and they could only express it from a repressed *GAL1* promoter. There are two reasons that forced recruitment of these proteins at the SPB could cause growth defects. The first is that forced localization of MEN proteins could cause MEN activation outside of mitosis. This could prevent Cdc14 re-sequestration, prohibiting cellular events in G1- and S-phase and early mitosis. Cdc14 has a tendency to undergo cycles of release and re-sequestration, so it is possible that these SPIs could cause bursty release of

Cdc14 throughout the cell cycle. This would lead to a pleiotropic phenotype. This would be in contrast to mutants such as *bfa1*Δ, in which Cdc14 release is still restricted to mitosis. The second reason is that forced localization may prevent movement of these proteins to other regions of the cell. It has been established that a Mob1-Nud1 fusion is lethal because it prevents Mob1 from localizing to the nucleus to release Cdc14 (Rock et al. (2013)). In a recent paper, Tamborrini et al. (2018) showed that forcing interaction between Cdc14 and Nud1 could rescue the cytokinesis defect of *DMA2* overexpression. Furthermore, Whalen et al. (2018) found that overexpression of *BFA1* could rescue the cytokinesis defect of *tem1*Δ *CDC15-UP* cells, suggesting roles for both Bfa1 and Tem1 in cytokinesis. While there is no characterised role for Cdc15 or Tem1 at any location other than the SPB yet, this could explain their SPIs with the SPB. Microscopy analysis of the SPI strains could be used to establish whether they show defects in cytokinesis.

3.6.5 Limitations of the SPI method

Throughout this chapter, I have described the results of SPI screens with the SPB. While a powerful tool for probing the effect of forced localization across the proteome, this method has its limitations.

A first criticism of the method is that it is not clear that the phenotypes observed arise as a specific result of forced interaction between query and target protein. It could be argued that fusion of SPB proteins to *RFP-GBP* could reduce their functionality. With the exception of Spc72, the target proteins are essential but as I have only used these fusions in strains bearing an endogeneous version of the SPB gene, I cannot rule out that these fusions are not functional. However, it is worth pointing out that each of N-terminal fusions used in this study are present in the GFP collection (Huh et al. (2003)), suggesting that they are tolerant to some degree of N-terminal tagging. A key argument against the view that these SPIs are non-specific is that most GFP strains are tolerant of these fusions

and only specific strains are sensitive. Therefore, at very worst it can be argued that these forced interactions are only detrimental to the fusion SPB proteins, and would not cause this phenotype if forced to interact with the wild type SPB protein.

A second criticism is that as I have introduced an additional copy of the SPB gene, under the control of the *CUP1* promoter, I have created a hybrid SPB containing both wild type and fusion proteins. This is problematic as it may impair SPB function and it also means that I have not recruited as much protein to the SPB as could be theoretically achieved if the wild type protein was not present. However, this second criticism really only shows that this method may miss interactions with the potential to cause a phenotype if more protein were recruited. This is supported by the fact that when I used the stronger *GALS* promoter in the MEN mini-screens, I found that the LGR of SPIs increased. A related issue is that the stoichiometry of GBP to GFP fusions will vary from one GFP strain to the next. In the cases of highly expressed proteins, it may only be a small proportion of the overall protein in the cell that is recruited to the SPB. Additionally, as I showed by fluorescence microscopy, only a proportion of strains actually show relocalization of GFP tagged protein to the SPB, and in some of these the relocalization is only partial. Again this limitation is only likely to prevent potential SPIs from causing a measurable growth defect. Overall, we can say that the method can identify specific interactions which cause a growth defect under these specific conditions of expression level.

A more profound criticism of using this approach to address the problem of which proteins are regulated at the SPB is that it does not necessarily show that these proteins are regulated at the SPB under physiological conditions. Indeed, I showed that the growth defect caused by forcing the sole copy of Cdc28 to interact with Nud1 is likely a result of sequestration of CDK outside of the nucleus, rather than an SPB-specific result. However, previous studies have shown that SPIs are enriched for physical interactions (Ólafsson and Thorpe (2015); Berry

et al. (2016)) suggesting that generally SPIs are caused by interactions that do occur under physiological conditions. It is also evident from my results that proteins involved in the same pathways and complexes respond cause SPIs with similar target proteins. Therefore I propose that SPI screens can help to answer the question of which proteins are regulated at the SPB. However, any specific interaction must be treated carefully and cross-referenced against other data, such as the protein localization screens of Huh et al. (2003).

3.6.6 Summary

In this chapter, I have presented the results of several genome-wide screens exploring the impact of forced localization at the SPB, and their follow-up. I found that the SPB is especially sensitive to forced localization of proteins. The central plaque protein is sensitive to forced localization of nuclear pore and SPB duplication proteins, and I showed that some of these interactions results in abberant SPB numbers. I repeated my analysis with a smaller selection of MEN proteins, including in a *kar9*Δ background, with Spc72, Nud1 and nud1-2 target proteins. I found a number of site-specific effects, with the phenotypes of some proteins depending on the exact outer plaque protein they are forced to interact with. Finally, I tested a *GALSp* driven, conditional version of the SPI system. I used this conditional system to show that forced localization of Cdc28 at the outer plaque of the SPB can inhibit mitotic entry. These results are particularly relevant to the first aim of my project, to discover which proteins are regulated by interaction with the SPB. However, the follow up experiments have also gone some way to address the other aims, which are to uncover how and why proteins are regulated through localization at the SPB.

In the next chapter I will attempt to address the question of how localization at the SPB is used to regulate proteins by presenting a computational model of mitotic exit. In order to represent the effects of spatial organisation of the MEN, I

developed a compartmental logical modelling formalism. I use this framework to represent some of the SPIs between MEN proteins and the SPB and predict their phenotypes.

Chapter 4

Results 2: Spatio-temporal modelling of the Mitotic Exit Network

4.1 Introduction

In the previous chapter I described an approach to systematically recruit proteins to the SPB. I found that the screens with Spc72 and Nud1 were enriched for proteins involved in control of mitotic exit. This fits into an existing body of work showing that localization of MEN proteins at the SPB is necessary and can be sufficient for Cdc14 release. Therefore, I decided to turn my attention to the problem of understanding how localization of MEN proteins at the SPB functions as a regulatory mechanism.

The MEN, and the related FEAR network, regulate mitotic exit through control of Cdc14 phosphatase (see Figure 1.4). The core MEN proteins, namely Bub2-Bfa1, Tem1, Cdc15 and Dbf2-Mob1, all localize at the SPB. They integrate temporal (anaphase-specific) signals with spatial (spindle alignment) signals in order to restrict mitotic exit until the spindle is properly aligned and the cell has

finished metaphase. The FEAR pathway causes limited Cdc14 release in early anaphase, while this is insufficient to initiate mitotic exit, it feeds back to amplify MEN activity. When the MEN is fully active, Cdc14 is released throughout the cell, leading to mitotic exit and the initiation of cytokinesis.

In order to study this problem, I built a computational model of mitotic exit control in budding yeast. The lack of quantitative data on this network, lead me to use the logical modelling formalism. My first approach was to train a Boolean model against literature data using CellNOptR (Terfve et al. (2012)). The training was effective, resulting in a model capable of fitting 88% of the training dataset. However, it lead to a problem in model identifiability, with multiple optimal models found. More importantly, this approach could not represent spatial aspects of MEN regulation.

In order to overcome these limitations, I decided to hand-build a model using a novel formalism, which I call compartmental logical modelling. This new model format allows spatial regulation to be represented in a logical model. Using the compartmental logical modelling framework I built a spatio-temporal model of the MEN. Through development of the model I uncovered important insights into MEN regulation. I then validated the model against literature phenotypes and found it could predict 80% of phenotypes tested. I converted the model to a continuous time framework (Stoll et al. (2017)) and showed it could make and predict changes in the timing of mitotic exit in FEAR mutants. I then linked timing effects to observed cell-cell variability in the checkpoint competence of SPoC mutants. Finally, I use the model to compare predicted and observed behaviour of cells where MEN proteins are forced to localize at the SPB. Altogether, I found that the compartmental logical model is a powerful tool to study and explore the interaction between localization and other aspects of regulation in mitotic exit control.

4.2 Training a model of the mitotic exit network

4.2.1 Aims

My first approach to building a model of the MEN was to train a Boolean model of the MEN with CellNOptR (Terfve et al. (2012)). Using this approach, a Prior-Knowledge Network (PKN) is trained against a list of known phenotypes, for example that a knock-down of *CDC15* prevents mitotic exit (Shirayama et al. (1996)). A Boolean model does not have parameters so the training acts on the architecture of the network and the logical rules of each node. This is important because if each node, i, has in-degree n_i then there are $2^{2^{n_i}}$ possible truth tables defining the node's update rule. As each of these rules are independent of the others, the number of possible models, N, is given by

$$N = \prod_i 2^{2^{n_i}}.$$

The vast majority of these models are totally non-sensical or incorrect so the problem becomes a search through this space to identify good models. An exhaustive search is not feasible for any reasonably sized network so heuristic algorithms are required. CellNOptR applies an evolutionary algorithm to search through the space of models (Figure 4.1A). It takes a model and randomly mutates the rules to create a population of new models. It tests these against the training dataset and scores them based on how many phenotypes they fit and then feeds the best model back into the first step. It will continue this process until no improvement occurs over 100 consecutive iterations.

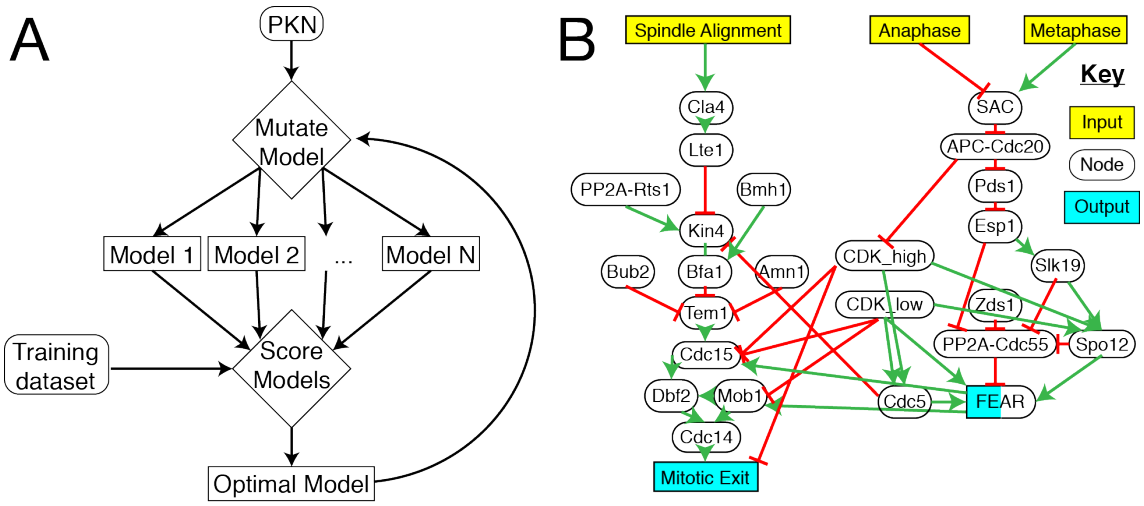

Figure 4.1: Training a model of the MEN with CellNOptR. A: Schematic showing the evolutionary algorithm used by CellNOptR to train a model. B: The PKN used as a basis for the MEN model. Yellow nodes are inputs reflecting cell cycle events beyond the scope of the model. Blue nodes are the phenotypic outputs used by the model to test the phentoype of a mutant.

4.2.2 Preparation of the prior knowledge network and training dataset

I constructed a PKN from the literature based primarily on 3 review articles (Rock and Amon (2009); Weiss (2012); Scarfone and Piatti (2015)) and 24 articles of primary literature, resulting in 48 signed and directed interactions between 46 nodes (Figure 4.1B). Some edges were added without literature justification in order to fill gaps in the network. There are 3 input nodes: Spindle Alignment, Anaphase and Metaphase, which reflect events outside of the scope of the model. Additionally, there are 7 unregulated nodes, which are set to their physiological states in all simulations. The outputs of the model are the Mitotic Exit and FEAR nodes, which are measured and tested against literature values during scoring.

I compiled a training dataset of 148 literature phenotypes from 39 primary literature articles, resulting in 117 unique phenotypes. In a wild type cell, Cdc14 is released from the nucleolus only in anaphase. For each mutant in the dataset I defined the phenotype by whether it caused the release of Cdc14 from the nucle-

olus in either metaphase or anaphase.

Both the PKN and training data were converted into the format specified by CellNOptR using custom R scripts.

4.2.3 Analysis of trained models

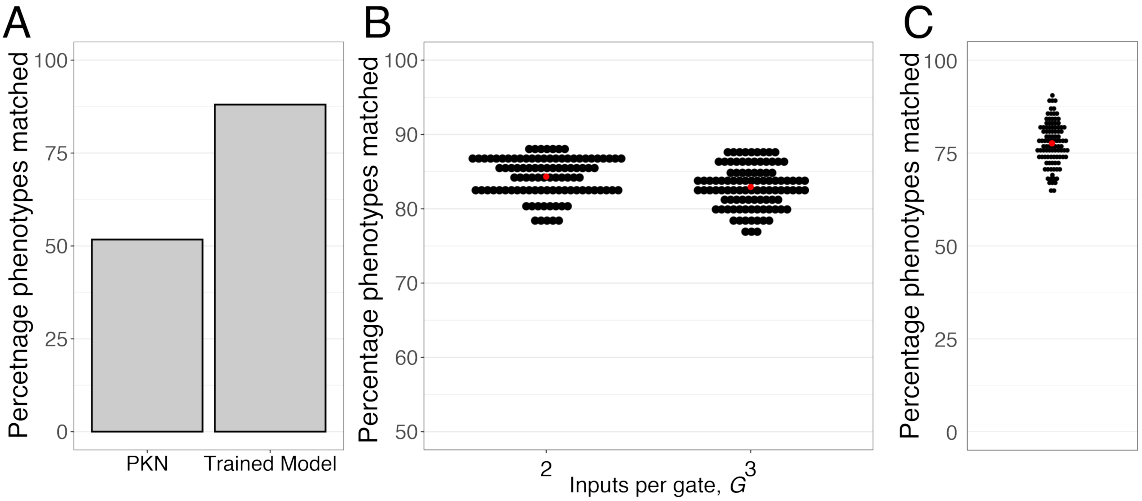

Figure 4.2: Evaluation of the training of the MEN model. A: Percentage of phenotypes matched by the untrained PKN and by the optimal trained model identified by training using 2 inputs per gate. B: The performance of all trained models identified using either 2 or 3 inputs per gate. The red circle shows the mean value. C: Distribution of bootstrap performances. The red circle shows the mean value.

I found that training the model once, with a population of 200 models per step, took around 10 minutes and there was significant variation in the fitted models between independent runs. Therefore, I used a bash script to run CellNOptR in parallel across different CPU nodes on the Francis Crick Institute's HPC cluster. Using this approach I generated an ensemble of 100 trained models in reasonable time.

Training the model greatly improved its ability to fit the training dataset; the optimal model fit improved from 51% to 88% (Figure 4.2A). CellNOptR does not actually explore the entire space of possible models, so I was interested to see if increasing the space explored could improve the optimal fit. CellNOptR uses a

parameter, G, to determine the inputs per gate used when expanding the model during preprocessing. Essentially, this means the program considers only AND gates containing up to G in-edges, note that this does not affect OR gates. Increasing the number of inputs per gate can greatly increase the number of possible models, meaning the algorithm runs much more slowly. Initially, I ran the algorithm using $G = 2$, but I repeated this analysis with $G = 3$. Despite increasing the search space, I found no improvement in the optimal fit to the data found and actually saw a decrease in the mean fit over the ensemble of models found (Figure 4.2B). Therefore, I continued analysis using the ensemble of models produced using $G = 2$. To test the dependence of the training process on the training dataset, I performed bootstrapping. I randomly split the training dataset into 80% of the phenotypes to use for training and 20% to use to test the models. I ran CellNOptR 100 times in parallel, using different random seeds to split the training sets. I found that generally the models trained using 80% of the data performed reasonably well on the unseen data, correctly predicting about 80% of the unseen phenotypes (Figure 4.2C). The results of this analysis convinced me that the ensemble of models have been effectively trained and cannot be improved by changing parameters of the algorithm.

Next, I investigated how similar the trained models are to each other. CellNOptR makes use of the disjunct normal form of logical statements, treating each node as a single OR gate over multiple AND gates, each potentially integrating both positive and negative interactions (Klamt et al. (2009)). This means CellNOptR considers each model as a list of edges, with the relevant edges combined in an OR gate for each node. A small proportion of edges were included in every model (Figure 4.3A), while a large number of edges were not included in any model. Each model can be represented by an edge-inclusion vector, $\{E_i\}$,

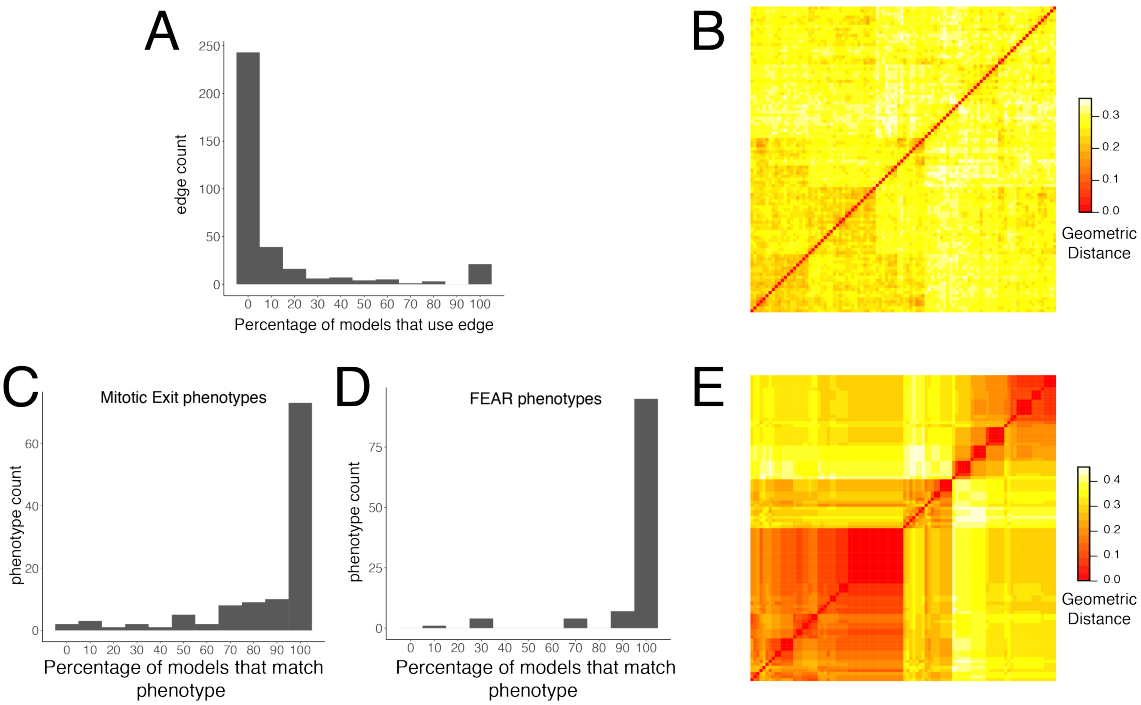

Figure 4.3: Comparison of the ensemble of models trained using 2 inputs per gate. A: Histogram showing the percentage of models using a given edge. B: Clustergram of the models, each coloured square shows the geometric distance between the edge-inclusion vector of two models. Hierarchical clustering was performed using the complete linkage method. C: Histogram showing the percentage of models correctly matching a given Mitotic Exit phenotype. D: Histogram showing the percentage of models correctly matching a given FEAR phenotype. E: Clustergram of the models, each coloured square shows the geometric distance between the phenotype-prediction vector of two models. Hierarchical clustering was performed using the complete linkage method.

where

$$E_i = \begin{cases} 1, & \text{if edge } i \text{ included in model} \\ 0, & \text{otherwise.} \end{cases} \tag{4.1}$$

I calculated the geometric distance between the edge-inclusion vector of each model and represented this information as a clustergram (Figure 4.3B). The hierarchical clustering algorithm does not identify any clear clusters, suggesting the models vary significantly in which edges are included. However, the edge inclusion structure of the models does not necessarily define the model's behaviour. In particular the disjunct normal form is not a unique representation of a rule so

there may be cases where the same rule is represented in different ways in different models. Unlike the edges, most phenotypes were matched by every model, as reflected by the high fit to the training data that was achieved. A small number of phenotypes were matched by none of the models but many more were fit by some but not all models (Figure 4.3C&D). This was true of both MEN and FEAR phenotypes, although a higher proportion of FEAR phenotypes were matched by every model than MEN phenotypes. In order to determine whether the models functionally converge, I defined a phenotype-prediction vector $\{P_i\}$ for each model, where

$$P_i = \begin{cases} 1, & \text{if phenotype } i \text{ is matched by the model} \\ 0, & \text{otherwise.} \end{cases} \tag{4.2}$$

Similarly to the edge-inclusion vector analysis, I constructed a clustergram for the phenotype-prediction vectors (Figure 4.3E). This shows much more structure than the edge version, suggesting the models converge functionally rather than structurally. The models cluster in a number of highly similar units, suggesting that the evolutionary algorithm could find models that were capable of fitting different subsets of the training dataset.

Among the 100 models trained using 2 inputs per gate, 7 achieved the maximum match to the dataset (88%). These optimal models fit nearly the same phenotypes: 11 phenotypes were never fit by the data, 2 were fit by some but not all and the rest were fit by every optimal model. However, there was limited structural convergence. There are 16 edges which were not forced during training that were present in every model, and 42 present in some but not all models. The majority (263) were present in none of these models.

4.2.4 Evaluation of trained models

While CellNOptR has proven to be a useful tool to train a model of the MEN, the trained model has limitations. In particular, it cannot account for spatial regulation of the MEN. This is because control of protein localization can occur both in series and in parallel to control of protein activity. This means that a spatial model must take account of both localization and activity independently. In order to create such a model, I decided to take an alternative approach, using CellNOptR to train subsections of the model while building other parts by hand.

4.3 A compartmental, logical model of mitotic exit

In order to build a spatio-temporal model of the MEN, I developed a compartmental logical modelling framework, capable of representing the spatial aspects of MEN regulation.

4.3.1 Model construction

The compartmental logical modelling framework is best understood through comparison with the compartmental ODE modelling framework. In the compartmental ODE modelling framework, independent variables are used to model the concentration of protein in each compartment. In a similar way, in a compartmental logical model, each protein has multiple nodes. In each compartment, each protein has a localization node whose state describes whether the protein is present in this compartment (1) or not (0). Additionally, there is an activity node for each protein and each compartment describing whether this protein is enzymatically active in this compartment. The network linking these nodes can be built from the superposition of an activity and localization network, which describe how the proteins regulate each others' enzymatic activity and localization respectively.

Due to the success of CellNOptR in training the model described above, I considered using CellNOptR to train the activity network for the mitotic exit model. However some aspects of MEN regulation are inherently spatial, for example the importance of enzymatic funneling to ensure Cdc15 phosphorylates Dbf2 only at the SPB (Rock et al. (2013)). In principle, a compartmental logical model could be trained with a genetic algorithm. However this algorithm would have to mutate the underlying activity or localization network and then compile a compartmental logical model to test. This is not currently supported with CellNOptR. Therefore, I took a combined approach, using CellNOptR to train the FEAR network, which is largely self-contained and restricted to the nucleus, and building the MEN section of the model by hand, before combining them to create a single model.

In order to train the FEAR network model, I built a PKN consisting of 22 edges and 15 nodes. I built a training datatset of 52 mutants from 11 publications, in this case using only Cdc14 release from the nucleolus as the phenotypic output. As described in the previous section, I generated an ensemble of 100 trained FEAR models. As I would not be training the MEN model, initially I decided to avoid allowing overexpression to feed forward and target downstream components of the pathway. However, I found this approach led to particular problems with phenotypes relating to Cdc5 overexpression. Overexpression of Cdc5 can cause release of Cdc14 (Visintin et al. (2003)), but Cdc5 activity is not thought to change throughout mitosis suggesting it is not targeted by other FEAR components. Therefore to match the phenotype of overexpression, I decided to allow Cdc5 only to feed forward. As the FEAR network is smaller than the full MEN model, I was able to use CellNOptR with 4 inputs per logical gate, the maximum supported by the package. This was particularly important as unlike the previous model, the FEAR model includes Net1, which has an in-degree of 7 in the PKN. This approach allowed for identification of models which could fit 88% of the training dataset. Of the 100 runs of the algorithm, 94 resulted in a model

with a score of 88%. In some cases, different runs of the algorithm identified the same model, as a result the ensemble identified 42 unique optimal models. These unique models could all fit exactly the same set of phenotypes in the training dataset. The variation between these 42 models centred on regulation of Spo12 and Net1. Relatively little is known about Spo12 regulation, except that it interacts with Fob1 (Stegmeier et al. (2004)) and it is phosphorylated by CDK (Tomson et al. (2009)). I included exploratory edges from Slk19 and Esp1 in the PKN, in case these were found to be necessary. However, as some models could explain the behaviour of Spo12 with only CDK and Fob1 regulation, we prioritised these models. While there were a variety of rules for Net1 regulation, these are likely to be functionally redundant. Therefore we chose a model based on the treatement of Spo12 regulation to take forward for use in the full model of mitotic exit.

I treated the trained FEAR network as an activity network, with the exception of PP2A-Cdc55 (Rossio and Yoshida (2011)) and Cdc14 which are controlled by localization. I combined the FEAR model with a hand-built model of MEN control of Cdc14, to create Model 0. The resulting network is shown in Figure 4.4A. The model is distributed across 5 compartments: the cytoplasm (mother compartment), the bud, the nucleus, the mSPB and the dSPB (Figure 4.4B). In metaphase and early anaphase, both SPBs reside in the mother compartment and exchange proteins with that compartment. Upon spindle alignment, the dSPB enters the bud compartment and exchanges proteins there. In this model, the SPBs are distinguished only by fate.

I decided to include multiple levels for the CDK, Cdc14 and Cdc15 nodes in the model. CDK activity decreases significantly at the metaphase-anaphase transition as a result of Cdc20 activity, however it does not reduce to G1 levels until activation of Cdh1 at mitotic exit. Rather than model specific cyclin specific effects, I included a high (metaphase) and a low (anaphase) level of CDK activity.

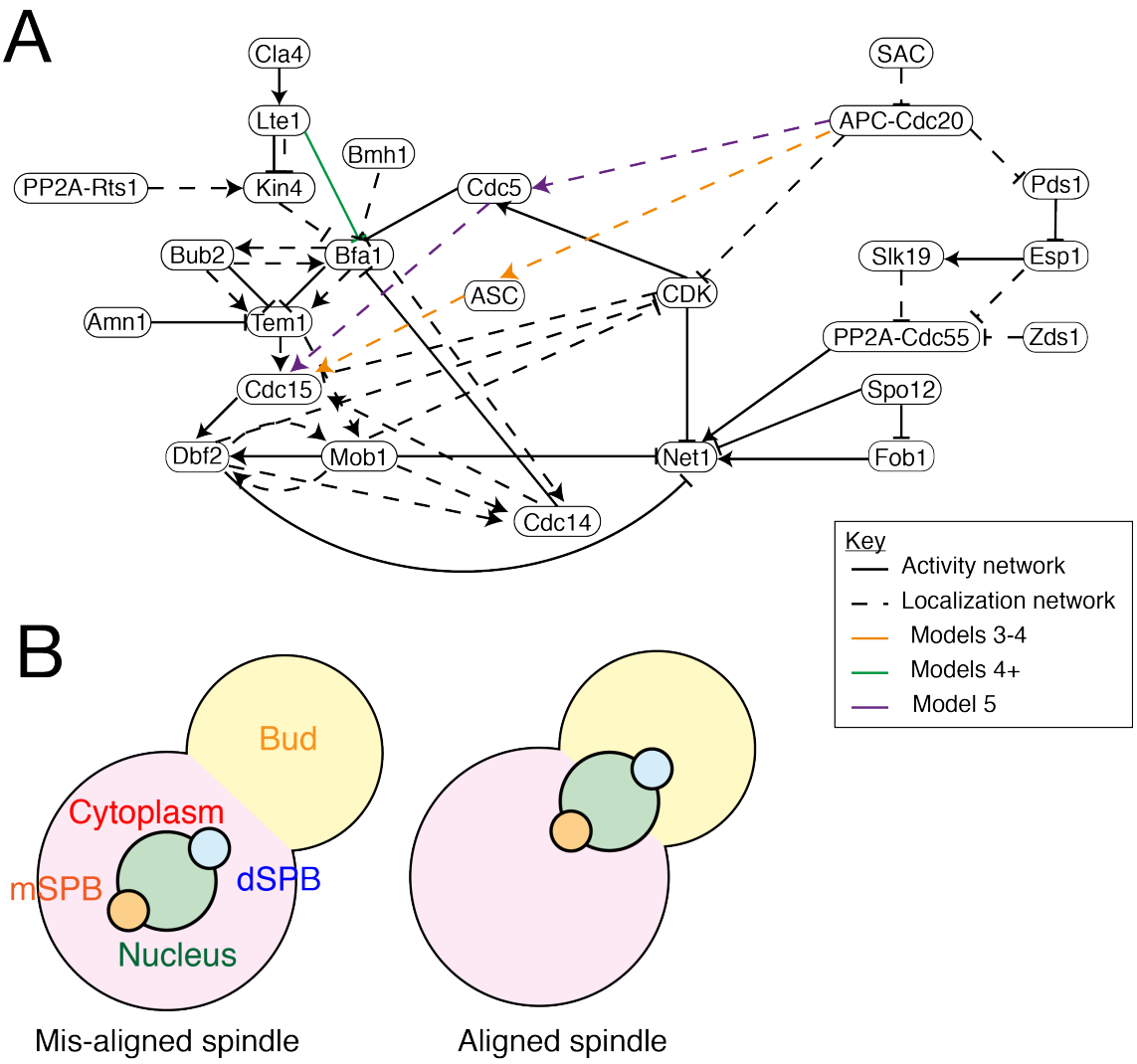

Figure 4.4: A: Network representation of Model 0. B: Compartments of the model.

Cdc14 also has two levels of activity throughout mitosis. FEAR-mediated release of Cdc14 in anaphase is largely restricted to the nucleus, however for FEAR to interact with MEN proteins in the cytoplasm, a low level of Cdc14 must exit the nucleus in early anaphase. Therefore, the model contains a low (FEAR) and high level of Cdc14. I also found it necessary to include two levels of Cdc15 activity. Cdc15's enzymatic activity does not change substantially throughout mitosis, instead the function of Cdc15 is controlled through localization. There are two stages of Cdc15 localization. Firstly, Cdc15 localizes at the SPB to a limited extent, where it engages in a negative feedback loop with with Nud1 and CDK

Model	Modification
0	Base model.
1	As 0 and the low (anaphase) level of CDK inhibit Cdc15 loading in absence of Tem1.
2	As 1 and the ASC inhibits Cdc15 loading in metaphase, in the absence of Tem1 and CDK.
3	As 2 and multi-level Tem1, Bub2 and Bfa1.
3a	As 3 and Identification of ASC as Cdc5.
4	As 3 and Lte1 can inhibit Bfa1 activity in a mechanism parallel to Kin4.
4a	As 3 and Lte1 can activate Tem1 activity in a mechanism parallel to Bfa1 inhibition.
5	As 4 and identification of ASC as Cdc5 and above.
6	As 5 but Lte1 regulation of Bfa1 can influence speed of Tem1 activation (MaBoSS implementation).

Table 4.1: Model versions

(König et al. (2010)). This loop is broken by Cdc14 activity or through localization of Tem1 which stabilises Cdc15 localization at the SPB and leads to a higher level of Cdc15 at the SPB. This high level of Cdc15 at the SPB is then capable of phosphorylating Dbf2.

Due to the constraints of the logical framework I had to simplify the mechanism of Bfa1 regulation by Kin4. Kin4 phosphorylation is thought to increase turnover of Bfa1 at the SPB, protecting it from inhibitory phosphorylation by Cdc5 (Caydasi and Pereira (2009)). In the model, Kin4 prevents Bfa1 localization at the SPB, with a similar effect.

I used an R script to convert the activity and localization networks into a single compartmental logical model. The resulting network consists of 270 nodes and 523 edges. In order to model the effects of overexpression I produced a second version of the network with overexpression nodes (see Materials and Methods, Chapter 2). This version of the network has 296 nodes and 748 edges.

4.3.2 An Anaphase-Specific Component is required to limit Cdc15 activity in metaphase

I developed the model by testing its behaviour against mutants with well-characterised phenotypes. The first mutant I simulated was *CDC15-7A* and *MOB1-2A* and the double mutant (Jaspersen and Morgan (2000); König et al. (2010); Campbell et al. (2019)). Alone, *CDC15-7A* allows cells to exit mitosis with a misaligned spindle (Falk et al. (2016a)). When combined with *MOB1-2A*, it will also allow exit from mitosis in metaphase, but in this case only if the spindle is aligned (Campbell et al. (2019)). I simulated the phospho-mutants by creating modified versions of the model in which edges from CDK and Cdc14 to Cdc15 and Mob1 were removed.

Model 0 was unable to fit the phenotype of *CDC15-7A* cells (Figure 4.5). This issue was resolved by modifying the rule for Cdc15 localization so that it could localize at the SPB in the absence of CDK (Model 1). However, this model could not fit the phenotype of the *CDC15-7A MOB1-2A* mutant (Figure 4.5). Model 1 predicts that this mutant should exit mitosis in metaphase regardless of spindle alignment. This suggested that an additional level of regulation is required to restrict Cdc15 activity in metaphase. I introduced an Anaphase-Specific Component (ASC) that is required for Cdc15 loading at the SPB in the absence of CDK (Model 2). This modification resulted in the model correctly fitting the phenotype of the double phospho-mutant (Figure 4.5).

4.3.3 Multi-level logic is required for Bub2, Bfa1 and Tem1

Model 2 is capable of predicting when *CDC15-7A MOB1-2A* cells can exit mitosis in metaphase, so I decided to test whether it could fit the behaviour of *bfa1*Δ and *bub2*Δ cells, which can also exit mitosis in metaphase (Fraschini et al. (1999)). Model 2 predicts that *bfa1*Δ cells would exit mitosis only in anaphase, although

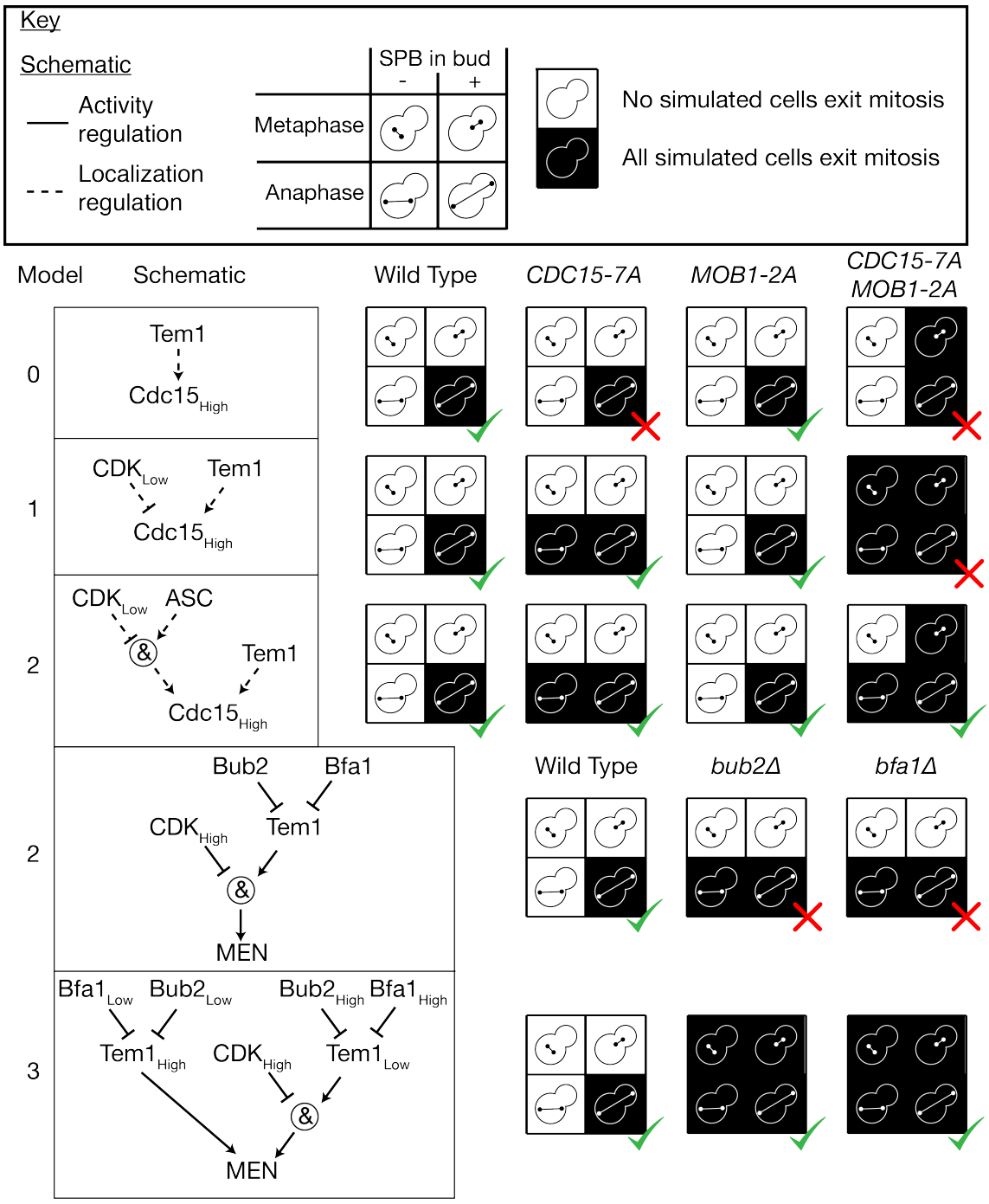

Figure 4.5: Caption located on next page.

independently of spindle alignment (Figure 4.5). In Model 2, Cdc15 and Mob1 are inhibited by the high level of CDK activity in metaphase, preventing mitotic exit even in the absence of Bub2-Bfa1 activity. To address this it is necessary to introduce multiple levels of activity for Bub2 and Bfa1 as well as Tem1, in order for this state to be transmissible to lower parts of the pathway (Model 3). In this model

Figure 4.5: Refinement of the MEN model based on mutants that can release Cdc14 in metaphase. All simulations are performed using the random asynchronous update scheme, 100 cells were simulated for each mutant starting from realistic initial conditions. In the original model, the *CDC15-7A* mutant has an intact SPoC, in contradiction of the experimental evidence. Introducing regulation of the $Cdc15_{High}$ SPB localization node by CDK fixes this issue (Model 1) however this model cannot fit the behaviour of the *CDC15-7A MOB1-2A* double mutant. This double mutant can exit mitosis in metaphase but only when the spindle aligns and an SPB enters the bud (Campbell et al. (2019)). The inclusion of an Anaphase-Specific Component (ASC) that limits Cdc15 loading in metaphase resolves this problem (Model 2). Deletion of either component of the Bub2-Bfa1 GAP complex also permits exit from mitosis in metaphase, however simulations of Model 2 do not agree with this. Introducing two levels of Bub2, Bfa1 and Tem1 activity (Model 3) is sufficient to represent this effect. All simulation data can be found in Supplementary File 17.

under physiological conditions, Bub2 and Bfa1 vary from a high level of activity where Tem1 is fully inhibited, to a low level where it is active enough to engage MEN signalling. In the case of Bub2 or Bfa1 deletion, Tem1 becomes hyperactivated, reaching its high level of activity. In this state it can localize to the SPB independently of Bub2-Bfa1 and recruit Cdc15, and then together with Cdc15, recruit Mob1 even in the presence of CDK. This modelling decision is justified by two experimental observations. Firstly, a constitutively active mutant protein, Tem1-Q79L, localises to SPBs independently of Bub2-Bfa1 at a much higher frequency than wild type Tem1 (Scarfone et al. (2015)). Secondly, Tem1 and Cdc15 function in a complex (Bardin et al. (2000); Asakawa et al. (2001)), meaning it is possible that Tem1 may help Cdc15 to load Mob1. By making these alterations, Model 3 is capable of fitting the behaviour of *bfa1*Δ and *bub2*Δ mutants.

4.3.4 Lte1 regulates Bub2-Bfa1 independently of Kin4

The Bub2-Bfa1 complex and Kin4 are both essential for the SPoC but there are differences between the phenotypes of the two deletions. While deletion of FEAR components has no impact on the phenotype of *bub2*Δ mutants, a *kin4*Δ*spo12*Δ double mutant has a functional SPoC (Falk et al. (2016a)). I tested whether Model

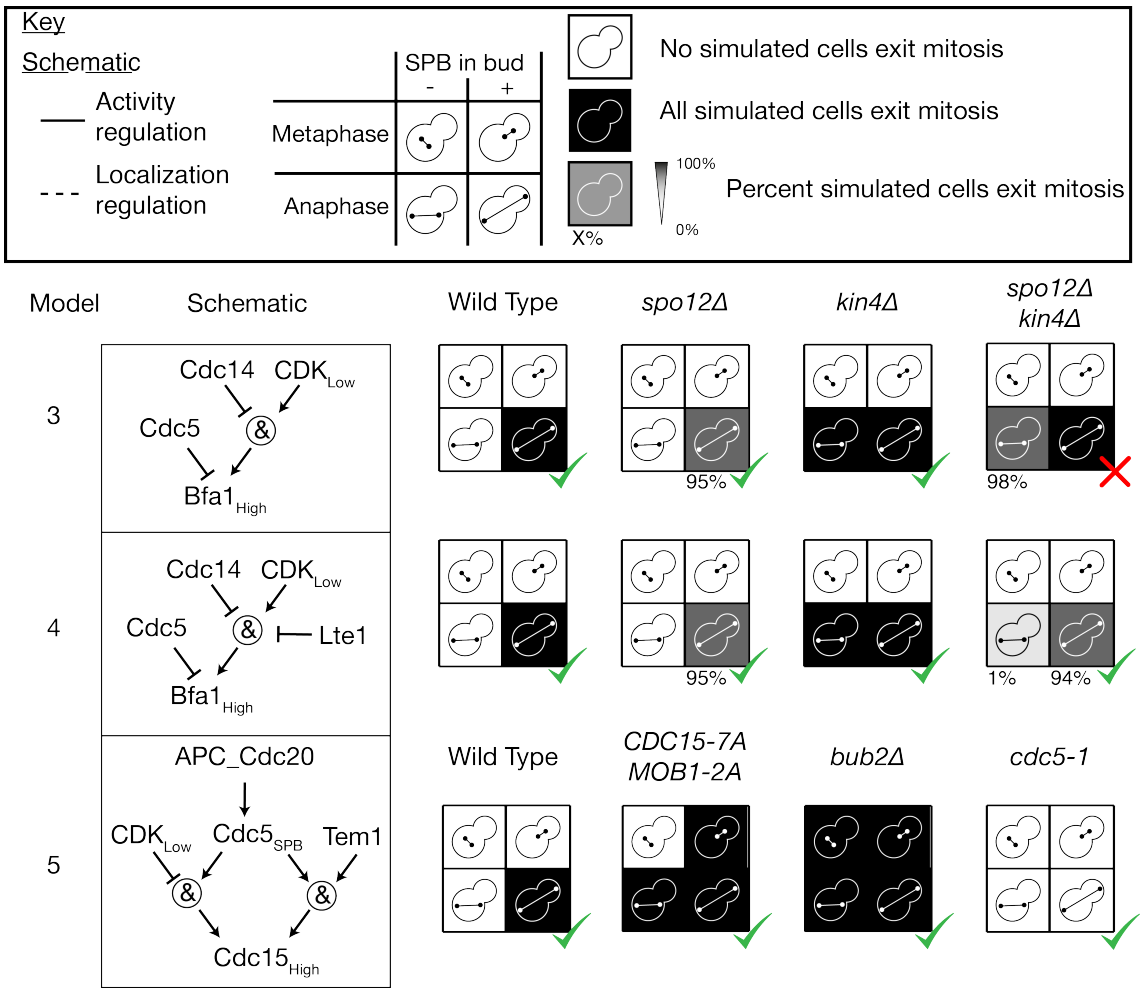

Figure 4.6: Refinement of the MEN model based on the phenotype of *kin4*Δ*spo12*Δ cells. All simulations are performed using the random asynchronous update scheme, 100 cells were simulated for each mutant starting from realistic initial conditions. In Model 3, the double mutant *kin4*Δ*spo12*Δ did not have a SPoC, in disagreement with experimental evidence (Falk et al. (2016a)). By introducing an additional level of regulation of Bfa1 by Lte1, this issue was resolved in Model 4. This change also allowed for identification of the ASC with Cdc5, while maintaining the correct behaviour of related phenotypes, such as *CDC15-7A MOB1-2A*, *kin4*Δ and *cdc5-1*.

3 could correctly fit the phentoype of the double mutant (Figure 4.6). In Model 3, the *kin4*Δ*spo12*Δ double mutant behaves like the single *kin4*Δ mutant. This is because Kin4 is the only spatial signal restricting mitotic exit prior to spindle alignment in Model 3. The ability of *kin4*Δ*spo12*Δ cells to delay mitotic exit until after spindle alignment suggests alternative MEN-activating spatial signals exist. A plausible candidate for this mechanism is Lte1 as *lte1*Δ*kin4*Δ*spo12*Δ are signifi-

cantly delayed in mitotic exit (Falk et al. (2016a)). I introduced Lte1 regulation of Bfa1 into the model (Model 4) and this version of the model can faithfully reproduce the phenotype of both single and double *kin4*Δ and *spo12*Δ mutants.

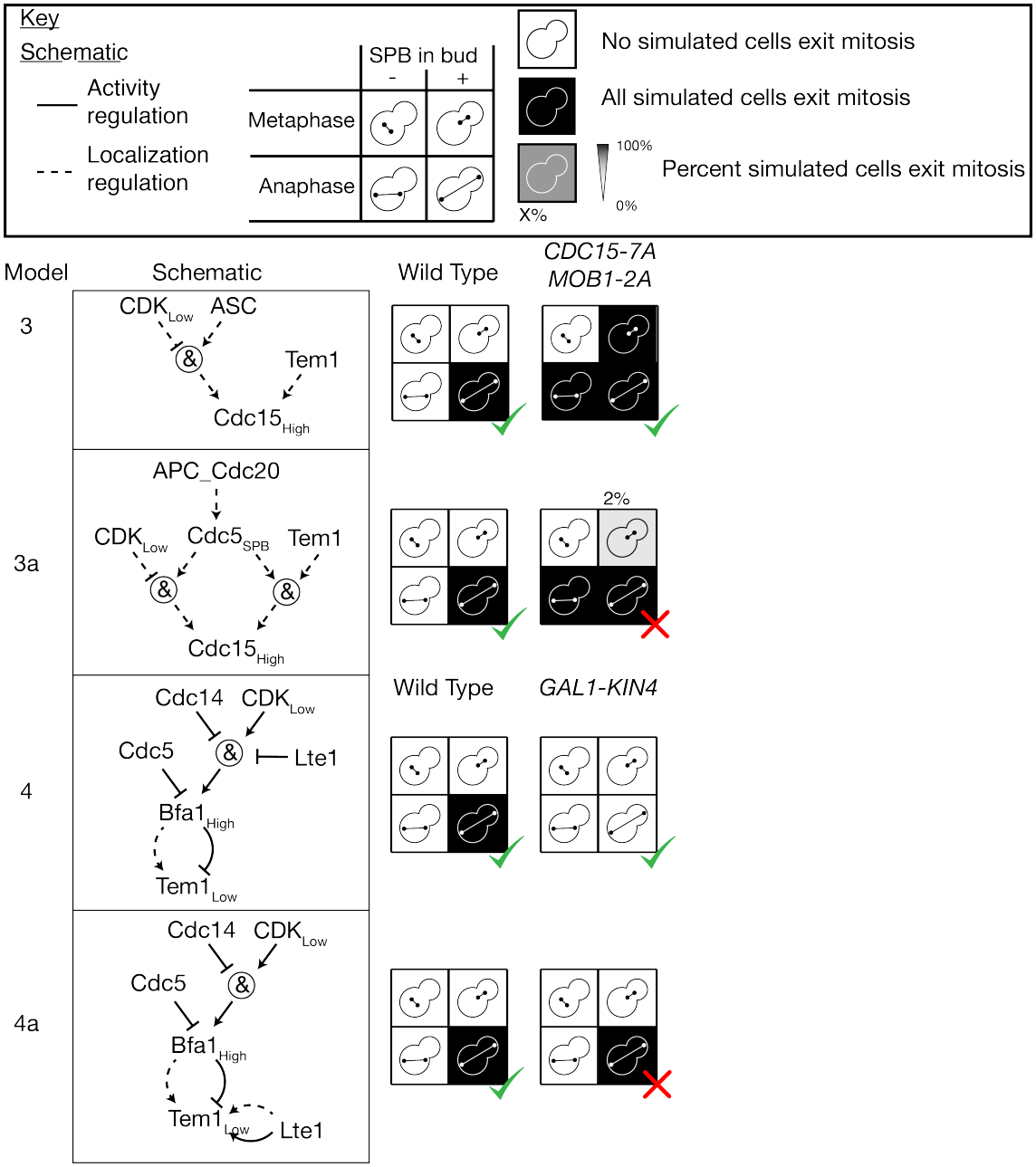

Figure 4.7: Identifying the ASC as Cdc5 in Model 3 (Model 3a) leads to incorrect behaviour of *CDC15-7A MOB1-2A*. Model 3 requires an additional pathway linking Lte1 to Tem1. In Model 4 Lte1 directly inhibits Bfa1 activity, leading to correct prediction of the phenotype of $GAL1p-KIN4$ cells. A version where Lte1 directly activates Tem1 (Model 4a) predicts behaviour of $GAL1p-KIN4$ incorrectly.

Lte1 shares homology with other GEFs, and so was long thought to act as a

GEF for Tem1 (Bardin and Amon (2001)). However, it has been demonstrated that Lte1 has no GEF activity towards Tem1 *in vitro* (Geymonat et al. (2009)). As there is no clear mechanism for regulation of Bfa1 by Lte1, I decided to test whether a model in which Lte1 regulates Tem1 rather than Bfa1 could fit experimental observations (Model 4a). This version of the model could not explain the phenotype of Kin4 overexpression (Figure 4.7), whereas Model 4 could. This lends support to the idea that Bfa1 is the recipient of the alternative MEN-activating signal.

4.3.5 Cdc5 is the anaphase specific component

The ASC was introduced to the model to promote localization of Cdc15 at the SPB in anaphase but not metaphase. A likely candidate for the ASC is Cdc5, which is necessary for localization of Cdc15 at the SPB in cells lacking Tem1 (Rock and Amon (2011)). Cdc5 is present at the SPBs at all times in mitosis, but recently evidence has emerged that suggests Cdc5 translocates from the nuclear to the cytoplasmic face of the SPB at the onset of anaphase (Botchkarev et al. (2017, 2014)). Taken together, these findings suggest a mechanism for Cdc5 to act as the ASC. I modified the model to include these effects (Model 5). Model 5 also requires a modified version of the rule for Bfa1, as Bfa1 must be inhibited in metaphase cells with aligned spindles to correctly fit the phenotype of the *CDC15-7A MOB1-2A* double mutant. This version of the model can fit all related phenotypes including *CDC15-7A MOB1-2A*, *bub2*Δ and *cdc5-1* (Jaspersen et al. (1998)) (Figure 4.6). Interestingly, I attempted to identify the ASC as Cdc5 in an earlier version of the model (Model 3a), however this version could not fit the phenotype of the *CDC15-7A MOB1-2A* double mutant (Figure 4.7). Introduction of the alternative MEN-activating pathway from Lte1 to Bfa1 allows for inhibition of Bfa1 in metaphase in the absence of Cdc5, allowing this mechanism to work.

4.4 Model Validation

Having refined the model against well characterised mutant phenotypes, I decided to validate Model 5 against an array of literature phenotypes.

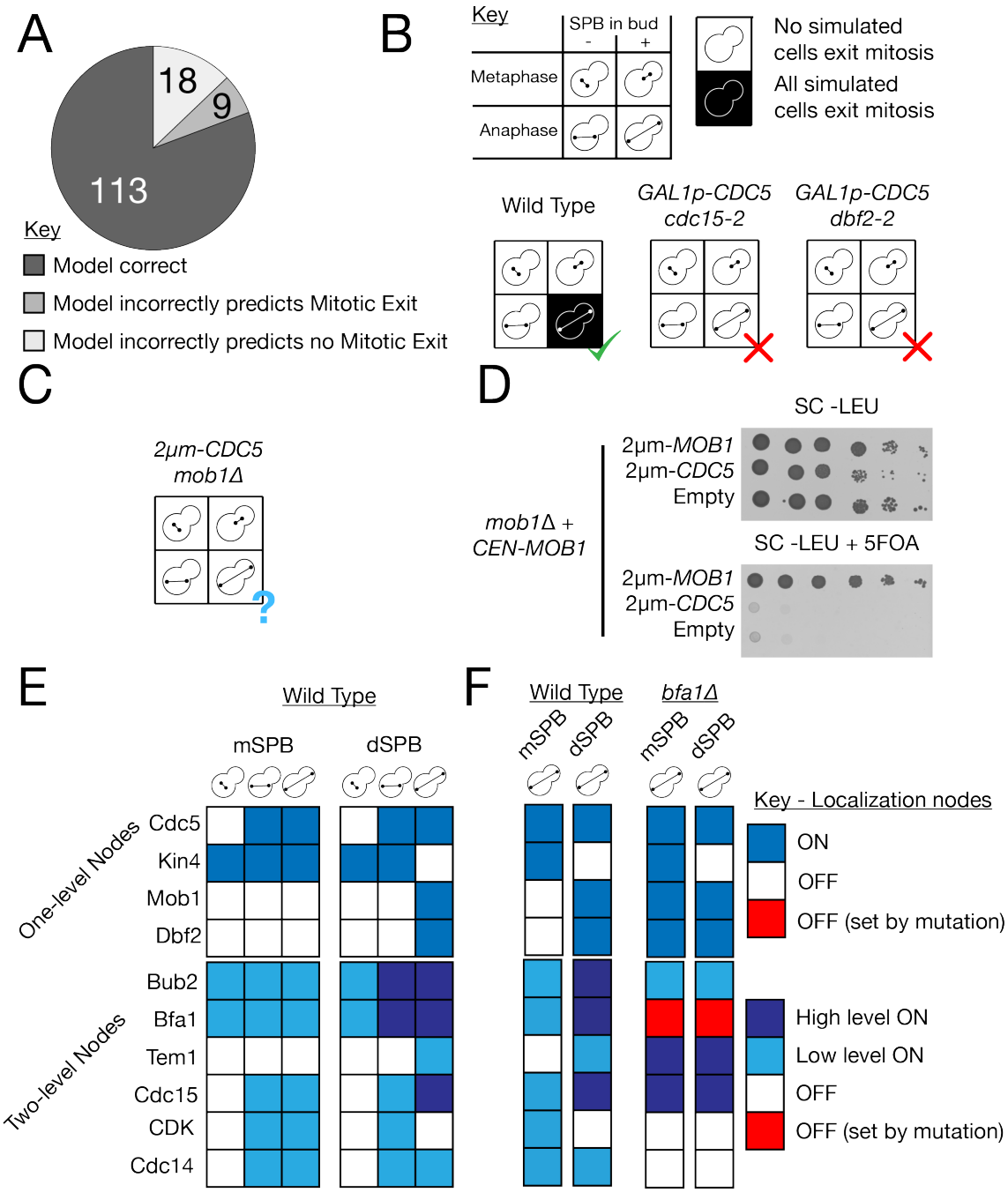

Figure 4.8: Caption located on next page.

Figure 4.8: Validation of Model 5 against literature phenotypes. A: The model correctly predicted 81% of the 140 tested literature phenotypes. B: The model often failed at predicting the phenotype of cells with a genotype that mixes overexpression with other mutations, such as the rescue of the temperature sensitive alleles *cdc15-2* and *dbf2-2* by overexpression of *CDC5*. C: The model predicts that overexpression of *CDC5* cannot rescue the *mob1*Δ mutation. D: Spot test confirming the model prediction that overexpression of *CDC5* can not rescue full deletion of *MOB1*. A *mob1*Δ strain kept alive by provision of a *CEN-MOB1* plasmid with uracil selection, was transformed with either a 2μm plasmid bearing *MOB1* or *CDC5* or an empty plasmid. The *CEN-MOB1* plasmid was counter-selected by addition of 5FOA, showing that moderate overexpression of Cdc5 is not sufficient for rescue of the *mob1*Δ phenotype. E: The localization state of MEN proteins on the SPBs in the three physiological stages of mitotic exit in the model. Steady states determined from synchronous update scheme. F: Comparison of (a)symmetry of SPBs in the steady states of wild type and *bfa1*Δ cells.

4.4.1 The model matches 80% of literature phenotypes

I searched the literature for MEN mutants, identifying 140 mutants from 37 publications. These mutants include knock-downs (deletions and temperature sensitive alleles), overexpressions (from the *GAL1* promoter or expressed on high copy number plasmids) and mis-localizing proteins. Each mutant was classified depending on the stage of mitosis in which they exit mitosis: metaphase, early anaphase (prior to spindle alignment) or late anaphase (after spindle alignment). Note that SPoC mutants (mutants that release Cdc14 in early anaphase) were detected in *kar9*Δ or *dyn1*Δ cells. Some mutants were classified differently between publications, in these cases we chose a single account to test, prioritising the S288C/BY4741 genetic background.

I used the asynchronous update scheme to simulate each mutant 100 times, and calculated the percentage of simulate cells that released Cdc14 fully into the cytoplasm. I then compared the simulated data to the literature phenotypes and recorded whether the majority of simulated cells behaved according to the literature phenotype. The model predicted 81% (113/140) of the phenotypes tested (Figure 4.8A).

4.4.2 The model fails to represent behaviour of partial knock-downs

While the model was broadly successful at predicting the phenotype of literature mutants, there were some types of mutant it struggled to capture. Overexpression of *CDC5* is capable of rescuing temperature sensitive MEN alleles, such as *tem1-3* (Jaspersen et al. (1998)), as well as initiating release of Cdc14 in a metaphase arrest (Hu et al. (2001)). Model 5 predicts that *CDC5* overexpession can cause mitotic exit however, it requires MEN proteins and therefore cannot alleviate their temperature sensitivity (Figure 4.8B). There is an interesting parallel here with the case of Spo12, a FEAR protein. Overexpression of *SPO12* can rescue a number of temperature sensitive MEN alleles (Jaspersen et al. (1998)). However, a recent study showed that while *SPO12* overexpression can rescue temperature sensitive alleles of MEN proteins, it cannot rescue their deletion (Caydasi et al. (2017)). When I used Model 5 to simulate *SPO12* overexpression combined with knock-down of MEN proteins, it predicted the phenotype of the deletion rather than the temperature sensitive allele. This suggests that excitation of the FEAR pathway or other MEN activators, such as Cdc5, may allow MEN signalling to occur at a lower, but not zero, threshold of MEN activity. I reasoned that a similar effect may apply to the case of *CDC5* overexpression. To test this hypothesis, I tested whether provision of *CDC5* on a $2\mu m$ plasmid could rescue deletion of *MOB1* (Figure 4.8D). This experiment showed that additional copies of *CDC5* could not suppress the lethality of *mob1*Δ, as predicted by Model 5 (Figure 4.8C). This supports the view that the model is effective at simulating the effects of full deletions of genes but struggles to represent the impact of knock-downs, such as temperature sensitive alleles. This is likely a broader issue with logical models, where protein activity is limited to a number of discrete states.

4.4.3 The model struggles to represent overexpression

Many of the phenotypes which the model could not correctly predict involve overexpression (19/27), in particular when combined with other mutations (18/27). These issues likely relate to the rules describing how overexpression functions in the model. In this framework, an overexpressed protein localizes everywhere it normally can go (all of the localization nodes for that protein are switched ON). I made this decision based on the fact that when *CDC15* is overexpressed, it localizes to the SPB even in *tem1*Δ cells(Rock and Amon (2011)). As Tem1 is usually required for Cdc15 localization at the SPB, it must be the case that overexpression can force Cdc15 to load in all conditions. However this pattern is not reproduced for all proteins, PP2A-Rts1 is required for Kin4 localization at the SPB and *rts1*Δ can rescue *GALp-Kin4* by preventing localization of Kin4 at the SPB (Chan and Amon (2009)). As no general rule can accommodate both these behaviours, it is inevitable that the impact of combining some of these mutations will be unpredictable.

4.4.4 Steady states of the model

The steady states of Model 5 accurately represent the known distribution of MEN proteins in the cell. There is a single steady state for each of the cell cycle stages we modelled: metaphase, early anaphase (prior to spindle alignment) and late anaphase. In each of these states, the localization pattern of MEN proteins fits experimental observations (Figure 4.8D). The *bfa1*Δ mutation disrupts the asymmetry of MEN proteins (Caydasi et al. (2012)) and this effect is captured by the model (Figure 4.8E).

In conclusion, Model 5 can predict the majority (88%) of literature phenotypes and its steady states are representative of our understanding of protein localization during mitosis.

4.5 Timing of mitotic exit

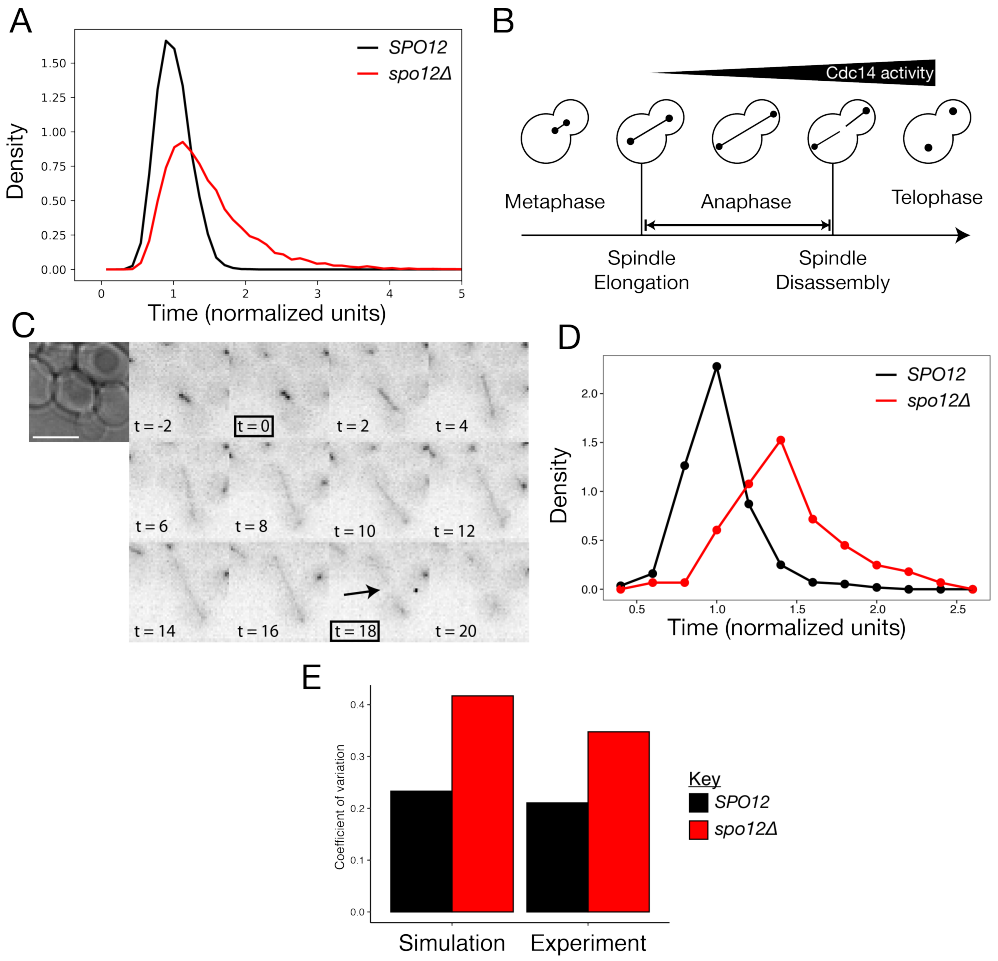

Figure 4.9: The role of FEAR in regulating anaphase length. A: We simulated 10,000 *SPO12* and *spo12*Δ cells and the length of anaphase (time from model initiation until mitotic exit) was calculated, and was normalized to the mean of the wild type cells. B: Schematic showing the key cell cycle events used to calculate the length of time spent in anaphase. C: Time course showing mRuby2-Tub1 fluorescence in a representative cell during exit from mitosis. Images were taken at 2 minute intervals and used to determine the length of anaphase. The image at 0 minutes shows the final frame where the cell has an un-extended spindle and spindle disassembly after 18 minutes. D: Distribution of anaphase lengths in *SPO12* and *spo12*Δ cells. 5 time course were performed, each with 3 fields of view per strain, (*SPO12* $n = 281$, *spo12*Δ $n = 223$). Due to differences in mean exit times between time courses, exit times from each time course were normalized to the mean exit time of *SPO12* cells in that time course. E: The coefficient of variation of exit times for *SPO12* and *spo12*Δ cells in simulation and experiment.

4.5.1 Simulations predict FEAR required for robust mitotic exit timing

The FEAR network is not essential for mitotic exit; however, FEAR mutants are delayed in exit from mitosis (Stegmeier et al. (2002)). In my model Cdc14 disrupts a negative feedback loop involving Cdc15, CDK and Nud1, allowing stable localization of Cdc15 at the SPB, suggesting the model could represent this temporal effect of FEAR disruption.

In order to test this hypothesis, I simulated the model using the MaBoSS package (Stoll et al. (2012, 2017)). MaBoSS treats a logical model as a continuous time Markov chain applied on the state space of the model, meaning that the model can be simulated in continuous time. This is an advantage over the asynchronous update scheme, which updates in discrete time steps. I simulated wild type and *spo12*Δ cells in late anaphase (Figure 4.9A). As hypothesised, the simulations revealed a delay in Cdc14 release in the *spo12*Δ mutant. Furthermore, the distribution of exit times in the FEAR mutant was different to the wild type. The exit time distribution of the *spo12*Δ cells has a long tail, indicating that the variance, as well as the mean, is higher than the wild type.

4.5.2 Experimental measurement of anaphase length confirm prediction

I decided to test whether this difference in the variance of mitosis length was observable in living cells. In order to get information on the full distribution of exit times, I used time-lapse microscopy to get single-cell data. This differs from previous studies, which relied on bulk measurements, for example (Stegmeier et al. (2002)). I used a *CDC14-CFP mRuby2-TUB1* strain, using Tub1 as a marker of the mitotic spindle. I measured the length of anaphase by recording the time stamp of the first frame showing an extended mitotic spindle and the first frame

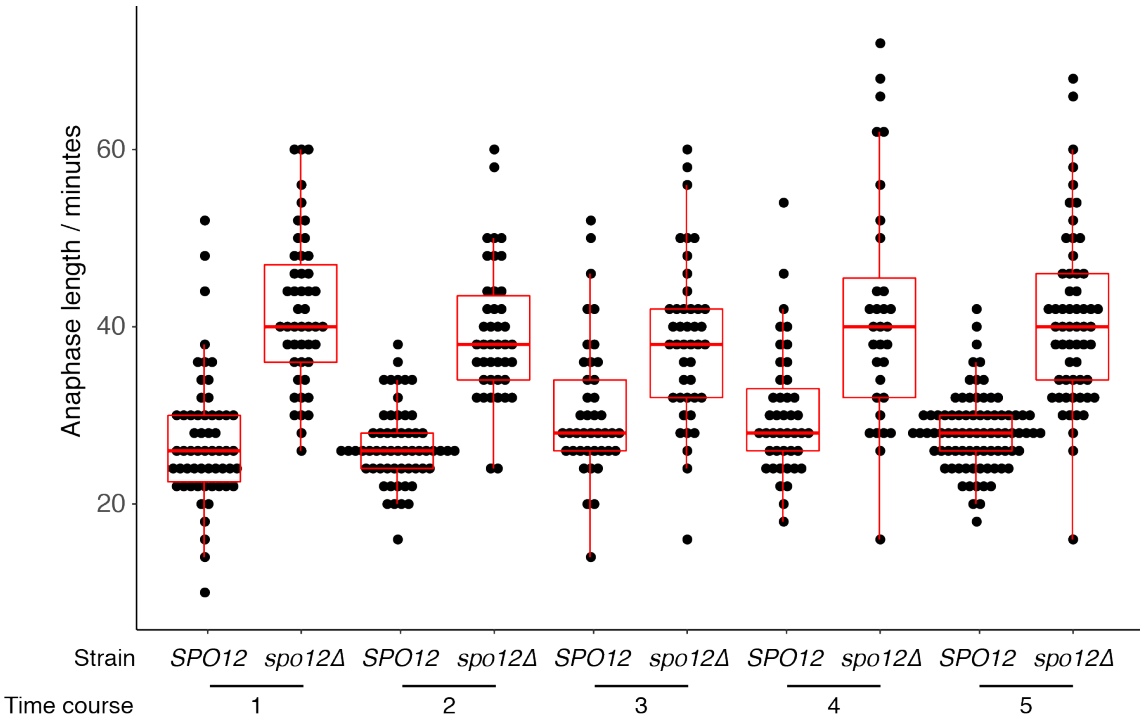

Figure 4.10: Raw measurements of anaphase length, grouped by strain and time course. Box plots show the median and the upper and lower quartiles, whiskers show 1.5 times the inter-quartile range or the closest measurement, whichever is closest.

of spindle disassembly (Figure 4.9B&C). I placed *SPO12* and *spo12*△ strains in side-by-side chambers and ran time courses for 2 hours, with 2 minute time intervals (Figure 4.10A). There were some differences in mean anaphase length in *SPO12* cells between different time courses, possibly due to the amount of time cells spend in the chamber before imaging. To account for this, I normalized the anaphase length measurements to the mean of the *SPO12* cells during each time course. The experimentally derived distributions of anaphase length qualitatively match the simulations (Figure 4.9D). In particular, the *spo12*△ distribution is both shifted right and has a heavier tail than the *SPO12* distribution. I used the Coefficient of Variation (CV) as a scale-free measure of variability to compare the effect of FEAR disruption in both the simulated and experimentally observed distributions of anaphase length (4.9E). Both simulation and experiment show a marked increase in CV in *spo12*△ cells when compared to *SPO12* cells. Further-

more, the simulations predict that the distribution of exit times in FEAR mutant cells would show a power law tail (Figure 4.10A). This is confirmed by experimental measurements, although intriguingly the wild type also shows this behaviour, albeit with a much less shallow tail. This suggests that anaphase length in FEAR mutant cells is highly variable. Altogether this evidence suggests that the FEAR network is important for the robustness of the timing of mitotic exit.

4.6 Predicting the strength of spindle position checkpoint mutants

In the previous section, I established that the compartmental logical modelling framework is capable of representing both temporal and spatial aspects of regulation, and can make predictions about single cell behaviour. Therefore, I decided to apply it to the problem of distinguishing the strength of SPoC mutants. All SPoC mutants, such as *kin4*Δ or *bub2*Δ, permit exit from mitosis while the spindle is misaligned. However, they differ in the penetrance of the phenotype: only a fraction of cells ever exit mitosis with misaligned spindles and in some mutants this fraction is higher than in others. For example, Falk et al. (2016a) found that around 25% of *kin4*Δ cells will exit mitosis with a misaligned spindle while 50% of *bub2*Δ cells will do so. This difference means we can distinguish between "strong" SPoC mutants like *bub2*Δ and "weak" mutants like *kin4*Δ cells. I decided to test whether my model of mitotic exit could tell strong and weak SPoC mutants apart.

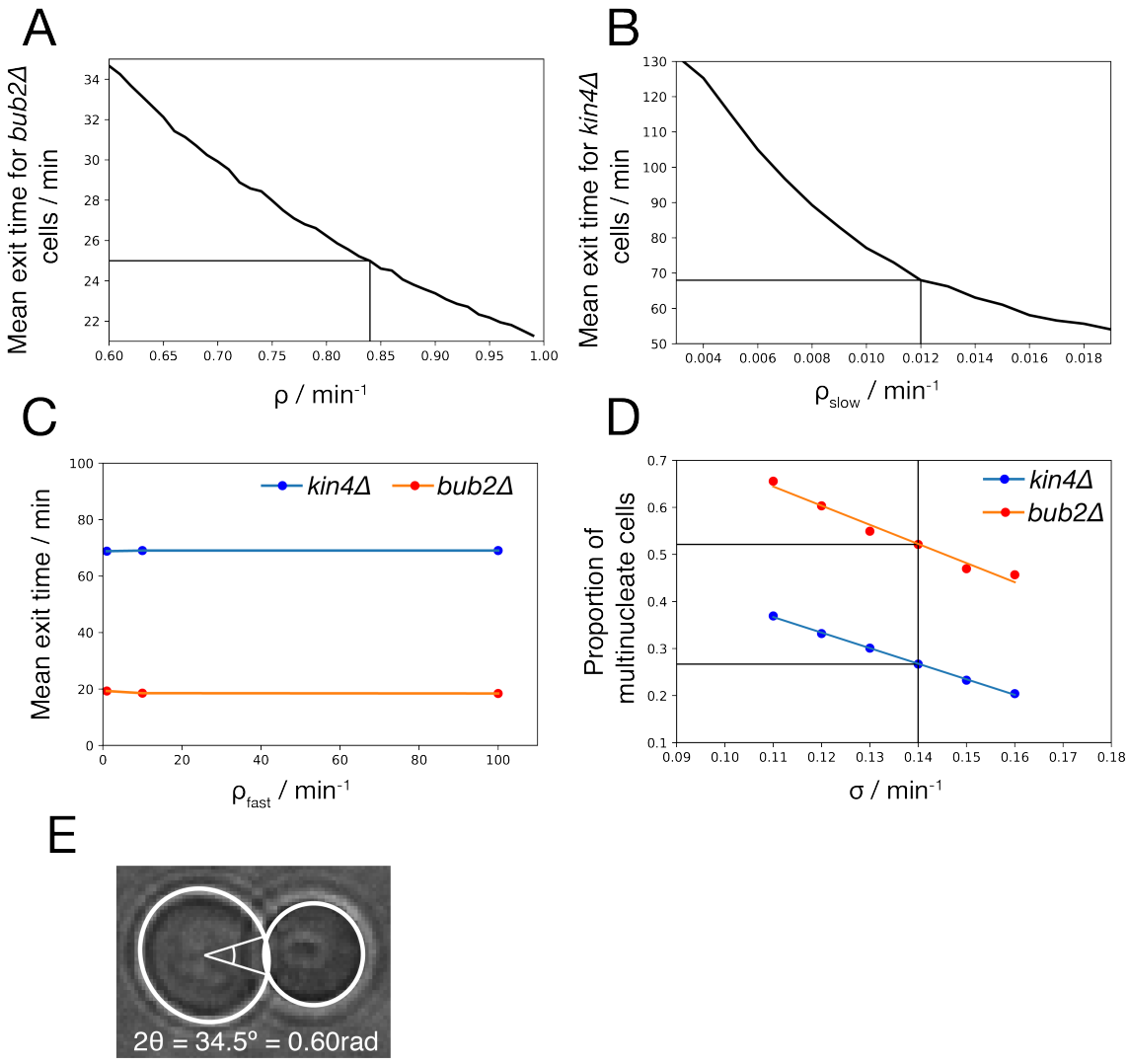

Figure 4.11: Caption located on next page.

4.6.1 Distribution of exit times in spindle position checkpoint mutants

A key difference between strong and weak SPoC mutants is the time spent in anaphase with a misaligned spindle before exiting mitosis. Falk et al. (2016a) used *kar9*Δ *osTIR1 dyn1-AID* cells, which align spindles very slowly due to disruption of both parallel spindle alignment pathways. They found that *kin4*Δ cells with misaligned spindles spent considerably longer in mitosis than *bub2*Δ cells. I

Figure 4.11: Parameter selection for the dimensional model (Model 6). A: The basic rate, ρ, was chosen so that the mean of the exit time distribution of *bub2*Δ is 25. I simulated 10,000 anaphase cells with misaligned spindles for 40 values of ρ between 0.6 and 1.0 and calculated the mean exit time. The closest to the target value ($\rho = 0.84$) was selected. B: The slow rate of Bfa1 inhibition, ρ_{slow}, was chosen so that the mean of the exit time distribution of *kin4*Δ is 70. I simulated 10,000 anaphase cells with misaligned spindles for 18 values of ρ_{slow} between 0.004 and 0.018 and calculated the mean exit time. The closest to the target value ($\rho_{slow} = 0.012$) was selected. C: I tried varying the fast rate of Bfa1 inhibition, ρ_{fast} over 2 orders of magnitude but found it had little effect on the length of mitosis in either mutant, so it was left at $\rho_{fast} = 1$. Mean exit times were derived from simulations of 10,000 anaphase cells with misaligned spindles. D: The parameter, σ, representing the rate of spindle alignment, was chosen to match both the measured proportions of multinucleate cell formation in *bub2*Δ (~ 0.5) and *kin4*Δ (~ 0.25). We tested 6 values of σ between 0.11 and 0.16. Fortunately, the value $\sigma = 0.14$ fits both proportions closely. Mean exit times were derived from simulations of 10,000 anaphase cells with misaligned spindles. E: Measurement of the half-angular bud width, θ, from a microscope image of a large-budded wild type cell. Based on this measurement we use a value of $\theta = 0.3$.

hypothesised that this difference in speed of MEN activation could be key to the difference in SPoC strength.

In order to represent this effect, I modified the MaBoSS model to make a new model (Model 6). The wiring of Model 6 is identical to Model 5, but Tem1 is activated more rapidly in the presence of Lte1. This decision was based on my earlier finding that Lte1 inhibits Bub2-Bfa1 activity. Lte1 is an attractive choice as its bud localization means that MEN activation will take less time when the spindle is correctly aligned. In order to match the experimental measurements of Falk et al. (2016a), I introduced parameters to dimensionalize the model:

- ρ_{fast}, the rate of Tem1 activation in the presence of Lte1.
- ρ_{slow}, the rate of Tem1 activation without Lte1.
- ρ, the rate of all other reactions.

These parameters were fit to match timing data from Falk et al. (2016a). I chose ρ so that the mean length of anaphase for *bub2*Δ cells with misaligned spindles was

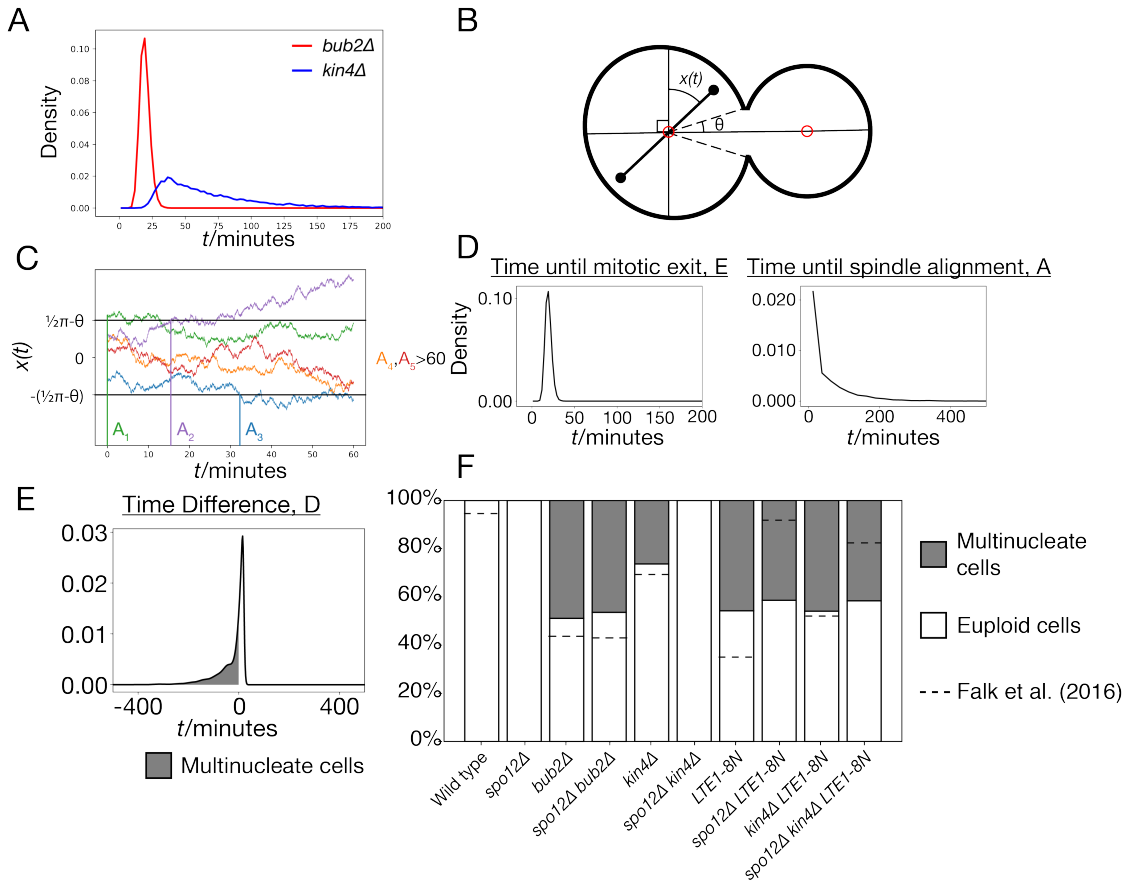

Figure 4.12: Caption located on next page.

25 minutes (Figure 4.11A). Similarly ρ_{slow} was chosen so that the mean length of anaphase for *kin4*Δ cells with misaligned spindles was 70 minutes (Figure 4.11B). I tried varying ρ_{fast} over 3 orders of magnitude however, it had minimal effect on the length of anaphase in cells with misaligned spindles for both mutants and so it was left at 1 (Figure 4.11C). All parameter values are summarised in Table 4.2. I used simulations of 10,000 cells to generate exit time distributions for both *kin4*Δ and *bub2*Δ cells (Figure 4.12A). I used cubic spline interpolation of these histograms to generate approximate PDFs for the random variable, E, representing the time from anaphase onset until exit from mitosis. Note that E is strain specific and must be re-calculated for each mutant.

Figure 4.12: Use of the parameterised model to predict and explore cell-cell variability in SPoC mutants. A: Simulated exit times of *bub2*Δ and *kin4*Δ cells with misaligned spindles, from 10,000 runs of the model. B: Schematic of a *kar9*Δ *osTIR1 dyn1-AID* cell, showing the spindle angle $x(t)$ and the half-angular neck width, θ. C: Simulations of $x(t)$, the spindle angle starting from uniformly distributed initial conditions and varying as a Brownian motion. The time until alignment A_i is indicated for each simulation. $A_1 = 0$ as in this case the initial condition of the simulation is within the bud neck ($x(0) > \frac{\pi}{2} - \theta$), corresponding to the scenario where the spindle is aligned at the point of extension. A_2 and A_3 can be measured as the point where $x(t)$ crosses either of the boundaries, as it is not important which SPB enters the bud. The final two simulations do not achieve alignment during the 60 minutes simulated so $A_4, A_5 > 60$. D: The distribution of exit times, E, for a simulated *bub2*Δ mutant and the distribution of alignment times, A, for a simulated *kar9*Δ *osTir1 dyn1-AID* cell. These distributions were inferred from cubic spline interpolation of histograms generated from 10,000 runs of the model or 10,000 Brownian motion simulations respectively. E: Distribution of the difference between exit time and alignment time, D, for the simulated *bub2*Δ *kar9*Δ *osTir1 dyn1-AID*. The area between the x-axis, the curve and $x = 0$ gives the predicted probability of a given cell exiting mitosis before spindle alignment occurs, giving rise to a multinucleate cell. F: Predicted proportions of multinucleate cells for various genetic backgrounds. Dotted lines show the measured proportions of multinucleate cells in Falk et al. (2016a).

4.6.2 Distribution of alignment times

In the previous section, I outlined how Model 6 can be used to predict the time taken for cells with misaligned spindles to exit mitosis. In order to predict the proportion cells exiting mitosis prior to spindle alignment, we also need a way to predict the time taken for a cell to align its spindle. As the analysis of Falk et al. (2016a) was gathered using *kar9*Δ *osTIR1 dyn1-AID* cells, I decided to model spindle alignment in this strain upon auxin-mediated Dyn1 degradation.

As neither spindle alignment pathway is present in these cells, alignment will occur as a result of random motion of the fluid inside the cell. A basic model of this is to consider the spindle to align by rotation around the geometric centre of the mother compartment. The angular displacement, $x(t)$, then acts as a Brownian motion (Figure 4.12B) over the region $(-\frac{\pi}{2}, \frac{\pi}{2})$. The spindle becomes aligned if the SPB enters the bud neck, and we assume it will not become misaligned again. Then, the Brownian motion ends if it ever passes above $\frac{\pi}{2} - \theta$

Parameter	Definition	Value
ρ	Standard rate of reactions in Model 6	0.84
ρ_{slow}	Rate of Tem1 activation in absence of Lte1	0.012
ρ_{fast}	Rate of Tem1 activation in presence of Lte1	1
σ	Rate constant of spindle alignment	0.14
θ	Half-angular bud width	0.3

Table 4.2: Parameters used to simulate SPoC competence.

or below $-\left(\frac{\pi}{2}-\theta\right)$, where θ is the half-angular bud width. The orientation of the spindle during metaphase is considered to be random so the initial condition $x(0) \sim U(-\frac{\pi}{2}, \frac{\pi}{2})$. This process requires two parameters: σ, the rate of alignment, and θ, the half-angular bud width. I approximated θ from a microscope image (Figure 4.11E), while σ was fit to checkpoint competency data as described below. Running simulations of this Brownian motion generates example trajectories for $x(t)$ (Figure 4.12C). The time until spindle alignment - the random variable, A - is then the time when $x(t)$ first escapes $\pm\left(\frac{\pi}{2}-\theta\right)$. It is important to note that $\mathbb{P}(A=0)>0$, as there is a non-zero chance that the spindle is already aligned at the onset of anaphase. Using a similar approach to the approximation of the PDF of E, I simulated alignment and measured A for 10,000 cells and performed cubic spline interpolation of the histogram of this data (Figure 4.12D).

4.6.3 Prediction of spindle position checkpoint strength

PDFs for the random variables E and A are sufficient to determine the penetrance of the SPoC mutant phenotype. I define the distribution of the difference of the variables to be $D = E - A$. This variable is distributed as the convolution of the other two

$$f_D(t) = \int_0^\infty f_E(t+s) f_A(s) ds.$$

This distribution can be used to determine $\mathbb{P}(D<0)$, the probability that exit from mitosis happens before spindle alignment is complete. This probability can be approximated by numerically integrating the area between the x-axis, f_D and

the line $x = 0$ (Figure 4.12E). Using this approach, I generated computational predictions of the proportion of cells exiting mitosis before spindle alignment in 10 strains tested in Falk et al. (2016a) (Figure 4.12F). This included strains expressing the *LTE1-8N* allele, which localizes throughout the cell unlike the wild type Lte1, which is limited to the bud (Geymonat et al. (2009)). These predictions closely match the experimentally observed proportions of multinucleate cells in most cases. However, the model could not quite match the reduction in SPoC efficiency caused by the *spo12*$\triangle$ mutation in the *LTE1-8N* and *LTE1-8N kin4*$\triangle$ backgrounds.

This framework provides a mechanism to link the speed of anaphase progression to the proportion of experimentally observed multinucleate cells. The success of this approach in predicting the strength of SPoC mutants suggests that the compartmental logical modelling framework is capable of making continuous predictions about the properties of mutant phenotypes.

4.7 Predicting the impact of forced localization

In the compartmental logical modelling framework it is easy to simulate mutant proteins that mislocalize within the cell, a clear advantage over non-spatial models. In order to examine the effects of forced localization at the SPB, I simulated the effects of forcing MEN proteins to localize there.

4.7.1 Forcing proteins to the spindle pole body

There are 10 MEN proteins that localize to the SPB in the model, I simulated forcing each of these, and Lte1, to the SPB using Model 5 under the asynchronous update scheme (Figure 4.13A). As Lte1 does not usually localize to the SPB, a modified version of the model incorporating an Lte1-SPB node was used to simulate this phenotype. In the cases where these experiments have already

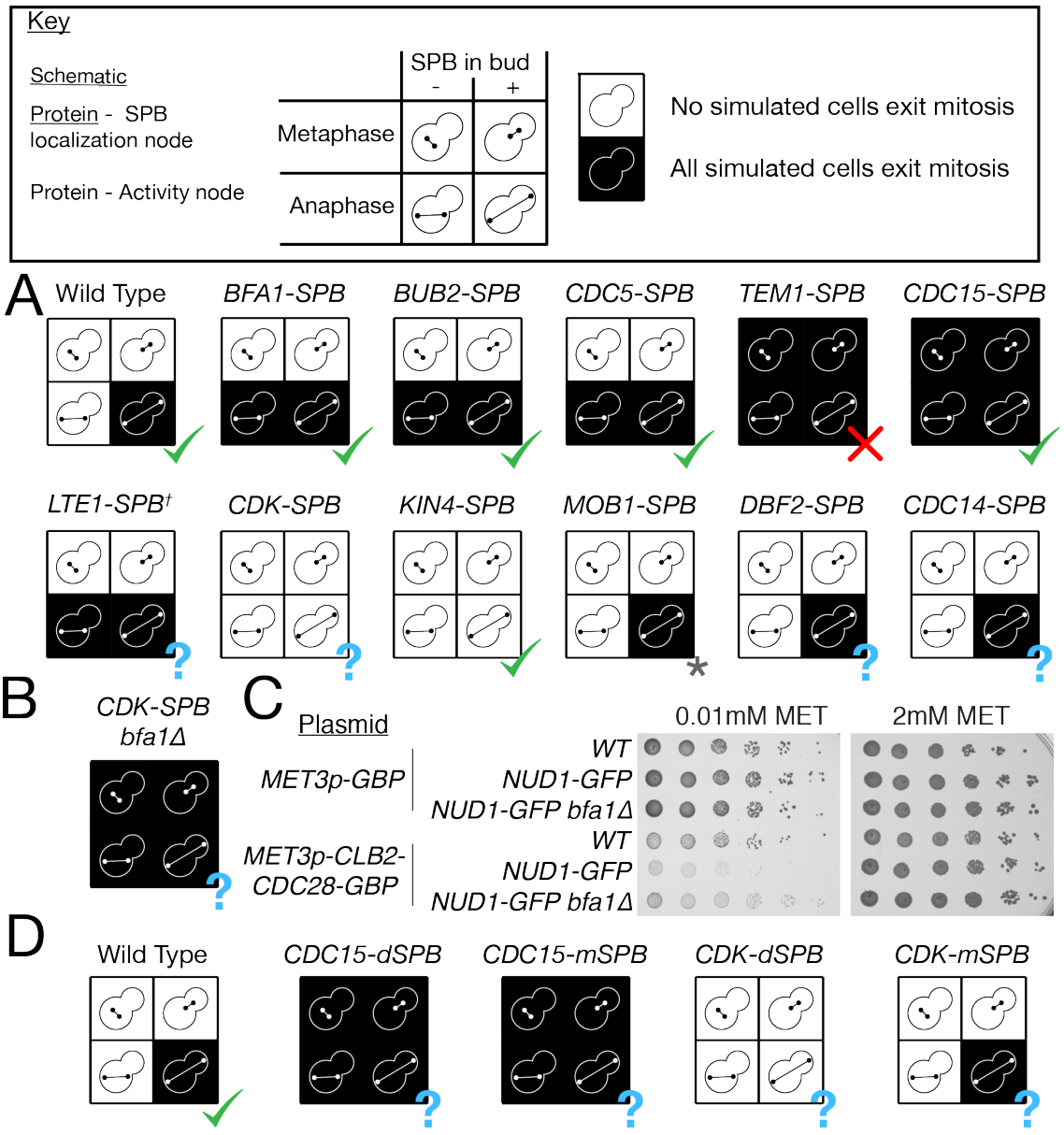

Figure 4.13: Caption located on next page.

been performed, the simulated phenotypes mostly match the experimental findings (5/6).

Bub2-Bfa1 is an inhibitor of MEN signalling so it is surprising to see that forced localization of these proteins induces mitotic exit in cells with misaligned spindles (Figure 4.13A). However, this has been experimentally observed (Scarfone et al. (2015); Gryaznova et al. (2016)). This is because Bfa1 is inhibited by Cdc5 at the SPB so forcing Bub2-Bfa1 to the SPB abolishes the protective effect of Kin4 phos-

Figure 4.13: Simulated forced localization phenotypes. A: Predicted phenotype of cells where each of the SPB-localized proteins in the model are forced to localise to the SPB. A question mark (?) indicates an phenotype that has not been experimentally verified in the literature. A star (*) is used to indicate that the *MOB1-SPB* phenotype differs from literature accounts due to factors beyond the scope of the model. B: Predicted rescue of the *CDK-SPB* phenotype by *bfa1*Δ. The dagger symbol (†) is used to indicate that the *LTE1-SPB* phenotype was tested on an updated version of the model. As Lte1 does not usually localize to the SPB, a modified version of the model was used to test this phenotype. C: Spot tests showing growth defect of Nud1-GFP cells expressing a fusion Clb2-CDK-GBP protein from the *MET3* promoter and rescue of this defect by *bfa1*Δ. Activity of the *MET3p* promoter was tuned by addition of 10μM methionine to media. D: Predicted phenotype of cells where Cdc15 or CDK are forced to either the mSPB or dSPB.

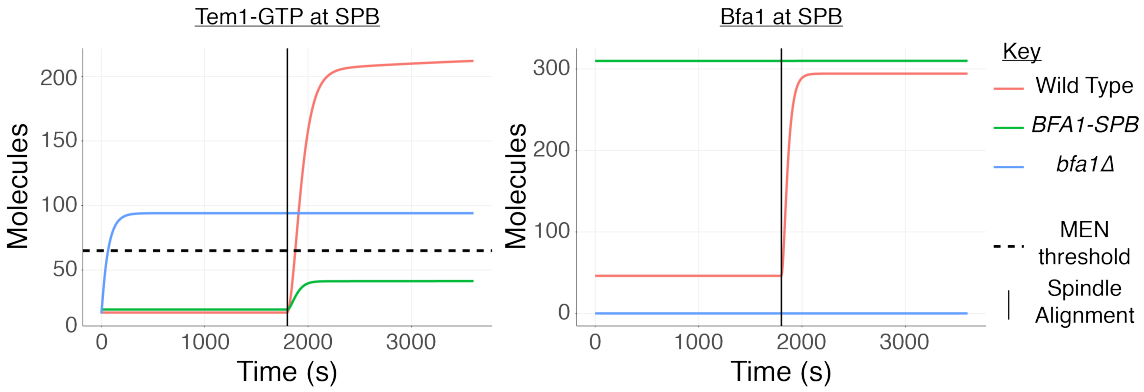

Figure 4.14: Simulations of wild type, *BFA1-SPB* and *bfa1*Δ cells using the model of Caydasi et al. (2012). The graph on the left shows how the number of Tem1-GTP (active Tem1) molecules at the SPB, while the graph on the right shows total Bfa1 molecules at the SPB. In this model, activation of the MEN is signalled by the number of Tem1-GTP molecules exceeding 65 (the MEN threshold). Simulations were performed using the same parameters as Caydasi et al. (2012), with custom initial conditions matching the pre-alignment steady states of the model.

phorylation. Previous computational models of the SPoC struggled to represent this effect, with the model of Caydasi et al. (2012) predicting the opposite effect (Figure 4.14). Model 5 also predicts that forced localization of Cdc5 at the SPB would disrupt SPoC function (Figure 4.13A), as experimentally observed (Caydasi et al. (2017)). The model also predicts that forced localization of Lte1 at the SPB would compromise the SPoC, a prediction that would be interesting to test experimentally.

My simulations show forced localization of Tem1 and Cdc15 abolish all control

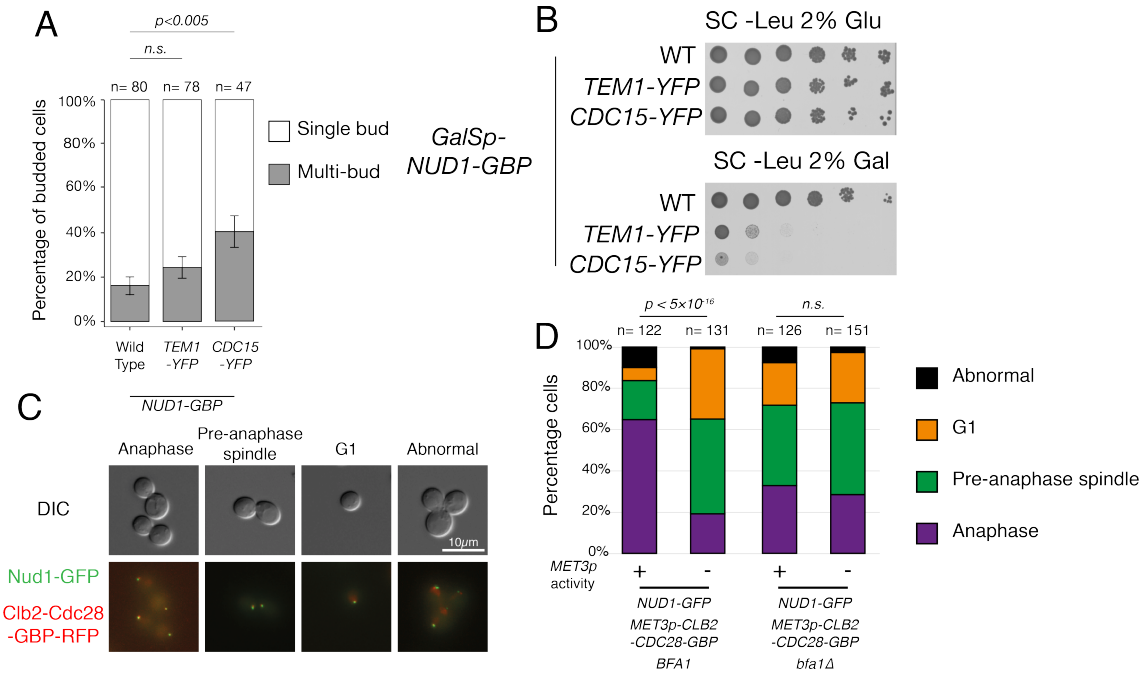

Figure 4.15: Experimental validation of simulated forced localization phenotypes. A: Recruiting Cdc15 but not Tem1 to the SPB promotes mitotic exit in metaphase. Wild type, *TEM1-YFP* and *CDC15-YFP* cells expressing *NUD1-GBP* from a plasmid were synchronized with alpha factor and then arrested in metaphase with nocodazole. After 3 hours the number of single and multi-budded cells was counted. Error bars represent 95% confidence intervals calculated with the Clopper-Pearson method. P-values were calculated using the two-tailed Fisher's exact test. B: Forced interaction of both Tem1 and Cdc15 with Nud1 is lethal. C: Representative images of *NUD1-GFP MET3p-CLB2-CDC28-GBP-RFP* cells, grown in media containing $10\mu M$ methionine. We placed cells into 4 categories: G1, pre-anaphase spindle (S or early M cells with 2 SPBs less than $3\mu m$ apart), anaphase (SPBs over $3\mu m$ apart) and abnormal cells (aberrant SPB or bud number). D: Quantification of the percentage of cells in each category. *NUD1-GFP MET3p-CLB2-CDC28-GBP-RFP* cells showed a high proportion of anaphase cells, which could be rescued by repression of the *MET3* promoter by addition of methionine or by the *bfa1*Δ mutation. *MET3p* activity was tuned by addition of 0.01mM methionine (+) or 2mM methionine (-). P-values calculated using the two-tailed Fisher's exact test.

of Cdc14 release during mitosis (Figure 4.13A). This is expected of Cdc15, which has been shown to induce exit from mitosis in metaphase when forced to the SPB (Rock and Amon (2011)). However, this is not true of Tem1. Valerio-Santiago and Monje-Casas (2011) showed that a Tem1-Cnm67 fusion protein could induce exit from mitosis in cells with misaligned spindles but not in metaphase. Nud1, rather than Cnm67, is the scaffold for Tem1 at the SPB (Scarfone and Piatti (2015)) so I

decided to test whether forcing Tem1 to interact with Nud1 would result in the predicted phenotype. I transformed wild type, *CDC15-YFP* and *TEM1-YFP* strains with a plasmid expressing *NUD1-GBP* from the reduced strength *GALS* promoter, as described in the previous chapter. I found that forced recruitment of Cdc15 but not Tem1 to Nud1 could induce mitotic exit in cells arrested in metaphase with Nocodazole (Figure 4.15A). Intriguingly, induction of *NUD1-GBP* was lethal in either strain (Figure 4.15B). This evidence suggests there may be aspects of Tem1 regulation not yet captured in the model.

Not all forced localizations induced mitotic exit, Kin4 is predicted to prevent mitotic exit when forced to the SPB (Figure 4.13A). There is conflicting experimental evidence on this point. A *KIN4* mutation that causes symmetrical localization had no effect on mitotic exit control (Chan and Amon (2010)) while a Kin4-Spc72 fusion protein was found to delay Cdc14 release (Maekawa et al. (2007)). Kin4 was identified as causing a SPI with Spc72 and Nud1 in the screens described in Chapter 3. Cdc14, Dbf2 and Mob1 are predicted to have no effect when forced to the SPB; the only case that has been tested experimentally is Mob1. A Mob1-Nud1 fusion was shown to be lethal because in this strain Mob1-Dbf2 could not leave the SPB and consequently could not release Cdc14 from the nucleus (Rock et al. (2013)). This effect is not captured in the model. Like Kin4, CDK is predicted to prevent mitotic exit when forced to localize to the SPB (Figure 4.13A). Additionally, the model predicts that this effect will be rescued by *bfa1*Δ (Figure 4.13B). I decided to test these predictions experimentally in collaboration with Cinzia Klemm from the Thorpe Lab.

We used plasmids that express either *GBP* or a *CLB2-CDC28-GBP* fusion protein from the *MET3* promoter in a yeast strain expressing *NUD1-GFP*. The *MET3* promoter is inducible, with very low expression in the presence of 2mM methionine, and a reasonably high level of expression in media containing 10μM methionine (Mao et al. (2002)). We found that the forced interaction of CDK

with Nud1 was lethal and that, as predicted, the *bfa1*Δ mutation rescued this effect (Figure 4.13C). Microscopy of these strains show that cells arrest with an extended spindle and large bud (Figure 4.15C), indicative of a late anaphase arrest. Quantification of cell cycle stage shows that deletion of *bfa1*Δ rescues this phenotype (4.15C).

4.7.2 Forcing proteins to localize asymmetrically

Tools to force protein localization at both SPBs, such as the GBP-GFP system, have been used to study the effect of forcible localization on the MEN for many years. However forcing proteins to interact with a single SPB is more difficult to achieve genetically. A system using optogenetics to activate binding at a single SPB has been used to recruit Clb2 to one SPB at a time (Yang et al. (2013)) but the effect of this on mitotic exit control has not been fully investigated. However, the impact of such perturbations can be explored using the compartmental logical model. The model predicts differing types of behaviour for CDK and Cdc15. Cdc15 is predicted to cause unscheduled mitotic exit when forced to localize at either SPB (Figure 4.13D), suggesting that MEN signalling could occur at the mSPB. On the other hand, the impact of forced localization of CDK at the SPB is only felt when forced to the dSPB and not the mSPB (Figure 4.13D).

4.8 Discussion

In this chapter I have presented and analyzed a spatio-temporal model of mitotic exit control in yeast. This model helps to answer the second of my key questions in this project: how is localization at the SPB used to regulate proteins? By formalizing the mechanism of mitotic exit control it allows us to examine how regulation of localization contributes to regulation of MEN proteins. In this section, I will begin by discussing the compartmental, logical modelling formalism and then

move on to discuss how the model contributes to our understanding of mitotic exit control.

4.8.1 Model training

My first approach to building a model of the MEN was to use CellNOptR to train a model against established MEN phenotypes. CellNOptR allowed me to find an ensemble of reasonable models, including 7 which could fit 88% of the provided phenotypes. I was surprised by the diversity of models produced by the genetic algorithm. Generally, the models converged functionally to fit the same phenotypes but not structurally. This suggests that the issue of finding unique logical models may generally be quite hard as multiple models may show the same phenotypic behaviour. This is a common problem in systems biology and is recognised by the authors of CellNOptR, who also found that the algorithm identified multiple optimal models (Saez-Rodriguez et al. (2009)). One solution to the issue is to identify specific experiments that will aid in model identification. This idea of a cyclical process of computational prediction and experimentation guided by these predictions is well-established in systems biology (reviewed in Kitano (2002); Kreutz and Timmer (2009)). Algorithms to identify experiments to distinguish Boolean models already exist (Ideker et al. (2000)) and these could be utilised to automatically infer the most informative perturbations.

An alternative approach could be to make use of the diversity of fitted models. In the field of machine learning, the random decision tree method has similar limitations: a single tree can be easily found and verified but repeated applications of the algorithm generally identify different trees. This method was improved by generalising it to the random forest method, in which a “forest” of trees is generated and the decision is determined by a democratic decision made by the entire forest. A similar approach could be considered for logical models, where the behaviour of an ensemble of models could be considered instead of an individual

model. This could be implemented as a form of probabilistic Boolean network, where the rule for a given node is selected randomly weighted by the frequency of this rule within the ensemble of trained models.

However, the failure of the method to identify a single model may reflect the fact that the Boolean framework is a significant abstraction of the underlying system. There were 11 phenotypes that were never fit by the training algorithm. Many of these were phenotypes I later identified issues with, in particular rescue of temperature sensitive MEN strains by Cdc5 overexpression and interaction of FEAR and Kin4 regulation of Bfa1. Two phenotypes were mutually exclusive among the optimal models, these were the SPoC phenotype of *rts1*Δ and its rescue by deletion of *LTE1*. This issue was resolved in the later model by introduction of spatial regulation of Kin4. The issues this model had achieving a perfect fit to the data are similar to the issues of the later model which are discussed below.

4.8.2 Spatio-temporal logical models

The primary issue with the models trained by CellNOptR was that they could not represent spatial organization of the MEN. In order to address this issue, I developed a novel modelling formalism: compartmental logical models. In principle, this kind of model could be trained with a genetic algorithm, like CellNOptR, but this algorithm would have to apply mutations to the underlying activity and localization networks and then test the compiled compartmental model.

This framework is similar to the compartmental ODE formalism and can represent most of the same kinds of spatial regulation. However it would currently struggle to represent sequestration in a compartment. In a compartmental ODE model there is a total number of molecules in the cell, meaning that localization in one compartment can effectively inhibit localization elsewhere. This is not represented in my MEN model, although additional rules could be included to make localization of some species in different compartments mutually exclusive.

In my model, the nucleolus is not explicitly represented so sequestration is modelled by inhibiting localization in the nucleus. The explicit representation of these compartments forces the researcher to consider the implications of some interactions. In this case, for example, it was essential for a small amount of FEAR to enter the cytoplasm in order for FEAR to have an effect on MEN regulation. One disadvantage of making logical models compartmental is the large increase in the number of nodes in the network. In the case of my model, the number of nodes is increased by a factor of 10. Certainly, it would not be advisable to use a compartmental logical model where a standard logical model would suffice. However, this increase in size may be justified in cases where spatial regulation is important. Logical models are already generally less computationally intensive to simulate and analyze than ODE models, so this increase in size has not proven to be a significant issue.

4.8.3 Modelling overexpression and forced localization

My model can represent different kinds of mutant including deletions, overexpressions and mislocalizing proteins. Loss-of-function mutants are straightforward to model, in this case we set the corresponding node to 0, regardless of the activity of regulators. I found that overexpression and forced localization were more difficult to model. I found that simply forcing the respective activity or localization node to 1 was not sufficient to model the behaviour of these mutants. Overexpression is a complex phenotype that can have multiple effects, including rewiring existing networks (Moriya (2015)). In my model, overexpression is controlled by an additional node representing the behaviour of the overexpressed gene. This node can over-ride other aspects of regulation, for example overexpression of an inhibitor could prevent activation of a protein even in conditions which would otherwise lead to its activation. I applied a similar approach to modelling forced localization at the SPB, with this perturbation resembling a local overexpression. This ap-

proach allows the model to represent 80% of genetic phenotypes. However these assumptions do have shortcomings. As discussed earlier in the chapter, we assume overexpression forces localization at the SPB, this is necessary to represent the phenotype of *GAL1p-CDC15 tem1*Δ but incorrectly predicts the phentoype of the *GAL1p-KIN4 rts1*Δ mutant. While the rule I have used here is a good heuristic it is clearly not applicable in all circumstances. To improve this would require more quantitative detail about the overexpression phenotype and how it could interact with other aspects of regulation. If this information became available then a hybrid logical-ODE model (such as described in Bornholdt (2008)) could be used to integrate this data into the existing model.

4.8.4 Limitations of logical modelling

In this chapter I have shown that a compartmental logical model of the MEN can accurately model control of mitotic exit in yeast. However, the simplifying assumptions behind these models lead to inevitable limitations. Certain mechanisms are inherently quantitative, for example the high turnover of Bub2-Bfa1 at the SPB as a result of Kin4 phosphorylation which protects Bfa1 from Cdc5 inhibition. In this case I was able to model the regulation by a simpler mechanism where Kin4 prevents Bfa1 localizing at the SPB. However there are some interesting MEN phenomena that my model does not reproduce, for example the asymmetry of MEN proteins at the SPB prior to spindle alignment or localization of MEN protein at the mSPB in telophase. These phenomena were left out as they were suspected not to have a functional role on the outcome of signalling, but they likely have an impact on the dynamics of mitotic exit signalling. While the model was able to make predictions about the impact of FEAR on the dynamics of mitotic exit, these other factors are not accounted for.

I found that the inability of logical models to represent partial loss-of-function mutations, like temperature sensitive alleles, was a significant limitation to the

model. Many of the phenotypes that could not be matched by the model were rescues of temperature sensitivity by overexpression of other genes. These could not be represented by the model as it could not distinguish between a deletion, which is lethal, and a temperature sensitive strain. One could argue that these effects would be more effectively modelled by a system of ODEs, which could account for quantitative changes. Technically this is true but in practice the quantitative details required to make such predictions are often lacking, for example the difference in activity between a wild-type and temperature-sensitive enzyme at restrictive temperature. However, if this kind of information were to become available this would be a viable option for ODE models. In order for logical models to be able to make such predictions, some kind of quantitative modification would be required.

4.8.5 Biological implications of the model

Through development of the model, I have arrived at several conclusions about the regulation of mitotic exit in yeast. Some of these are new ideas, but most are affirmations or combinations of earlier ideas. However, putting these pieces together in a computational model constitutes a comprehensive and unified view of mitotic exit.

The anaphase specific component and Cdc5

I introduced the ASC as a regulator of Cdc15 localization in order to fit the phenotype of *CDC15-7A MOB1-2A* cells. By combining the ideas of Rock and Amon (2011) and Botchkarev et al. (2017), I propose that Cdc5 could play this role (Figure 4.16). In this model, Cdc5's localization at the cytoplasmic face of the SPB in early anaphase is the signal required for mitotic exit to be initiated in *CDC15-7A MOB1-2A* cells with a misaligned spindle. Botchkarev et al. (2017) argue that

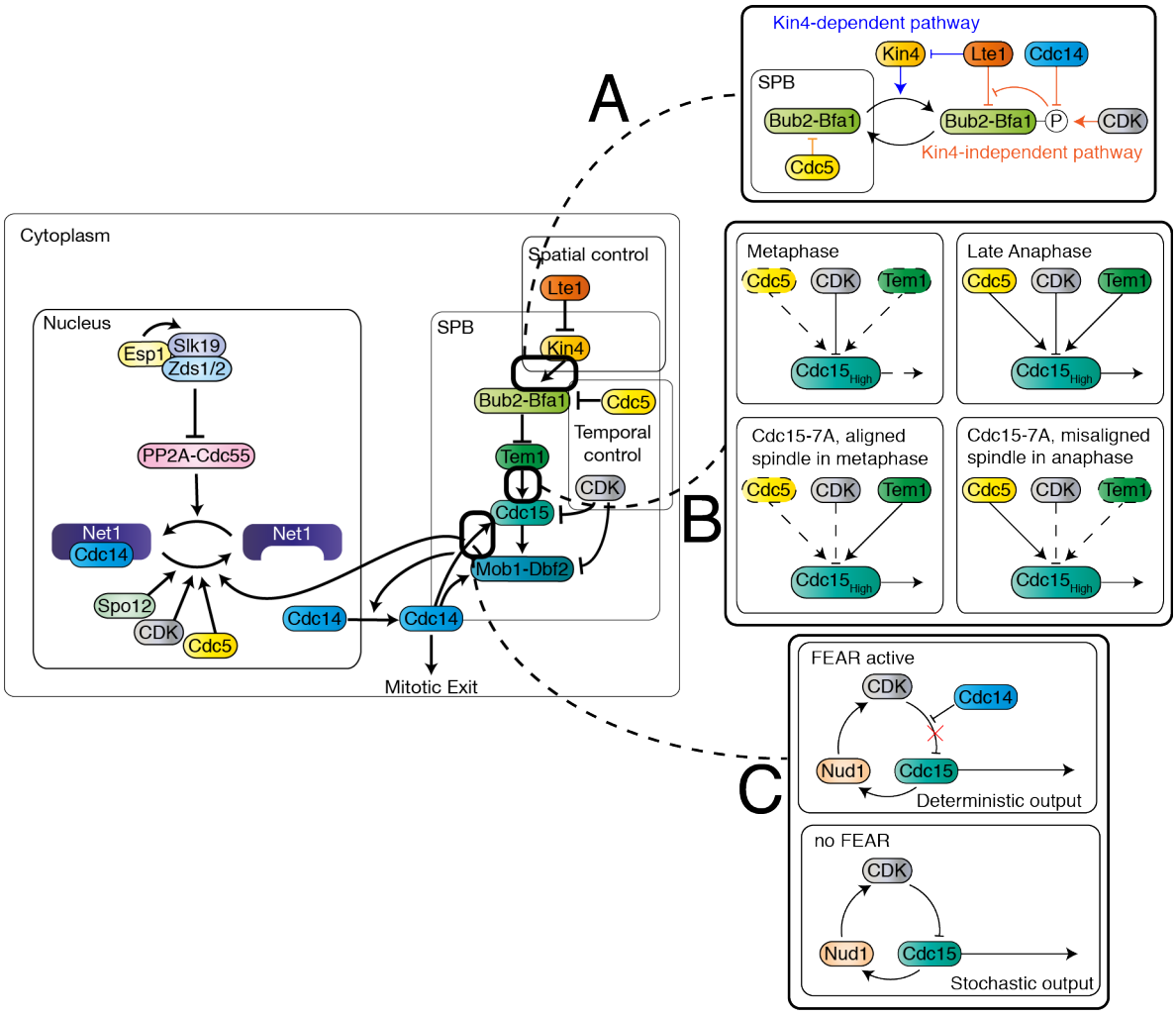

Figure 4.16: Model of the MEN including the developments contributed in this chapter. A: Lte1 regulates Bub2-Bfa1 via two pathways, only one of which is dependent on Kin4. B: Cdc5 is required for recruitment of Cdc15 to the SPB in the absence of Tem1 or CDK regulation. C: FEAR breaks a Cdc15-Nud1-CDK negative feedback loop, leading to deterministic timing of mitosis.

Cdc5's movement from nuclear to cytoplasmic face of the SPB is controlled by the FEAR network, and this could be explored in the model. A key prediction of this model is that Lte1 is responsible for Bfa1 inhibition in *CDC15-7A MOB1-2A* cells which exit mitosis in metaphase with an aligned spindle. It would be an interesting test of the model to see whether deletion of *LTE1* prevents exit from mitosis in these conditions.

The role of Lte1 beyond Kin4 regulation

As noted by Falk et al. (2016a), *kin4*Δ*spo12*Δ cells can maintain the SPoC despite the absence of Kin4. I found that the model therefore required two parallel SPoC pathways, one via Kin4 and another independent of it (Figure 4.16). I further built on this mechanism in Model 6, proposing that MEN signalling could proceed more rapidly in the presence of Lte1 than in its absence. A tempting mechanism would be that Lte1, which contains a GEF-like domain, could act as a GEF for Tem1. However, it has been shown that Lte1 has no GEF activity towards Tem1 *in vitro* (Geymonat et al. (2009)), although other factors such as Ras, were not included in these experiments (Seshan and Amon (2005)). Furthermore, I found that Lte1's alternative MEN-promoting activity must be directed towards Bfa1 rather than Tem1. My choice of Lte1 was based on the requirement that the signal must be bud-localized to meet the spatial requirements. However, there are potentially other bud-localized proteins that could perform this role. While sick, the *lte1*Δ*kin4*Δ*spo12*Δ triple mutant can exit mitosis but requires the bud-localized kinase Ste20 (Caydasi et al. (2017)). Additional polarity proteins, such as Kel1, Kel2, Cdc24 and Cdc42 have also been shown to play a role in control of mitotic exit (Höfken and Schiebel (2002)). Therefore it may be that it is these proteins, rather than just Lte1 which contribute to SPoC maintenance in the absence of Kin4. Examining the contribution of these proteins could be an interesting future direction for the model. .

The role of Cdc14 early anaphase release in the control of mitotic exit

While control of FEAR has been extensively studied, its purpose is not entirely clear. FEAR proteins have genetic interactions with MEN proteins, leading to the view that the FEAR 'primes' the MEN. This is backed up by the observation that mitotic exit is delayed in FEAR mutants. I simulated my model in continuous time using MaBoSS and found that in these simulations, FEAR mutants not only spent longer in mitosis but the length of mitosis was also more variable. This finding was verified using time-lapse microscopy. In this model, the key determinant of mitosis length was localization of Cdc15 at the SPB, which occurs deterministically in the presence of FEAR and stochastically in its absence (Figure 4.16). The FEAR has many other roles, some of which could also regulate the length of mitosis, for example reversing CDK-phosphorylation of securin, accelerating the metaphase-anaphase transition (Holt et al. (2008)).

The logical formalism is fairly abstract and so it is reasonable to question whether we would really expect it to capture temporal effects. In the continuous-time Markov chain simulation strategy used by MaBoSS, waiting times such as the length of mitosis are effectively the sum of sequential waiting times for individual nodes to update. Each node is selected to update as a Poisson process with a rate parameter ρ, meaning the waiting time between the previous node in the cascade updating and the next node changing state is an exponential variable with rate ρ. In the case of a linear cascade with k components, the waiting time would be

$$T = \sum_{i=1}^{k} t_i,$$

where t_i are independent exponential variables with rate parameter ρ_i. If the ρ_i are all the same then T fits the definition of an Erlang distribution. Recent research measuring the length of cell cycle stages in human cells found that they were modelled well by an Erlang distribution (Chao et al. (2019); Gelens and San-

tos (2019)). Together with my own findings on mitosis length, this suggests that continuous-time implementations of logical models can be effective at representing biological timing processes.

4.8.6 A stochastic view of checkpoint competence

For much of this chapter I have dealt with mutant phenotypes as deterministic outcomes however in reality only a fraction of cells ever display a mutant phenotype. By considering the waiting times until either mitotic exit occurs or the spindle aligns, I was able to predict the proportion of cells showing a binucleate phenotype in SPoC mutant backgrounds. I used existing data to fit rate parameters to get a dimensional model, and eventually found that by varying a single parameter, σ, I could fit the percentage of binucleate cells in both *kin4*Δ and *bub2*Δ backgrounds. The fact that varying this single parameter could fit both phenotypes suggests the model is not over-fitted.

In this view of checkpoints, two kinds of mutant may affect the percentage of cells affected: SPoC machinery and timing mutants. Obviously, mutants affecting the machinery detecting spindle alignment will affect SPoC competence but additionally mutants affecting the rate of mitotic exit signalling could also change the percentage of cells affected in a SPoC mutant background. As FEAR mutants are delayed in mitotic exit, it is possible that the SPoC rescue of *kin4*Δ*spo12*Δ cells could be caused simply by the delay in signalling. Notably, the model was not able to fully predict the impact of *spo12*Δ in *LTE1-8N* strains. Although I was able to show a delay in mitotic exit in FEAR mutants in the non-parameterised model, I did not fit this delay to quantitative data. It would be interesting to add parameters to the model to allow it to quantitatively represent the delay caused by FEAR mutations. Until this mechanism has been fully explored, it remains an open question whether the impact of FEAR mutants on SPoC competence is a result of changes to the logic or the timing of the MEN.

More generally, this framework would apply to other checkpoints such as the SAC and in other organisms. It would be interesting to compare the stochastic properties of checkpoints such as the SAC between single-celled yeasts and multi-cellular organisms. It is sometimes speculated that single-celled organisms have intentionally leaky checkpoints as they have a vested interest in their own survival even if this causes aneuploidy. Multi-cellular organisms may be more careful as they face an evolutionary pressure from cancer, which may outweigh the benefits of an individual cell's survival.

4.8.7 The role of SPB localization in the MEN

A key aim of this project was to establish a mathematical model that could help us to understand the role of localization of MEN proteins at the SPB. A key test of this model is therefore whether it can correctly predict the impact of forced localization of MEN proteins at the SPB. I found that the model could correctly predict the phenotype of forced localization of all MEN proteins except for Tem1. In collaboration with Cinzia Klemm I have also verified the prediction of the model that forced localization of CDK at the SPB would prevent mitotic exit and that this could be rescued by *BFA1* deletion. Both the experiments of myself and Valerio-Santiago and Monje-Casas (2011) show that forced recruitment of Tem1 at the SPB does not induce mitotic exit in metaphase, in contradiction of the prediction of the model. It will be interesting to explore the factors restraining mitotic exit in metaphase in such cells, especially as deletion of Bub2-Bfa1 components, which act through Tem1, are sufficient to cause premature Cdc14 release.

Forced localization of proteins at both SPBs is already a standard technique in the molecular biologist's toolbox. However, my model is able to predict the outcome of experiments that are not yet widely practiced, such as recruitment to a single SPB. The model predicts that forcing Cdc15 to either SPB would initiate mitotic exit, raising the interesting prospect of driving MEN activity from the mSPB.

On the other hand, the model also predicts that the effects of forced localization of CDK would prevent mitotic exit only at the dSPB. There are two possible ways to achieve this asymmetric localization. The first would be to make use of existing asymmetries between the SPBs. Kar9 localizes at the dSPB and so fusing proteins to Kar9 using the GFP-GBP system could achieve this. The identity of the SPB is controlled by phosphorlyation of Nud1 and so it is theoretically possible that with further work to understand how this modification defines the SPB's identity, this modification could be leveraged to control localization at one SPB or the other. Alternatively, an optogenetic system could be used to target proteins to one SPB or the other in a microscope. Yang et al. (2013) use the PhyB-PIF optogenetic system to target proteins to interact with Spc72 and show that they can target proteins directly to one SPB or another. My own preliminary research has shown the potential to use a Nud1-PIF fusion to target PhyB-YFP to the SPBs upon exposure to light. Therefore this strategy could be used to test the predictions made by the model about the impact of forced localization at a single SPB.

4.8.8 Summary

In this chapter I have set out two approaches to modelling control of mitotic exit. In the first approach, I used a model-fitting algorithm to train a logical model against a dataset of literature phenotypes. This approach proved effective, however it could not represent the spatial apsects of regulation of the MEN. Therefore, I developed a novel approach, building a compartmental logical model. This approach allowed me to produce a model of mitotic exit which can explicitly represent the localization of MEN proteins at the SPB and predict the impact of altering this localization. This model allows us to address the question of how localization is used to regulate MEN proteins. For example, it reveals how the Bub2-Bfa1 complex is able to have both MEN activating and inhibiting behaviours as a result of the distinction between regulation of its localization and GAP activity. Develop-

ing this model yielded several interesting insights into the regulation of mitotic exit control. Furthermore, a continuous time implementation of the model, allowed me to make and test predictions about the timing of mitosis. Additionally, I was able to adapt this approach to investigate the role of timing in cell-cell variation of SPoC mutants. Overall, the compartmental logical model of the MEN has proved a powerful tool to study mitotic exit and the role of localization at the SPB.

Chapter 5

Conclusion and Future Directions

In this chapter I will present the key discoveries from the project then revisit the aims of the project and highlight how they have been addressed in this thesis. I will then outline the future work that could be performed to build on the work presented here.

5.1 Key discoveries

- **The SPB is especially sensitive to forced localization.** I fitted mixture models to the SPB SPI data as well as 23 SPI screens published by Berry et al. (2016). The fitted parameters of these models suggest that the SPB screens have more and stronger SPIs than other regions of the cell.

- **SPIs can induce SPB overduplication.** I showed that forced interactions between Spc42 and Bbp1, Nup133 and YJL021C lead to cells showing additional SPBs and multi-polar spindles. I also found evidence of additional SPBs resulting from forced interactions between Spc42 and 11 SPIN and nuclear pore proteins.

- **A compartmental, logical model of mitotic exit fits 80% of literature phenotypes.** Construction of the model revealed the importance of sev-

eral aspects of MEN regulation. I found that translocation of Cdc5 across the nuclear membrane is an important anaphase-specific signal, limiting MEN activity in metaphase. Bub2-Bfa1 is found in low levels at the SPBs from metaphase, and this is also important to restrain MEN activity prior to anaphase. If found that, aside from the Kin4-mediated pathway, an additional bud-specific signal targeting Bub2-Bfa1 is also necessary, in this model Lte1 plays this role.

- **FEAR regulates the robustness of anaphase length.** The model predicts that deletion of FEAR network components should lead to more variability in anaphase length. I verified this with time-lapse microscopy. This effect is mediated by low levels of Cdc14 interrupting a negative feedback loop between Cdc15, Nud1 and CDK, leading to deterministic loading of Cdc15 at the SPB.

- **A stochastic view of checkpoints predicts the proportion of SPoC deficient cells.** By combining the model with a model of spindle alignment I constructed a framework to predict the proportion of cells showing a binucleate phenotype.

- **The logic of spatial regulation in the MEN.** The compartmental model can simulate mislocalizing mutants and in most cases correctly predicts their phenotypes. I demonstrate that the model correctly predicts the phenotype and rescue of forcing CDK to localize at the SPB. The model can also make predictions about the impact of localizing proteins to a single SPB.

5.2 Meeting the aims of the project

Which proteins are regulated through interactions with the SPB?

I performed SPI screens using GBP fusions with 5 different regions of the SPB. These screens identified proteins that cause a growth defect when forced to localize at the SPB.

The hits from the SPI screens were enriched for proteins involved in processes that are known to be regulated from the SPB. I found that a number of MEN proteins were SPIs with the SPB. Further analysis of these interactions showed that some were scaffold-dependent, in particular Tem1 had a different phenotype when recruited to Spc72 than Nud1. These findings fit into an established body of work demonstrating mitotic exit is controlled from the SPBs. I also found that the screen with Spc42 was enriched for nuclear pore components. A growing body of work has implicated nuclear pore proteins in the process of SPB insertion. I found that forced recruitment of both nuclear pore components and SPIN proteins (known insertion regulators) induced SPB overduplication. These results imply that either an additional, as-yet-uncharacterized SPB duplication pathway exists or that recruitment of these proteins to the SPB is a novel aspect of regulation of SPB duplication. These strains show potential to be developed into a yeast model to study the impact of multiple MTOCs on chromosome division, this is a promising avenue for future work.

By comparing my SPB screens to a number of already published SPI screens, I was able to establish that the SPB is especially sensitive to forced localization. This means that my SPI screens had more and stronger hits than other screens. The hits from my screens were enriched for a number of processes that are not currently known to occur at the SPBs, for example lipid biosynthesis. One possible explanation for this is that the SPB is a particularly effective structure to sequester proteins. By this logic, proteins that play an essential role in the cell

can be effectively prevented from playing this role by keeping them tied up at the SPB. This is a possible explanation for the Cdc28-Nud1 SPI, which appears to cause a mitotic entry defect. In any case, these screens show that many proteins have the potential to have their functionality modified through localization at the SPB.

How is localization at the SPB used as an aspect of protein regulation?

I have developed a novel modelling formalism in order to integrate spatial information into a logical model of the MEN. This has allowed me to investigate the role of localization in the MEN both experimentally and computationally. Clearly, logical modelling is a simplistic representation of a complex system. However, with the compartmental adaptation of the formalism, it seems to be sufficient to explain the behaviour of the MEN under many different genetic perturbations.

Localization of MEN proteins at the SPB is clearly a key aspect of their regulation and is necessary for the key positive regulators of the MEN: Tem1, Cdc15 and Mob1-Dbf2. Cdc15 is a particularly interesting case, as unlike many other MEN proteins, it's activity does not appear to be regulated through post-translational modification. Instead, its activity towards Dbf2 is regulated only through localization at the SPB. The local increase in concentration of both proteins at the outer plaque of the SPB is then sufficient for Cdc15 to phosphorylate and activate Dbf2. This is mediated by phosphorylation of Nud1 by Cdc15. Interestingly, phosphorylation of Nud1 by Cdc15 is also thought to be necessary for a negative feedback loop which leads to recruitment of CDK, and ultimately to loss of Cdc15 from the SPB. FEAR release reverses CDK phosphorylation of Cdc15, allowing it to localize stably at the SPB. In the absence of CDK and Tem1 regulation, Cdc15 localizes at the SPB in anaphase, a finding we attribute to the localization of Cdc5 at the SPB at that time. Therefore, localization of Cdc15 at the SPB acts as an integrator of temporal and spatial signals. It is interesting to note that my model

predicts that localization of Cdc15 at the mSPB should induce MEN activation there in cells with a misaligned spindle and this would be a key test of the model's accuracy.

Unlike Cdc15, the Bub2-Bfa1 complex is an inhibitor of the MEN but its localization at the SPB also promotes MEN activity. This contradictory behaviour results from the distinction between its role as a scaffold for Tem1 at the SPB and its GAP activity towards Tem1. By making a distinction between localization and activity of a protein in the compartmental logical modelling framework, these effects can be accurately modelled, resulting in the correct prediction of the phenotype caused by forced localization of the complex at the SPB. Therefore, for Bub2-Bfa1, localization at the SPB allows for tight spatial control of Tem1 activity. In the cytoplasm, the complex effectively inhibits Tem1 activity and prior to spindle alignment Kin4 acts to keep Bub2-Bfa1 exchanging regularly with between the cytoplasm and SPB. Upon spindle alignment, the complex accumulates at the dSPB, where it's activity is inhibited by Cdc5 and by a bud-specific protein which has been proposed to be Lte1. This regulation of Bub2-Bfa1 ensures that Tem1 can only become active at an SPB in the bud.

The localization of Tem1 at the SPB is also clearly highly regulated. My model predicts that forced localization of Tem1 should induce Cdc14 release in metaphase, but experimental observations indicate this is not the case. It will be interesting to study what factors are limiting MEN activity in metaphase when Tem1 is localized there. My SPI mini-screens suggested that Tem1 is highly sensitive to the specific region it is localized to. The forced interaction of Tem1 with Nud1 is always lethal, while the SPI between Tem1 and Spc72 depended on the *kar9*$\triangle$ mutation. Forced interaction of Tem1 with the temperature sensitive *nud1-2* allele had no effect on fitness at all. This information suggests that Nud1 may do more than just act as a passive scaffold for Tem1.

Beyond well-characterised MEN proteins, some other cell cycle regulators

showed a growth defect when recruited to the SPB. One such protein is Tpd3, the regulatory subunit of the PP2A complex. PP2A has well understood roles in mitotic exit, in particular the Cdc55 isoform is important in the FEAR network and the Rts1 isoform regulates Kin4 localization at the SPB. However there is significant biochemical evidence that PP2A also regulates Mob1 and Bfa1 (Baro et al. (2013, 2018); Touati et al. (2019)). An interesting future direction for this research will be to expand the treatment of PP2A. Glc7, the catalytic subunit of PP1, was also identified as a SPI with the SPB. PP1 is known to play a role in mitotic exit of other eukaryotes, but has no known function in this process in budding yeast.

Why does the cell use localization at the SPB to regulate proteins?

On the face of it, my model of mitotic exit provides an easy answer to this question. A number of proteins are required to localize at the SPB for mitotic exit to occur. Any mutation preventing their localization there would prevent mitotic exit. However, perhaps a more interesting question is why localization, rather than more widely-used mechanisms like post-translational modification, is used.

The SPB acts as a sensor for the SPoC, sensing the entry of the SPB into the bud compartment as an indicator of spindle alignment. Other mechanisms, such as interactions between astral microtubules and the bud neck have been proposed however further experimental observations have lead to their rejection. While these other mechanisms seem convincing, clearly an SPB-based mechanism was selected for. It seems likely that this is the root cause for MEN proteins to localize at the SPB. The obvious counterpoint to this suggestion is that *S. pombe* regulates the SIN from the SPBs but does not have a SPoC. Certainly, other budding yeasts, such as *Candida albicans* have been shown to possess a SPoC (Finley et al. (2008)) so it could be that *S. pombe* descended from a yeast which required a SPoC and has maintained regulation at the SPB while losing the checkpoint. However, even this argument does suggest that regulation of the

MEN or SIN at the SPB offers some advantage beyond its role as a sensor.

Scaffolds are common in biology, however they usually consist of a protein that brings together two proteins to increase the activity of one towards the other. Large multi-protein assemblies like the SPB acting as a scaffold are more rare. Scaffolds have a number of useful theoretical properties, in particular they can greatly increase the rate of reaction (Levchenko et al. (2000)). This is particularly evident in the case of Cdc15 phosphorylation of Dbf2, which can occur in the cytoplasm but proceeds too slowly to reach the threshold of Dbf2 activity required for mitotic exit.

An interesting way to investigate this effect would be to engineer a synthetic signalling pathway. This pathway could then be studied in isolation from its impact on growth. Various versions of the pathway could be developed to test the effect of introducing a scaffold based on a single protein or a multi-protein assembly.

5.3 Future directions in systems biology

Systems biology is a young and developing field, here I will outline a few areas touched upon in my research which I expect to lead to major developments in the field.

Integrating data into models

In recent years the amount of biological data has increased exponentially. High-throughput and robotics-assisted methodologies mean that assays can be performed on much larger scales than previously attempted. For example, genome-wide phosphoproteomic screening is now a widely used technique and has been used to study exit from mitosis in yeast (Touati et al. (2018)). Developments in artificial intelligence and machine learning are beginning to allow for automated analysis of complex datasets on a large scale. For example, Mattiazzi Usaj et al.

(2020) have recently performed automated phenotyping of cellular morphology across the entire yeast deletion collection. These new kinds of datasets provide both an opportunity and a challenge for systems biology. On the one hand they offer a window into the kind of specific, quantitative details that for so long have been lacking from our understanding of biological systems. However their interpretation is often not straightforward and comparison between methods and even between groups performing the same kinds of experiments is difficult. Therefore it will be critical to develop tools to allow for integration of heterogeneous datasets into mechanistic models.

Logical model inference

As I found in my own attempts at model inference, this is currently a difficult problem, with significant issues of model identifiability. As the model spaces of logical models (as well as quantitative modelling formalisms) are very large, heuristic methods such as the genetic algorithm will always be limited. Some alternative approaches such as those based on linear programming (Leifeld et al. (2018)) and answer set programming (Videla et al. (2015)) have been proposed. Attempts have even been made to assemble ODE models directly from the scientific literature using natural language processing (Gyori et al. (2017)), and this could be extended to logical models. Currently we lack a thorough theoretical understanding of how knowledge of mutant phenotypes can constrain the model space, and as a result there is no clear idea about how much data is required to specify a unique model. Therefore, improvements in both our theoretical understanding of logical models and also the toolbox of algorithms to approach these problems are likely to prove valuable.

Genome-scale models

Logical models have been proposed as a framework to build genome-scale models of cells as a tool for personalised medicine. While some diseases have been identified that are caused by particular alleles of a single gene, some such as Type 2 diabetes clearly have a genetic component but this cannot be isolated to a single locus (Jackson et al. (2018)). Clearly, it would be of medical interest to be able to identify when someone is at risk of a disease based on the sequence of their DNA. In order to achieve this, it will be necessary to understand how alleles of one gene may interact with alleles of others. The complexity of the human genome means that computational models are likely to be necessary to achieve this aim, and the scalability of logical models makes them a strong contender. Logical models have already been used to formulate patient-specific tumour models in order to predict response to combination therapies (Eduati et al. (2020)). However, most of the genetic risk factors for diseases are not whole-scale deletions of genes but are rather small mutations to the gene or regulatory regions. Therefore, it will be important to develop tools to predict the impact of quantitative changes in activity or expression level of enzymes from logical models.

Chapter 6

Appendix

6.1 Copyright

- Figure 1.1 is adapted from D'Amours and Amon (2004), and is licensed under CC BY-NC 4.0.
- Figure 1.3 adapted from Fu et al. (2015). Copyright 2015 Cold Spring Harbor Laboratory Press.
- Figure 1.7 reproduced from Simanis (2015)) with permission of The Journal of Cell Science.
- Figure 1.8 reproduced from Costanzo et al. (2010). Reprinted with permission from AAAS.
- Figure 1.9 is adapted from Abou-Jaoudé et al. (2016), and is licensed under CC BY 4.0.
- Figure 1.12A adapted from Bornholdt (2008) with permission of The Royal Society.
- Figure 1.12B is reproduced from Li et al. (2004). Copyright 2004 National Academy of Sciences.

6.2 Data Accessibility

Most of the data from chapter 3 can be accessed at `https://doi.org/10.1534/g3.119.400117`. All data can be provided upon request by the author.

6.3 Supporting Code

All supporting code may be accessed at `https://github.com/RowanHowell`.

- **SPIdatashell.R** R script providing interface to perform tidying and standard analysis of SPI data, assuming data formatted as output from ScreenMill.
- **SPIscripts.R** R script providing functions for tidying and standard analysis of SPI data.
- **MMfit.R** R script providing interface to perform mixture model analysis of SPI screen, assuming data formatted as output from above scripts.
- **MMfuns.R** R script providing functions for mixture model analysus of SPI data.
- **CreateFEARPKN.R** R script to create the FEAR PKN in CellNOptR format from Supplementary File 14.
- **ReadFEARPhenotypes.R** R script to create a list of FEAR phenotypes in CellNOptR format from Supplementary File 15.
- **TrainFEARNetwork.R** R script using CellNOptR to train a FEAR model.
- **TrainingFuncs.R** R script providing functions to train a model with CellNOptR.

- **CLMshell.R** R script providing interface to construct and simulate the compartmental logical model of mitotic exit.
- **Activity5.txt** Text file containing the activity network of MEN proteins in BoolNet format.
- **FEARnet3.txt** Text file containing the activity network of FEAR proteins in BoolNet format.
- **Localization5.txt** Text file containing most of the localization network of MEN proteins in BoolNet format.
- **LocSpecificActivity.txt** Text file containing additional part of localization network of MEN proteins in BoolNet format. This is required when localization depends on activity of protein in a specific location or when activity is regulated differently in a specific location.
- **CreateCLM.R** R script that assembles the model from the constituent activity and localization networks.
- **model5.sbml** Systems Biology Markup Language file containing the model.
- **simulateMutantSync.R** R script containing function sued to perform synchronous update scheme simulations of the model.
- **simulateMutantAsync.R** R script containing function sued to perform asynchronous-random, update scheme simulations of the model.
- **CLMfunctions.R** R script containing additional functions used in construction and simulation of the model.
- **model5.bnd** Text file containing rules of Model 5 in MaBoSS format.
- **model5.cfg** Text file containing configuration information of Model 5 in MaBoSS format.

- **model6.bnd** Text file containing rules of Model 6 in MaBoSS format.
- **model6.cfg** Text file containing configuration information of Model 6 in MaBoSS format.
- **model6parameterised.cfg** Text file containing configuration and parameter information of Model 6 in MaBoSS format.
- **AnaphaseLength.ipynb** Jupyter notebook containing python scripts to perform simulations and measurements of anaphase length.
- **SPoCmutants.ipynb** Jupyter notebook containing python scripts to perform simulations and measurements of SPoC mutants.
- **ParameterEstimation.ipynb** Jupyter notebook containing python scripts to perform simulations required to estimate parameters of Model 6.

Bibliography

Abou-Jaoudé, W., Traynard, P., Monteiro, P. T., Saez-Rodriguez, J., Helikar, T., Thieffry, D., and Chaouiya, C. Logical Modeling and Dynamical Analysis of Cellular Networks. *Frontiers in Genetics*, 7(86):353–20, May 2016.

Adames, N. R., Oberle, J. R., and Cooper, J. A. The surveillance mechanism of the spindle position checkpoint in yeast. *The Journal of Cell Biology*, 153(1): 159–168, Apr. 2001.

Adams, I. R. and Kilmartin, J. V. Localization of Core Spindle Pole Body (SPB) Components during SPB Duplication in Saccharomyces cerevisiae. *The Journal of Cell Biology*, 145(4):809–823, May 1999.

Ahmadian, M., Tyson, J. J., Peccoud, J., and Cao, Y. A hybrid stochastic model of the budding yeast cell cycle. *npj Systems Biology and Applications*, pages 1–10, Mar. 2020.

Albert, R. and Thakar, J. Boolean modeling: a logic-based dynamic approach for understanding signaling and regulatory networks and for making useful predictions. *Wiley Interdisciplinary Reviews: Systems Biology and Medicine*, 6(5): 353–369, July 2014.

Andrews, B. and Measday, V. The cyclin family of budding yeast: abundant use of a good idea. *Trends in genetics : TIG*, 14(2):66–72, Feb. 1998.

Arquint, C., Gabryjonczyk, A.-M., and Nigg, E. A. Centrosomes as signalling

centres. *Philosophical transactions of the Royal Society of London. Series B, Biological sciences*, 369(1650):20130464–20130464, Sept. 2014.

Asakawa, K., Yoshida, S., Otake, F., and Toh-E, A. A novel functional domain of Cdc15 kinase is required for its interaction with Tem1 GTPase in Saccharomyces cerevisiae. *Genetics*, 157(4):1437–1450, Apr. 2001.

Avena, J. S., Burns, S., Yu, Z., Ebmeier, C. C., Old, W. M., Jaspersen, S. L., and Winey, M. Licensing of Yeast Centrosome Duplication Requires Phosphoregulation of Sfi1. *PLOS Genetics*, 10(10):e1004666–10, Oct. 2014.

Azzam, R., Chen, S. L., Shou, W., Mah, A. S., Alexandru, G., Nasmyth, K., Annan, R. S., Carr, S. A., and Deshaies, R. J. Phosphorylation by cyclin B-Cdk underlies release of mitotic exit activator Cdc14 from the nucleolus. *Science*, 305(5683):516–519, July 2004.

Bajpai, A., Feoktistova, A., Chen, J.-S., McCollum, D., Sato, M., Carazo-Salas, R. E., Gould, K. L., and Csikasz-Nagy, A. Dynamics of SIN Asymmetry Establishment. *PLoS Computational Biology*, 9(7):e1003147, July 2013.

Barberis, M., Todd, R. G., and van der Zee, L. Advances and challenges in logical modeling of cell cycle regulation: perspective for multi-scale, integrative yeast cell models. *FEMS Yeast Research*, 17(1):fow103–15, Jan. 2017.

Bardin, A. J. and Amon, A. Men and sin: what's the difference? *Nature Reviews Molecular Cell Biology*, 2(11):815–826, Nov. 2001.

Bardin, A. J., Visintin, R., and Amon, A. A mechanism for coupling exit from mitosis to partitioning of the nucleus. *Cell*, 102(1):21–31, July 2000.

Barik, D., Baumann, W. T., Paul, M. R., Novák, B., and Tyson, J. J. A model of yeast cell-cycle regulation based on multisite phosphorylation. *Molecular Systems Biology*, 6:1–18, Aug. 2010.

Barik, D., Ball, D. A., Peccoud, J., and Tyson, J. J. A Stochastic Model of the Yeast Cell Cycle Reveals Roles for Feedback Regulation in Limiting Cellular Variability. *PLoS Computational Biology*, 12(12):e1005230–36, Dec. 2016.

Baro, B., Rodriguez-Rodriguez, J.-A., Calabria, I., Hernáez, M. L., Gil, C., and Queralt, E. Dual Regulation of the Mitotic Exit Network (MEN) by PP2A-Cdc55 Phosphatase. *PLOS Genetics*, 9(12):e1003966–15, Dec. 2013.

Baro, B., Játiva, S., Calabria, I., Vinaixa, J., Bech-Serra, J.-J., de LaTorre, C., Rodrigues, J., Hernáez, M. L., Gil, C., Barceló-Batllori, S., Larsen, M. R., and Queralt, E. SILAC-based phosphoproteomics reveals new PP2A-Cdc55-regulated processes in budding yeast. *GigaScience*, 7(5):9–18, May 2018.

Baryshnikova, A. Systematic Functional Annotation and Visualization of Biological Networks. *Cell Systems*, 2(6):412–421, June 2016.

Baryshnikova, A., Costanzo, M., Kim, Y., Ding, H., Koh, J., Toufighi, K., Youn, J.-Y., Ou, J., San Luis, B.-J., Bandyopadhyay, S., Hibbs, M., Hess, D., Gingras, A.-C., Bader, G. D., Troyanskaya, O. G., Brown, G. W., Andrews, B., Boone, C., and Myers, C. L. Quantitative analysis of fitness and genetic interactions in yeast on a genome scale. *Nature Methods*, 7(12):1017–1024, Nov. 2010.

Baryshnikova, A., Costanzo, M., Myers, C. L., Andrews, B., and Boone, C. Genetic interaction networks: toward an understanding of heritability. *Annual review of genomics and human genetics*, 14:111–133, 2013.

Basu, S., Roberts, E. L., Jones, A. W., Swaffer, M. P., Snijders, A. P., and Nurse, P. The Hydrophobic Patch Directs Cyclin B to Centrosomes to Promote Global CDK Phosphorylation at Mitosis. *Current Biology*, 30(5):883–892.e4, Mar. 2020.

Baum, P., Furlong, C., and Byers, B. Yeast gene required for spindle pole body

duplication: homology of its product with Ca2+-binding proteins. *Proceedings of the National Academy of Sciences*, 83(15):5512–5516, Aug. 1986.

Benjamini, Y. and Hochberg, Y. Controlling the False Discovery Rate: A Practical and Powerful Approach to Multiple Testing. *Journal of the Royal Statistical Society. Series B Methodological*, 57(1):289–300, Oct. 1995.

Bérenguier, D., Chaouiya, C., Monteiro, P. T., Naldi, A., Remy, E., Thieffry, D., and Tichit, L. Dynamical modeling and analysis of large cellular regulatory networks. *Chaos: An Interdisciplinary Journal of Nonlinear Science*, 23(2): 025114, 2013.

Berry, L. K., Ólafsson, G., Ledesma-Fernandez, E., and Thorpe, P. H. Synthetic protein interactions reveal a functional map of the cell. *eLife*, 5:e13053–17, Apr. 2016.

Bertazzi, D. T., Kurtulmus, B., and Pereira, G. The cortical protein Lte1 promotes mitotic exit by inhibiting the spindle position checkpoint kinase Kin4. *The Journal of Cell Biology*, 193(6):1033–1048, June 2011.

Biere, A. PicoSAT Essentials. *Journal on Satisfiability, Boolean Modeling and Computation*, 4:75–97, June 2008.

Bornholdt, S. Boolean network models of cellular regulation: prospects and limitations. *Journal of The Royal Society Interface*, 5 Suppl 1:S85–94, Aug. 2008.

Bose, A. and Dalal, S. N. Centrosome amplification and tumorigenesis: Cause or effect? In *The Golgi Apparatus and Centriole*, pages 413–440. Springer, 2019.

Botchkarev, V. V. and Haber, J. E. Functions and regulation of the Polo-like kinase Cdc5 in the absence and presence of DNA damage. *Current Genetics*, 64(1): 87–96, July 2017.

Botchkarev, V. V., Rossio, V., and Yoshida, S. The budding yeast Polo-like kinase Cdc5 is released from the nucleus during anaphase for timely mitotic exit. *Cell cycle (Georgetown, Tex.)*, 13(20):3260–3270, 2014.

Botchkarev, V. V., Garabedian, M. V., Lemos, B., Paulissen, E., and Haber, J. E. The budding yeast Polo-like kinase localizes to distinct populations at centrosomes during mitosis. *Molecular Biology of the Cell*, pages mbc.E16–05–0324, Feb. 2017.

Brachat, S., Dietrich, F. S., Voegeli, S., Zhang, Z., Stuart, L., Lerch, A., Gates, K., Gaffney, T., and Philippsen, P. Reinvestigation of the Saccharomyces cerevisiae genome annotation by comparison to the genome of a related fungus: Ashbya gossypii. *Genome biology*, 4(7):R45, 2003.

Brachmann, C. B., Davies, A., Cost, G. J., Caputo, E., Li, J., Hieter, P., and Boeke, J. D. Designer deletion strains derived from Saccharomyces cerevisiae S288C: a useful set of strains and plasmids for PCR-mediated gene disruption and other applications. *Yeast*, 14(2):115–132, Jan. 1998.

Brenner, S. Theoretical biology in the third millennium. *Philosophical Transactions of the Royal Society B: Biological Sciences*, 354(1392):1963–1965, Dec. 1999.

Bullitt, E., Rout, M. P., Kilmartin, J. V., and Akey, C. W. The yeast spindle pole body is assembled around a central crystal of Spc42p. *Cell*, 89(7):1077–1086, June 1997.

Byers, B. and Goetsch, L. Duplication of spindle plaques and integration of the yeast cell cycle. In *Cold Spring Harbor Symposia on Quantitative Biology*, volume 38, pages 123–131. Cold Spring Harbor Laboratory Press, 1974.

Campbell, I., Zhou, X., and Amon, A. Spindle pole bodies function as signal amplifiers in the mitotic exit network. *Molecular Biology of the Cell*, pages 1–29, Feb. 2020.

Campbell, I. W., Zhou, X., and Amon, A. The Mitotic Exit Network integrates temporal and spatial signals by distributing regulation across multiple components. *eLife*, 8, Jan. 2019.

Castillon, G. A., Adames, N. R., Rosello, C. H., Seidel, H. S., Longtine, M. S., Cooper, J. A., and Heil-Chapdelaine, R. A. Septins Have a Dual Role in Controlling Mitotic Exit in Budding Yeast. *Current Biology*, 13(8):654–658, Apr. 2003.

Cavanaugh, A. M. and Jaspersen, S. L. Big Lessons from Little Yeast: Budding and Fission Yeast Centrosome Structure, Duplication, and Function. *Annual Review of Genetics*, 51:361–383, Nov. 2017.

Caydasi, A. K. and Pereira, G. Spindle alignment regulates the dynamic association of checkpoint proteins with yeast spindle pole bodies. *Developmental Cell*, 16(1):146–156, 2009.

Caydasi, A. K., Kurtulmus, B., Orrico, M. I. L., Hofmann, A., Ibrahim, B., and Pereira, G. Elm1 kinase activates the spindle position checkpoint kinase Kin4. *The Journal of Cell Biology*, 190(6):975–989, Sept. 2010.

Caydasi, A. K., Lohel, M., Grünert, G., Dittrich, P., Pereira, G., and Ibrahim, B. A dynamical model of the spindle position checkpoint. *Molecular Systems Biology*, 8:582, May 2012.

Caydasi, A. K., Micoogullari, Y., Kurtulmus, B., Palani, S., and Pereira, G. The 14-3-3 protein Bmh1 functions in the spindle position checkpoint by breaking Bfa1 asymmetry at yeast centrosomes. *Molecular Biology of the Cell*, 25(14): 2143–2151, July 2014.

Caydasi, A. K., Khmelinskii, A., Duenas-Sanchez, R., Kurtulmus, B., Knop, M., and Pereira, G. Temporal and compartment-specific signals coordinate mitotic exit with spindle position. *Nature Communications*, 8:14129, Jan. 2017.

Chan, L. Y. and Amon, A. The protein phosphatase 2A functions in the spindle position checkpoint by regulating the checkpoint kinase Kin4. *Genes & development*, 23(14):1639–1649, July 2009.

Chan, L. Y. and Amon, A. Spindle Position Is Coordinated with Cell-Cycle Progression through Establishment of Mitotic Exit-Activating and -Inhibitory Zones. *Molecular Cell*, 39(3):444–454, Aug. 2010.

Chao, H. X., Fakhreddin, R. I., Shimerov, H. K., Kedziora, K. M., Kumar, R. J., Perez, J., Limas, J. C., Grant, G. D., Cook, J. G., Gupta, G. P., and Purvis, J. E. Evidence that the human cell cycle is a series of uncoupled, memoryless phases. *Molecular Systems Biology*, 15(3):e0185637–19, Mar. 2019.

Chaouiya, C., Bérenguier, D., Keating, S. M., Naldi, A., van Iersel, M. P., Rodriguez, N., Dräger, A., Büchel, F., Cokelaer, T., Kowal, B., Wicks, B., Gonçalves, E., Dorier, J., Page, M., Monteiro, P. T., von Kamp, A., Xenarios, I., de Jong, H., Hucka, M., Klamt, S., Thieffry, D., Le Novère, N., Saez-Rodriguez, J., and Helikar, T. SBML qualitative models: a model representation format and infrastructure to foster interactions between qualitative modelling formalisms and tools. *BMC Systems Biology*, 7(1):135, Dec. 2013.

Chasapi, A., Wachowicz, P., Niknejad, A., Collin, P., Krapp, A., Cano, E., Simanis, V., and Xenarios, I. An Extended, Boolean Model of the Septation Initiation Network in S.Pombe Provides Insights into Its Regulation. *PLoS ONE*, 10(8): e0134214–22, Aug. 2015.

Chen, K. C., Csikasz-Nagy, A., Gyorffy, B., Val, J., Novak, B., and Tyson, J. J. Kinetic analysis of a molecular model of the budding yeast cell cycle. *Yeast*, 11 (1):369–391, Jan. 2000.

Chen, K. C., Calzone, L., Csikasz-Nagy, A., Cross, F. R., Novák, B., and Tyson,

J. J. Integrative Analysis of Cell Cycle Control in Budding Yeast. *Molecular Biology of the Cell*, pages 1–22, July 2004.

Chen, M., Amos, B., Watson, L. T., Tyson, J., Cao, Y., Shaffer, C., Trosset, M., Oguz, C., and Kakoti, G. Quasi-Newton Stochastic Optimization Algorithm for Parameter Estimation of a Stochastic Model of the Budding Yeast Cell Cycle. *IEEE/ACM Transactions on Computational Biology and Bioinformatics*, pages 1–1, Nov. 2017.

Cheng, L., Hunke, L., and Hardy, C. F. Cell cycle regulation of the Saccharomyces cerevisiae polo-like kinase cdc5p. *Molecular and Cellular Biology*, 18(12):7360–7370, Dec. 1998.

Chial, H. J., Rout, M. P., Giddings, T. H., and Winey, M. Saccharomyces cerevisiae Ndc1p is a shared component of nuclear pore complexes and spindle pole bodies. *The Journal of Cell Biology*, 143(7):1789–1800, Dec. 1998.

Chiroli, E., Fraschini, R., Beretta, A., Tonelli, M., Lucchini, G., and Piatti, S. Budding yeast PAK kinases regulate mitotic exit by two different mechanisms. *The Journal of Cell Biology*, 160(6):857–874, Mar. 2003.

Clemente-Blanco, A., Mayán-Santos, M., Schneider, D. A., Machín, F., Jarmuz, A., Tschochner, H., and Aragón, L. Cdc14 inhibits transcription by RNA polymerase I during anaphase. *Nature Publishing Group*, 457(7235):219–222, Mar. 2009.

Costanzo, M., Baryshnikova, A., Bellay, J., Kim, Y., Spear, E. D., Sevier, C. S., Ding, H., Koh, J. L. Y., Toufighi, K., Mostafavi, S., Prinz, J., St Onge, R. P., VanderSluis, B., Makhnevych, T., Vizeacoumar, F. J., Alizadeh, S., Bahr, S., Brost, R. L., Chen, Y., Cokol, M., Deshpande, R., Li, Z., Lin, Z.-Y., Liang, W., Marback, M., Paw, J., San Luis, B.-J., Shuteriqi, E., Tong, A. H. Y., van Dyk, N., Wallace, I. M., Whitney, J. A., Weirauch, M. T., Zhong, G., Zhu, H., Houry,

W. A., Brudno, M., Ragibizadeh, S., Papp, B., Pál, C., Roth, F. P., Giaever, G., Nislow, C., Troyanskaya, O. G., Bussey, H., Bader, G. D., Gingras, A.-C., Morris, Q. D., Kim, P. M., Kaiser, C. A., Myers, C. L., Andrews, B. J., and Boone, C. The genetic landscape of a cell. *Science*, 327(5964):425–431, Jan. 2010.

Costanzo, M., VanderSluis, B., Koch, E. N., Baryshnikova, A., Pons, C., Tan, G., Wang, W., Usaj, M., Hanchard, J., Lee, S. D., Pelechano, V., Styles, E. B., Billmann, M., van Leeuwen, J., van Dyk, N., Lin, Z.-Y., Kuzmin, E., Nelson, J., Piotrowski, J. S., Srikumar, T., Bahr, S., Chen, Y., Deshpande, R., Kurat, C. F., Li, S. C., Li, Z., Usaj, M. M., Okada, H., Pascoe, N., San Luis, B.-J., Sharifpoor, S., Shuteriqi, E., Simpkins, S. W., Snider, J., Suresh, H. G., Tan, Y., Zhu, H., Malod-Dognin, N., Janjic, V., Przulj, N., Troyanskaya, O. G., Stagljar, I., Xia, T., Ohya, Y., Gingras, A.-C., Raught, B., Boutros, M., Steinmetz, L. M., Moore, C. L., Rosebrock, A. P., Caudy, A. A., Myers, C. L., Andrews, B., and Boone, C. A global genetic interaction network maps a wiring diagram of cellular function. *Science*, 353(6306):aaf1420–aaf1420, Sept. 2016.

Csikasz-Nagy, A., Battogtokh, D., Chen, K. C., Novák, B., and Tyson, J. J. Analysis of a Generic Model of Eukaryotic Cell-Cycle Regulation. *Biophysical Journal*, 90(12):4361–4379, June 2006.

Csikasz-Nagy, A., Kapuy, O., Győrffy, B., Tyson, J. J., and Novák, B. Modeling the septation initiation network (SIN) in fission yeast cells. *Current Genetics*, 51(4):245–255, Mar. 2007.

Cueille, N., Salimova, E., Esteban, V., Blanco, M., Moreno, S., Bueno, A., and Simanis, V. Flp1, a fission yeast orthologue of the s. cerevisiae CDC14 gene, is not required for cyclin degradation or rum1p stabilisation at the end of mitosis. *Journal of Cell Science*, 114(Pt 14):2649–2664, July 2001.

D'Amours, D. and Amon, A. At the interface between signaling and executing

anaphase—Cdc14 and the FEAR network. *Genes & development*, 18(21): 2581–2595, Nov. 2004.

D'Aquino, K. E., Monje-Casas, F., Paulson, J., Reiser, V., Charles, G. M., Lai, L., Shokat, K. M., and Amon, A. The Protein Kinase Kin4 Inhibits Exit from Mitosis in Response to Spindle Position Defects. *Molecular Cell*, 19(2):223–234, July 2005.

de los Santos-Velázquez, A. I., de Oya, I. G., Manzano-López, J., and Monje-Casas, F. Late rDNA Condensation Ensures Timely Cdc14 Release and Coordination of Mitotic Exit Signaling with Nucleolar Segregation. *Current biology*, 27(21):3248–3263.e5, Nov. 2017.

De Wulf, P., Montani, F., and Visintin, R. Protein phosphatases take the mitotic stage. *Current Opinion in Cell Biology*, 21(6):806–815, Dec. 2009.

Dittmar, J. C., Reid, R. J., and Rothstein, R. ScreenMill: a freely available software suite for growth measurement, analysis and visualization of high-throughput screen data. *BMC Bioinformatics*, 11(1):353, June 2010.

Dubrova, E. and Teslenko, M. A SAT-Based Algorithm for Finding Attractors in Synchronous Boolean Networks. *IEEE/ACM Transactions on Computational Biology and Bioinformatics*, 8(5):1393–1399, July 2011.

Dujon, B. The yeast genome project: what did we learn? *Trends in genetics : TIG*, 12(7):263–270, July 1996.

Durrett, R. *Probability: theory and examples*, volume 49. Cambridge university press, 2019.

Eden, E., Navon, R., Steinfeld, I., Lipson, D., and Yakhini, Z. GOrilla: a tool for discovery and visualization of enriched GO terms in ranked gene lists. *BMC Bioinformatics*, 10(1):48–7, 2009.

Eduati, F., Jaaks, P., Wappler, J., Cramer, T., Merten, C. A., Garnett, M. J., and Saez-Rodriguez, J. Patient-specific logic models of signaling pathways from screenings on cancer biopsies to prioritize personalized combination therapies. *Molecular Systems Biology*, 16(2):2452–13, Feb. 2020.

Efron, B. Large-Scale Simultaneous Hypothesis Testing. *Journal of the American Statistical Association*, 99(465):96–104, Mar. 2004.

Eisen, M. B., Spellman, P. T., Brown, P. O., and Botstein, D. Cluster analysis and display of genome-wide expression patterns. *Proceedings of the National Academy of Sciences*, 95(25):14863–14868, Dec. 1998.

Elowitz, M. B., Levine, A. J., Siggia, E. D., and Swain, P. S. Stochastic gene expression in a single cell. *Science*, 297(5584):1183–1186, Aug. 2002.

Elserafy, M., Šarić, M., Neuner, A., Lin, T.-c., Zhang, W., Seybold, C., Sivashanmugam, L., and Schiebel, E. Molecular Mechanisms that Restrict Yeast Centrosome Duplication to One Event per Cell Cycle. *Current Biology*, 24(13): 1456–1466, July 2014.

Falk, J. E., Chan, L. Y., and Amon, A. Lte1 promotes mitotic exit by controlling the localization of the spindle position checkpoint kinase Kin4. *Proceedings of the National Academy of Sciences*, 108(31):12584–12590, Aug. 2011.

Falk, J. E., Campbell, I. W., Joyce, K., Whalen, J., Seshan, A., and Amon, A. LTE1 promotes exit from mitosis by multiple mechanisms. *Molecular Biology of the Cell*, 27(25):3991–4001, Dec. 2016a.

Falk, J. E., Tsuchiya, D., Verdaasdonk, J., Lacefield, S., Bloom, K., and Amon, A. Spatial signals link exit from mitosis to spindle position. *eLife*, 5:159–23, May 2016b.

Fauré, A., Naldi, A., Lopez, F., Chaouiya, C., Ciliberto, A., and Thieffry, D. Modular logical modelling of the budding yeast cell cycle. *Molecular BioSystems*, 5(12): 1787–11, 2009.

Finley, K. R., Bouchonville, K. J., Quick, A., and Berman, J. Dynein-dependent nuclear dynamics affect morphogenesis in Candida albicans by means of the Bub2p spindle checkpoint. *Journal of Cell Science*, 121(5):724–724, Feb. 2008.

Fisher, J. and Henzinger, T. A. Executable cell biology. *Nature Biotechnology*, 25 (11):1239–1249, Nov. 2007.

Fraley, C. and Raftery, A. E. Model-Based Clustering, Discriminant Analysis, and Density Estimation. *Journal of the American Statistical Association*, 97(458): 611–631, June 2002.

Fraschini, R., Formenti, E., Lucchini, G., and Piatti, S. Budding yeast Bub2 is localized at spindle pole bodies and activates the mitotic checkpoint via a different pathway from Mad2. *The Journal of Cell Biology*, 145(5):979–991, May 1999.

Frenz, L. M., Lee, S. E., Fesquet, D., and Johnston, L. H. The budding yeast Dbf2 protein kinase localises to the centrosome and moves to the bud neck in late mitosis. *Journal of Cell Science*, 113 Pt 19:3399–3408, Oct. 2000.

Fu, J., Hagan, I. M., and Glover, D. M. The Centrosome and Its Duplication Cycle. *Cold Spring Harbor Perspectives in Biology*, 7(2):a015800, Feb. 2015.

Gardner, M. The fantastic combinations of john conway's new solitaire game "life". *Scientific American*, 223:120–123, 1970.

Garg, A., Di Cara, A., Xenarios, I., Mendoza, L., and De Micheli, G. Synchronous versus asynchronous modeling of gene regulatory networks. *Bioinformatics*, 24(17):1917–1925, Aug. 2008.

Gelens, L. and Santos, S. D. Eternal sunshine of the spotless cycle. *Molecular Systems Biology*, 15(4):e8864–2, Apr. 2019.

Geymonat, M., Spanos, A., Smith, S. J. M., Wheatley, E., Rittinger, K., Johnston, L. H., and Sedgwick, S. G. Control of mitotic exit in budding yeast. In vitro regulation of Tem1 GTPase by Bub2 and Bfa1. *Journal of Biological Chemistry*, 277(32):28439–28445, Aug. 2002.

Geymonat, M., Spanos, A., Walker, P. A., Johnston, L. H., and Sedgwick, S. G. In vitro regulation of budding yeast Bfa1/Bub2 GAP activity by Cdc5. *Journal of Biological Chemistry*, 278(17):14591–14594, Apr. 2003.

Geymonat, M., Spanos, A., de Bettignies, G., and Sedgwick, S. G. Lte1 contributes to Bfa1 localization rather than stimulating nucleotide exchange by Tem1. *The Journal of Cell Biology*, 187(4):497–511, Nov. 2009.

Geymonat, M., Peng, Q., Guo, Z., Yu, Z., Unruh, J. R., Jaspersen, S. L., and Segal, M. Orderly assembly underpinning built-in asymmetry in the yeast centrosome duplication cycle requires cyclin-dependent kinase. *eLife*, 9:809–29, Aug. 2020.

Giaever, G. and Nislow, C. The Yeast Deletion Collection: A Decade of Functional Genomics. *Genetics*, 197(2):451–465, June 2014.

Giaever, G., Chu, A. M., Ni, L., Connelly, C., Riles, L., Véronneau, S., Dow, S., Lucau-Danila, A., Anderson, K., André, B., Arkin, A. P., Astromoff, A., El-Bakkoury, M., Bangham, R., Benito, R., Brachat, S., Campanaro, S., Curtiss, M., Davis, K., Deutschbauer, A., Entian, K.-D., Flaherty, P., Foury, F., Garfinkel, D. J., Gerstein, M., Gotte, D., Güldener, U., Hegemann, J. H., Hempel, S., Herman, Z., Jaramillo, D. F., Kelly, D. E., Kelly, S. L., Kötter, P., LaBonte, D., Lamb, D. C., Lan, N., Liang, H., Liao, H., Liu, L., Luo, C., Lussier, M., Mao,

R., Ménard, P., Ooi, S. L., Revuelta, J. L., Roberts, C. J., Rose, M., Ross-Macdonald, P., Scherens, B., Schimmack, G., Shafer, B., Shoemaker, D. D., Sookhai-Mahadeo, S., Storms, R. K., Strathern, J. N., Valle, G., Voet, M., Volckaert, G., Wang, C.-y., Ward, T. R., Wilhelmy, J., Winzeler, E. A., Yang, Y., Yen, G., Youngman, E., Yu, K., Bussey, H., Boeke, J. D., Snyder, M., Philippsen, P., Davis, R. W., and Johnston, M. Functional profiling of the Saccharomyces cerevisiae genome. *Nature*, 418(6896):387–391, July 2002.

Glass, L. and Kauffman, S. A. The logical analysis of continuous, non-linear biochemical control networks. *Journal of theoretical Biology*, 39(1):103–129, 1973.

Goodson, H. V., Anderson, B. L., Warrick, H. M., Pon, L. A., and Spudich, J. A. Synthetic lethality screen identifies a novel yeast myosin I gene (MYO5): myosin I proteins are required for polarization of the actin cytoskeleton. *The Journal of Cell Biology*, 133(6):1277–1291, June 1996.

Grallert, A., Patel, A., Tallada, V. A., Chan, K. Y., Bagley, S., Krapp, A., Simanis, V., and Hagan, I. M. Centrosomal MPF triggers the mitotic and morphogenetic switches of fission yeast. *Nature Cell Biology*, 15(1):88–95, Dec. 2012.

Gruneberg, U., Campbell, K., Simpson, C., Grindlay, J., and Schiebel, E. Nud1p links astral microtubule organization and the control of exit from mitosis. *The EMBO journal*, 19(23):6475–6488, Dec. 2000.

Gryaznova, Y., Caydasi, A. K., Malengo, G., and Sourjik, V. A FRET-based study reveals site-specific regulation of spindle position checkpoint proteins at yeast centrosomes. *eLife*, 5, 2016.

Gunawardena, J. Models in biology: 'accurate descriptions of our pathetic thinking'. *BMC Biology*, 12(1):29, Apr. 2014.

Gyori, B. M., Bachman, J. A., Subramanian, K., Muhlich, J. L., Galescu, L., and Sorger, P. K. From word models to executable models of signaling networks using automated assembly. *Molecular Systems Biology*, 13(11):954–26, Nov. 2017.

Haase, S. B., Winey, M., and Reed, S. I. Multi-step control of spindle pole body duplication by cyclin-dependent kinase. *Nature Cell Biology*, 3(1):38–42, Jan. 2001.

Hancioglu, B. and Tyson, J. J. A Mathematical Model of Mitotic Exit in Budding Yeast: The Role of Polo Kinase. *PLoS ONE*, 7(2):e30810, 2012.

Harvey, K. F., Zhang, X., and Thomas, D. M. The Hippo pathway and human cancer. *Nature reviews. Cancer*, 13(4):246–257, Apr. 2013.

Heldt, F. S., Lunstone, R., Tyson, J. J., and Novák, B. Dilution and titration of cell-cycle regulators may control cell size in budding yeast. *PLoS Computational Biology*, 14(10):e1006548, Oct. 2018.

Hergovich, A., Cornils, H., and Hemmings, B. A. Mammalian NDR protein kinases: from regulation to a role in centrosome duplication. *Biochimica et biophysica acta*, 1784(1):3–15, Jan. 2008.

Higuchi, T. and Uhlmann, F. Stabilization of microtubule dynamics at anaphase onset promotes chromosome segregation. *Nature Publishing Group*, 433 (7022):171–176, Jan. 2005.

Höfken, T. and Schiebel, E. A role for cell polarity proteins in mitotic exit. *The EMBO journal*, 21(18):4851–4862, Sept. 2002.

Holt, L. J., Krutchinsky, A. N., and Morgan, D. O. Positive feedback sharpens the anaphase switch. *Nature*, 454(7202):353–357, June 2008.

Hoops, S., Sahle, S., Gauges, R., Lee, C., Pahle, J., Simus, N., Singhal, M., Xu, L., Mendes, P., and Kummer, U. COPASI–a COmplex PAthway SImulator. *Bioinformatics*, 22(24):3067–3074, Dec. 2006.

Hotz, M. and Barral, Y. The Mitotic Exit Network: new turns on old pathways. *Trends in Cell Biology*, 24(3):145–152, Mar. 2014.

Hotz, M., Leisner, C., Chen, D., Manatschal, C., Wegleiter, T., Ouellet, J., Lindstrom, D., Gottschling, D. E., Vogel, J., and Barral, Y. Spindle Pole Bodies Exploit the Mitotic Exit Network in Metaphase to Drive Their Age-Dependent Segregation. *Cell*, 148(5):958–972, Mar. 2012a.

Hotz, M., Lengefeld, J., and Barral, Y. The MEN mediates the effects of the spindle assembly checkpoint on Kar9-dependent spindle pole body inheritance in budding yeast. *Cell cycle (Georgetown, Tex.)*, 11(16):3109–3116, Aug. 2012b.

Howell, R. S. M., Csikasz-Nagy, A., and Thorpe, P. H. Synthetic Physical Interactions with the Yeast Centrosome. *G3 (Bethesda, Md.)*, 9(7):2183–2194, July 2019.

Hu, F., Wang, Y., Liu, D., Li, Y., Qin, J., and Elledge, S. J. Regulation of the Bub2/Bfa1 GAP complex by Cdc5 and cell cycle checkpoints. *Cell*, 107(5): 655–665, Nov. 2001.

Huh, W.-K., Falvo, J. V., Gerke, L. C., Carroll, A. S., Howson, R. W., Weissman, J. S., and OShea, E. K. Global analysis of protein localization in budding yeast. *Nature*, 425(6959):686–691, Oct. 2003.

Ibrahim, B. Toward a systems-level view of mitotic checkpoints. *Progress in Biophysics and Molecular Biology*, 117(2-3):217–224, Mar. 2015.

Ibrahim, B., Henze, R., Gruenert, G., Egbert, M., Huwald, J., and Dittrich, P. Spa-

tial Rule-Based Modeling: A Method and Its Application to the Human Mitotic Kinetochore. *Cells*, 2(3):506–544, July 2013.

Ideker, T. E., Thorsson, V., and Karp, R. M. Discovery of regulatory interactions through perturbation: inference and experimental design. *Pacific Symposium on Biocomputing. Pacific Symposium on Biocomputing*, pages 305–316, 2000.

Irons, D. J. Logical analysis of the budding yeast cell cycle. *Journal of Theoretical Biology*, 257(4):543–559, Apr. 2009.

Jackson, M., Marks, L., May, G. H. W., and Wilson, J. B. The genetic basis of disease. *Essays In Biochemistry*, 62(5):643–723, Dec. 2018.

Jaspersen, S. L. and Ghosh, S. Nuclear envelope insertion of spindle pole bodies and nuclear pore complexes. *Nucleus*, 3(3):226–236, May 2012.

Jaspersen, S. L. and Morgan, D. O. Cdc14 activates cdc15 to promote mitotic exit in budding yeast. *Current Biology*, 10(10):615–618, May 2000.

Jaspersen, S. L. and Winey, M. The budding yeast spindle pole body: structure, duplication, and function. *Annual review of cell and developmental biology*, 20: 1–28, 2004.

Jaspersen, S. L., Charles, J. F., Tinker-Kulberg, R. L., and Morgan, D. O. A late mitotic regulatory network controlling cyclin destruction in Saccharomyces cerevisiae. *Molecular Biology of the Cell*, 9(10):2803–2817, Oct. 1998.

Játiva, S., Calabria, I., Moyano-Rodriguez, Y., Garcia, P., and Queralt, E. Cdc14 activation requires coordinated Cdk1-dependent phosphorylation of Net1 and PP2A-Cdc55 at anaphase onset. *Cellular and Molecular Life Sciences*, 76(18): 3601–3620, Sept. 2019.

Jiménez, J., Cid, V. J., Cenamor, R., Yuste, M., Molero, G., Nombela, C., and

Sánchez, M. Morphogenesis beyond cytokinetic arrest in Saccharomyces cerevisiae. *The Journal of Cell Biology*, 143(6):1617–1634, Dec. 1998.

Juanes, M. A. and Piatti, S. The final cut: cell polarity meets cytokinesis at the bud neck in S. cerevisiae. *Cellular and Molecular Life Sciences*, 73(16):3115–3136, July 2016.

Kauffman, S. A. Metabolic stability and epigenesis in randomly constructed genetic nets. *Journal of Theoretical Biology*, 22(3):437–467, Mar. 1969.

Khmelinskii, A., Lawrence, C., Roostalu, J., and Schiebel, E. Cdc14-regulated midzone assembly controls anaphase B. *The Journal of Cell Biology*, 177(6): 981–993, June 2007.

Kholodenko, B. N. Cell-signalling dynamics in time and space. *Nature Reviews Molecular Cell Biology*, 7(3):165–176, Feb. 2006.

Kilmartin, J. V. Lessons from yeast: the spindle pole body and the centrosome. *Phil Trans R Soc B*, 2014.

Kitano, H. Systems biology: a brief overview. *Science*, 295(5560):1662–1664, Mar. 2002.

Klamt, S., Haus, U.-U., and Theis, F. Hypergraphs and Cellular Networks. *PLoS Computational Biology*, 5(5):e1000385–6, May 2009.

Klarner, H., Streck, A., and Siebert, H. Pyboolnet: a python package for the generation, analysis and visualization of boolean networks. *Bioinformatics*, 33 (5):770–772, 2017.

Kocakaplan, D., Karabürk, H., Kirdok, I., Erkan, Ş. N., Dilege, C., and Caydasi, A. K. Protein Phosphatase 1 in association with Bud14 inhibits mitotic exit in Saccharomyces cerevisiae. *bioRxiv*, Aug. 2020.

Komarnitsky, S. I., Chiang, Y. C., Luca, F. C., Chen, J., Toyn, J. H., Winey, M., Johnston, L. H., and Denis, C. L. DBF2 protein kinase binds to and acts through the cell cycle-regulated MOB1 protein. *Molecular and Cellular Biology*, 18(4): 2100–2107, Apr. 1998.

König, C., Maekawa, H., and Schiebel, E. Mutual regulation of cyclin-dependent kinase and the mitotic exit network. *The Journal of Cell Biology*, 188(3):351–368, Feb. 2010.

Kraikivski, P., Chen, K. C., Laomettachit, T., Murali, T. M., and Tyson, J. J. From START to FINISH: computational analysis of cell cycle control in budding yeast. *Nature Publishing Group*, 1:1–9, Dec. 2015.

Kreutz, C. and Timmer, J. Systems biology: experimental design. *FEBS Journal*, 276(4):923–942, Jan. 2009.

Krumsiek, J., Pölsterl, S., Wittmann, D. M., and Theis, F. J. Odefy–from discrete to continuous models. *BMC Bioinformatics*, 11(1):233, May 2010.

Kuilman, T., Maiolica, A., Godfrey, M., Scheidel, N., Aebersold, R., and Uhlmann, F. Identification of Cdk targets that control cytokinesis. *The EMBO journal*, 34 (1):81–96, Jan. 2015.

Laomettachit, T., Chen, K. C., Baumann, W. T., and Tyson, J. J. A Model of Yeast Cell-Cycle Regulation Based on a Standard Component Modeling Strategy for Protein Regulatory Networks. *PLoS ONE*, 11(5):e0153738–43, May 2016.

Lazebnik, Y. Can a biologist fix a radio?—or, what i learned while studying apoptosis. *Cancer cell*, 2(3):179–182, 2002.

Lee, S. E., Frenz, L. M., Wells, N. J., Johnson, A. L., and Johnston, L. H. Order of function of the budding-yeast mitotic exit-network proteins Tem1, Cdc15, Mob1, Dbf2, and Cdc5. *Current Biology*, 11(10):784–788, 2001.

Leifeld, T., Zhang, Z., and Zhang, P. Identification of Boolean Network Models From Time Series Data Incorporating Prior Knowledge. *Frontiers in Physiology*, 9:17–12, June 2018.

Lengefeld, J. and Barral, Y. Asymmetric Segregation of Aged Spindle Pole Bodies During Cell Division: Mechanisms and Relevance Beyond Budding Yeast? *BioEssays*, 14:1800038–9, July 2018.

Lengefeld, J., Hotz, M., Rollins, M., Baetz, K., and Barral, Y. Budding yeast Wee1 distinguishes spindle pole bodies to guide their pattern of age-dependent segregation. *Nature Cell Biology*, 19(8):941–951, July 2017.

Lengefeld, J., Yen, E., Chen, X., Leary, A., Vogel, J., and Barral, Y. Spatial cues and not spindle pole maturation drive the asymmetry of astral microtubules between new and preexisting spindle poles. *Molecular Biology of the Cell*, 29 (1):10–28, Jan. 2018.

Levchenko, A., Bruck, J., and Sternberg, P. W. Scaffold proteins may biphasically affect the levels of mitogen-activated protein kinase signaling and reduce its threshold properties. *Proceedings of the National Academy of Sciences*, 97 (11):5818–5823, May 2000.

Levine, M. S., Bakker, B., Boeckx, B., Moyett, J., Lu, J., Vitre, B., Spierings, D. C., Lansdorp, P. M., Cleveland, D. W., Lambrechts, D., Foijer, F., and Holland, A. J. Centrosome Amplification Is Sufficient to Promote Spontaneous Tumorigenesis in Mammals. *Developmental Cell*, 40(3):313–322.e5, Feb. 2017.

Lew, D. J. and Reed, S. I. Morphogenesis in the yeast cell cycle: regulation by Cdc28 and cyclins. *The Journal of Cell Biology*, 120(6):1305–1320, Mar. 1993.

Li, F., Long, T., Lu, Y., Ouyang, Q., and Tang, C. The yeast cell-cycle network is robustly designed. *Proceedings of the National Academy of Sciences*, 101(14): 4781–4786, Apr. 2004.

Li, R. Bifurcation of the mitotic checkpoint pathway in budding yeast. *Proceedings of the National Academy of Sciences*, 96(9):4989–4994, Apr. 1999.

Li, S., Sandercock, A. M., Conduit, P., Robinson, C. V., Williams, R. L., and Kilmartin, J. V. Structural role of Sfi1p-centrin filaments in budding yeast spindle pole body duplication. *The Journal of Cell Biology*, 173(6):867–877, June 2006.

Linke, C., Chasapi, A., González-Novo, A., Al Sawad, I., Tognetti, S., Klipp, E., Loog, M., Krobitsch, S., Posas, F., Xenarios, I., and Barberis, M. A Clb/Cdk1-mediated regulation of Fkh2 synchronizes CLB expression in the budding yeast cell cycle. *Nature Publishing Group*, pages 1–11, Feb. 2017.

Linkert, M., Rueden, C. T., Allan, C., Burel, J.-M., Moore, W., Patterson, A., Loranger, B., Moore, J., Neves, C., MacDonald, D., Tarkowska, A., Sticco, C., Hill, E., Rossner, M., Eliceiri, K. W., and Swedlow, J. R. Metadata matters: access to image data in the real world. *The Journal of Cell Biology*, 189(5):777–782, May 2010.

Lippincott, J., Shannon, K. B., Shou, W., Deshaies, R. J., and Li, R. The Tem1 small GTPase controls actomyosin and septin dynamics during cytokinesis. *Journal of Cell Science*, 114(Pt 7):1379–1386, Apr. 2001.

Lu, Y. and Cross, F. R. Periodic Cyclin-Cdk Activity Entrains an Autonomous Cdc14 Release Oscillator. *Cell*, 141(2):268–279, Apr. 2010.

Luca, F. C. and Winey, M. MOB1, an essential yeast gene required for completion of mitosis and maintenance of ploidy. *Molecular Biology of the Cell*, 9(1):29–46, Jan. 1998.

Maekawa, H., Priest, C., Lechner, J., Pereira, G., and Schiebel, E. The yeast centrosome translates the positional information of the anaphase spindle into a cell cycle signal. *The Journal of Cell Biology*, 179(3):423–436, Nov. 2007.

Mah, A. S., Jang, J., and Deshaies, R. J. Protein kinase Cdc15 activates the Dbf2-Mob1 kinase complex. *Proceedings of the National Academy of Sciences*, 98 (13):7325–7330, June 2001.

Manzano-López, J., Matellán, L., Álvarez-Llamas, A., Blanco-Mira, J. C., and Monje-Casas, F. Asymmetric inheritance of spindle microtubule-organizing centres preserves replicative lifespan. *Nature Cell Biology*, 21(8):952–965, Aug. 2019.

Manzoni, R., Montani, F., Visintin, C., Caudron, F., Ciliberto, A., and Visintin, R. Oscillations in Cdc14 release and sequestration reveal a circuit underlying mitotic exit. *The Journal of Cell Biology*, 190(2):209–222, July 2010.

Mao, X., Hu, Y., Liang, C., and Lu, C. MET3 Promoter: A Tightly Regulated Promoter and Its Application in Construction of Conditional Lethal Strain. *Current Microbiology*, 45(1):37–40, July 2002.

Markus, S. M., Omer, S., Baranowski, K., and Lee, W.-L. Improved Plasmids for Fluorescent Protein Tagging of Microtubules in Saccharomyces cerevisiae. *Traffic*, 16(7):773–786, Apr. 2015.

Matellán, L. and Monje-Casas, F. Regulation of Mitotic Exit by Cell Cycle Checkpoints: Lessons From Saccharomyces cerevisiae. *Genes*, 11(2), Feb. 2020.

Mattiazzi Usaj, M., Sahin, N., Friesen, H., Pons, C., Usaj, M., Masinas, M. P. D., Shuteriqi, E., Shkurin, A., Aloy, P., Morris, Q., Boone, C., and Andrews, B. J. Systematic genetics and single-cell imaging reveal widespread morphological pleiotropy and cell-to-cell variability. *Molecular Systems Biology*, 16(2):30–27, Feb. 2020.

Meng, Z., Moroishi, T., and Guan, K.-L. Mechanisms of Hippo pathway regulation. *Genes & development*, 30(1):1–17, Jan. 2016.

Menssen, R., Neutzner, A., and Seufert, W. Asymmetric spindle pole localization of yeast Cdc15 kinase links mitotic exit and cytokinesis. *Current Biology*, 11(5): 345–350, 2001.

Merlini, L., Fraschini, R., Boettcher, B., Barral, Y., Lucchini, G., and Piatti, S. Budding Yeast Dma Proteins Control Septin Dynamics and the Spindle Position Checkpoint by Promoting the Recruitment of the Elm1 Kinase to the Bud Neck. *PLOS Genetics*, 8(4):e1002670–18, Apr. 2012.

Messier, V., Zenklusen, D., and Michnick, S. W. A nutrient-responsive pathway that determines M phase timing through control of B-cyclin mRNA stability. *Cell*, 153(5):1080–1093, May 2013.

Miller, R. K. and Rose, M. D. Kar9p is a novel cortical protein required for cytoplasmic microtubule orientation in yeast. *The Journal of Cell Biology*, 140(2): 377–390, Jan. 1998a.

Miller, R. K. and Rose, M. D. Kar9p is a novel cortical protein required for cytoplasmic microtubule orientation in yeast. *The Journal of Cell Biology*, 140(2): 377–390, Jan. 1998b.

Mohl, D. A., Huddleston, M. J., Collingwood, T. S., Annan, R. S., and Deshaies, R. J. Dbf2–Mob1 drives relocalization of protein phosphatase Cdc14 to the cytoplasm during exit from mitosis. *The Journal of Cell Biology*, 184(4):527–539, Feb. 2009.

Monje-Casas, F. and Amon, A. Cell polarity determinants establish asymmetry in MEN signaling. *Developmental Cell*, 16(1):132–145, Jan. 2009.

Moore, J. K., Chudalayandi, P., Heil-Chapdelaine, R. A., and Cooper, J. A. The spindle position checkpoint is coordinated by the Elm1 kinase. *The Journal of Cell Biology*, 191(3):493–503, Nov. 2010.

Moriya, H. Quantitative nature of overexpression experiments. *Molecular Biology of the Cell*, 26(22):3932–3939, Nov. 2015.

Mortensen, E. M., Haas, W., Gygi, M., Gygi, S. P., and Kellogg, D. R. Cdc28-Dependent Regulation of the Cdc5/Polo Kinase. *Current Biology*, 15(22):2033–2037, Nov. 2005.

Muller, E. G. D., Snydsman, B. E., Novik, I., Hailey, D. W., Gestaut, D. R., Niemann, C. A., O'Toole, E. T., Giddings, T. H., Sundin, B. A., and Davis, T. N. The organization of the core proteins of the yeast spindle pole body. *Molecular Biology of the Cell*, 16(7):3341–3352, July 2005.

Mumberg, D., Müller, R., and Funk, M. Regulatable promoters of Saccharomyces cerevisiae: comparison of transcriptional activity and their use for heterologous expression. *Nucleic Acids Research*, 22(25):5767–5768, Dec. 1994.

Münzner, U., Klipp, E., and Krantz, M. A comprehensive, mechanistically detailed, and executable model of the cell division cycle in Saccharomyces cerevisiae. *Nature Communications*, pages 1–12, Mar. 2019.

Mura, I. and Csikasz-Nagy, A. Stochastic Petri Net extension of a yeast cell cycle model. *Journal of Theoretical Biology*, 254(4):850–860, Oct. 2008.

Müssel, C., Hopfensitz, M., and Kestler, H. A. BoolNet—an R package for generation, reconstruction and analysis of Boolean networks. *Bioinformatics*, 26(10): 1378–1380, Apr. 2010.

Naldi, A., Berenguier, D., Faure, A., Lopez, F., Thieffry, D., and Chaouiya, C. Logical modelling of regulatory networks with GINsim 2.3. *Bio Systems*, 97(2): 134–139, Aug. 2009.

Nigg, E. A. Origins and consequences of centrosome aberrations in human cancers. *International Journal of Cancer*, 119(12):2717–2723, 2006.

Nislow, C., Lee, A. Y., Allen, P. L., Giaever, G., Smith, A., Gebbia, M., Stodieck, L. S., Hammond, J. S., Birdsall, H. H., and Hammond, T. G. Genes required for survival in microgravity revealed by genome-wide yeast deletion collections cultured during spaceflight. *BioMed research international*, 2015:976458, 2015.

Oh, Y., Chang, K.-J., Orlean, P., Wloka, C., Deshaies, R., and Bi, E. Mitotic exit kinase Dbf2 directly phosphorylates chitin synthase Chs2 to regulate cytokinesis in budding yeast. *Molecular Biology of the Cell*, 23(13):2445–2456, July 2012.

Ólafsson, G. and Thorpe, P. H. Synthetic physical interactions map kinetochore regulators and regions sensitive to constitutive Cdc14 localization. *Proceedings of the National Academy of Sciences*, 112(33):10413–10418, Aug. 2015.

Ólafsson, G. and Thorpe, P. H. Synthetic Physical Interactions Map Kinetochore-Checkpoint Activation Regions. *G3 (Bethesda, Md.)*, 6(8):2531–2542, Aug. 2016.

Ólafsson, G. and Thorpe, P. H. Rewiring the Budding Yeast Proteome using Synthetic Physical Interactions. In *Genome Instability*, pages 599–612. Humana Press, New York, NY, New York, NY, 2018.

Pereira, G. and Schiebel, E. Kin4 Kinase Delays Mitotic Exit in Response to Spindle Alignment Defects. *Molecular Cell*, 19(2):209–221, July 2005.

Pereira, G., Höfken, T., Grindlay, J., Manson, C., and Schiebel, E. The Bub2p spindle checkpoint links nuclear migration with mitotic exit. *Molecular Cell*, 6 (1):1–10, July 2000.

Pereira, G., Tanaka, T. U., Nasmyth, K., and Schiebel, E. Modes of spindle pole body inheritance and segregation of the Bfa1p-Bub2p checkpoint protein complex. *The EMBO journal*, 20(22):6359–6370, Nov. 2001.

Pereira, G., Manson, C., Grindlay, J., and Schiebel, E. Regulation of the Bfa1p-Bub2p complex at spindle pole bodies by the cell cycle phosphatase Cdc14p. *The Journal of Cell Biology*, 157(3):367–379, Apr. 2002.

Perez-Carrasco, R., Barnes, C. P., Schaerli, Y., Isalan, M., Briscoe, J., and Page, K. M. Combining a Toggle Switch and a Repressilator within the AC-DC Circuit Generates Distinct Dynamical Behaviors. *Cell Systems*, pages 1–14, Mar. 2018.

Ptacek, J., Devgan, G., Michaud, G., Zhu, H., Zhu, X., Fasolo, J., Guo, H., Jona, G., Breitkreutz, A., Sopko, R., McCartney, R. R., Schmidt, M. C., Rachidi, N., Lee, S.-J., Mah, A. S., Meng, L., Stark, M. J. R., Stern, D. F., De Virgilio, C., Tyers, M., Andrews, B., Gerstein, M., Schweitzer, B., Predki, P. F., and Snyder, M. Global analysis of protein phosphorylation in yeast. *Nature*, 438(7068): 679–684, Dec. 2005.

Qu, X., Aldana, M., and Kadanoff, L. P. Numerical and theoretical studies of noise effects in the kauffman model. *Journal of Statistical Physics*, 109(5-6): 967–986, 2002.

Queralt, E. and Uhlmann, F. Separase cooperates with Zds1 and Zds2 to activate Cdc14 phosphatase in early anaphase. *The Journal of Cell Biology*, 182(5): 873–883, Sept. 2008a.

Queralt, E. and Uhlmann, F. Cdk-counteracting phosphatases unlock mitotic exit. *Current Opinion in Cell Biology*, 20(6):661–668, Dec. 2008b.

Queralt, E., Lehane, C., Novák, B., and Uhlmann, F. Downregulation of PP2A(Cdc55) phosphatase by separase initiates mitotic exit in budding yeast. *Cell*, 125(4):719–732, May 2006.

Rahal, R. and Amon, A. The Polo-like kinase Cdc5 interacts with FEAR network

components and Cdc14. *Cell cycle (Georgetown, Tex.)*, 7(20):3262–3272, Oct. 2014.

Reid, R. J. D., Gonzalez-Barrera, S., Sunjevaric, I., Alvaro, D., Ciccone, S., Wagner, M., and Rothstein, R. Selective ploidy ablation, a high-throughput plasmid transfer protocol, identifies new genes affecting topoisomerase I-induced DNA damage. *Genome Research*, 21(3):477–486, Mar. 2011.

Ro, H.-S., Song, S., and Lee, K. S. Bfa1 can regulate Tem1 function independently of Bub2 in the mitotic exit network of Saccharomyces cerevisiae. *Proceedings of the National Academy of Sciences*, 99(8):5436–5441, Apr. 2002.

Rock, J. M. and Amon, A. The FEAR network. *Current Biology*, 19(23):R1063–R1068, Dec. 2009.

Rock, J. M. and Amon, A. Cdc15 integrates Tem1 GTPase-mediated spatial signals with Polo kinase-mediated temporal cues to activate mitotic exit. *Genes & development*, 25(18):1943–1954, Sept. 2011.

Rock, J. M., Lim, D., Stach, L., Ogrodowicz, R. W., Keck, J. M., Jones, M. H., Wong, C. C. L., Yates, J. R., Winey, M., Smerdon, S. J., Yaffe, M. B., and Amon, A. Activation of the Yeast Hippo Pathway by Phosphorylation-Dependent Assembly of Signaling Complexes. *Science*, 340(6134):871–875, May 2013.

Rodriguez-Rodriguez, J.-A., Moyano, Y., Játiva, S., and Queralt, E. Mitotic Exit Function of Polo-like Kinase Cdc5 Is Dependent on Sequential Activation by Cdk1. *CellReports*, 15(9):2050–2062, May 2016.

Rossio, V. and Yoshida, S. Spatial regulation of Cdc55–PP2A by Zds1/Zds2 controls mitotic entry and mitotic exit in budding yeast. *The Journal of Cell Biology*, 193(3):445–454, May 2011.

Rothbauer, U., Zolghadr, K., Muyldermans, S., Schepers, A., Cardoso, M. C., and Leonhardt, H. A Versatile Nanotrap for Biochemical and Functional Studies with Fluorescent Fusion Proteins. *Molecular & Cellular Proteomics*, 7(2):282–289, 2007.

Rubinstein, A., Hazan, O., Chor, B., Pinter, R. Y., and Kassir, Y. The effective application of a discrete transition model to explore cell-cycle regulation in yeast. *BMC research notes*, 6(1):311–13, Aug. 2013.

Rüthnick, D. and Schiebel, E. Duplication of the Yeast Spindle Pole Body Once per Cell Cycle. *Molecular and Cellular Biology*, 36(9):1324–1331, Apr. 2016.

Rüthnick, D. and Schiebel, E. Duplication and Nuclear Envelope Insertion of the Yeast Microtubule Organizing Centre, the Spindle Pole Body. *Cells*, 7(5), May 2018.

Rüthnick, D., Neuner, A., Dietrich, F., Kirrmaier, D., Engel, U., Knop, M., and Schiebel, E. Characterization of spindle pole body duplication reveals a regulatory role for nuclear pore complexes. *The Journal of Cell Biology*, 216(8): 2425–2442, Aug. 2017.

Saez-Rodriguez, J., Alexopoulos, L. G., Epperlein, J., Samaga, R., Lauffenburger, D. A., Klamt, S., and Sorger, P. K. Discrete logic modelling as a means to link protein signalling networks with functional analysis of mammalian signal transduction. *Molecular Systems Biology*, 5:1–19, Dec. 2009.

Saldanha, A. J. Java Treeview–extensible visualization of microarray data. *Bioinformatics*, 20(17):3246–3248, Nov. 2004.

Salzberg, S. L. Open questions: How many genes do we have? *BMC Biology*, 16(1):94–3, Aug. 2018.

Sanchez-Diaz, A., Nkosi, P. J., Murray, S., and Labib, K. The Mitotic Exit Network and Cdc14 phosphatase initiate cytokinesis by counteracting CDK phosphorylations and blocking polarised growth. *The EMBO journal*, 31(17):3620–3634, Aug. 2012.

Scarfone, I. and Piatti, S. Coupling spindle position with mitotic exit in budding yeast: The multifaceted role of the small GTPase Tem1. *Small GTPases*, 6(4): 196–201, Oct. 2015.

Scarfone, I., Venturetti, M., Hotz, M., Lengefeld, J., Barral, Y., and Piatti, S. Asymmetry of the Budding Yeast Tem1 GTPase at Spindle Poles Is Required for Spindle Positioning But Not for Mitotic Exit. *PLOS Genetics*, 11(2):e1004938–29, Feb. 2015.

Schindelin, J., Arganda-Carreras, I., Frise, E., Kaynig, V., Longair, M., Pietzsch, T., Preibisch, S., Rueden, C., Saalfeld, S., Schmid, B., Tinevez, J.-Y., White, D. J., Hartenstein, V., Eliceiri, K., Tomancak, P., and Cardona, A. Fiji: an open-source platform for biological-image analysis. *Nature Methods*, 9(7):676–682, June 2012.

Scrucca, L., Fop, M., Murphy, T. B., and Raftery, A. E. mclust 5: Clustering, Classification and Density Estimation Using Gaussian Finite Mixture Models. *The R journal*, 8(1):289–317, Aug. 2016.

Seshan, A. and Amon, A. Ras and the Rho effector Cla4 collaborate to target and anchor Lte1 at the bud cortex. *Cell cycle (Georgetown, Tex.)*, 4(7):940–946, July 2005.

Shalem, O., Sanjana, N. E., and Zhang, F. High-throughput functional genomics using CRISPR-Cas9. *Nature Reviews Genetics*, 16(5):299–311, May 2015.

Shirayama, M., Matsui, Y., Tanaka, K., and Toh-E, A. Isolation of a cdc25 fam-

ily gene, msi2/lte1, as a multicopy suppressor of ira1. *Yeast*, 10(4):451–461, 1994a.

Shirayama, M., Matsui, Y., and Toh-E, A. The yeast TEM1 gene, which encodes a GTP-binding protein, is involved in termination of M phase. *Molecular and Cellular Biology*, 14(11):7476–7482, Nov. 1994b.

Shirayama, M., Matsui, Y., and Toh-E, A. Dominant mutant alleles of yeast protein kinase gene CDC15 suppress the lte1 defect in termination of M phase and genetically interact with CDC14. *Molecular & general genetics : MGG*, 251(2): 176–185, May 1996.

Shirayama, M., Tóth, A., Gálová, M., and Nasmyth, K. APC(Cdc20) promotes exit from mitosis by destroying the anaphase inhibitor Pds1 and cyclin Clb5. *Nature*, 402(6758):203–207, Nov. 1999.

Shmulevich, I., Dougherty, E. R., Kim, S., and Zhang, W. Probabilistic Boolean Networks: a rule-based uncertainty model for gene regulatory networks. *Bioinformatics*, 18(2):261–274, Feb. 2002.

Shou, W., Seol, J. H., Baskerville, C., Moazed, D., Chen, Z. W., Jang, J., Shevchenko, A., Charbonneau, H., and Deshaies, R. J. Exit from mitosis is triggered by Tem1-dependent release of the protein phosphatase Cdc14 from nucleolar RENT complex. *Cell*, 97(2):233–244, Apr. 1999.

Shou, W., Azzam, R., Chen, S. L., Huddleston, M. J., Baskerville, C., Charbonneau, H., Annan, R. S., Carr, S. A., and Deshaies, R. J. Cdc5 influences phosphorylation of Net1 and disassembly of the RENT complex. *BMC molecular biology*, 3(1):3, Apr. 2002.

Simanis, V. Pombe's thirteen - control of fission yeast cell division by the septation initiation network. *Journal of Cell Science*, 128(8):1465–1474, Apr. 2015.

Singhania, R., Sramkoski, R. M., Jacobberger, J. W., and Tyson, J. J. A hybrid model of mammalian cell cycle regulation. *PLoS Computational Biology*, 7(2): e1001077, Feb. 2011.

Snead, J. L., Sullivan, M., Lowery, D. M., Cohen, M. S., Zhang, C., Randle, D. H., Taunton, J., Yaffe, M. B., Morgan, D. O., and Shokat, K. M. A Coupled Chemical-Genetic and Bioinformatic Approach to Polo-like Kinase Pathway Exploration. *Chemistry & Biology*, 14(11):1261–1272, Nov. 2007.

Song, K., Mach, K. E., Chen, C. Y., Reynolds, T., and Albright, C. F. A novel suppressor of ras1 in fission yeast, byr4, is a dosage-dependent inhibitor of cytokinesis. *The Journal of Cell Biology*, 133(6):1307–1319, June 1996.

Song, S., Grenfell, T. Z., Garfield, S., Erikson, R. L., and Lee, K. S. Essential function of the polo box of Cdc5 in subcellular localization and induction of cytokinetic structures. *Molecular and Cellular Biology*, 20(1):286–298, Jan. 2000.

Stegmeier, F. and Amon, A. Closing Mitosis: The Functions of the Cdc14 Phosphatase and Its Regulation. *Annual Review of Genetics*, 38(1):203–232, Dec. 2004.

Stegmeier, F., Visintin, R., and Amon, A. Separase, polo kinase, the kinetochore protein Slk19, and Spo12 function in a network that controls Cdc14 localization during early anaphase. *Cell*, 108(2):207–220, Jan. 2002.

Stegmeier, F., Huang, J., Rahal, R., Zmolik, J., Moazed, D., and Amon, A. The Replication Fork Block Protein Fob1 Functions as a Negative Regulator of the FEAR Network. *Current Biology*, 14(6):467–480, Mar. 2004.

Stoepel, J., Ottey, M. A., Kurischko, C., Hieter, P., and Luca, F. C. The mitotic exit network Mob1p-Dbf2p kinase complex localizes to the nucleus and regulates passenger protein localization. *Molecular Biology of the Cell*, 16(12):5465–5479, Dec. 2005.

Stoll, G., Viara, E., Barillot, E., and Calzone, L. Continuous time Boolean modeling for biological signaling: application of Gillespie algorithm. *BMC Systems Biology*, 6(1):116–18, Aug. 2012.

Stoll, G., Caron, B., Viara, E., Dugourd, A., Zinovyev, A., Naldi, A., Kroemer, G., Barillot, E., and Calzone, L. MaBoSS 2.0: an environment for stochastic Boolean modeling. *Bioinformatics*, 33(14):2226–2228, Mar. 2017.

Strogatz, S. *Nonlinear Dynamics And Chaos: With Applications To Physics, Biology, Chemistry, And Engineering (Studies in Nonlinearity)*. Westview Press, 2001.

Sullivan, M. and Morgan, D. O. Finishing mitosis, one step at a time. *Nature Reviews Molecular Cell Biology*, 8(11):894–903, Nov. 2007.

Sullivan, M. and Uhlmann, F. A non-proteolytic function of separase links the onset of anaphase to mitotic exit. *Nature Cell Biology*, 5(3):249–254, Feb. 2003.

Tamborrini, D. and Piatti, S. Septin clearance from the division site triggers cytokinesis in budding yeast. *Microbial cell (Graz, Austria)*, 6(6):295–298, May 2019.

Tamborrini, D., Juanes, M. A., Ibanes, S., Rancati, G., and Piatti, S. Recruitment of the mitotic exit network to yeast centrosomes couples septin displacement to actomyosin constriction. *Nature Communications*, 9(1):4308, Oct. 2018.

Terfve, C., Cokelaer, T., Henriques, D., MacNamara, A., Gonçalves, E., Morris, M. K., van Iersel, M., Lauffenburger, D. A., and Saez-Rodriguez, J. CellNOptR: a flexible toolkit to train protein signaling networks to data using multiple logic formalisms. *BMC Systems Biology*, 6(1):133, Oct. 2012.

Thomas, R. Boolean formalization of genetic control circuits. *Journal of theoretical biology*, 42(3):563–585, 1973.

Tkach, J. M., Yimit, A., Lee, A. Y., Riffle, M., Costanzo, M., Jaschob, D., Hendry, J. A., Ou, J., Moffat, J., Boone, C., Davis, T. N., Nislow, C., and Brown, G. W. Dissecting DNA damage response pathways by analysing protein localization and abundance changes during DNA replication stress. *Nature Cell Biology*, 14(9):966–976, July 2012.

Todd, R. G. and Helikar, T. Ergodic Sets as Cell Phenotype of Budding Yeast Cell Cycle. *PLoS ONE*, 7(10):e45780–10, Oct. 2012.

Tomson, B. N., Rahal, R., Reiser, V., Monje-Casas, F., Mekhail, K., Moazed, D., and Amon, A. Regulation of Spo12 Phosphorylation and Its Essential Role in the FEAR Network. *Current Biology*, 19(6):449–460, Mar. 2009.

Tong, A. H. Y., Lesage, G., Bader, G. D., Ding, H., Xu, H., Xin, X., Young, J., Berriz, G. F., Brost, R. L., Chang, M., Chen, Y., Cheng, X., Chua, G., Friesen, H., Goldberg, D. S., Haynes, J., Humphries, C., He, G., Hussein, S., Ke, L., Krogan, N., Li, Z., Levinson, J. N., Lu, H., Ménard, P., Munyana, C., Parsons, A. B., Ryan, O., Tonikian, R., Roberts, T., Sdicu, A.-M., Shapiro, J., Sheikh, B., Suter, B., Wong, S. L., Zhang, L. V., Zhu, H., Burd, C. G., Munro, S., Sander, C., Rine, J., Greenblatt, J., Peter, M., Bretscher, A., Bell, G., Roth, F. P., Brown, G. W., Andrews, B., Bussey, H., and Boone, C. Global mapping of the yeast genetic interaction network. *Science*, 303(5659):808–813, Feb. 2004.

Tóth, A., Queralt, E., Uhlmann, F., and Novák, B. Mitotic exit in two dimensions. *Journal of Theoretical Biology*, 248(3):560–573, Oct. 2007.

Touati, S. A., Kataria, M., Jones, A. W., Snijders, A. P., and Uhlmann, F. Phosphoproteome dynamics during mitotic exit in budding yeast. *The EMBO journal*, 37 (10):e98745–4, May 2018.

Touati, S. A., Hofbauer, L., Jones, A. W., Snijders, A. P., Kelly, G., and Uhlmann, F. Cdc14 and PP2A Phosphatases Cooperate to Shape Phosphoproteome Dynamics during Mitotic Exit. *CellReports*, 29(7):2105–2119.e4, Nov. 2019.

Toyn, J. H., Araki, H., Sugino, A., and Johnston, L. H. The cell-cycle-regulated budding yeast gene DBF2, encoding a putative protein kinase, has a homologue that is not under cell-cycle control. *Gene*, 104(1):63–70, July 1991.

Trcek, T., Larson, D. R., Moldón, A., Query, C. C., and Singer, R. H. Single-molecule mRNA decay measurements reveal promoter- regulated mRNA stability in yeast. *Cell*, 147(7):1484–1497, Dec. 2011.

Tyson, J. J. Bringing cartoons to life. *Nature Publishing Group*, 1(1):E1–E9, Feb. 2007.

Tyson, J. J. and Novák, B. Functional Motifs in Biochemical Reaction Networks. *Annual Review of Physical Chemistry*, 61(1):219–240, Mar. 2010.

Tyson, J. J. and Novák, B. A Dynamical Paradigm for Molecular Cell Biology. *Trends in Cell Biology*, Apr. 2020.

Tyson, J. J., Chen, K. C., and Novák, B. Sniffers, buzzers, toggles and blinkers: dynamics of regulatory and signaling pathways in the cell. *Current Opinion in Cell Biology*, 15(2):221–231, Apr. 2003.

Usaj, M., Tan, Y., Wang, W., VanderSluis, B., Zou, A., Myers, C. L., Costanzo, M., Andrews, B., and Boone, C. TheCellMap.org: A Web-Accessible Database for Visualizing and Mining the Global Yeast Genetic Interaction Network. *G3 (Bethesda, Md.)*, page g3.117.040220, Mar. 2017.

Valerio-Santiago, M. and Monje-Casas, F. Tem1 localization to the spindle pole bodies is essential for mitotic exit and impairs spindle checkpoint function. *The Journal of Cell Biology*, 192(4):599–614, Feb. 2011.

Varela, P. L., Ramos, C. V., Monteiro, P. T., and Chaouiya, C. EpiLog: A software for the logical modelling of epithelial dynamics. *F1000Research*, 7:1145, 2018.

Videla, S., Guziolowski, C., Eduati, F., Thiele, S., Gebser, M., Nicolas, J., Saez-Rodriguez, J., Schaub, T., and Siegel, A. Learning Boolean logic models of signaling networks with ASP. *Theoretical Computer Science*, 599(C):79–101, Sept. 2015.

Vinod, P. K., Freire, P., Rattani, A., Ciliberto, A., Uhlmann, F., and Novak, B. Computational modelling of mitotic exit in budding yeast: the role of separase and Cdc14 endocycles. *Journal of The Royal Society Interface*, 8(61):1128–1141, 2011.

Visintin, R., Stegmeier, F., and Amon, A. The role of the polo kinase Cdc5 in controlling Cdc14 localization. *Molecular Biology of the Cell*, 14(11):4486–4498, Nov. 2003.

Viswanath, S., Bonomi, M., Kim, S. J., Klenchin, V. A., Taylor, K. C., Yabut, K. C., Umbreit, N. T., Van Epps, H. A., Meehl, J., Jones, M. H., Russel, D., Velazquez-Muriel, J. A., Winey, M., Rayment, I., Davis, T. N., Sali, A., and Muller, E. G. The molecular architecture of the yeast spindle pole body core determined by Bayesian integrative modeling. *Molecular Biology of the Cell*, 28(23):3298–3314, Nov. 2017.

Wang, X., Tsai, J.-W., Imai, J. H., Lian, W.-N., Vallee, R. B., and Shi, S.-H. Asymmetric centrosome inheritance maintains neural progenitors in the neocortex. *Nature Publishing Group*, 461(7266):947–955, Oct. 2009.

Wang, Y. and Ng, T.-Y. Phosphatase 2A negatively regulates mitotic exit in Saccharomyces cerevisiae. *Molecular Biology of the Cell*, 17(1):80–89, Jan. 2006.

Wang, Y., Shirogane, T., Liu, D., Harper, J. W., and Elledge, S. J. Exit from exit:

resetting the cell cycle through Amn1 inhibition of G protein signaling. *Cell*, 112 (5):697–709, Mar. 2003.

Warne, D. J., Baker, R. E., and Simpson, M. J. Simulation and inference algorithms for stochastic biochemical reaction networks: from basic concepts to state-of-the-art. *Journal of The Royal Society Interface*, 16(151):20180943, Feb. 2019.

Weiss, E. L. Mitotic Exit and Separation of Mother and Daughter Cells. *Genetics*, 192(4):1165–1202, Dec. 2012.

Whalen, J., Sniffen, C., Gartland, S., Vannini, M., and Seshan, A. Budding Yeast BFA1 Has Multiple Positive Roles in Directing Late Mitotic Events. *G3 (Bethesda, Md.)*, 8(11):3397–3410, Nov. 2018.

Whitaker, W. R., Davis, S. A., Arkin, A. P., and Dueber, J. E. Engineering robust control of two-component system phosphotransfer using modular scaffolds. *Proceedings of the National Academy of Sciences of the United States of America*, 109(44):18090–18095, Oct. 2012.

Wilkinson, D. J. Stochastic modelling for quantitative description of heterogeneous biological systems. *Nature Reviews Genetics*, 10(2):122–133, Feb. 2009.

Winey, M., Goetsch, L., Baum, P., and Byers, B. MPS1 and MPS2: novel yeast genes defining distinct steps of spindle pole body duplication. *The Journal of Cell Biology*, 114(4):745–754, Aug. 1991.

Winzeler, E. A., Shoemaker, D. D., Astromoff, A., Liang, H., Anderson, K., Andre, B., Bangham, R., Benito, R., Boeke, J. D., Bussey, H., Chu, A. M., Connelly, C., Davis, K., Dietrich, F., Dow, S. W., El Bakkoury, M., Foury, F., Friend, S. H., Gentalen, E., Giaever, G., Hegemann, J. H., Jones, T., Laub, M., Liao,

H., Liebundguth, N., Lockhart, D. J., Lucau-Danila, A., Lussier, M., M'Rabet, N., Menard, P., Mittmann, M., Pai, C., Rebischung, C., Revuelta, J. L., Riles, L., Roberts, C. J., Ross-MacDonald, P., Scherens, B., Snyder, M., Sookhai-Mahadeo, S., Storms, R. K., Véronneau, S., Voet, M., Volckaert, G., Ward, T. R., Wysocki, R., Yen, G. S., Yu, K., Zimmermann, K., Philippsen, P., Johnston, M., and Davis, R. W. Functional characterization of the S. cerevisiae genome by gene deletion and parallel analysis. *Science*, 285(5429):901–906, Aug. 1999.

Witkin, K. L., Friederichs, J. M., Cohen-Fix, O., and Jaspersen, S. L. Changes in the nuclear envelope environment affect spindle pole body duplication in Saccharomyces cerevisiae. *Genetics*, 186(3):867–883, Nov. 2010.

Wong, J., Nakajima, Y., Westermann, S., Shang, C., Kang, J.-S., Goodner, C., Houshmand, P., Fields, S., Chan, C. S. M., Drubin, D., Barnes, G., and Hazbun, T. A protein interaction map of the mitotic spindle. *Molecular Biology of the Cell*, 18(10):3800–3809, Oct. 2007.

Yang, X., Jost, A. P.-T., Weiner, O. D., and Tang, C. A light-inducible organelle-targeting system for dynamically activating and inactivating signaling in budding yeast. *Molecular Biology of the Cell*, 24(15):2419–2430, Aug. 2013.

Yellman, C. M. and Roeder, G. S. Cdc14 Early Anaphase Release, FEAR, Is Limited to the Nucleus and Dispensable for Efficient Mitotic Exit. *PLoS ONE*, 10(6):e0128604–24, June 2015.

Yoshida, S. and Toh-e, A. Budding yeast Cdc5 phosphorylates Net1 and assists Cdc14 release from the nucleolus. *Biochemical and biophysical research communications*, 294(3):687–691, June 2002.

Zackrisson, M., Hallin, J., Ottosson, L.-G., Dahl, P., Fernandez-Parada, E., Ländström, E., Fernandez-Ricaud, L., Kaferle, P., Skyman, A., Stenberg, S., Omholt,

S., Petrovič, U., Warringer, J., and Blomberg, A. Scan-o-matic: High-Resolution Microbial Phenomics at a Massive Scale. *G3 (Bethesda, Md.)*, 6(9):3003–3014, Sept. 2016.

Zhang, Y., Qian, M., Ouyang, Q., Deng, M., Li, F., and Tang, C. Stochastic model of yeast cell-cycle network. *Physica D: Nonlinear Phenomena*, 219(1):35–39, July 2006.

Zhou, X., Li, W., Liu, Y., and Amon, A. Cross-compartment signal propagation in the Mitotic Exit Network. *bioRxiv*, Oct. 2020.